

ELECTROFORMING AND ELECTRON EMISSION IN
METAL-BOROSILICATE GLASS-METAL STRUCTURES

BY

EBRAHIM HOSSEIN ZADEH TAHERI, B.Sc.

This thesis was submitted in fulfilment
of the requirements for the degree of
Doctor of Philosophy at Brunel University.

August 1974

Man's brain has never solved the eternal Why
Nor foraged past the frontier set for thought.
All intellect be sure, proves nugatory,
However hard we either teach or learn.

Not you, not I, can learn the inmost secret:
The eternal Cypher proves too hard to break.

from The Rubaiyyat of

Omar Khayaam.

"In the Name of Allah, the Compassionate, the Merciful."

Here's...to those that I love

Here's...to those that love me

Here's...to those that love them

that love those that love them

that love those that love me.

Anon.

ABSTRACT

Electrical conduction properties of thin co-evaporated $\text{SiO}_x/\text{B}_2\text{O}_3$ (borosilicate) films in the form of sandwich structures of $\text{M-SiO}_x/\text{B}_2\text{O}_3\text{-M}$ (diode) and $\text{M-SiO}_x/\text{B}_2\text{O}_3\text{-M-SiO}_x/\text{B}_2\text{O}_3\text{-M}$ (triode) have been studied. Diode and triode systems show electroforming effects and subsequently electron emission, voltage-controlled negative resistance, electroluminescence, and switching phenomena.

Previous work in this field is reviewed. By making certain modifications to the filamentary conduction theory of Dearnaley, the time dependence of the circulating current and electron emission may be explained. The theory is also supported by topographical studies of the structures in a scanning electron microscope. The voltage breakdown strength in borosilicate glasses is found to be very high, in particular for devices which carry aluminium electrodes in comparison to those carry silver, copper or gold electrodes. Breakdown depends on both the electrode and insulating materials and on the insulator thickness. Since the circulating current in borosilicate films which carry noble metal electrodes such as Ag or Au, is much higher than those which carry reactive electrode materials such as Al, i.e. the device temperature is very high ($400\text{-}700^\circ\text{C}$), and these have led us to the conclusion that this type of breakdown in fact is at least partly thermal in origin.

Experiments on triode systems yielded extremely interesting results such as dependence of potential distribution on the forming direction, non-uniformity of conducting filaments, and finally controllability of the circulating and emission currents by the grid voltage.

The films deposited between Al electrodes, show evidence of electroforming and of electron emission. Formed devices also showed a region of differential negative resistance at high voltages. These devices could withstand high voltages and give improved emission efficiency. Diode and triode systems having thickness greater than $10,000 \text{ \AA}$ were formed. The effects of electrode materials, by using combinations of Al, Ag and Cu in triode electrodes were studied. Peak voltage and peak current showed a dependence on the electrode materials.

Scanning electron microscope observations of films showed localised effects at the electrode surfaces and physical changes in the dielectric structure, while the sandwich structures were being operated as electron emitters. Consequently electroforming is believed more likely to take place by means of the production of filaments of mostly electrode and insulator materials by diffusion and electrolytic processes. Since borosilicate films show a high sensitivity to water vapour for concentrations of B_2O_3 greater than 50%, a 30% concentration of B_2O_3 was found experimentally suitable to work with, and therefore all devices made use of 70% SiO_x and 30% B_2O_3 insulating films.

ACKNOWLEDGEMENTS

The author would like to thank all those who have contributed, or helped in any way, towards this work. He would particularly like to mention, by name, these people without whose help this work might not have been accomplished:-

Professor C.A. Hogarth for his supervision and guidance throughout this project.

Mr. R.M. Creamer, Mr. R.B. Hall, Dr. R.D. Gould, Dr. A.A. Abidi, Mr. H. Bidadi and Mr. G.R. Moridi for critical discussions which proved to be of valuable help.

Thanks are also due to Mr. D.J. Pacey and Mr. K.R. Schlachter for advice concerning vacuum problems and Mr. S. Woodisse, Mr. L. Lightowler, Mr. A.J. Cowie and the other Physics Department Technical Staff, who have always been available to help and advise.

Mr. B. Fookes and Mr. R. Bulpett of the Metallurgy Department for the experimental assistance and for the useful discussions on the production of the S.E.M. pictures in Chapter 5.

Mr. L.E.L. Chandrasekera for the photograph of the apparatus and developing the pictures which were taken in the S.E.M. and Monique for typing this manuscript.

I would also like to take this opportunity of thanking Alison for all the help she has given and The Pahlavi Foundation of Iran for financial assistance.

CONTENTS	Page
Abstract	(i)
Acknowledgements	(iii)
Contents	(iv)
1. A Review of Electrical Conduction in Amorphous Thin Films	1
1.1. Introduction	1
1.2. D.C. Conduction Mechanisms in M-I-M Systems	5
1.3. Electroforming in M-I-M Structures	13
1.4. Differential Negative Resistance and Switching Phenomena in M-I-M Systems	29
1.4.1. Current-Controlled Negative Resistance	31
1.4.2. Voltage-Controlled Negative Resistance	33
1.5. Electroforming and Electroluminescence Phenomena in M-I-M Structures	34
1.6. M-I-M-I-M (Triode) Systems	39
1.7. Models of the Forming Process and Conduction Phenomena in Formed M-I-M Structures	43
1.7.1. Hickmott	43
1.7.2. Simmons, Verderber and Eales	45
1.7.3. Greene, Bush and Rawlings	52
1.7.4. Barriac, Pinard and Davoine	54
1.7.5. Dearnaley, Morgan and Stoneham	56
1.7.6. Ralph and Woodcock	61
1.7.7. Discussion	65
1.8. Breakdown in Solid Dielectric Films	67
1.9. Aim of the Experimental Work	73

2. Device Preparation and Experimental Techniques	75
2.1. Preparation of Devices	75
2.1.1. The Evaporation System	75
2.1.2. Deposition Procedures	77
2.1.3. Thickness Measurements	82
2.2. Electrical Measurements	83
2.2.1. The Vacuum Test System	83
2.2.2. Electrical Circuits	84
2.2.3. Electroforming	85
2.2.4. Temperature Measurements	85
2.2.5. Topography of the Devices in a S.E.M.	86
3. M-I-M Systems	88
3.1. D.C. Stability and Characteristics of M- $\text{SiO}_x/\text{B}_2\text{O}_3$ -M Structures	88
3.1.1. Variation of I_c and I_e with Bias Voltage	88
3.1.2. Variation of Device Temperature with Bias Voltage during Operation	94
3.1.3. Time Dependence of the Electroforming Process	95
3.1.4. Breakdown	95
3.2. The High Field Region	97
3.2.1. Breakdown Voltage and its Dependence on Insulator Thickness and on Electrode Material	97
3.2.2. Low Temperature Characteristics	99
3.3. Discussion of Results	101
4. M-I-M-I-M Systems	105
4.1. Forming Direction and Potential Distribution	105

4.2. Potential Distribution and its Variation with Grid Voltage in the Two Insulator Regions (D_1 and D_2)	111
4.2.1. Effect of a Negatively-Biased Grid	112
4.3. General Circuit Arrangement in Triode Systems	113
4.4. Discussion of the Results on the Triode Systems	126
5. Observation of the Behaviour of M-I-M structure in the Scanning Electron Microscope during the Dynamic Operation of the Devices	133
5.1. Introduction	133
5.2. Results of Topography of the Device Surfaces during the Dynamic Operation	135
6. Summary and Conclusion	142
References	149
Figures	154

CHAPTER 1.A review of electrical conduction in amorphous thin films1.1. Introduction

While thin films of liquids and the associated phenomenon of interference colours have been studied for over three centuries, thin solid films were probably first obtained by electrolysis in 1838. In the recorded literature, however, Bunsen and Grove obtained metal films in 1852 by means of a chemical reaction and by glow-discharge sputtering, respectively. Faraday obtained metal films in 1857 by the thermal evaporation on explosion of a current-carrying metal wire. The usefulness of the optical properties of metal films, and scientific curiosity about the behaviour of effectively two-dimensional solids have been responsible for the immense interest in the study of the science and technology of thin films. Physical phenomena peculiar to thin films, and the basis for their study, are generally the consequence of their planar geometry, size, and unique structures. Size-limited electron and phonon transport process in metals, insulators and semiconductors, quantum-mechanical tunnelling through normal and super-conducting metal-insulator junctions are some examples of contributions of thin film phenomena to solid-state physics. The very useful book 'Thin Film Phenomena' by Chopra published in 1969, has many excellent articles and data in this subject.

Insulating films are coming into widespread use in electronic devices and integrated circuits. As a result their academic properties are currently of great interest both in industrial research

laboratories and universities. Various techniques such as evaporating, sputtering, chemical deposition and certain other methods are used to prepare particular materials in their thin film form.

Metal-insulator-metal structures were considered as capacitors, since these structures for number of reasons have advantages compared to previous conventional devices. Only in relatively recent times has it been possible from the conductivity point of view to prepare thin dielectric films with any degree of reproducibility. The usual and common means of film preparations these days are by sputtering or vacuum deposition techniques. Even at the present time, there is a good deal of art required to obtain reproducibility. This is because the properties of films which determine conductivity, such as structure, impurity, etc., are dependent on a number of factors during film deposition, including rate of deposition, substrate temperature, residual ambient pressure, purity of evaporant, etc. In other words the conductivity of the film can be due to its extrinsic nature as well as its intrinsic properties. During recent years vacuum coating plants and auxiliary equipments have reached the level of sophistication required to permit some reasonable degree of control over the films.

Amorphous materials are of current topical interest and one class of such materials consists of thin layers of mixed oxides which possess a 'glassy' structure.

In this thesis the electrical properties of silicon oxide-boric oxide mixtures (borosilicate glass) in M-I-M (diode) and M-I-M-I-M

(triode) forms are studied. Since there is evidence as I shall discuss later, that breakdown in such structures is due to the thermal effects, borosilicate glass films are quite suitable from this point of view in remaining undamaged at a high device temperature. As a result, for a number of particular reasons which will be discussed in later chapters, borosilicate films have an advantage over other monoxide films such as silicon oxide films, etc., to be formed at high applied voltage with reactive electrode materials such as aluminium.

In the past, experimental results have often been interpreted without taking into account the extrinsic nature of the films. A further complicating factor in interpreting experimental data is that, because of the wide range of electric fields under which the data is usually gathered, the observations often cannot be described by a single conduction mechanism; it is not unusual for various field strength ranges to involve different electrical phenomena. Because of the defect nature of the films, it is not also uncommon for co-operative phenomena to occur; for example, space-charge (due to trapped carriers) modulation of Poole-Frenkel effect or Schottky effect. Due to the impurities incorporated into the films during deposition and the defect nature of the films, amorphous material may contain a large number of donor and acceptor centres and traps¹. In these materials donor and acceptors do not form discrete energy levels. In crystalline insulators the conduction and valence bands and energy gap are well-defined; but in amorphous materials band edges do not undergo a sudden transition from allowed to forbidden energy levels.

In other words, in these materials, there are not such well-defined regions. Since in amorphous materials the local binding forces in the short range are essentially the same as in the crystalline forms, band theory which is strictly applicable to crystalline materials, in its modified case may however, be applicable to amorphous films².

In strictly amorphous materials there is another important consideration which leads to the existence of so called 'impurity bands'. Because of the lack of long-range order in these films, there is a smearing of the conduction and valence band edges (impurity bands)³. Similar effects also take place in heavily-doped semiconductors. Because the band edges are diffuse, there is a gradual transition from a quasi-continuous state (conduction and valence bands), in which the carriers can move freely, to strictly localised states (density-of-states tail) or traps in which the carriers are immobilised¹. These traps are an intrinsic property of amorphous insulators and probably exist in large quantities ($\sim 10^{19} \text{ cm}^{-3}$)¹.

⁴Mott has shown that a one-dimensional energy band model for completely amorphous materials, results in a series of localised states. Transition takes place from the band to localised tail of states. This transition at which a significant change in the mobility of these materials occurs is called the 'mobility edge' and the gap between the mobility edges is then termed the 'mobility gap' similar in terminology to 'energy gap' employed for crystalline semiconductors.

1.2. D.C. Conduction Mechanisms in M-I-M Systems

There are several reasons for believing that the observed conductivity in vacuum-deposited thin dielectric films is often due to the extrinsic properties rather than to the intrinsic properties. For example, the current density is often much higher than would be expected, and the activation energy associated with the conductivity is usually less than half of the insulator energy gap. The source of the extrinsic conductivity is thought to be the inherent defect nature of evaporated chemical films⁵.

An insulator, in practice, abounds with traps. Traps positioned above and below the Fermi level are essentially empty (shallow) and filled (deep) respectively. Simmons has shown that non-degenerate equilibrium statistics require

$$N_{td} \exp\left(\frac{E_{td} - E_{Fi}}{kT}\right) + N_v \exp\left(\frac{E_v - E_{Fi}}{kT}\right)$$

$$= N_{ts} \exp\left(\frac{E_{Fi} - E_{ts}}{kT}\right) + N_c \exp\left(\frac{E_{Fi} - E_c}{kT}\right) \dots 1-1$$

where N_{td} and N_{ts} are respectively the deep and shallow trap densities and E_{td} and E_{ts} are respectively the energies of the deep and shallow trap levels. For particular values of trap parameters, the two terms involving the conduction and valence bands can be neglected. Thus the insulator Fermi energy is obtained.

(6)

$$E_{Fi} = \frac{E_{ts} + E_{td}}{2} + \frac{kT}{2} \ln \frac{N_{td}}{N_{ts}} \dots\dots\dots 1-2$$

From this equation it is seen that E_{Fi} is determined only by the trap parameters, and it is normally positioned between the two trap levels.

When the electrodes are applied to the insulator (MIM), the height of the potential barrier and the shape of the bottom of the insulator conduction band are such that the vacuum and Fermi levels of the electrode and insulator are one and the same level known as "The System Fermi Level E_{Fs} ". The continuity of the vacuum levels determines the height of the interfacial barrier ϕ_0 .

$$\phi_0 = \psi_m - \chi$$

Where ψ_m is the metal work function and χ the insulator affinity. Normally before the electrodes are applied, $\psi_m \neq \psi_i$ (ψ_i is the original work function of the insulator). When electrodes are applied, charge is exchanged between the electrode and insulator such that the relative change in position of the Fermi level of the insulator reduces the energy difference between the electrode and insulator Fermi levels. The charge exchange ceases when the two Fermi levels come together to form a discrete monoenergetic system Fermi level⁶. The types of contact at a metal-insulator interface fall into three categories. When conduction is electronic, Simmons⁶ has shown that conduction depends upon the types of contact.

(a) Ohmic contact and this is when $\psi_m < \psi_i$. Under this condition, electrons are injected from the electrode into the conduction band of the insulator, giving rise to a space-charge region. This region is termed 'accumulation region'.

(b) Blocking contact, and this is when $\psi_m > \psi_i$.

The thermal equilibrium in this condition requires that electrons flow from the insulator into the metal. A depletion region and positive space charge are created in the insulator and an equal negative charge resides on the metal electrode.

Electrostatic interaction between the surface of the insulator, creates a local field in this surface. This field bends the bottom of the insulator conduction band downwards within the bulk of the insulator until it lies an energy $\psi_m - \psi_i$ below the top of the interface. The place at which this occurs determines the edge of the depletion region.

(c) Neutral contact, and this is when $\psi_m = \psi_i$.

The Fermi levels of insulator and electrode and vacuum line up without the necessity of charge transfer. Since no space charge exists within the insulator, the conduction band is flat right up to the interface.

Conduction usually takes place by the transference of electrons or holes, or ions across the insulating layers. We begin by considering electronic motion in M-I-M systems. When conduction is by electronic means, two different-process can be distinguished:

(i) Electrode-Limited Conduction

When the conductivity is dominated by a potential barrier at

the electrode-insulator interface, the free-electron density at the interface is much lower than that in the bulk of the insulator. Thus the rate of electron flow through the system will be limited by the rate at which they flow over the interfacial barrier, hence the conduction process is electrode limited.

(ii) Bulk-Limited Conduction

In this case, the conductivity is dominated by the high resistivity of the insulator. The contact is ohmic and is capable of supply the electrons to the insulator, as required by bias conditions. Thus with this type of contact, the conduction process through the system is limited by the rate at which the electrons can flow through the bulk of the insulator rather than the rate at which they are supplied by the electrode, hence the condition is bulk limited.

(iii) Ionic Conduction

Current density J , in M-I-M systems is a function of applied electric field, F , activation energy ϕ and temperature T .

$$J = f(F, \phi, T) \quad \dots\dots 1-3$$

In ionic conduction the transference of ionic charge takes place between adjacent defect sites under the influence of the applied field. Conduction takes place by a series of ionic jumps between neighbouring sites over a potential barrier ϕ .

The electric field lowers the potential barrier ϕ , by a fraction of $\beta_I F$ in the forward direction (β_I is a constant) and increases it by the same factor in backward direction. For a DC electric field where $\beta_I F$ is not negligible compared to kT , the probability of ionic jumps in the backward direction can be neglected.

Current density is given by:-

$$J = J_I \exp\left(\frac{-\phi}{kT}\right) \exp\left(\frac{\beta_I E}{kT}\right) \dots\dots\dots 1-4$$

where k is Boltzmann's constant.

(iv) Quantum-mechanical Tunnelling

According to the quantum theory, the wave function of an electron has finite values within the classically forbidden barrier of insulator separate by two metal electrodes (M-I-M). The wave function decays exponentially within the thickness of the barrier. Therefore, if the barrier is extremely thin, the electron has a finite penetration probability which depends on the geometrical configuration of the potential barrier. Tunnelling (field emission) may also take place through barrier whose effective thickness is reduced by the high applied field. This type of conduction, however, falls into the electrode-limited processes category.

The insulator must be thin, ($< 100\text{\AA}$) so that the electron wave function is not fully attenuated at the opposite electrode. If, however, the insulator is sufficiently thin, the predominant contribution to the current is derived from electrons in the cathode, tunnelling through the insulator potential barrier. As we shall discuss later, for thicker films at higher temperatures, current will be due to the thermal excitation of electrons (thermionic emission) over the insulator barrier. The tunnelling process is temperature-dependent. The tunnelling equation, however, gives a complicated dependence of current on the barrier heights at the two electrodes, which differs for forward and reverse bias voltages.

It has been shown that the logarithmic derivative of tunnel current with respect to voltage ($\frac{dJ}{dV}$ versus V) rises sharply at $V = \phi_1$ and $V = \phi_2$, ($\phi_1 < \phi_2$) where ϕ_1 and ϕ_2 are the barrier heights (in electron volts) for forward and reverse bias respectively.^{7,8,9.}

Grundlach and Heldman¹⁰ used this technique ($\frac{dJ}{dV}$ versus V) to determine the barrier heights in tunnel junctions prepared by a thermal method. At higher voltage i.e. $V \gg \frac{\phi}{e}$ complicated forms of the current density equation reduce to the well-known Fowler-Nordheim equation which does not depend on temperature.

$$J = J_{FN} F^2 \exp \left(- \frac{\beta_{FN} \phi^{3/2}}{F} \right) \dots\dots 1-5$$

where J_{FN} and β_{FN} are Fowler-Nordheim constants and F is the electric field.

In thicker films where the potential barrier is too high to permit tunnelling to occur, or at sufficiently high temperatures the current flowing through the insulator is limited by the rate at which electrons are thermally excited over the potential barrier into the insulator band (thermionic or Schottky emission).

The thermionic emission equation of Richardson then is applied:

$$J = J_R^- T^2 \exp \left(- \frac{\phi}{kT} \right) \dots\dots\dots 1-6$$

where J_R^- is the Richardson constant and ϕ is potential barrier which is independent of voltage bias. The presence of a high field causes a reduction in barrier height ϕ , which is known as the Schottky effect. The Richardson thermionic emission equation then is modified to the Richardson - Schottky equation.

(11.)

$$J = J_R T^2 \exp\left(\frac{-\phi}{kT}\right) \exp\left(\frac{\beta_s F^2}{kT}\right) \dots\dots 1-7$$

where β_s is the Schottky constant and F is the electric field.

In the case of ohmic contact (bulk-limited conduction) sometimes the space-charge limited (SCL) conduction occurs. In this type of contact as mentioned, a negative space charge region exists inside the surfaces of the insulator, and an equal and opposite (positive) surface charge exists on the electrodes. The application of a voltage bias to the system (MIM) results in an increase in and redistribution of the space charge in the insulator and an increase and decrease respectively in the positive surface charge existing on the anode and the cathode. The positive charge on the cathode is just equal to the negative space charge existing in the cathode region, that is the region between the cathode-insulator interface and the virtual cathode (the place at which the field in the cathode is zero). Similarly, the positive charge exists throughout the anode region (the region between the virtual cathode and the anode-insulator interface). In the virtual cathode region current is carried by diffusion processes only. The free component of the space charge existing in the insulator conducts the current, hence the term space-charge-limited current. In fact the cathode region provides the required charge to the anode region by voltage bias conditions. Thus, provided the cathode region exists, that is positive charge exists on the cathode, the conduction process will be space-charge-limited. Mott and Gurney¹¹ studied SCL currents theoretically in a trap-free insulator for the first time and predicted that

$$J = \text{const} \frac{V^2}{S^3} \dots\dots\dots 1-8$$

The expression becomes more complicated in a defect insulator when a single discrete trap level is introduced. The current density shows a power law dependence on V with the exponent greater than 2.

The most important high-field bulk effect in an insulator is the Poole-Frenkel effect, which is directly analogous to the Schottky effect at an interfacial barrier. In this case when an electric field interacts with the coulombic potential barrier of a donor centre or trap, the height of the barrier is lowered. The Poole-Frenkel equation associated with the thin film insulator is ¹.

$$J = J_{PF} F \exp\left(-\frac{\phi}{kT}\right) \exp\left(\frac{\beta_{PF} F^{1/2}}{kT}\right) \dots\dots\dots 1-9$$

where $\beta_{PF} = 2 \beta_s$.

The higher value of β in the Poole-Frenkel equation is related to the different geometry of the potential barriers at the immobile positive charge centres. Frenkel ^{19, 20} suggested that the ionisation potential of the atoms in a solid is lowered by amount of $\beta_{PF} F^{1/2} \equiv \Delta\phi_{PF}$ where $\Delta\phi_{PF}$ is the Poole-Frenkel attenuation of a coulombic barrier in a uniform electric field. Thus the conductivity is field dependent and the current density equation is

$$J = J_0 \exp\left(\frac{\beta_{PF} F^{1/2}}{2kT}\right) \dots\dots\dots 1-10$$

where $J_0 = \sigma_0 E$ and J_0 and σ_0 are respectively the low-field current density and low-field conductivity. However, the

original Frenkel equation has a factor $2kT$ in the denominators of the Poole-Frenkel equation. Certain modifications to equation (1-9) sometimes apply.

Mead¹¹ has suggested that the experimental behaviour described by equation (1-9) is a result of existence of a large number of shallow traps which exhibit Poole-Frenkel emission at high fields. Simmons¹ has shown that if a more realistic value of dielectric constant is used, Mead's results are compatible with Schottky emission. Nevertheless equation (1-9) is still generally used to describe the Poole-Frenkel effect in thin film insulators.

Conduction often takes place by means of the transference of electrons between neighbouring localised impurities, hence the term impurity conduction. In this case, there is no need for electrons to be excited into the insulator conduction band. Electrons can be transferred between adjacent sites either by tunnelling through or by hopping over the potential barrier between the sites. Both the tunnelling and the hopping type of impurity conduction give a thermally-activated equation of the form

$$J = J_{Th} F \exp \left(- \frac{\phi}{kT} \right) \quad \dots 1-11$$

where ϕ is the potential barrier or activation energy and J_{Th} is constant and a function of the majority carrier concentration and the activation energy differs for the hopping and tunnelling processes.

1.3 Electroforming in M-I-M Structures

Thin insulator films, from 100 \AA - $20,000 \text{ \AA}$ thick have a number of interesting electrical properties. These properties include forming, which is a profound and essentially permanent change produced by application of a voltage greater than a forming voltage V_F , to MIM structures. Application of a voltage pulse $V \gg V_F$ of a few seconds at

room temperature in vacuum produces a profound change in the current-voltage characteristic. The current at a given voltage is increased sometimes by as much as a factor of 10^8 , and the new characteristic shows a differential negative resistance at low frequencies. The occurrence of forming depends on the insulator, on the electrodes, and on the temperature and environment during the forming process. The forming voltage depends slightly on the thickness of insulator. The forming process is voltage-controlled. The degree of formation depends on the thickness of the insulator and electrode material. Forming sometimes does not occur for insulators thicker than 3000 \AA , but, however formation of some insulators up to $20,000 \text{ \AA}$, has been reported¹³. Forming occurs most readily in insulators with reactive anions such as oxides like SiO_x , Al_2O_3 and the fluorides CaF_2 , MgF_2 , MnF_2 , and appears to be easier when the insulator is non-stoichiometric. During the forming process there is emission of gas-oxygen from the oxides and fluorine from the fluorides and bubbles are produced between the insulator and electrode¹⁴. The dependence of forming on electrode material is different for the anode, to which forming is sensitive, and the cathode which does not significantly affect forming. Dearnaley et al¹⁴ tabulated the anode metals which have been used by Simmons and Verderber and Hickmott in M-SiO-M and M- Al_2O_3 -M respectively in order of their formability. Some of these metals such as Al in the devices, reported by Hickmott, only formed at high voltage, and in the devices described by Simmons and Verderber (SiO) did not form. Metals with high work function and which do not readily form stable oxides or fluorides are formable. Reactive metals on the contrary either form with difficulty at high voltages (Al) or never form (Mg).

Pollack et al^{15,16} observed a field-dependent forming process in evaporated Pb-Al₂O₃-Pb diodes, which occurred even in air at atmospheric pressure. Forming took place at about 12V for a 340 Å thick insulator. The forming effects disappeared when the bias was removed. Forming was uni-directional and current levels were low if the applied voltage was in a different direction from that used to induce forming. The ease of forming was greatly reduced at low temperatures. and for the samples at room temperature, the current fell rapidly between 300 to 235 K. Below this temperature the current remained relatively constant. A qualitative model was presented to explain these results. The model included the establishment of a positive ionic space-charge which drifted towards the cathode producing a local field as high as 10^8 V cm⁻¹ in the cathode region. The high-field region is also consistent with a lowered metal-insulator work function, which allows Schottky emission of electrons into the insulating layer.

Hickmott¹⁷ observed forming and negative resistance phenomena in a number of oxides, such as SiO, Al₂O₃, Ta₂O₅, ZrO₂ and TiO₂. For a 350 Å film, a sharp increase in current occurred at 4.1 volts. On lowering the voltage, the circulating current increased and reached a peak value at 2.3V. This voltage for maximum current was independent of film thickness between 150 to 1000 Å, but varied if anode materials other than Au were used. Forming only occurred in vacuum conditions. The negative resistance region was observed for either polarity of applied

voltage. It was found that the current passed was considerably reduced as the temperature was lowered. The shape of the I-V characteristic remained unchanged down to a temperature of 195 K. The negative resistance region disappeared completely at low temperature. By increasing the temperature to a value exceeding 195 K, the negative resistance was re-established.

There appeared to be some correlation between purity of samples and their forming voltage. Impure bisulphate - anodised Al films showed a value of V_F (3.7-4.1V) nearly independent of thickness. For SiO and pure Al_2O_3 diodes, the forming voltage increased with oxide thickness. The dependence of forming on the purity of the insulator; together with the temperature dependence results led Hickmott to suggest that the device properties were probably dependent on impurity conduction through the insulator. Ag, Au, Cu, Co, Pb, Sn, Bi, In, Al, and Mg were used as counter electrodes since the insulator and base electrodes were Al_2O_3 and Al in each case respectively. In relatively thin films, Ag electrodes frequently induced shorting between the electrodes and with thicker films Ag appeared to be the optimum anode material. In the case of the thinner films having a Ag counter electrode, forming took place when the counter electrode was biased negatively. The conductivity for peak current using the other metals diminished in the order given above. Some device properties were dependent on the device polarity during forming, but forming itself would generally occur for either polarity.

Filaretov et al ¹⁸ conducted experiments with Al-Al₂O₃-M structures and found that the conducting properties were strongly affected by the nature of the counter electrode. It was proposed that a junction layer was formed in the insulator by the diffusion of metal atoms from the electrode. With respect to the thickness of the insulator (100 - 500 Å) it was suggested that the metal atoms could diffuse right across the insulator to form deep impurity levels in the forbidden band of the insulator which could behave as trapping or recombination centres. A space charge could be formed by ionisation of these centres which could decrease the density of free carriers and cause the negative-resistance region to be developed. The observed decrease in current density with oxygen may also be dependent on a decrease in conductivity due to the oxygen absorption of the surface of the Al₂O₃ layer.

Barriac et al ¹⁹ observed that forming in Al-Al₂O₃ (100 - 1000 Å) - Al films prepared by anodisation and atmospheric oxidation of Al, occurred more readily when the top electrode was positively biased, even though devices were of a symmetrical construction. After forming, the normal properties of the devices were not polarity dependent. Rare and inert gases did not modify the conduction properties, but the pressure of oxygen caused the complete disappearance of the negative resistance region. Increasing the temperature to 373 K did not

increase the conductivity and the usual low-temperature behaviour was observed at liquid nitrogen temperatures.

Simmons et al ^{3,20} studied the factors involved in the forming of Al-SiO-Au structures. Samples formed at a high temperature faster and current levels were higher than those formed at lower temperatures. Oxygen pressure had to be less than 10 torr or forming was inhibited. The reasons for the environmental effect were not discussed. A slight decrease was observed in the forming voltage with temperature over a range of 300 K. When the Al electrode was positive devices did not form. Formed samples could be un-formed by application of an increased reverse voltage bias. The temperature-dependent forming process and reversibility of forming were taken to be a strong indication of ionic migration. On the basis of these observations a new model of the forming process ²⁰ was developed in which a band of localised states were introduced in the forbidden band of the insulator. The model then was extended to include most of the subsequent conduction phenomena.

Dearnaley ²¹ proposed the novel theory that conduction took place through a matrix of conducting filaments which were propagated during the forming process.

Greene et al ²² studied the the dependence of device properties on the nature of the anode material. The most effective anode materials were those of low chemical reactivity,

while reactive metal gave poor results. They found that the effectiveness such as maximum current density under similar conditions, etc, of anode materials was in the following order: Pd, Ir, Pt, Au, Ag, Cu, C, Si, Ni, Co, Fe, Zn, Sn, Pb, Cr, In, Mn, Be, Al and Mg.

During the forming process, devices were monitored with a mass spectrometer and results indicated the evolution of fluorine from fluoride devices. Similar experiments on oxides were not attempted because of the high background level of atmospheric oxygen. A correlation was found between the observed forming voltage and values of the Gibbs free energy (proportional to the minimum voltage for normal solid-state electrolysis) of formation of various halides. The observed correlation was close enough for Greene et al ²² to suggest that forming was by an electrolytic process in the high fields which occur in certain localised regions of the insulator. A series of mechanical reactions takes place leading to the establishment of chains of defect centres across the insulator. Conduction then takes place through these chains by a tunnelling process.

Dearnaley ²¹ described a filamentary model to account for the properties of oxide-coated cathodes. In this model filaments consist of chains of metal atoms separated by oxygen vacancies which are produced when the cathodes are thermally activated. The vacancies can then take up oxygen atoms from an oxygen atmosphere and thus poisoning of the cathodes is adequately explained. Emission is originally field emission, but the filament

current raises the local temperature and initiates thermionic emission from the ends of the filaments to a suitable anode. Flicker noise which is characteristic of oxide coated cathodes is caused by the thermal rupture and subsequent field-assisted re-forming of the filamentary paths.

Barriac et al ²³ investigated the dependence of peak current and peak voltage with frequency of an AC signal applied to Al-Al₂O₃-Al or Au films. While the peak voltage (V_m) remained roughly independent of frequency, the value of peak current (I_m) dropped sharply between 0.1 and 10 Hz. Increasing the partial pressure of oxygen from 10^{-5} to 2×10^{-1} torr produced a significant change in the device properties.

Jawalekar ²⁴ noted two differences in normal negative resistance behaviour of formed Yb-YbO-M devices. Firstly the current in the negative resistance region was stable in contrast to the normal noisy behaviour; secondly, at higher voltages a sharp current increase was observed in agreement with the results of Barriac et al ²³. Electron emission was detected at voltages greater than 10 V. VCNR was explained by excess metal and oxygen atoms in the YbO layer. Negative resistance is then a result of a similar process to that in the tunnel diode, when the Fermi level drops into the valence band of the P-type layer due to heavy doping.

Doucas and Walsh²⁵ observed forming in four-layer structures of M-CdS-I-M. A typical thickness of the layers involved was 10,000 Å for CdS and 2000 Å for the insulator (usually SiO or MgF₂). The base electrode was Al while the top electrode was either Al or Au. The nature of the top electrode was found to have no effect on the properties of the samples. Room temperature measurements showed an increase in device current with voltage bias up to 10V, and the negative resistance region disappeared at 77 K. At liquid nitrogen temperature a power-law dependence was observed with $I_c \propto V_b^n$ where $3 \leq n \leq 5$ for $V > V_0$ while $2 > n > 3$ for $V < V_0$. V is the voltage at which negative resistance and electron emission appears and usually was constant between 10-12V. The variation of emission current (I_e) showed a $\log I_e/V_b^2$ versus $1/V_b$ dependence, indicative of a field-emission mechanism. Then it was suggested that for a field-emission effect, the slope of the straight line of I_e/V_b^2 v. $1/V_b$ characterised the height of the potential barrier through which tunnelling was taking place. When the biasing polarity was reversed no emission was observed, although the sample power was dissipated in the device. In the voltage region beyond 10V emission increased rapidly, while the power input to the device either decreased or remained approximately constant. The conductivity of M-CdS-M (diode) films was substantially higher (10-20 times) as expected, although they did not exhibit any negative resistance or electron emission.

There was no significant difference in the Ac frequency-response between M-CdS-I-M and M-I-CdS-M conductivity structures. Cooling the device did not reduce the number of the emitting spots but it affected their brightness. A poly-filamentary conduction model based on Dearnaley's filamentary model, was assumed and it was suggested that the filament density was much higher in the CdS than in the insulating layer. Thus higher conductivity in M-CdS-M structures was explained, as was the importance of the insulating layer. High current in the CdS layer caused thermal breakdown to occur before localised filamentary rupture. The insulating layer served the purpose of providing a region where this can take place.

Collins²⁶ suggested that preferential deposition of Cd atoms in the Doucas and Walsh²⁵ devices, may well have given rise to a Cd rich layer of CdS which would have exhibited metallic conduction properties. Apparent forming in the four-layer devices would therefore merely be the result of forming in the insulator. The similarity of the results of Doucas and Walsh with those for simple SiO_x films was then pointed out, as well as the peculiar behaviour observed by Collins for CdS devices. This included the time dependence of the voltage for voltage maximum, which also had been observed previously by Sutherland²⁵ in ZnS films. Doucas and Walsh²² instead of accepting metallic conduction in CdS, stressed that samples which are deposited at temperatures greater than 100°C show a

decrease in the number of Cd atoms, leading to an increase in the resistivity of the film. The probability of hot electron emission through the CdS (10,000 Å) layer would be much less (as required by Collins), and would not be in agreement with experimental results.

Hickmott²⁸ studied Al-Al₂O₃-M diodes where special care was taken to obtain a "clean" anodised layer. Results were compared with those previously obtained for so-called "dirty" Al₂O₃ films. "Cleaned" Al₂O₃ did not form with Al, Mg, Pb, and Sn counter electrodes for either polarity. Application of higher voltages caused destructive breakdown. Forming occurred with Ag and Au anodes. VCNR was observed, but the peak voltage for Au counter-electrodes was higher (14V) than for Ag. The forming voltage appeared to be field-dependent although it was not constant. Forming was observed with the base Al electrodes positive in "dirty" oxides where the forming voltage was independent of insulator thickness and of counter electrode material. Thus forming in films having less impurity and with the Al electrode positive was impossible. The forming process, however in "cleaned" oxides appeared to be field dependent.

VCNR and forming have been observed in monomolecular layers. Grundlach and Kadlec³² investigated cadmium arachidate. Preparation was achieved by depositing a series of layers 26 Å thick. Forming of the final assemblies took place at 5-6V when the counter-electrode was Al or Au and biased positively. The VCNR property was temperature-dependent, so that it was observed in the temperature range 110-225 K, although it disappeared completely at higher temperatures. On repeated voltage cycling, each time the peak voltage shifted towards

lower voltages so that after a number of cycles the VCNR disappeared. The ratio of peak-to-valley in I-V characteristic increased with the number of monolayers. VCNR for less than five monolayers was not observed. Since the binding force between monolayers is very weak, therefore it was proposed that the injection of metal ions could be easier in these devices. This could be the reason why monolayer sandwiches were formable at low temperatures. The disappearance of VCNR after a few voltage cycles can be due to the dead-time effects.

Sutherland et al²⁹ investigated forming phenomena particularly in Al-ZnS-Ag and Al-CdS-Au structures. The forming voltage for an Ag counter-electrode is lower than for Au, but nevertheless both occur at low voltages. There was a slight negative resistance, so that the peak-to-valley voltage ratio was slightly greater than unity. A large increase in current was observed after the valley region. Similar to SiO_x devices, the value of threshold voltage (V_t) in this case was greater than V_m . A two-stage forming process was observed in Al-CdS-Au and Al-CdS-Ag devices. Initially the current followed a low resistance ohmic characteristic, and finally this gave way to a bipolar VCNR characteristic. V_m was time dependent in common with M-ZnS-M structures.

Sutherland³⁰ proposed a scheme of classifying materials which would undergo forming. Greene²² had already suggested that forming of local regions can be due to a form of solid state electrolysis; similar to the phenomena which occurs in ionic crystals. The amount of ionic character for a given material can account for the suggested forming process.

Pauling³¹ has given an equation for the amount of ionic

character for a single bond between atoms A and B.

Amount of ionic character = $1 - e^{-(X_A - X_B)}$ where X_A and X_B are the electronegativities of atoms A and B. Sutherland showed that formable materials had an ionic content of greater than 50%. An exception to this is provided by the sulphides. It was thought, however, in sulphides that forming was initially probably by diffusion of electrode material into the insulator as a result of the heat dissipation at the beginning of the two-stage forming process.

Gundlach and Kadlec³² extended their work on cadmium arachidate to include triode structures using Al electrodes. At low temperature results were similar to those which had been observed by Hickmott¹³ for SiO_x layers during the initial stages of the forming process. Negative resistance was observed and the applied voltage divided equally over the two distinct regions. At high temperatures the voltage distribution was non-symmetric. Almost the whole of the applied voltage dropped in one region and every little in the other region. The probability of the high-field region appearing in either region of the triode structure was approximately equal. Hickmott¹³ estimated a 120 Å thick high-field region near the cathode and generally in Hickmott's devices the high-field region happened to be in the cathode region. The high-field region becomes firmly established after a number of voltage cycles and apparently no change could be induced in the potential distribution by change of polarity. We shall discuss later the proposition that the location of high-field region is due to the forming direction and independent of electrode polarity. However, a tentative explanation of some of these effects was given. It was suggested that conducting

filaments initially did not contact the grid structure, passing through pinholes from the cathode to the top electrode. The potential distribution was not then affected by the grid. At higher voltages and higher temperatures forming was developed in the grid-top electrode region. Conduction in this region along the filaments was ohmic, and the high field region was in the cathode region.

Thurstans et al³³ have observed large peak currents under single-shot pulses biased in electroformed Al-SiO_x-Au structures. They have noticed that continued application of pulses (200 μs to 0.5 sec. Width) enhanced this effect and modified the subsequent DC characteristics of the device. The effects have been explained in terms of models in which filaments are produced during pulse operation. They have estimated that on the basis of an unmodified filament population, the current flowing at a voltage corresponding to the DC peak current would increase by 25%. They have argued that the large increase in current is due to the change in the numbers of filaments and their resistance distribution.

∞ Hogarth and Taheri³⁴ reported electroforming in borosilicate (SiO_x/B₂O₃) glasses 3000 - 6000 Å thick. Forming took place at higher voltages and with difficulties, since both electrodes were Al. The borosilicate glasses are of very high resistivity (of order 10¹⁵ - 10¹⁶ ohm-cm at low fields). Forming voltage, V_F in these structures varied between 20 and 30 V. The time dependence of current through the devices with Al electrodes was observed and the required time to form was long, usually between 2-3 hours for perfect formation. VCNR in formed Al-SiO_x/B₂O₃ (3000 Å)-Al devices was clearly observed although peak current occurred at higher voltages (V_m = 30 - 80 V). Thicker films (~ 6000 Å) showed three closed peaks

which at the time was thought to be due to occurrence of pre-breakdown.

Taheri et al³⁵ extended the studying of Al-borosilicate glass-Al sandwiches. They have reported perfect electroforming in and electron emission from these devices. Samples have been produced by a co-evaporation technique with composition of 30% B₂O₃ and 70% SiO_x. The Subscript x in SiO_x relates to the uncertainty in composition of evaporated films of silicon monoxide although rapid evaporation of SiO is known to lead to a deposited composition tending to the formula SiO.

The emission current density was of the order 10^{-5} A cm⁻², and since the circulating current through the sandwich was lower than in similar films of SiO_x, the transmission efficiency ($\alpha = \frac{I_e}{I_c}$) was high. The behaviour of the devices, however, has been ascribed to the rupture of field-assisted formed filaments of the type discussed by Dearnaley et al³⁶, and by Sutherland²⁷. Measurements of the device temperature have shown that the temperature - voltage curves follow the I-V characteristic.

Hogarth and Taheri³⁷ continued studying the properties of M-SiO_x/B₂O₃-M structures, replacing Al anode with Cu, Ag and Au. The obtained results were similar to the other formed monoxide diodes and exhibited VCNR, electron emission and time dependence of forming process on different anode material and insulator thickness. The forming time in films carrying noble metals (Ag, Au) were very fast (between 0.1 and few seconds). Devices with Al electrode required a longer time (about 2-3 hours) and higher voltages. Emission current and circulating currents in films carrying Au or Ag electrodes were much higher than those carrying Al electrodes. Temperature measurements showed very much higher temperatures (up to 300°C) at

the peak current operation.

In extension of Taheri and Hogarth's^{34,35,37} work on borosilicate glasses, Hogarth and Bidadi³⁸ continued the studying of electron emission from $\text{Cu-SiO}_x/\text{B}_2\text{O}_3\text{-Cu}$ devices and measured the hot electron attenuation lengths in both the copper electrode and in the insulator. They have observed that attenuation of electron length increases from 1.2×10^{-5} cm at 5 V to 2.2×10^{-5} cm at 24 V in copper. Attenuation lengths in $\text{SiO}_x/\text{B}_2\text{O}_3$ also increase with bias voltage from 1.2×10^{-5} cm at 5 V to a peak value of 2.6×10^{-5} cm at 20 V, then decrease to 2.2×10^{-5} cm at 25 V.

Taheri and Hogarth³⁹ studied the forming process in $\text{Ag-SiO}_x/\text{B}_2\text{O}_3\text{-Ag}$ or Cu structures by direct observation of the devices in a scanning electron microscope during the operation of the devices. The spots formed on the metal electrode surface were believed to identify the positions of the ends of filaments and were believed to be related to the discrete spatial pattern of electron emission which was inferred from the individual scintillations observed when a fluorescent screen is used to study the electron emission pattern^{36,40,41}. The main observations made were of local apparent hot spots, believed to be the terminations of filaments, and evidence of disturbances to the surface region around them. Also there was evidence of tracks developing on or near the surface. The results for specimens having copper or silver electrodes showed similarities but also dissimilarities. These differences have been ascribed to differences in diffusivities of Cu and Ag and in their different affinities for oxygen. All the evidence pointed to considerable power dissipation at the ends of the filaments. Before forming, no special features were observed on the counter electrodes of the devices. The devices were formed by

application of 7 V (devices with Ag electrode) or 9 V (devices with Cu counter and Ag base electrodes). During the electroforming process a number of spots ranging in diameter from 7 to 15×10^{-4} cm were formed. The observations suggested that the temperature in the vicinity of the localised filamentary regions was high, since the density of filaments at any time was between 1 and 10 in a typical 3 mm x 3 mm active area, and if the excess current (over the normal bulk dielectric current) was mostly carried by the filaments, the power dissipation in very localised region would be high and a high temperature would result. The localised regions where filaments were observed vary from time to time, being formed, re-formed and destroyed. The effective current density was between $10^4 - 10^5$ A cm⁻² for a peak current of 100 mA, indicating that a considerable localised heating and melting of the counter electrode was highly probable. However, the high power dissipation in the vicinity of the filaments led to an evolution of energy and the patterns resulting from this were shown in the photographs (see also figures 62, 65 & 66). They have concluded that the scanning electron microscope provides a useful method for observing localised effects in MIM cathodes during their operation.

1.4 Differential Negative Resistance and Switching

Phenomena in MIM Systems

In MIM structures, after forming, differential negative resistance together with switching and memory phenomena also occur. The exhibited phenomena can be explained by a combination of one or more of the conduction mechanisms described in 1.7. Systems which show differential negative resistance are divided into two classes. These are S-type current-controlled negative resistance (CCNR) and N-type voltage-

controlled negative resistance (VCNR). Devices showing both types of characteristic, frequently exhibit related switching and memory phenomena¹⁴. The mechanisms which give rise to differential negative resistance fall into three broad categories, VIZ; processes in which the Joule heating of the conduction electrons causes a change in their number or in their mobility, processes in which special semi-permanent space-charge distributions are set up, and those which involve a phase change or atomic re-arrangement of the host insulator. The most commonly-considered mechanisms are those in the first category, a super heating mechanism providing an example in this category. Certain electronic scattering processes become less efficient at high electron energies. The electron mobility can then rise suddenly, giving an S-type characteristic. The second category is that in which a special space-charge distribution is set up and which gives rise to the differential negative resistance.

These are the models of Hickmott^{13,17} and Simmons and Verderber³ for oxide films, and of Mott² for the chalcogenide "threshold" switch. The model of Barriac et al²³ also falls into this category; although it does not involve other features, such as ionic conduction. Further discussion on these models will be given in 1.7. Finally, we refer to the theories which involve an atomic re-arrangement. This may be a bulk change, or it may involve only small regions of the insulator. In some oxides in which there are bulk transitions sometimes leading to switching, Joule heating may be sufficient to raise the oxide to a temperature above that required for a phase change. The high-temperature state is more highly conducting, and on S-type characteristic results. In the "bistable" switches, filaments have been observed directly, and their behaviour appears

to be associated with a glass transition, and possibly with recrystallisation.

1.4.1 Current-Controlled Negative Resistance

CCNR has been extensively observed in semi conducting chalcogenide glass thin films. The phenomena also has been observed in bulk devices. A review is given by Henisch⁴². Mott has suggested that the increase in conductivity, giving an S-type characteristic, results from an atomic rearrangement which leaves some atoms with incompletely saturated bonds. The low current state of these devices corresponds to an amorphous atomic configuration in which essentially all atoms have saturated bonds. Two approaches which have features in common are those of Gibbons and Beadle⁴³ and of Dearnaley²¹. In these models the conduction is ohmic along filaments which are physically different from the host matrix. In Dearnaley's model these filaments can fracture, becoming non-conducting, and the differential negative resistance results from this fall in conductivity on fracture. Gibbons and Beadle have one filament; switching occurs but there is no negative resistance. CCNR, however, is discussed, as a part of wider review, by Simmons⁹ and Dearnaley et al¹⁴. The switching and memory properties of the chalcogenide glass films divided into two categories⁴⁴. These are the threshold switch or Ovshinsky switch. In the threshold switch at low voltages a high impedance characteristic is exhibited. When the voltage is increased above a critical value V_t (threshold voltage), the device switches to a very low impedance "on" state. The device will only remain in this low impedance state provided the current is maintained above a critical value called the holding current I_h in this state $V_h < V_t$ where V_h is holding voltage. When the current is

reduced below I_h the device switches back to the high impedance "off" state. V_t follows an approximately linear variation with electrode separation, while V_h is almost independent of separation. The I-V characteristic is S-type. The second type of switch is the memory or bistable switch. The memory switch also shows a high impedance "off" state and a low impedance "on" state, but the switching behaviour is different. Switching from the "off" to the "on" state is accomplished by application of a high voltage pulse, whereas switching back to the "off" state can only occur after a high current power pulse is applied. The "off" state cannot be re-obtained merely by reducing the current through the device, and the "on" state is thus a stable memory state. Since the threshold-switching time ($\sim 10^{-10}$ S) is different from the memory-switching time ($\sim 10^{-6}$ S), different explanations for switching processes are proposed. The fast switching time of the threshold switch is an indication that electronic (probably space-charge-limited) processes are responsible. A thermal runaway effect can also be responsible for the switching process. Thermal runaway does not appear to be applicable to the thicker chalcogenide films. The rather slower switching time of the memory switch is compatible with atomic re-arrangement in the glass and this is normally ascribed to the growth of a crystallised filament between the electrodes. Erasure of the "on" state occurs when the filament is destroyed or when it undergoes a phase change due to the high current pulse.

Memory switching has also been observed in transition metal glasses⁴⁵. These consist of inorganic oxides containing an appreciable concentration of transition metal ions which can enter the glass in two or more valence states. As with the chalcogenide

glass memory switch, switching from high to low impedance state is by means of a voltage pulse, while switching from low to high impedance states is by means of a current pulse.

Chopra⁴⁶ observed CCNR is formed oxides of Nb, Ta and Ti.

Forming took place when the reverse current density was increased above 100 mA cm^{-2} . Below the peak current in the I-V characteristic he suggested a space-charge limited mechanism. The impedance of the device beyond the negative resistance was effectively zero.

1.4.2 Voltage-Controlled Negative Resistance

VCNR only occurs after a forming process. This type of conduction is observed in a wide variety of oxides, halides and sulphides. This phenomenon has been observed also in organic monomolecular layers of cadmium arachidate⁴⁷. Hickmott^{12 16} reported the first observation of the VCNR and made an extensive investigation of the phenomena in a number of oxide films. Before forming the device current shows $\log I_c \propto V_b^{1/2}$ dependence where I_c is the circulating current through the device and V_b is voltage bias. Since the circulating current is proportional to $V_b^{1/2}$, from equations (1-9) and (1-10) it can be seen that this is characteristic of Schottky or Poole-Frenkel emission.

When the voltage bias is increased to a value in excess of the forming voltage V_F , a large increase in conductivity takes place. Reducing the current to zero results in the permanent establishment of a VCNR characteristic. The negative resistance part of the characteristic is normally noisy. The maximum current through the device is denoted by I_m and the voltage at which this occurs by V_m . The voltage for the current minimum in the negative resistance region is denoted by V_u . The emission current is denoted by I_e and can be collected with a suitable anode. Figure 1 shows the general

characteristic of a formed device which exhibits VCNR. Switching behaviour also is observed. If the device is quickly turned off in the negative resistance region (in less than 0.1 ms); at the points B, C, or D, the new characteristic will follow the paths OB', OC', or OD'. At the threshold voltage $V_T < V_m$ the device switches back to the low-impedance characteristic. In practice there is an infinite number of memory states. AC characteristics do not show VCNR but follow the curve OA, OB, OC or OD (see figure 1).

1.5 Electron Emission and Electroluminescence Phenomena in M-I-M Structures

Some of the effects of forming other than those on the I-V characteristics in formed devices, are electron emission and electroluminescence phenomena. The electron emission from a formed device depends strongly on the bias voltage. At voltages below the peak voltage there is very little emission. As the voltage is further increased the emitted current rises slowly then starts to increase rapidly at a voltage which depends on the nature of the electrode and insulator material. A dependence of electron emission on the thickness of the insulator has also been reported. The emitted electrons are "hot" since they are not in equilibrium with other electrons in the device. The emission is not uniform over the device, and appears to come from small localised regions. The electrode through which emission occurs also affects the observed external current. In the simplest cases the current is simply attenuated. One of the reasons for the emission efficiency of the oxide devices, as opposed to thinner films (10-50 Å), which has been suggested is that higher voltages can be applied to thicker films without breakdown, and these higher voltages give emission with less

attenuation by diffraction.

Some important points in interpreting the emission are mentioned by many workers. These are as follows. Firstly, a significant fraction of the emitted electrons have energies close to eV , where V is the applied voltage. Secondly, much of the emission is localised at small regions in the electrode. Thirdly, the emission is not simply a result of the insulator becoming hot, while Verderber and Simmons²⁰ eliminate this probability by observing that the electron emission does not follow the power dissipation in the device.

Hanney et al¹⁷ observed that electron emission follows the growth of electrical conductivity through the device. Heinze and Wagener⁴⁸ studied the distribution of the emission from an oxide cathode at successive stages of activation. They formed electron images of the cathode and thereby observed that emission takes place from small bright centres. Initially only a few centres were present but as activation proceeded the number of sites increased rapidly.

In the formed oxide, the electroluminescence parallels electron emission to some extent. Visible electroluminescence develops simultaneously with the development of VCNR. The luminescence first appears at voltages just below the voltage maximum and falls again in the differential negative resistance regime, before starting a slow rise in intensity with applied voltage. The light which covers a wide spectral range, is emitted from a few bright spots; these spots are usually stable under repeated tracings of the current-voltage characteristic, although a few spots appear or disappear. The spots are typically a few microns in diameter and there is no conclusive evidence that they are the spots from which electron emission occurs.

Electroluminescence is not confined to oxide films which develop VCNR.

Hickmott^{49,50} has studied in detail the electroluminescence in Nb_2O_5 diodes which exhibit CCNR. The diodes are electroluminescent before forming; after the forming process, increased electroluminescence accompanies switching, and the emitted light is both polarity and voltage dependent. Microscopic observations indicated that forming and switching occur at small conducting regions. In both the Hickmott and Simmons and Verderber theories of electron emission and electroluminescence, electrons are excited by some means into the conduction band when they move through the insulator without attenuation. Emission can then occur at energies up to the sum of the energy received from the applied field (eV at most) and the energy received from the excitation mechanism. The excitation mechanisms suggested by Hickmott include the impact ionisation of levels in the insulator and some kind of recombination process.

According to Dearnaley's filamentary model, electron emission is due to the generation of hot carriers by the fields which exist at high-resistance spots in the filaments. In some of these spots, the voltage drop may be very nearly the whole bias voltage. Hickmott⁴⁹ has also discussed the luminescence and has proposed models based on recombination involving the impurity levels in the insulator. The origin of the decrease in the luminescence in the differential negative resistance regime is by no means certain, and may be a population effect (a decrease in the number of electrons capable of radiative transitions, or a decrease in the number of sites which can receive the electron), or an effect on the transition probability itself. Dearnaley⁵¹ suggested that the electronic conduction

is developed during activation by filamentary propagation through the oxide, assisted by reducing conditions and temperature the filaments were believed to be a defect state, possibly a chain of alternate cations and anion vacancies. In this way the small emission centres are satisfactorily explained. The high thermionic emission is explained by the field emission from such highly-localised "patches" coupled with the local Joule heating which is a consequence of conduction through filaments.

Kanter and Feibelman⁵² performed an exhaustive study of electron emission for Al-Al₂O₃-Au structures where the insulator thickness varied between 70-150 Å and anode thickness from 200-300 Å. For most samples the characteristic could be explained in terms of Fowler-Nordheim tunnelling although some exhibited different behaviour.

Verderber and Simmons⁵³ described the use of the devices as cold cathode electron emitters. The variation of circulating and emission current could be split up into four distinct voltage ranges. There is no emission between 0-2.5V and I_c is proportional to $\sinh K'V_b$ where V_b is the bias voltage and k' is a constant. For bias voltages in the range 2.5 to 3 V the current through the device is maximum and the emission current increases exponentially. Negative resistance occurs after, in the range of 3-7 V where the emission increases slowly but still exponentially. At voltages in excess of 7 V the circulating current increases slightly while the emission current increases sharply. Electron emission at voltages less than the work function of Au were attributed to the acquisition of energy from the lattice in agreement with the previous work of Hickmott⁵⁴. Lomax and Simmons⁵⁵ later described an alpha-numeric

display panel consisting of a 5 x 5 array of cold cathodes.

Barriac et al²³ studied various aspects of I_e/V_b characteristics in Al-Al₂O₃-Au devices. Emission current measurements showed a peak value at a voltage slightly above that of V_m and then a region of low emission at about 5V. Emission current then increased at about 6 V. Barriac et al extended their ionic/tunnelling theory noted earlier¹⁹ and gave experimental values for the constants used to characterise the electron emission.

Hartmann et al⁵⁶ measured the spatial distribution of the emission current from Al-Al₂O₃-Au devices. They observed emission from localised areas and noted that the intensity and number of emitting spots increased with time. Short circuits through the alumina at which localised heating caused increased emission, were tentatively suggested to be the predominant source of electron emission.

Collins and Gould⁵⁷ were able to form Au-SiO₂-Au devices of thickness up to 6400 Å in contrast to the results of Simmons et al²⁰ where forming was restricted to oxide layer of less than 3000 Å. The I-V characteristic showed the usual peak at 3V followed by a negative resistance region and a second peak at 16V which was not evident in previous work. This peak was voltage and not field-dependent, remaining at 16V for a wide range of insulator thickness. It was suggested that the gradual fall of I_c after the second peak was the result of a more permanent mechanism than that responsible for the first peak. It was proposed that normal dielectric breakdown which causes the destruction of regions of diameter up to $100\mu\text{m}$ ⁵⁸ and thus reduces the effective device area, was the mechanism responsible. Emission current measurement also revealed a secondary maximum at 16V which was very dependent on the same process.

Collins et al⁹¹ replaced the Au electrode by Ag to produce Al-SiO_x-Ag cathodes. Electron emission was more spatially uniform than in Au devices. Emission did appear to rise at certain localized areas of the device and transmission ratios were typically lower than in the corresponding Au devices. The hot electron attenuation length in Ag was also measured.

Sutherland et al²⁹ observed electron emission in Al-ZnS or CdS-Au devices. Al-ZnS-Ag films did not show electron emission. Some structure was observed in the emission patterns, but was not as well defined as emission patterns observed in Au-SiO-Au devices by Gould and Collins⁸⁵.

1.6 M-I-M-I-M (Triode) Systems

The experimental data discussed so far refer to the diode, that is to two-electrode M-I-M diodes. A few workers, notably Hickmott¹³, Mead⁵⁹, Nelson and Anderson⁶⁰, Antula⁶¹ and Gundlach and Kadlec³² have reported observations on triode systems. The use of the M-I-M-I-M configuration offers a number of advantages over simple M-I-M systems.

Hickmott¹³ carried out an important set of experiments on triodes. He studied the potential distribution and negative resistance phenomena in formed Al-SiO-Al-SiO-Au triodes with SiO thickness between 150-500 Å. The development of VCNR in Hickmott's triode was accompanied by the establishment of a high-field region about 120 Å in thickness near the negative electrode. The triode showed VCNR for both forward and reverse bias voltages but the potential distribution changed slightly. It was suggested that VCNR in the I-V characteristic was a high-field phenomenon but did not depend on field emission of electrons from the metal electrode. The behaviour of Al-SiO-Al-Au triodes was found to be generally

identical to that of Al-SiO-Au diodes. Experiments on triodes, however, led Hickmott to a phenomenological model of impurity conduction and VCNR in thin oxide films. Conductivity was developed in the triode by applying a voltage bias between top and base electrode, with the top electrode positive. Generally, triode currents were smaller for decreasing voltage than for increasing voltage. Before forming the potentials applied between the top and base electrodes divided as was expected between the grid-top electrode and the grid-base electrode regions. However, after forming, the potential distributions were highly non-linear. The most characteristic feature of the potential distribution in a triode, as negative resistance became fully developed, was that nearly all the potential drop appeared at the negative electrode, between grid and cathode. When the voltage is reversed the potential drop remains in the same region, although the high conductivity and differential negative resistance are still observed. Reversal of polarity of the voltage applied also results in a decrease of circulating current; a broadening of the peak in I-V characteristic and a shifting of V_m . It was suggested that the mechanism responsible for negative resistance does not depend on having a high field at the negative electrode of the triode; field emission from the negative electrode also did not determine the current-voltage characteristic or the negative resistance. It was noted that the potential in the triode could shift when the polarity was reversed although it was not essential for negative resistance. However, measurements of the potential distribution in triodes provided for Hickmott a basis for a model of conduction and negative resistance in thin insulator films. It has been argued that the establishment of conductivity in the diode

or triode resulted in the localisation of the potential drop in a fairly narrow region of the insulator, a region which was characterised by high fields when potentials less than the band gap of the insulator were applied. Processes occurring in this high-field region determined the current-voltage characteristic, negative resistance, electron emission and electroluminescence. Since this work by Hickmott there has been relatively little interest in measurements on triode devices. Gundlach and Kadlec³² have observed qualitatively similar behaviour in many of these properties using organic monomolecular layers of cadmium arachidate.

Taheri and Hogarth⁶² have studied in detail, electroforming, potential distribution and effect of grid voltage on I-V characteristic in MIMIM structures, where I is borosilicate glass (70% SiO₂, 30% B₂O₃) and is a chosen metal (Al, Cu, Ag). An electroforming process was considered with respect to the polarity of applied voltage and was found that potential distribution in the triode depends on the direction of forming. Effects of positively or negatively biasing of the grid on potential distribution, on circulating and emission current, and on V_m were also studied. Further details are given in experimental section of chapter (see Chapter 4) in this thesis.

Raby and Collins⁶³ have studied the electroforming and potential distribution in M-SiO-M-SiO-M thin film triodes. They have also measured attenuation lengths of hot electrons in Ag, Au and SiO_x using a triode system. They have reported that the behaviour of an individual device after both layers had been formed was unpredictable. They have argued that because of two reasons this was expected. Firstly the triode has been considered as two diodes, in series, each displaying VCNR and each with the other diode plus associated

circuit resistance as its load. Each diode constituted a bistable element with the possibility of switching along the load line to a higher or lower impedance state. It has been argued that with two such devices in series there is the possibility of switching in one diode triggering switching in the other and could be in such a way the rapid switching back and forth of potential qualitatively explained. Secondly, the forming phenomenon has been considered as a continuous process which carries on throughout the device lifetime and is often the limiting factor in determining the useful life time of a device. They have also observed that the attenuation of electrons passing through a thin film experimentally follows an exponential thickness dependence.

They have argued that the non-linear dependence of α on t_g^{-1} (where t_g is the grid thickness) is not specific to a particular electrode material but it should be a consequence either of the device configuration and structure, of the transport mechanism through this structure, or of the measurement technique. They have come to the conclusion that, however, the asymmetry in the fields in the two oxide layers in agreement with observations of Hickmott¹³, could be due to the natural consequence of having two diodes in series with an I-V characteristic showing VCNR. No evidence has been found however that nearly all of the applied voltage is dropped in a sub-120 Å^o layer with effectively zero field in the rest of the oxide. The switching of potentials from one oxide layer to other has been assumed to the association of switching along the respective diode load line, together with

changes in the I-V characteristics associated with continued device forming. It has been suggested that the usefulness of triode devices in measurement of electron attenuation lengths is critically dependent on the presence of pinholes in the various layers and that such measurements could only be meaningfully compared with those made using other techniques if pinhole effects are eliminated or compensated for.

Abidi and Hogarth⁶⁴ have reported potential distribution measurements in BaO/SiO using triode configuration. The results obtained are in general agreement with those of Hickmott.

1.7. Models of the Forming Process and Conduction Phenomena in formed M-I-M Structures

1.7.1. Hickmott

This model assumes that in the unformed insulator there are present an appreciable number of neutral impurity centres of energy E_I , situated approximately at the centre of the band gap. The existence of a high field in the insulator dominates the conduction process. This high field has been estimated to be 120 Å thick normally near the cathode, although it can shift in any region of the insulator¹³. Figures 2-a and 2-b show the band diagrams of unformed and formed Al-SiO-Au diodes respectively. E_C and E_V are conduction and valence band edges and E_F is the Fermi level. ψ_{Au} is the Au work-function. When a dc bias voltage is applied across the device, Schottky emission takes place from both the cathode and the impurity centres. At sufficiently high values of bias voltage, ionised centres form an impurity band in the insulator which can assist the subsequent conduction process through the insulator. Thus conductivity of the structure is determined

by these positive impurity centres. The process is followed by modifications occurring to the metal-insulator interface such that electrons can easily enter into the insulator without thermal activation. The carriers are low-mobility electrons which hop from one centre to another. Conduction in the low-field regions of the insulator is also by this process. In figure 2-b the process is indicated by (1).

The hopping process which determines the conduction mechanism at voltages below V_m , is not able to explain the observed phenomena such as negative resistance, electron emission and electroluminescence in formed devices. Therefore Hickmott¹³ suggested that there is an immobile hole level at energy E_H , between the impurity band and the valence band. As the voltage is increased the hole levels are filled by electrons tunnelling from the valence band or excited by impact ionisation (2). As a result of electrons tunnelling from the valence band, mobile holes are left in this band which are accelerated toward the negative electrode under the influence of the high field (3). As the accelerated holes reach the impurity levels, they are neutralised by electrons in this level (4). By this motion the electrons in turn impart their recombination energy to other electrons trapped in an impurity case. These electrons are then excited into the conduction band of the insulator (5), where the high field accelerates them towards the positive electrode (6), Direct tunnelling of electrons from the impurity band to the conduction band of the insulator at sufficient voltages also is more likely. Electrons having sufficient energy overcome the Au work-function barrier and may be emitted from the surface of the

top electrode (electron emission) while other electrons can be captured by the impurity band (7), with emission of light. Radiative transitions between the valence band, hole levels and impurity levels can also contribute to the observed electroluminescence.

The occurrence of negative resistance after the voltage maximum at 2.8 V is caused by neutralisation of impurity sites by electrons tunnelling from the hole levels under the influence of the high-field, (8). Since neutralisation has been assumed to be an exponential function of applied voltage, when the voltage is increased beyond V_m the number of impurity centres that are ionised and take part in conduction decreases rapidly, and the current level decreases. In fact the current is limited by a fall in the number of ionised impurity levels in the high-field region.

Hicknott¹³ confirms, however, that forming is not the same as electrical breakdown, since breakdown occurs at higher voltages. The difficulties with this model lie in part in the features which are not explained explicitly like the dependence on atmosphere, the release of gas and the dependence on the electrode, and in part in that rather severe demands are placed on the impurity levels. The impurities must be sufficiently dense that a satisfactory impurity band be formed and in the correct energy range for injection to occur without thermal activation.

1.7.2 Simmons, Verderber and Eales

This model is based on injection of metal ions from the anode into the insulator. This gives a broad band of impurity states which allow conduction. Their model explains the dependence on electrodes, since the energy spectrum of the impurity levels depends on which species of ions is injected. The temperature dependence of forming follows since

the ionic mobility is temperature-dependent. Further, by making assumptions about the distribution of ionic space-charge and the resulting fields it is possible to argue that forming should be voltage-dependent.

In more detail, when an insulator is brought into contact with a metal electrode there is in general a flow of charge from one layer to the other in order that thermal equilibrium requirements be satisfied. This means that the vacuum and Fermi levels of the two layers must be continuous.

Two types of contact (ohmic and blocking) determine the direction of charge flow which depends only on the relative work-functions of the metal and the insulator, ψ_m and ψ_i . In this model usually the insulator-work function is not defined, but, however, it can be expressed in terms of electron affinity, χ_i and bulk activation energy, ϕ_b as :

$$\psi_i = \chi_i + \phi_b$$

Bulk activation energy is the height of the bottom of the insulator conduction band above the Fermi level in the un-formed device.

In the Al-SiO-Al devices considered by Verderber et al²⁰, $\psi_m > \chi_i + \phi_b$ indicating that electrons flow from the insulator to the metal. A depletion region of positive charge is created in the insulator and an equal negative charge on the metal electrode. As a result of these two charge accumulations a local field exists within the surface of the insulator. This field bends the bottom of the insulator conduction band in the centre of the insulator downwards until it lies at an energy ϕ_b above the Fermi level. Figure 3-a shows the band structure of an Al-SiO-Al structure for a zero bias.

Barrier heights at both interfaces have been taken as equal and from figure 3-a, can be seen to be

$$\phi_0 = \psi_m - \chi_i \quad \dots\dots\dots 1-12$$

Ionisable centres are assumed to exist in the SiO probably due to the presence of free silicon. These centres possibly form a depletion region in the SiO.

Figure 3-b shows the energy diagram of the un-formed device for $V_b < V_F$, where V_F is the forming voltage. At the negative electrode the field at the interface and width of the depletion region are increased, while at the positive electrode, on the contrary, the field at the interface and width of the depletion region are decreased. Since a reduced positive field still exists at the anode and exhibits migration, ions are not yet able to migrate from the anode into the insulator.

At voltages $V_b > V_F$, the field at the anode interface falls to zero. There is now no retarding field to inhibit injection and positive ions migrate through the insulator freely. The condition for the field to be zero is when $V_d = \phi_0 - \phi_b$. Assuming that a similar voltage is dropped across the depletion region at the negative electrode the forming voltage is given by :

$$V_F = 2 V_d = 2 (\phi_0 - \phi_b) \quad \dots\dots\dots 1-13$$

Where V_d is the voltage drop across the depletion region. Since

ϕ_0 and ϕ_b are constants independent of oxide thickness and evaporating

conditions, thus V_F is not affected by variations in evaporating procedure. Figure 3 -C shows the band diagrams in the case of $V_b > V_F$. Equation (1-13) gives theoretical values of forming voltage. In the given example, where $\phi_o = 3$ eV and $\phi_b = 0.4$ eV the value of V_F is 5.2 V which is in excellent agreement with experimental results.

The Au ions injected into the insulator and which act as donor centres are in different discrete energy levels³. Two reasons for this have been given. Firstly, in an amorphous material there is neither consistency of nearest neighbour distances nor a recognisable lattice; therefore the Au ions are not restricted to predetermined lattice positions; with the result that their potential energies are not well-defined. Secondly, filling of traps present in the insulator up to the Fermi level gives a net negative charge. A coulombic interaction between positive donors and the negative traps perturbs the potential energy of the donor centres. Because of these two effects, a band of localised states is created within the energy of the insulator. Figure 4 -a shows the band diagram of a formed device when $V_b = 0$. ψ_m is the metal work-function, ϕ_o the metal-insulator barrier height and ψ_I and ψ_i the energies of the bottom of the conduction band and the top of the localised levels. All energies are measured from the Fermi level.

Figure 4-b shows the band diagram when a voltage less than ϕ_i is applied. In this case an electron at the Fermi level can pass straight through the band of allowed states to the other electrode by a tunnel hopping process. At voltages greater than ϕ_i electrons at the Fermi level can only tunnel as far as the top of the allowed band and therefore effectively cannot contribute to the conduction process. The case is shown in figure 4-C. These

electrons are stored in local levels near the top of the allowed band. Electrons with an energy greater than $V_b - \phi_i$ below the Fermi level can still contribute to conduction, but, since the contribution to current of injected electrons falls off rapidly with energy below the Fermi level, the current through the device decreases.

According to the above discussion, the maximum current must flow when $V_b = \phi_i$ independently of the thickness of the insulator. It is suggested that the processes which are responsible for the rising tail in the $I_c - V_b$ characteristic at voltages greater than 8V take place by transport of electrons, injected at the Fermi level of the metal, into the conduction band of the insulator. Thermal excitation (Ac in figure 4-C) and tunnelling through the gap between the allowed state and the conduction band (AB in figure 4-C) becomes possible.

The memory phenomenon is also explained on the basis of the stored charge. As previously mentioned at voltages $V_b < \phi_i$ electrons with energies between E_F and $E_F - (V_b - \phi_i)$ are not able to contribute to the conduction process. These are stored near the top of the band of allowed states. When the voltage is removed slowly, the stored charge leaks out via the anode and the device remains in its original state. In the case of quick removal of applied voltage the electrons remain in the same state in which they are stored. After a while the electrons will diffuse through the insulator by tunnelling towards the centre of the insulator in the direction of lowered potential barriers. Potential barriers rise on both sides at the centre of the insulator so that the charge remains in this position. Since the probability of electrons falling below

the Fermi level or to another lower state is less than that for simple oscillation of the electrons between two states of equal energy, electrons do not drop from their state. Energetically, the stored charge is still near the top of the allowed band. Thus the stored charge within the insulator reduced the field at the metal-insulator interfaces. It is evident that by substituting the reduced field in the theoretical $I_c - V_b$ characteristic equation (equation 5 of reference 3), for $V_b < \phi_i$ the circulating current is reduced. The higher the voltage at which the circulating current falls off rapidly, the higher the charge stored and hence the lower the field at the interface. Therefore, the subsequent impedance of the device can be predetermined by the voltage at which the memory is induced. Consequently the memory is not restricted to an "on" and "off" state, but in principle gives an infinite number of analogue memory states.

The device switches back into the low impedance state at the threshold voltage V_T , which appears to be a natural consequence of the stored charge located just below the top of the band of allowed states. However, since V_b is less than ϕ_i the stored charge is energetically higher than the Fermi level of both the anode and cathode. The occupation probabilities of energy levels in the cathode and anode, of equal energy to those occupied by the stored electrons, are approximately equal to zero. This indicates that electron densities for these levels at the cathode and anode is zero. Therefore the absence of an electron concentration gradient between cathode and anode, necessary to drive the stored charge through the potential barrier region at the anode, causes stabilization of the stored charge. As V_b is increased towards

Φ_i the cathode Fermi level moves up towards the stored charge levels. Thus the occupation probability for electrons in the cathode, at the equivalent energy to that of the stored charge, approaches that of Fermi level. Therefore the density of electrons in the cathode is high while the electron density in the anode remains approximately zero. Consequently the stored charge is swept away to the anode due to existence of the electron concentration gradient and the device switches back into its low impedance state. Switching occurs when the stored charge lines up with the cathode Fermi level and negative resistance starts when the top of the impurity band in the bulk lines up with the same level (cathode Fermi level). Switching must always occur just before the start of the negative resistance region, as is observed. The reason is, since the stored charge is located just below the top of the allowed band, switching occurs at $V_b - V_T$ which is slightly lower than the voltage at which the onset of negative resistance occurs ($V_b = \Phi_i$).

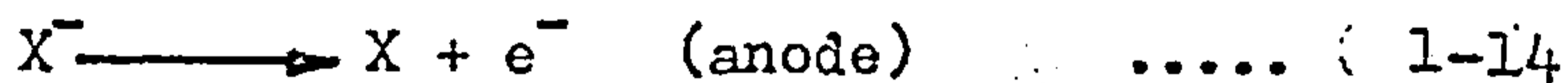
According to this model, electron emission arises when hot electrons are injected from the base electrode into and through the top electrode. Electrons, by a tunnel-hopping process through the insulator, arrive at the anode with a maximum energy ψ_i . Since Φ_i is less than the electron work-function ψ_m , no electron can surmount the barrier at $V_b < \Phi_i$ and be emitted (figure 4-b). When $V_b > \Phi_i$ electrons injected at the Fermi level can only reach the point A in the insulator (figure 4-c) there is, however, probability of obtaining energy from the lattice (AC) and becoming excited in the conduction band.

The objections to this theory are two-fold. Firstly the forming process seems to show none of the dependence on preparation

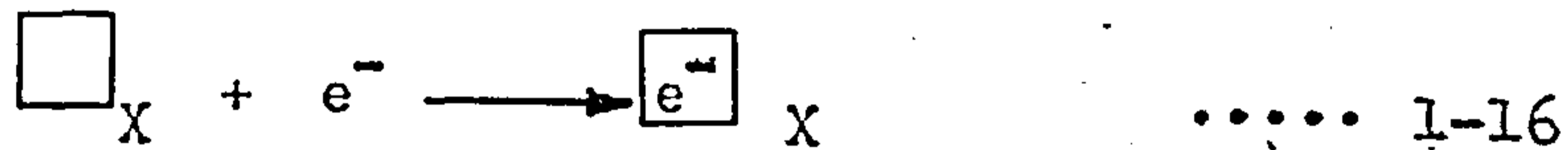
or on insulator thickness and on electrode ionic mobility which could be expected from the wide range of cases studied. Nor is the dependence on atmosphere satisfactorily treated.

1.7.3 Greene, Bush and Rawlings

Greene et al²² argued that the forming mechanism is a high-field electrolytic process in which anion vacancies are injected into the insulator. These vacancies give rise to localised conduction paths through the layer. The theory is developed for a hypothetical insulator MX consisting of M^+ and X^- ions, which is applicable to many different systems. At low fields the reactions at the electrodes for an insulator MX are :



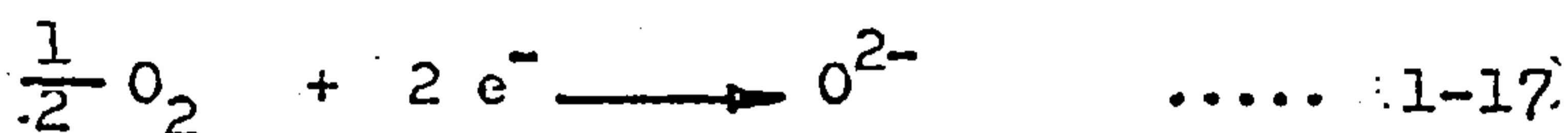
At the anode the X^- anions liberate an electron with the evolution of oxygen when the insular is an oxide. For halide devices the corresponding halogen is given off. At high fields a further cathode process occurs. This is injection of electrons into anion vacancies at the cathode.



(where $\boxed{e^-}_X$ is the X vacancy with trapped electron).

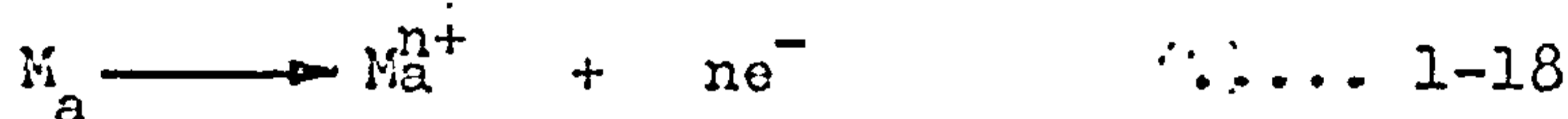
The diffusion of such vacancies towards the anode under the influence of the high electric field leads to the establishment of chains of defect centres which extend across the insulator from cathode to anode. These defect centres are probably of the F-centre type. Throughout the lifetime of the device F-centres continuously diffuse towards the anode, where they are discharged leaving vacancies. Injection of electrons into vacancies at the cathode fills up again

the F-centres lost at the anode. Thus the forming process is a continuous process. Conduction in the formed device takes place by tunnelling of electrons, through the chains of diffusing F-centres, towards the anode. In an oxygen environment a further reaction can occur at the cathode.



In the presence of oxygen the supply of electrons at the cathode is reduced to such an extent that reactions 1-14 and 1-15 are limited. At high oxygen concentrations reaction 1-16 is completely inhibited so that continuous forming cannot occur.

In reactive anode material the following reaction takes place.



Under the influence of the high electric field, the positive metal ions together with oxygen ions resulting from 1-17 will both be absorbed into the insulator. Thus material is entering the insulator by reaction 1-17 and 1-18 and leaving by 1-14 and 1-15. If the rate of material entering exceeds the rate of material leaving the insulator, thickness and field across it will be reduced so that forming via reaction 1-16 is diminished. Therefore less reactive anode material is recommended for optimum forming. The ambient oxygen pressure also should be kept to a minimum.

Apart from minor modifications to the theory of Simmons and Verderber³, the properties of the formed device are explained in similar terms. Tunnelling takes place between allowed states, where these states are defects of the F-centre type. At sufficient voltages electrons tunnelling from the cathode may reach the conduction band of the insulator and then be able to enter the

un-formed regions of the insulator. Negative resistance and memory are thought to be a consequence of a long lived space charge produced by trapping in the un-formed regions. At voltages greater than that at which trapping starts, the current falls, but it starts to rise once more when the traps are filled. Assumption of remaining trapped charge after the device has been switched off, modifies the characteristic up to threshold voltage. The trapped charge can then be released by excitation out of the traps. Excitation by some form of energy transfer from electrons in the tunnelling path is suggested although the excitation mechanism is not clear.

Noise in the negative resistance region is explained by a dynamic equilibrium process between the conducting paths, some switching on and some off in a similar way to the rapturing and re-forming of filaments in Dearnaley's model³⁶.

Electron emission is caused by electrons in the conduction band being accelerated by the field to an energy sufficient to overcome the barrier at the anode.

The model, however, accounts rather well for the forming in ionic crystals. It is not clear if the suggested mechanism can be adapted to other insulators, such as SiO_2 , which show forming.

1.7.4 Barriac, Pinard and Davoine

Their model involves the injection of ions from the anode, giving the ionic conduction and space charge needed for the origin of negative resistance. The injection is initiated by a local fusion of the insulator and electrode by a spark, accompanied by a large heat release. The assumption is based on existence of imperfect regions in an un-formed device, where the insulator is thinner than normal. Electrical arcing across the region takes place at a critical value

of the applied field. Considerable heat release causes local melting of the insulator resulting in the establishment of holes or cavities in the insulator. Vaporised metal atoms are absorbed on the surface of the cavities and current of positive ions in the direction of cathode. A positive space-charge is created by ions in the cathode region. The space-charge perturbs the field in such a way that the applied voltage is dropped over a narrow region much less than the whole thickness of insulator. The region is termed "effective thickness" which varies with the amount of space-charge at low voltages. Tunnelling of electrons from the cathode begins after a given voltage when the effective thickness reaches a saturated value. Since the tunnelling electrons have low energy, the majority of them cannot surmount the "ionic barrier" and contribute to the total current. These low-energy electrons create electrically-neutral pairs with the positive ionic charge carriers termed "pseudo-atoms". Instability of chemical bonding of positive and negative carriers at high-fields diminishes the ionic current by an amount equal to the tunnelling current in the cathode region. The resulting drop in ionic current is the beginning of the negative resistance region. However, in the low-voltage range the conduction is purely ionic and effective thickness is voltage dependent. The ionic current is given as a function of surface diffusion of the ions; the ionic vibration frequency; surface activation energy and effective field. The I-V characteristic is divided into four ranges corresponding to four different voltage ranges. Each part is interpreted by combinations of different conduction mechanism and values of effective thickness^{23,65}.

Current in the first and second regions is exponentially

proportional to the bias voltage, while in the third and fourth regions they are reduced by an amount proportional to the square of the applied voltage. The magnitude of the current in any region is given by the relevant equations. The values of the constant also can be obtained by graphical means. This theory predicts the value of the voltage for maximum current. Since the peak current occurs in the third region, the voltage for maximum current can be calculated from the zero of dI_3/dV_b , where I_3 is current in the third region and V_b is the bias voltage.

At low voltages, since there are neutral pairs, no emission occurs. In order for emission to take place the electrons must have sufficient energy, after passing the "ionic barrier", to overcome the anode work-function.

Environmental effects are discussed in the case of the device performance at high oxygen pressure. The following reaction takes place



According to above reaction, the ions form a stable metallic oxide in performance to neutral pairs and thus are permanently neutralised. As a result, a space-charge region is not maintained in the cathode region. In this model, however, the nature of the electron traps and the dependence of forming voltage on the electrodes and on the insulator is not discussed.

1.7.5 Dearnaley, Morgan and Stoneham

This model is based on the formation of filaments during the electroforming process. These filaments exhibit ohmic conduction, without thermal activation. This is because, perhaps, the sites

involved are considered to very close together so that hopping without activation energy may occur⁴. Dearnaley¹⁴ suggested that under the influence of an electric field oxide films which are deficient in oxygen can undergo a process whereby conducting channels are propagated. The growth of chains of metal atoms alternating with anion vacancies is a possibility, while gas release observed during the forming supports this view. Conduction subsequently occurs through the conducting chains. The filaments are characterised by two important features. The first is that the filament may fracture, and cease to contribute to the conduction. The second is that the filament can reform under suitable conditions. The reforming of the filament is related to the basic forming process of propagation of the filament through the insulator. The fracture of the filament is a consequence of Joule heating, raising the temperature of a part of the filament so that there is local atomic re-organisation, as in melting or other phase changes. The phonon scattering of electrons also increases as the filament temperature rises. The fracture is probably localised in some small region of the filament, since then the switching is voltage, rather than field-dependent. The localisation of the fracture results from the non-uniformity of the filaments which are assumed to have at least one weak spot along their length and their effective resistances are taken to be determined by these. The existence of weak spots in the filaments is a consequence of their growth and the amorphous nature of the insulator. Each filament is assumed to exhibit ohmic conduction. As the voltage is increased the lattice temperature rises, particularly at the weak spots. At a certain voltage thermal vibration at a weak spot attains such a

level that rupture of the filament occurs and conduction ceases. The combined effect of many filaments rupturing at slightly different voltages is a gradual fall of current with voltage in the negative resistance region.

Once each filament bridges the gap between the electrodes, conduction begins and Joule heating occurs. The rupture of filaments occurs when the associated lattice temperature exceeds a certain value. The filaments can reform subsequently, but it depends on their temperature; the ambient temperature; the electric field and possible space charge effects. The filament temperature is not a thermodynamically well-defined quantity. Therefore it is used as a measure of the local heating in the filament. Physically both temperature and the resistance of the filament are assumed by associating them with local regions of high resistance on a highly-conducting filament or chain of defects. Two terms contribute to change the filament temperature, viz. the Joule heating, and heat loss to the insulator, which is assumed simply to be proportional to the temperature difference between the filament and its environment. The total current is given by

$$I = \int_{\min}^{\infty} d\rho \frac{V}{\rho} P(\rho) \dots\dots 1-20$$

where ρ is the resistance of the filament and $P(\rho)$ gives the probability distribution of the various resistances and

$$\int_0^{\infty} d\rho P(\rho) = 1 \dots\dots 1-21$$

The filaments are assumed to be either permanently broken or permanently unbroken at the given voltage and that an

equilibrium has been achieved so that the previous history of the specimen can be ignored. However, the detailed shape of the characteristic is determined by the distribution $P(\rho)$. Two features of $P(\rho)$ are immediately apparent. First, there are very few filaments with resistance below ρ_T since the devices can be cycled below threshold voltage, V_T , without showing signs of filament breakdown. Secondly there are very few filaments with resistances above ρ_u when the devices are cycled at V_u where at this voltage the circulating current is a minimum. At voltages in excess of V_u , the conductivity is small and the filamentary contribution cannot be appreciable and we can take it that all filaments are broken.

The probability distribution of filaments, $P(\rho)$ is derived from the $I_c - V_b$ characteristic by noting

$$\frac{P(\rho)}{\rho} \propto \frac{d(I_c/V_b)}{d(V^2)} \quad \dots\dots\dots 1-22$$

which yields a roughly triangular distribution of filament resistance as shown in figure 5. The current voltage behaviour deduced from a simplified triangular filament distribution, neglecting tunnelling effects gives excellent agreement with measured characteristics. The apparently negative values of $P(\rho)$ for small ρ reflects the contribution of tunnelling or space-charge effects at low voltages. The absence of very-low-resistance filaments is just a consequence of finite specific resistance and the absence of very high-resistance filaments perhaps reflects a natural selection mechanism in the forming process. This is because presumably a filament will cease to propagate rather than continue as high resistance path, if conditions such as the local structure of the insulator, are not favourable.

Deadtime, is a measure of the time between the filament breaking

and reaching a state from which it may reform. This transition appears to be thermally activated. A possible microscopic model which predicts the dead time is assumed. According to this model, during the rupture of the filament at a weak spot, electrons are scattered into the surrounding insulator. The insulator will be highly polarised locally, and will return to equilibrium by thermally-activated processes, such as Poole-Frenkel emissions from traps. At low temperatures this "polarised" state will exist for a long time reforming will not occur. At high temperatures the system may relax rapidly to a state in which the filament is broken but the polarisation is absent. The filament may then rejoin by ionic migration in the electric field. The relaxation takes a finite time and hence the transient phenomena which appear at frequencies between 50 and 100 Hz is explained. Filaments which have been broken remain non-conducting for almost the whole of the time since the time constant for the heating process is short compared with the time to re-establish conduction. In this way the reason why switching time from high to low impedance state is relatively long (approximately 10^{-7} sec.) while switching back to the high impedance state is rapid (approximately 10^{-9} sec.) becomes apparent. It is likely that the difference occurs because in the former case ionic migration must take place, while in the latter the controlling mechanism is the scattering of "hot" electrons leading to polarisation of the dielectric. Then it can be understood why the "dead time" of many milliseconds must elapse before the cycle can be repeated. This corresponds to the relaxation of space charge polarisation.

In the negative resistance region filaments are continually breaking and re-joining to large current fluctuations. The noise level is therefore much higher than at lower voltages where the filaments are either all unbroken or all ruptured.

Hot electrons produced at weak spots near the anode will not be

heavily scattered and will be emitted with energies corresponding to the full bias across the device. However, hot electrons produced by the high fields at the filamentary weak spots are responsible for electron emission into vacuum.

1.7.6 Ralph and Woodcock

This model in fact is an extension of the filamentary model of the type postulated by Dearnaley in which the theories of impurity band tailing in amorphous insulators are accepted, and, although conduction is assumed to take place through filamentary regions, a band structure is ascribed to each filament. Conduction and other related properties are determined by certain modifications to the energy band diagram under bias conditions.

In common with the models of Simmons³ and Hickmott, conduction takes place via an impurity or defect bands somewhere within the insulator energy gap. Because of the lack of long range order in amorphous material the conduction and valence band edges smear out into a range of low mobility localised states. The boundary, where the mobility between the non-localised high mobility states and localised states changes sharply, is termed the mobility edge and the energy difference between the mobility edges of the conduction and valence bands is referred to as the mobility gap. The edges of the impurity band will also smear out into a localised states⁶⁷, giving a mobility band width which is less than the density-of-states bandwidth. The distribution of states is determined by the ratio of V_0/J' , where $V_0^2 = \langle V^2 \rangle$; V is the random excess potential at each impurity site and J' is the bandwidth due to the overlap of the individual state wavefunctions. Above a critical value of V_0/J' all the levels in the band are localised. The critical value of V_0/J' has been estimated by Ziman⁶⁸ to be 2.8 while Anderson⁶⁹ has given a value of 5.0. Below the

critical value the impurity band is divided into a range of propagating states with localised density-of-states tails.

Each filament is assumed to consist of a region containing a high density of defect (or impurity) levels sufficient to form a wide band of states which for convenience is referred to as an impurity band. If Greene's theory of forming is accepted, these defects would be oxygen vacancies in oxide films. Furthermore it is assumed that along each filament the energy width of this impurity band may vary considerably with position as a result of the fluctuations in the density of defects and variation in the random potential V , which these defects experience in an amorphous material. As a result there will be corresponding fluctuations along the filaments. There will also be a region where the mobility bandwidth is low; a corresponding increase in the density-of-states bandwidth also occurs. These regions are referred to as constrictions. The dominant constriction of the mobility band of a given filament under zero bias condition is shown by the band diagram of figure 6.

Isoenergetic tunnelling between the non-localised level within the mobility band (E_m) gives rise to a voltage current relationship of the form $I \propto \sinh k'V$ at voltages below that at which the filaments begin to switch to high resistance. The detail of this mechanism of current flow have been considered by Simmons et al³.

At sufficiently high voltage electrons are hot enough to leave the centre of the impurity band and enter the localised states. This is shown as (a) in figure 6-a. Conduction through a filament may continue via the trapping states by recombination (b) thermal degeneration (c) and field emission (d), but finally will

The memory phenomena are interpreted as a result of the retention of trapped charge when the applied bias is reduced. Some filaments remain non-conducting as long as the trapped charge persists, since the current level also will be lower than the case when the trapped charges are not present. Erasure of the memory state occurs when a trapped charge is released by field emission into the conduction or valence band. The field is a maximum at the constrictions inside the filaments and when this reaches a sufficient level, electrons trapped in the localised states within the filaments will be rapidly released. Other trapped charges outside the filaments and which contribute to reduce the conduction must also be released before all the filaments can be returned to the conducting state. Since there is relatively low field intensity in the un-formed insulator, the trapped charge outside the filaments must relax into the traps inside the filaments where in this way it is then released by field emission. The threshold voltage V_T at which memory erasure is initiated, is determined by the traps inside the filaments. The value of V_T is determined by traps inside the filaments, since the value of dead-time between switching cycles and which is time dependent, is a consequence of the time constant associated with the relaxation process and is determined by traps in the un-formed insulator.

Electron emission takes place by transport of hot electrons from the traps within the filaments to the conduction band by field emission. Therefore, according to above discussion about the memory phenomena, the onset of electron emission will occur at the same voltage as that at which memory erasure occurs. In the negative resistance region, where electrons are entering traps progressively

with subsequent release by field emission, the emission current rises quickly.

Electroluminescence is caused by radiative recombination between hot electrons and holes as has been discussed by Hickmott¹³. The upper limit of photon energies measured by Ralph and Woodcock corresponded to the applied voltage, as expected.

In common with the model of Dearnaley the noise levels in the negative resistance region are taken to be due to the different switching thresholds of many different filaments.

1.7.7. Discussion

From the time of the first observations of the forming effect by Kreynina et al⁷⁰; the related phenomena have been investigated by many workers in this field as has been briefly reviewed.

The earlier theories of conduction were based on band models, and later a uniform conduction medium was assumed by the conduction models of Hickmott¹³ and of Simmons and Verderber^{3,20}, although electron emission was observed to occur at discrete spots. The proposed models were able to explain most of the phenomena observed even though some phenomena in different models were left unexplained. Nevertheless, these models were in good agreement with various device parameters quantitatively as well as qualitatively.

Forming effects have been studied in a wide range of materials. Hickmott¹³ investigated the phenomena using Al_2O_3 since which Simmons²⁰ studied SiO and was able to predict forming voltage in this material. A type of solid state electrolysis mechanism was proposed by Greene et al²², where, by this model, the effect of gaseous environment and the emission of gas during the forming

process were explained. The observations led them to the fact that conduction takes place through a chain of defect centres rather than a uniform medium.

The model of Barriac et al ^{23, 65} accommodated the concept of the high-field region, but assuming a uniform conduction through the device, successfully explained the effect of an oxygen environment,

Dearnaley et al ¹⁴ suggested the filamentary theory which successfully explained the phenomena observed in oxide films, although the nature of filaments was not clearly understood. The model is not only applicable to insulators and semiconductors, but also to organic monomolecular layers ⁷¹. Modification of the theory by Sutherland ²⁷ is able to explain the high values of V_m in sulphides and increase in V_m with time. Dearnaley et al ¹⁴ have fully reviewed the earlier various conduction mechanisms and shown that by a filamentary model most of the observed phenomena can be explained. Experimental evidence for this model is given by the emission of electrons from point sources ⁷². The rupturing and re-jointing of the filaments in localised regions is taken to account for the difference in switching times between the high to low, and vice versa, states. Noise in the negative-resistance region also has been explained due to rupturing and re-joining of the filaments. More recently Ralph and Woodcock ⁶⁶ attempted to extend the phenomenological filamentary model of the type postulated by Dearnaley. In this model a band model is proposed for the conducting filaments and seems to provide a more realistic mechanism through the filaments in amorphous materials.

1.8 Breakdown in Solid Dielectric Films

All materials conduct electrically and all suffer some form of breakdown in a sufficiently strong electric field. For low field strengths the conduction process in most materials is ohmic but as the field strength is increased the conductivity usually becomes field dependent; if the field strength is increased further some form of destructive irreversible conduction takes place.

Dielectric solids usually exhibit a permanently damaged discharge track, and this occurs whether the breakdown has been due to the thermal instability or the other causes. The other causes that may determine dielectric breakdown of solids are not still completely known. Purely electrical breakdown can be subclassified into intrinsic and avalanche breakdown.

In a typical breakdown experiment one measures the current--voltage response of the specimen up to the final destructive breakdown.

The forming processes in M-I-M systems also bear some resemblance to dielectric breakdown, but however, forming is not breakdown, although there are similarities.

The classical theory of breakdown reviewed by Whitehead⁷³ and O'Dwyer⁷⁴ is based on the concept of an electron avalanche. The simplest forms, for examples, as has been discussed by Mott⁴, indicate that breakdown occurs when electrons in the insulator gain energy from the applied field at a rate which exceeds their energy loss. Developments of this theory have been made by O'Dwyer⁷⁴ and by Forlani and Minnaja⁷⁵. These avalanche theories predict a

breakdown field as a function of film thickness and temperature. Detailed experimental studies of thin films confirm that the breakdown voltage depends on film thickness. However breakdown in solid dielectric falls into two categories:

a) Breakdown as a continuation of the conduction process - Thermal breakdown

In a sense all breakdown is a continuation of the conduction process (continuous forming). In thermal breakdown, theory and experiment are in good agreement without the postulation of any physical processes additional to those which operated in a continuous way from the initial application of the voltage. These processes are the Joule heat generated by the current flow, and the conduction of this heat away to the surroundings. If thermal conduction is the only significant heat-loss process, the fundamental breakdown equation is given by ⁷⁴.

$$C_v \frac{dT}{dt} - \text{div} (k \text{ grad } T) = \sigma F^2 \quad \dots\dots\dots 1-23$$

where C_v is the specific heat per unit volume, k is the thermal conductivity, σ is the electrical conductivity, F the field, $\frac{dT}{dt}$ is the time derivative, and $\text{grad } T$ takes the space gradient of the temperature. Since σ is temperature dependent, even approximate analytic solutions of equation (1-23) are not possible for any but the simplest boundary conditions. A complete solution would give T as a function of time and position, but all of this information is not required, since failure of the dielectric will depend of the temperature of its hottest part. For a numerical solution we need calculate only the temperature of the hottest part as a function of time for some specified manner of application of the field. The principal result is that there exists a critical field

strength, F_m for which the temperature of the hottest part of the dielectric asymptotically approaches some temperature T_m (not necessarily the melting point of the dielectric - in fact a very much lower temperature) with time. For field strengths greater than F_m the temperature reaches the value T_m in a finite time and thereafter increases without limit, while for lower field strengths the temperature rises slowly to some upper limit that depends on the field strength. It is evident that ⁷⁴ that the thermal critical field strength depends on the time application of the field.

Figure 7 shows a schematic diagram of solution to equation (1-23).

When the temperature of the hottest part of the dielectric is equal to T_m , the time-dependent term of the equation (1-23) then vanishes and the solution of

$$- \operatorname{div} (k \operatorname{grad} T) = \sigma F^2 \quad \dots\dots\dots 1-24$$

gives the minimum thermal critical field F_m appropriate to the case in which the field is applied for a very long time. In the literature F_m has simply been called the thermal breakdown strength. When the field is applied as a short pulse (of the order of seconds or less-, the heat conduction term in equation (1-23) can be neglected and we obtain the equation

$$C_v - \frac{dT}{dt} = \sigma F^2 \quad \dots\dots\dots 1-25$$

For thin films it is assumed that the power dissipation results in a constant temperature T in the dielectric, which is different from the temperature of the surroundings. If the rate of energy loss to the surroundings is proportional to $\Delta T = T - T_0$, then the relationship can be written as:

$$\lambda \cdot \Delta T = IV \quad \dots\dots\dots 1-26$$

where λ is a constant for the particular test set up. Equation

(1-26) in fact is the basis for one approximate approach for the thermal breakdown of thin films.

It should also be mentioned that in many cases the field will not be uniform within the dielectric, so that it is more logical to speak of a critical voltage than a critical field strength. Thermal breakdown in thin films with field-dependent conductivity, however, involves complicated equations. It is possible to include an explicit field-strength dependence in the electrical conductivity if thermal-conduction process can be treated in the simplified manner of equation(1-26) appropriate to thin dielectric films. A simpler analysis also results if the temperature and field-strength dependence of the conductivity are separable.

The general experimental characteristics of the thermal breakdown have been summarised by O'Dwyer⁷⁴ as follows:-

(1) High temperatures favour thermal breakdown, since in general the electrical conductivity increases and thermal conductivity decreases as the temperature increases.

(2) The thermal breakdown strength depends on the size and shape of the sample, and on the geometry, and thermal properties of the electrodes and the ambient medium. It takes milliseconds or longer for breakdown to develop.

(3) In an impulse thermal breakdown, the strength does not depend generally on the size and shape of the sample, provided the electrode arrangement is such that heat is not conducted away too rapidly. The breakdown strength varies greatly with time of the application of the field, being larger for voltage pulses of short duration.

(4) For AC electric fields the breakdown strength is usually lower than the DC breakdown strength, since the power loss in a dielectric usually increases with frequency.

(b) Breakdown as caused by the onset of collision ionisation - purely electrical breakdown

Collision ionisation is known to occur in semi-conductors which differ from dielectrics chiefly by having a narrower forbidden band gap. From this point of view the theories of intrinsic breakdown yield values of the field strength for which collision ionisation becomes an important process.

Seitz⁷⁶ considered the conditions in which a single electron (or very few electrons) starting at the cathode can cause an avalanche of electrons of sufficient size to destroy the dielectric. If a single electron leaving the cathode can succeed in producing another conduction electron by collision ionisation, and these two produce a further two, an avalanche of n electrons will be produced in n generations. This type of theory of avalanche breakdown attempts to incorporate the more soundly based features of the intrinsic and thermal theories into one, at least for those cases in which the initial instability is electronic in nature.

Both types of avalanche theory are assumed on the basis of uniformity of the field strength or continuity of the current. For thin films there would normally be a few generations of collision ionisation and the uniform-field assumption should be

approximately correct provided that the current is not too large. Distortion of the field depends on the charge density, and even a single collision ionization between cathode and anode would make the distortion large if the current were large. On the other hand, it is unlikely that the field distortion can ever be ignored in thicker films, in which, relatively, many generations of collision ionization will occur; the assumption of continuous current is therefore probably a better starting point, although not an adequate one. Similar to thermal breakdown, the general experimental features of purely electrical breakdown, and the circumstances under which it occurs, are summarised by O'Dwyer⁷⁴ as follows:-

(1) It occurs at low temperature - for many substances this means room temperature or lower.

(2) The breakdown field strength does not appear to depend on the electrode material, if the electrodes are metallic.

(3) To a certain extent, crystalline dielectrics show preferential directions for the formation of the discharge path.

(4) The breakdown field strength is not a function of the voltage wave form from DC to a single-shot impulse with microsecond rise time, or greater; it is therefore inferred that the breakdown process occurs in a time of order of microseconds or less.

(5) The breakdown field strength depends on the thickness of the dielectric; for thick samples the breakdown strength is an extremely slowly-varying function of thickness; for thin samples the variation is more rapid.

1.9 Aim of the experimental work

Amorphous materials are of current topical interest at this time and one class of such materials consists of thin layers of mixed oxides which possess a glassy structure. Glassy mixtures of silicon oxide and boric oxide have long been known to have good electrical characteristics, an example of this mixture being Pyrex glass. An amorphous mixture of the two oxides has been prepared by Wright ⁷⁷ who observed good mixing quality and uniformity of the non-crystalline structure using transmission electron microscopy. There are few reports on the properties of this mixture, in film form, but existing evidence suggested that enhanced oxygen absorption is present when co-evaporating this mixture and that this leads to improved dielectric properties. Timson ⁷⁸ has reported that increased oxidation may have led to considerable reduction in the unsatisfied bond concentration, which is the main cause of high dielectric loss in silicon oxide.

In this thesis some electrical conduction properties of thin co-evaporated films of SiO_x (70%) - B_2O_3 (30%) are studied. M - $\text{SiO}_x/\text{B}_2\text{O}_3$ - M structures were investigated in detail, using Al, Ag, Cu and Au electrodes in order to understand the effects of electrode material on forming. Devices with Al electrodes show little electroforming since it takes place with difficulty and needs an extremely long time to be formed in comparison with other noble electrode materials.

The electroforming process is also studied by using triode systems and experimental observations on potential distribution measurement led us to recognition of a certain forming direction

within the formed insulator. Different circuit arrangements in triode systems also revealed a number of interesting results, especially the effect of application of bias voltage at the grid on the potential distribution in the insulator layer and on levels of circulating and emission currents.

The proportion of 30% B_2O_3 and 70% SiO_x was found after a number of different percentages in the preparation were used. This percentage was found quite suitable for electrical measurements since increasing the molar concentration of B_2O_3 more than 30% greatly increases the sensitivity of the mixture to atmosphere so that the film properties will be affected a great deal.

The topography of the devices was studied in a scanning electron microscope during the dynamic operation of the samples and was an attempt to achieve direct observation of electron emission from the surface of the top electrode and any physical change on this surface.

The high temperatures of some devices during the conduction, particularly when the maximum current flows through them, and which has already been measured ³⁷ was inferred by the topographical features of the surface observed during the dynamic operation of the devices in the S.E.M.

Electroforming of the samples and their subsequent operation as negative resistance and electron emitting devices led to characteristic disturbances of the top electrodes which were consistent with the idea of filamentary conduction processes.

Since the borosilicate films containing more than 50% B_2O_3 are highly effected by atmosphere, the isolation of some specimens from the ambient surroundings was achieved by a coating technique and the current-voltage characteristics could then be measured.

CHAPTER 2.

Device Preparation and Experimental Techniques

2.1. Preparation of Devices

2.1.1. The Evaporation System

Thin films of metals and insulators were produced by vacuum evaporation in a BALZERS BA 510, 19 inch coating unit.

The vacuum chamber was of stainless steel and of double-walled construction. This double wall facilitated the heating or cooling of the chamber by the passage of hot or cold water.

A large substrate heater controlled by a variac transformer was mounted in the top of the vacuum chamber. The pumping of this plant consisted of a DIFF 1500, 9 inch diffusion pump and a DUO 25 rotary pump. These two pumps together were capable of producing an ultimate chamber pressure of 10^{-6} torr and this could be improved to 10^{-7} torr when liquid nitrogen cooling was employed. The bell-jar could be raised by a hydraulic hoist. The interior of the chamber was visible during the evaporation through a reinforced pyrex glass window. The chamber and backing pressures were continuously monitored with Balzers Pirani and Penning gauges. The working arrangement inside the bell-jar of the system has been fully described by Wright⁷⁷. Facilities for ionic bombardment cleaning of substrates were available in the chamber. Using a source-to-substrate distance of 30 cm, a large area of substrate could be coated uniformly. The evaporating sources were screened from each other to avoid contamination. Power for the evaporating sources was drawn from an internal 2 kVA supply with secondary transformer windings delivering 4-32 V. For co-evaporation purposes an external supply was also used. The techniques of co-evaporation

have been previously described by Hogarth and Wright.⁷⁹

Quartz crystal thickness were used to measure the evaporation rate and total thicknesses of oxide or metal film and were located directly above each evaporating source. For their operation, the monitors depend on the change in frequency of vibration of a thin quartz crystal when its mass changes due to the deposition of a thin film on its surface.

Quartz is kept in vibration by application of an alternating voltage at the natural frequency of the crystal to stimulate the piezoelectric properties of the material. Their dependence on mass, however, means that monitors must be calibrated for different density materials if absolute thickness measurement is required. The crystals were shielded to minimise temperature-induced frequency drifts and were collimated so that each crystal detected material deposited only from its own evaporation source. The effect of temperature drift on the monitors was reduced further by allowing radiation effects from a hot source to stabilize before opening the shield and beginning the coating process. The movable shield was capable of being rotated from outside the vacuum system. A rotary substrate holder was employed which was capable of holding four 3" x 1" substrates at a time. Masks could be rotated below the substrates by an external rotary seal, and a maximum of four different layers could be deposited. An aluminium shield, located directly below the masks enabled the substrates to be isolated from the evaporant until the initial evaporating conditions had been established. A shutter was let into the bell-jar through one of the ports provided. This enabled part of the masks to be completely shut off during evaporation,

allowing samples of different electrode or insulator thickness to be deposited on a single substrate.

2.1.2. Deposition Procedures

Films were deposited on Corning 7059 borosilicate glass substrates. These substrates were used for all electrical specimens, as the low surface roughness and low alkali ion concentration in this glass were most suitable properties for work on small current measurements in thin films. The less expensive Chance microscope slides were used when depositing material for thickness measurements. The cleaning procedure for every substrate was as follows:

- a) Boil in a solution of Teepol in distilled water for 10 minutes,
- b) rinse in hot distilled water,
- c) remove final traces of grease and Teepol by immersing in warm isopropyl alcohol,
- d) air dry and dust with Selvyt cloth,
- e) mount in the substrate holder and blow off remaining dust particles by using a stream of compressed nitrogen,
- f) finally clean by ionic bombardment during the pump-down sequence.

On each substrate a maximum of nine devices (four devices in the case of the triode configuration) could be deposited. Figures 8 and 9 show the geometry of masks used for diode (M-I-M) and triode (M-I-M-I-M) systems respectively.

Evaporation sources were usually made in the form of boats from sheets of tantalum, molybdenum or tungsten, 0.004 inch thick.

The design and material used for boat fabrication depended on its working temperature. Figure 10-a shows some of the designs used for boric oxide and silicon oxide (molybdenum for boric oxide since for evaporation it requires higher temperature about 2000°C and a tantalum boat for SiO_x as this requires a lower temperature to be evaporated, about 1000°C) and for the Cu, Ag or Au electrodes (figure 10-b). Aluminium was always evaporated by hanging pieces of Al wire on a tungsten spiral (figure 10-c). When using three sources simultaneously, aluminium sheet shields placed in between sources prevented one source from coating another.

In the case of the M-I-M structure preparation, firstly a base electrode of thickness $300\text{-}500 \text{ \AA}$ was deposited on the clean substrate. This was followed by the insulating layer of $\text{SiO}_x/\text{B}_2\text{O}_3$ and finally deposition of the top electrode completed the structure. Figure 11-a shows a diagram of the device arrangement produced by using masks as shown in figure 8.

Preparation of triode systems (M-I-M-I-M) was as the following order:-

- a) deposition of the base electrode of thickness 500 \AA (B).
- b) deposition of the first dielectric layer (D_1),
- c) deposition of the grid of thickness 300 \AA , (G)
- d) deposition of the second dielectric layer (D_2)
- e) deposition of the top electrode of thickness 500 \AA , (T)

Figure 11-b shows a diagram of the triode arrangement produced by using masks as shown in figure 9.

The depositions were carried out at a pressure of 5×10^{-6} — 1×10^{-6} torr at a substrate temperature of $150 - 300^{\circ} \text{C}$. Films showed greater adhesion to the substrates when deposited at these temperatures, and the electrical behaviour was more stable.

Boric oxide has a lower vapour pressure than silicon monoxide and consequently requires a higher source temperature for evaporation, in the region of 2000°C . Even at this temperature, no boat/evaporant reaction appeared to take place and the evaporation rate was very stable. However, boric oxide was evaporated from a molybdenum source as shown in figure 10-a. The oxide contains large quantities of water (approximately 30% by weight) which had to be removed before evaporation of the material. The outgassing was found to be so violent and prolonged that at least 50% of the charge was lost during the initial stages. For this reason, the oxide before placing in the source was heated up to 700°C in an alumina crucible in air for 20 minutes. Outgassing was still necessary in vacuum but was found to be considerably less violent and lengthy.

The affinity of boric oxide for water presented other problems. On exposure to air the boric oxide film on the quartz crystal absorbed water vapour. This water vapour was subsequently driven off by radiation from the source. The result was a continuously decreasing reading on the film thickness meter. Therefore not only was it necessary to outgas the evaporant charge but also the quartz crystal film. Wright^{??} has found that by evaporating a fresh oxide film on the crystal the evolution of water vapour could be arrested.

However, for similar reasons, frequent cleaning of the chamber was necessary in order to achieve the required ultimate pressures.

$\text{SiO}_x/\text{B}_2\text{O}_3$ mixture films also show that great sensitivity to water vapour, particularly for concentrations of boric oxide more than 50% molar. Calculations of molar concentration were made, using thickness measurement and a density calculated from the response of quartz crystal thickness monitors, using the response for silicon oxide as a standard of mass/thickness. With a density of 2.2 gm cm^{-3} for silicon oxide, the boric oxide film density was found to be 1.85 gm cm^{-3} which is very close to that of bulk vitreous boric oxide. Crystalline boric oxide, however, has a considerably greater density of 2.46 gm.cm^{-3} which was strong evidence that the evaporated films were open-structured and probably non-crystalline as expected.

Standardised optimum evaporation rates were adhered to throughout. These were $7 \text{ \AA} \cdot \text{sec}^{-1}$ (Al), $5 \text{ \AA} \cdot \text{sec}^{-1}$ (Au), $10 \text{ \AA} \cdot \text{sec}^{-1}$ (Ag), $10 \text{ \AA} \cdot \text{sec}^{-1}$ (Cu), and $30 \text{ \AA} \cdot \text{sec}^{-1}$ ($\text{SiO}_x/\text{B}_2\text{O}_3$).

The deposition sequence proceeded in the following order :

- a) the interior of the evaporator chamber assembly was cleaned to reduce the risk of contamination of the evaporated films.
- b) the cleaned substrates and evaporating boats were loaded into the chamber, and aluminium shields to prevent soiling of the chamber by evaporants were inserted,
- c) the stability of the quartz crystal monitor was checked before starting the pumpdown sequence.

- d) when the chamber pressure had reached 0.5 torr the roughing valve was closed and the high vacuum valve opened so that the chamber was then pumped by the diffusion pump,
- e) the chamber needle valve control was adjusted to give a chamber pressure of 0.1 torr and the substrates were cleaned by ionic bombardment for a few minutes.
- f) the needle valve was then closed and the chamber pressure allowed to reach 10^{-5} torr.
- g) the substrate heater was turned on and the chamber temperature allowed to rise until the substrate temperature was approximately 200° C.
- h) the liquid nitrogen trap was filled to reduce the chamber pressure to less than 10^{-6} torr.

After these the deposition commenced.

The aluminium shield was positioned between the masks and boats while the currents through them were adjusted until uniform evaporation rates were attained. This was monitored using the calibrated quartz crystal monitors. The deposition was allowed to continue until the required thickness was reached, when the shutter was again used to close off the masks and the evaporation was curtailed. This procedure was repeated for the various layers of a device. In the case of devices with different layer thicknesses on a single substrate, an additional shutter which could be moved horizontally between the masks and the sources was used. This enabled sections of the masks to be shut off during deposition. Since the boric oxide source produced large amounts of heat, the substrate heater must be switched off and water-cooling system of the bell-jar must

be switched on to reduce the temperature, otherwise the high temperature of the bell-jar causes a rise in the pressure and disturbance of the evaporation rates. Controlling the evaporation rates in the co-evaporation case becomes more difficult due to the high temperature of the chamber, specially in the preparation of thicker films which require a longer deposition time. After deposition the whole system is allowed to cool before admitting air to the system. Since borosilicate films, as mentioned earlier, are very sensitive to atmospheric exposure, they must be removed as quickly as possible and put either in a vacuum test system for measurement or kept in an evacuated desiccator until required.

2.1.3. Thickness measurements

The thickness of films were monitored during evaporation using a conventional quartz crystal monitoring technique⁸⁰.

The frequency of the crystal, driven by an oscillator unit, varies with the thickness of the corresponding material deposited. Thickness could be determined once the frequency meter connected to the crystal had been accurately calibrated using either an interferometric technique or Talystep thickness measurements described below.

The deposition rate and change of frequency in the monitor crystal were read directly using SPEED 1 film thickness monitor Model 1.

The deposition rate is also proportional to rate of change of frequency.

Two methods, optical and mechanical were used to measure the film thickness:

a) Mechanical method

The Rank Taylor Hobson Talystep 1 measures the film thicknesses are measured by a diamond stylus which traverses the substrate.

Vertical movement of the stylus arm varies the inductance of a sensitive coil, which is electrically amplified and fed to a pen recorder which traces a greatly enlarged section of the film step. Film thickness could be obtained directly from the trace. Typical traces and a schematic diagram of the instrument are shown in figure 12 .

b) Optical method

Insulator thickness could be measured by an interferometric technique. Special specimens consisting only of an insulator layer and a partial covering of electrode material were used for this purpose. Fringes of equal distance were observed through a low-powered microscope illuminated with parallel monochromatic light of wavelength λ , when a semi-transparent aluminised substrate was placed in good contact with the film surface. This gives a sharply-defined fringe displacement at the oxide thickness step. By counting the number of fringes displaced (q), the film thickness (t) could be deduced by :

$$t = q \frac{\lambda}{2}$$

so that by measuring q to one fifth of a fringe, films one micron thick could be measured to an accuracy of 5%.

2.2. Electrical Measurements

2.2.1. The Vacuum Test System

Since forming and related characteristics of formed borosilicate devices only take place under vacuum conditions, all electrical measurements were performed in a subsidiary high vacuum system. A photograph of the test system is shown in figure 13. . Glass-to-metal seals in the top-plate of the test chamber allowed screened

leads for electrical connection and thermocouples to be introduced into the chamber. Leads were kept as short as practicable and were rigidly tied down and screened to reduce noise signals at low current levels measurement.

Substrates were mounted on a Perspex assembly fixed to the bottom of a copper cryostat. The substrates were in contact with the container so that in the case of liquid nitrogen measurement, they could have cooled down to the required temperature. A photograph of this part of the system is shown in figure 13. The devices were connected by means of spring contacts. A good contact also was ensured by lightly coating with silver paint. A thermocouple was attached to the top of some samples when temperature measurement data was required. For collecting emitted electrons from the top electrode, an aluminium anode was positioned 1 cm away and parallel to the surface of the films.

2.2.2. Electrical Circuits

The circulating and emission currents were measured by traditional methods. The basic requirement of the circuit was the DC Solartron stabilized power supply, and the Keithley power source 240A 1.2 kV, 10 mA for supplying an accelerating voltage. The emission current collected at the anode was measured with a Keithley 160 C electrometer, capable of detecting 10^{-13} A or less.

An acceleration potential of + 100 V related to the base electrode of the device was always applied. The emitted electrons collected by the anode circuit drained away to earth through the electrometer. A diagram of this circuit for diode examples is shown in figure 14-a. Figure 14-b shows the electrical circuit used for

potential measurement as well as emission and circulating current measurements in triode systems.

2.2.3. Electroforming

Diode and triode systems were formed at a pressure of about 10^{-6} torr in the test chamber. The Solartron stabilised DC power supply, capable of delivering voltage in steps of 0.1 V, was used. The voltage was increased in 1 V steps with an approximately 20 - 30 sec. delay between steps. Forming in devices carrying noble metal electrodes took place in a few seconds as soon as the forming voltage was reached.

Samples with Al electrodes required higher voltages and relatively longer time (15 min. to 2 hours) to be formed. After forming, devices were usually run for a few cycles before readings were taken. This allows forming to be established perfectly and results less noisy characteristics.

Forming in triode systems also simply takes place by application of bias voltage between base and top electrode in a similar way as described for diode systems. Since forming is established in these structures, forming of individual layers is not necessary.

2.2.4. Temperature measurements

When the maximum current is passed through the films with well-conducting metal electrodes then local temperatures of the sample can become very high. This has been demonstrated by mounting the specimen assembly on a slab of Perspex and when examined after use some localized melting or depolymerization of the Perspex, leaving a small cavity, has been found to have occurred. The temperature measurements of the active area during

operation were obtained by attaching a chromel-alumel thermocouple to the surface of the device with Araldite which is electrically a non-conducting adhesive. The results of this work have recently been reported by Hogarth and Taheri ³⁷.

Measurements of circulating and emission current at different ranges of temperature from liquid nitrogen temperature up to + 100^o C were achieved by design of a special system. The apparatus consisted of a copper box soldered to stainless steel tubes which were soldered to the top-plate of the vacuum test chamber. Copper and stainless steel were chosen for the parts of the system which required, respectively, a high a low thermal conductivity. Substrates were pressed firmly onto the flat base of the copper box by means of springs. Liquid nitrogen was introduced into the box from outside the vacuum system through the stainless steel tubes. A thermocouple attached to the substrate recorded the temperature. The readings were taken by a Comark electronic thermometer. Intermediate temperatures were obtained by using an electric heater inserted between the substrate and the base plate. The temperature could be varied by varying the voltage across the heater. A thermal equilibrium could be obtained between the heating and cooling processes. Higher temperatures were obtained by using the heater without the liquid nitrogen supply.

2.2.5. Topography of the devices in a S.E.M.

The sandwich structures of borosilicate films were electroformed in a scanning electron microscope (Cambridge Stereoscan 54) at a pressure of 10^{-5} torr. The local phenomena were observed at a point on the counter electrode surface before the maximum in the voltage-current characteristic and also beyond it. The main observations made were of local

apparent hot spots. The results were obtained for specimens having copper or silver counter electrode. During the forming process a number of spots ranging in the diameter from 7 to 15×10^{-4} cm were formed. The results and photographs of the counter electrode at different stages of the device conduction recently have been reported by Taheri and Hogarth³⁹.

CHAPTER 3.

M-I-M Systems

3.1. DC Stability and Characteristics of M-SiO_x/B₂O₃-M Structures3.1.1. Variation of I_c and I_e with bias voltage

At the time this work began there were only a few reports about borosilicate sandwich structures in the literature, notably by Hogarth and Wright^{77,79} who have given co-evaporation data of mixture films and by Timson and Hogarth⁸¹ who have reported some electrical properties of unformed Al-SiO_x/B₂O₃-Al structures.

Early studies, however, started by examining different compositions of B₂O₃ in SiO_x and it was found (practically) that 30% B₂O₃ in SiO_x gives a good dielectric stability in borosilicate films. Wright⁷⁷ on the calculation of values of dielectric strength proportional to film density for the composition of 30% B₂O₃ and 70% SiO_x, has noticed a similar mechanism to that found for glasses when "modifier" oxides were added.

Timson and Hogarth⁸¹ have shown that films of thickness $1-2 \times 10^{-4}$ cm with Al electrodes give a DC current-voltage relationship of the form $I_c \propto V_b^n$ where n was of the order of 4 - 6. The AC conductance σ_{ac} at frequency f was of the form $\sigma_{ac} \propto f^n$ where n varied between 0.9 and 1.0. They have also reported the results of electron-spin resonance measurements which show that one effect of admixture of B₂O₃ to SiO_x is to reduce the density of the dangling bonds.

In this work the early devices utilised Al electrodes. Such films of 3000 - 6000 Å thick showed electroforming and a region of differential negative resistance in the current-voltage characteristic³⁴. Films 6000 Å thick showed a slight negative resistance region having typically three peaks close together. The interesting point of these structures was their dielectric stability at high voltages: sometimes up to 500 - 600 volts, without occurrence of breakdown. The forming process with Al electrodes was lengthy and difficult in comparison with films carrying electrodes such as Ag or Au.

However, further studies on the borosilicate sandwiches were continued and improved forming was achieved. The formed devices show that typically higher currents were passed for a given voltage than with the thicker films of Timson and Hogarth⁸¹, although the resistivity was high (10^{15} - 10^{16} ohm-cm) and the current tended to decrease above a certain voltage level.

The observation of voltage-controlled negative resistance (VCNR) and the possibility of electron emission into vacuum, and also other properties of formed devices was considered worthy of investigation. Al electrodes were used in spite of early work which had suggested that forming with Al electrodes would not occur, on the contrary, the more recent work of Pivot et al⁸² and Doucas and Walsh²⁵ has shown that Al electrodes are not necessarily a barrier to forming.

The forming voltage, V_F , in these films was somewhat variable between samples but was usually in the range of 20-30 V. When forming was completed the bias voltage was reduced to zero and then reapplied to give the formed characteristic.

Figures 15 and 16 show the typical current-voltage characteristics of respectively 3000 Å and 6000 Å thick borosilicate films with Al electrodes as were reported in early studies of these structures³⁴.

In order to study the electron emission from Al-SiO_x/B₂O₃-Al structures, films of thickness approximately 3000 Å were used. At voltages of 30 V at which the negative resistance occurs, electron emission into a vacuum increases very rapidly with bias voltage. The emission current density is of order $10^{-5} \text{ A cm}^{-2}$ and since the circulating current through the sandwich is lower than in similar films of SiO_x, the transmission efficiency is high. The devices showed remarkable dielectric properties and some samples could withstand voltages up to 400 V. Figure 17 shows a typical characteristic of circulating current I_c against bias voltage V_b . A peak current is exhibited at 30 V followed by a differential negative resistance region. Above the maximum value the general level of current falls although there are sometimes small increases in current at voltages greater than the voltage for current maximum. Figure 18 shows the variation of the emission current I_e with bias voltage, V_b . This is apparent at quite low voltages and rises very steeply at about 10 V to a maximum which occurs at the same value of voltage as the maximum in I_c . I_e then slowly decreases until at some voltage usually about 100 V the emission current falls very steeply and sometimes disappears altogether. Subsequent retracing of the characteristic shows the same general form and current levels of the same order, thus

indicating that normal dielectric breakdown has not begun to destroy the samples. Figure 19 shows the variation of transmission ratio ($\alpha = I_e/I_c$) with V_b . The maximum value of α is 10^{-3} which is comparable with that for other thin film cold cathodes. The large rises and falls of current at applied voltages of order 10 V and 100 V respectively, correspond to similar changes in emission current.

In the following the current-voltage characteristics with film thickness have been investigated more thoroughly and have extended the composition range, over which borosilicate specimens may be prepared and measured by a technique involving partial encapsulation in silicon dioxide. This prevents the absorption of water vapour by complexes containing more than 40-50% B_2O_3 and also enables certain novel results to be obtained concerning power dissipation at the turnover voltage.

Metal films of aluminium, silver, gold and copper were deposited as electrodes of thicknesses $3 - 5 \times 10^{-6}$ cm. The active area of the M-I-M devices investigated was 6 mm^2 . Clearly currents for a given voltage will be higher in thinner films and, as has been shown previously, the results are quite complex. In an attempt to establish a more definite variation of voltage-current characteristics with thickness, specimens made, in the form indicated in Figure 20.-a, were prepared by moving the shutter by a definite amount in successive steps during the evaporation process.

Eight specimens of notionally the same controlled composition but of well-defined and different thicknesses could be made on one Corning substrate, the specimen being prepared

under the same pressure, temperature, deposition rate ($30 \text{ \AA}/\text{Sec}$) and with the same electrode type. This procedure was superior to earlier experiments using a wedge-shaped layer carrying several electrodes, defining specimens of only an "average" thickness.

The peak voltage (V_p) with Ag, Au and Cu electrodes is much lower and current levels are higher than for samples with Al electrodes. Current-Voltage characteristics are shown in figure 21 for borosilicate films with Al, Ag and Cu electrodes. All show a voltage-controlled negative resistance. Figure 22 shows voltage-current characteristics for a range of electroformed specimens of different thickness and made in steps on one substrate as described above. The electrode thicknesses were constant. It may be noted that current levels increase symmetrically with decreasing thickness and that the peak voltage (V_p) increases slightly with increasing dielectric thickness.

The isolation of some specimens from the ambient surroundings was achieved³⁷ using the structure shown in figure 20-b. With this system borosilicate specimens containing more than 50% B_2O_3 could be prepared and kept for subsequent measurement. The covered films described above and coated with a 2 - 3 μm layer of silicon dioxide were investigated and the voltage-current characteristics of one such film is shown in figure 23 and contrasted with a similar but uncoated film. It may be observed that the characteristics of coated and uncoated samples are generally of the same form but that the peak voltage has increased and the peak current has decreased for

the covered films.

Electron emission into a vacuum is very low (about 10^{-13} A) for voltages well below the peak but increases rapidly at just below this value as the applied voltage is increased. The emission current density is lower for samples with Al electrodes (about 10^{-5} Acm⁻²) than for samples with Ag or Cu electrodes and with the same thicknesses (about 10^{-4} Acm⁻² or higher).

Figures 24 and 25 show the variation of emission current with bias voltage from a Al-SiO_x/B₂O₃-Al film and from similar films carrying Ag and Cu electrodes. The emission current is a maximum at approximately the same applied voltage as that for which the circulating current is a maximum and then decreases fairly slowly until, at a somewhat higher applied voltage (100 - 150 V), it decreases rapidly. Retracing of the characteristic showed that this rapid decrease was not a consequence of an avalanche type of dielectric breakdown and was generally reversible. The electron emission also depends on the dielectric materials and top electrode thickness due to attenuation of electrons in these regions. Measurement of the attenuation lengths of hot electrons in borosilicate films has shown that these can exceed 2×10^{-5} cm in the SiO_x/B₂O₃ complex and thus are longer than the values reported for SiO_x⁸³.

Since there are fewer trapping centres in the form of dangling bonds in SiO_x/B₂O₃ than in SiO_x, this result is not unexpected⁸⁴.

Figure 26 shows the way in which the emission current, plotted as a function of applied voltage, varies with thickness of the oxide complex.

The emission current shown in Figure 27 is, as would

be expected, very low for the samples covered with silicon dioxide in comparison with that for similar but uncovered films.

When the maximum current is passed through the films with well-conducting metal electrodes the local temperatures can become very high. This has been demonstrated by mounting the specimen assembly on a slab of perspex and when examined after use some localised melting or depolymerization of the perspex, leaving a small cavity, has been found to have occurred.

3.1.2. Variation of device temperature with bias voltage during operation

In order to test whether any appreciable quantity of heat was dissipated in the device especially at very high voltage levels a thermocouple was attached to some devices and the device temperature (I_c) monitored. Typical results are shown in figures 28 and 29 respectively for Al-SiO_x/B₂O₃-Al and Cu-SiO_x/B₂O₃-Cu samples. The temperature was allowed to stabilise after each increase in voltage, so that a steady-state condition was achieved. The variation of I_c with V_b is also shown for comparison. The I_c - V_b curve, in general, follows the I_c - V_b curve and the maximum temperature occurs when the current flow is highest. At high voltages the temperature relaxes to the ambient temperature and no significant heat dissipation is detectable.

As expected the temperature increased as I_c increased but this is merely a consequence of Joule heat dissipation within the device. It can also be seen that the device temperature is dependent on the circulating current. Since current levels in films carrying Cu, Ag or Au electrodes are higher than films

having Al electrodes, temperature levels may be as high as 300°C or higher (Figure 29). In the negative resistance region as I_c starts to decrease, the device temperature falls drastically.

3.1.3. Time dependence of the electroforming process

The electroforming process of devices with Al electrodes is very slow and rather difficult so that sometimes forming does not always occur. However, the phenomena have been reported for the $\text{Al-SiO}_x/\text{B}_2\text{O}_3\text{-Al}$ system³⁵ where the insulator film thickness is of order $3 - 6 \times 10^{-5}\text{cm}$. The voltage required for electroforming (20 - 40 V) and the peak voltage (30 - 200 V) are much higher than for samples with gold, silver or copper electrodes. The resistivity of the unformed devices is high (of order $10^{15} - 10^{16}$ ohm cm) and thus current levels are low, but in formed films currents are much higher (for the same voltage applied) than in unformed devices.

As has been mentioned above, the forming process for Al electrodes is quite slow and may last from 5 minutes to 2 hours depending on the applied voltage, dielectric thickness and temperature. For the high-conductivity electrodes such as Cu, Ag or Au, forming takes place much more quickly, in typically between 1 to 30 seconds. Figure 30 shows the increase with time of current at a given voltage in an unformed $\text{Al-SiO}_x/\text{B}_2\text{O}_3\text{-Al}$ and this may be contrasted with the data for an unformed $\text{Ag-SiO}_x/\text{B}_2\text{O}_3\text{-Ag}$ film shown in figure 31.

3.1.4. Breakdown

Unformed samples show a uniform surface region. Observation of the top electrode after subjecting devices to various diffe-

rent voltage levels, indicates the destructive processes occurring in such devices. The general pattern of the formed films is quite similar, although breakdown holes and peeling of the top electrode are also sometimes observed. This is because forming is a continuous process which finally leads to a breakdown.

After forming some samples were cycled at voltages up to V_p (peak voltage) and were subsequently run at that voltage for a few minutes. Observations of such samples under the microscope revealed some areas of the active part of the device which had escaped damage, while other regions showed many areas of localised wrinkling. The existence of such regions is probably due to non-uniform heating of certain areas of the device, due to the high current passed at peak voltage which could lead to non-uniform expansion of the top electrode. The evolution of oxygen may also contribute to the appearance of such areas⁵⁸. As the maximum voltage level is increased the density of such breakdown regions and large areas of the top electrode are destroyed.

Current densities around the breakdown areas are likely to be higher than the average, due to localised melting of the top electrode and the destruction of part of the insulator, and thus the temperature in these areas is higher than that in the bulk of the devices. The burn-out process, which is accompanied by an increase in temperature finally destroys the active area of the sample. However, observation of breakdown areas shows many interesting features which will be discussed more fully in Chapter 5, where observation has carefully been

carried out by using a scanning electron microscope.

3.2. The high field region

3.2.1. Breakdown voltage and its dependence on insulator thickness and on electrode material

Since borosilicate films from the dielectric strength point of view are very strong in comparison with the other oxides or mixed oxides, thus the breakdown voltage, V_{β} of these films is very high.

In thicker films, however, breakdown occurs at higher voltages which is due to the low current density in these films. In order to investigate the dependence of V_{β} on insulator thickness, a series of sets of devices was fabricated with insulator thicknesses varying from 3000 to 12,000 Å. Figures 32 and 33 show the variation of V_{β} with insulator thickness t of Al-SiO_x/B₂O₃-Al and Ag-SiO_x/B₂O₃-Ag films respectively. Since current levels in films with noble electrode metals are much higher (see figure 215)) than the films carrying Al electrodes, breakdown voltage occurs at lower voltages than devices with Al electrodes. Note that in figures 32 and 33 the points are average values of V_{β} on a particular substrate and the extent of error bars indicate the spread of the values on the substrate.

It is apparent that within experimental error the value of V_{β} remains constant over the entire insulator thickness range. The average field when the first burn-out occurs varies between 5×10^6 Vcm⁻¹ to 5×10^5 V cm⁻¹ for samples with Al electrodes and between 10^6 V cm⁻¹ to 5×10^6 V cm⁻¹ for samples with Ag

electrodes.

In unformed materials the breakdown field normally decreases with insulator thickness and generally a relation of the type $F_B \propto d^{-\gamma}$ is obtained^{58,75}. F_B is the average field across the dielectric layer and the value of γ varies between 0.30 and 0.65. However, it is clear that there is no correlation between this type of relation and the above results unless we assume $\gamma = 1$ although the justification for such assumption is slim in view of the following. Firstly the thickness range over which such theories are normally applied is much greater than the thickness range of the films which were used. Secondly, the temperature variation of breakdown voltage is more in accordance with thermal breakdown characteristics than with electric breakdown as predicted by Forlani and Minnaja⁷⁵. Thirdly the assumption that the field is uniform within the formed insulator materials is unlikely. The experimental results of Hickmott¹³ suggest that most of the applied voltage is dropped over a high-field region. Similar results were obtained in the study of potential distribution in triode systems which are described more fully in Chapter 4. Furthermore both the theories of Hickmott¹³ and Barriac et al²³ predict the existence of a high field region within the insulator. In the latter case this saturates to a constant thickness at a voltage less than V_p .

An explanation of the experimental results may be given which is the assumption of a high field region within the insulator. The assumption appears to be more applicable to formed materials than a theory which does not take into account

the existence of the high field region. Assuming that the high field region is the region where breakdown is initiated, variation of V_{β} with different insulators can be explained.

The voltage distribution is such that an intrinsic burnout field (F_{β}) varies with the thickness of the high field (δ) region in some way analogous to that predicted by the Forlani-Minnaja theory, although Hickmott¹³ obtained a constant value of 120 Å for δ in SiO_x and Al_2O_3 films.

On forming, a high field region is set up at some region in the insulator. The thickness of this region (δ) probably remains roughly constant with voltage. Both self-heating and maximum-voltage breakdown processes are initiated in the high field region. Self-heating breakdowns will penetrate completely through the remaining insulator in the lower field across the high field region reaches a particular value F_{β} ; the burnout voltage V_{β} will then be given by $V_{\beta} = F_{\beta} \delta$. Destruction of that region is not probably due to thermal runaway. Complete device destruction does not occur since the low-field region may well escape relatively undamaged, although in some samples, complete destruction was observed.

The breakdown voltage also strongly depends on electrode material particularly when electrodes are Al. Films with Al electrodes withstand up to 500 - 700 V without breakdown occurring. This is due to the comparatively low current density in these devices.

3.2.2. Low temperature characteristics

Low-temperature characteristics of some oxide films have been reported by a number of authors^{85,17,86,87}. Similar effects

have also been observed, in borosilicate films. The results obtained are generally in good agreement with the results of Hickmott¹⁷.

The value of I_c at a given applied voltage falls as the temperature of the device is decreased. The negative resistance region persists until the temperature falls below a certain critical value.

The low-impedance negative resistance could not be obtained except by increasing the temperature above the critical value.

The critical value varied somewhat between samples but was usually in the range 160 - 200 K.

A set of I-V characteristics of a formed sample carrying Ag electrodes is shown in figure 34. The thickness of insulator ($\text{SiO}_x/\text{B}_2\text{O}_3$) is 6000 Å. It can be seen that the height of the peak current decreases with decreasing temperature. At temperatures lower than 160 K the region of negative resistance completely disappears.

The formed samples exhibit a voltage-temperature memory effect, i.e. after any change in the temperature the circulating current follows the original I-V characteristic during the first cycle until a certain voltage. Only after this voltage is exceeded, the conduction of the device changes and transition to another I-V characteristic, corresponding to the new temperature, occurs. The critical values of the voltage varies with electrode material, however, for samples with Ag electrodes the values are in the range of about 1.7 to 2.2 V for decreasing and increasing temperatures respectively.

This memory effect enables VCNR to be observed during the first cycle even at liquid nitrogen temperatures.

In further cycles the current becomes a monotonic function of the increasing voltage. After reheating the sample to 295 K. and applying a voltage greater than 2.2V, the original room temperature characteristic is restored. Thus if the voltage during the measurements does not exceed the value of the critical voltage (1.7V), the conductivity of the formed device is practically independent of changes in temperature.

3.3 Discussion of Results

The use of co-evaporated borosilicate glass in a metal insulator-metal (MIM) structure has shown some new results. It was found possible to form the devices electrically even though aluminium electrodes were employed and the circulating currents through the devices were quite low (a few mA) and certainly not so high as for the simple oxide devices previously reported. This result is consistent with the improved dielectric properties of these co-evaporated complexes as previously reported (78). The maximum value of transmission efficiency observed, $\alpha = 10^{-5}$, was on films 3×10^{-5} cm thick with Al electrodes of thickness about 5×10^{-6} cm. This value is comparable with the maximum estimated for SiO_x films of thickness 8×10^{-6} cm and assuming a top electrode having zero thickness and thus zero attenuation. We may expect to obtain even higher transmission ratios on thinner films and with a thinner top electrode.

The very high dielectric strength of the mixture allows high voltages to be applied across the insulator without breakdown occurring. Although current levels with Al electrodes are low, the

high applied voltage means that considerable power is being dissipated in the device. For example a value of $V_b = 300V$ and a circulating current of 0.33 mA corresponds to a power dissipated of order $0.1W$. Although this is of the same order as power dissipated in the simple oxide devices, the lower circulating currents would be expected to give more stable operation.

In $\text{Al-SiO}_x/\text{B}_2\text{O}_3\text{-Al}$ devices the general circulating current I_c against voltage bias V_b curve was of the form $I \propto V^n$, where n varies between 4 and 6 and is directly comparable with the earlier results of Hogarth and Taheri³⁴ for 3000 to 6000 Å films.

On increasing the bias above the forming voltage V_F , a substantial increase in I_c was observed. Typical increases were from 10^{-5} to 10^{-3} A. Current levels were substantially higher thereafter even at voltages below V_F and electron emission into a vacuum could now be detected. The films are amorphous in character but contain a smaller concentration of unpaired electrons on dangling bonds than films of SiO evaporated at similar rate. The negative resistance has been explained in terms of the polyfilamentary model of Dearnaley et al¹⁴ and which has been developed further by Ralph and Woodcock⁶⁶ and by Sutherland²⁷. The observation of VCNR in the voltage-current characteristic of a M-I-M diode was ascribed to the formation of field-assisted formed filaments which rupture when the current levels through them lead to high local power dissipation, so that the current then falls with increasing voltage.

The results on the rate of forming are primarily of practical interest in that not only are the emission currents obtainable from samples with high conductivity electrodes, higher than those for samples with aluminium electrodes, but they are also formed more

rapidly.

From a study of the curves of circulating current as a function of applied bias voltage, the power dissipated at the peak has been calculated and the pattern of behaviour indentified. For the three curves in figure 21 the peak powers were calculated as 0.30 W and 0.28W for the silver and copper electrodes respectively and only 0.035W for the aluminium electrodes. This suggests that the diffusion of aluminium only leads to the formation of thin filamentary paths which pass lower excess currents and thus are only capable of dissipating smaller amounts of energy before the voltage, at which they are ruptured, is applied. The diffusion of copper or silver is more favourable, higher currents are passed and a higher power can be dissipated before rupture of the filaments. When the data given in figure 22 are analysed in a similar manner the power dissipated at the peak voltage for given thickness values are given below.

Thickness (A.U.)	Peak Power (m W)
3000	26
5000	23
7000	18
10000	14
12000	10
15000	6.4

It may be observed that the higher power dissipation at the peak voltage is observed for the thinner films and that as a consequence more energy is available for communication to the free electrons.

Consequently a higher electron emission for a given bias voltage would be expected. It is clear from figure 25 that this is indeed the case. Thus in designing cold cathodes based on M-I-M structures and in which the insulator has an amorphous character and is consequently less liable to "pinhole" type of imperfections, improvements in performance may be achieved by using very thin layers, consistent with sufficient thickness to enable a coherent film to be deposited and to avoid simple destructive breakdown and tunnelling effects.

In studying the properties of M-I-M structures containing more than 50% of B_2O_3 in the SiO_2/B_2O_3 , it is of interest (a) that the structure protectively coated with silica can show comparable current-voltage characteristics to those of sandwiches using other compositions (figure 23) and (b) that the power dissipated at the peak voltage for two similar specimens, one covered with and one without silica coating, is the same, being about 26-30 mW for the sample used in figure 23.

Although the previous measurements of the temperature of the devices, during operation as electron emitters, have indicated fairly small rises³⁵, the results in figure 29 make it clear that with well-conducting metal electrodes the measured temperature of the device may rise to 300°C or so and the localized high temperatures may be sufficient to form small "pools" in the perspex. Nevertheless the cathodes are operating well below the temperature of conventional thermionic cathodes and, for applied voltages, at least two orders of magnitude below those needed for external field-emission devices.

CHAPTER 4

M-I-M-I-M Systems

Thin film metal-insulator-metal structures (MIM) have been investigated for more than ten years and have shown promise as voltage-controlled negative resistance (VCNR) media as well as cold electron emitters requiring only a few volts to excite them. In the further study of these structures, for example to determine the potential distribution across the insulating layers, triode systems of the form M-I-M-I-M are very suitable and work has already been reported by Hickmott¹³ on Al_2O_3 , Abidi and Hogarth⁶⁴ on BaO/SiO_x and by Gould and Hogarth⁸⁸ on SiO_x .

By using different circuits and by controlling the grid voltage, as well as by studying the actual borosilicate films, circulating and emission currents may be controlled. The observed current gain will depend on the precise circuit used and on the grid bias voltage. Voltage-controlled negative resistance (VCNR) and electron emission from the triode structures are also observed and some properties are similar to those of the diodes but some are characteristic only of triode structures.

A co-evaporation technique for depositing mixed oxide layers of controlled composition was used to prepare $\text{SiO}_x/\text{B}_2\text{O}_3$ (70% SiO_x and 30% B_2O_3). The dielectric thicknesses between grid and base electrode (D_1) and grid and electrode (D_2) were in the range of 3000-7000 Å; the metal layers of order 500Å, Al, Ag and Cu being used. Figure 35 shows a typical triode structure together with the symbols which will be used. The active area of the specimens used was 6 mm².

4.1 Forming Direction and Potential Distribution

Hickmott¹³ has reported measurements on triode structures using

Al_2O_3 as the insulator and has shown that the development of voltage-controlled negative resistance (VCNR) is accompanied by the establishment of a high-field region typically 120\AA thick near the negative electrode, which in Hickmott's experiments was usually of aluminium and formed the base electrode. In other similar works on triode systems, generally devices were formed with the base electrode negative as a usual procedure. If a certain direction is taken into account for forming then it can be seen that in most of the earlier works the forming process in triodes has a similar direction. Consequently, however, potential distribution measurements in previous reports show similar results, i.e. applied bias voltage between top and base electrodes drops between grid and negative electrode.

In this work the expression "Forming Direction" (FD) will be used to indicate the polarity of applied voltage producing the electroforming, a positive FD implying that the triode was formed with the base electrode negative and the top electrode positive, and vice versa.

Hickmott has observed that in some formed triodes, the potential distribution shifts when the polarity distribution depends on the direction ($-FD$), with the top electrode negative, show a high-field region between the grid and top electrode even if the polarity used for subsequent measurements is reversed. The high-resistance region (D_2) in this case will remain unchanged unless a large forming voltage of opposite sign is applied. In other words, so long as the forming direction has not been changed the potential distribution remains unchanged and the applied potential, independent of the polarity of the top electrode, drops between the grid and top electrode, i.e. in the forming direction. If now the reverse bias is exceeded by typically 3-5 V more than was needed to cause the initial

electroforming to take place, the potential drop shifts from one region to another, e.g. from D_2 to D_1 . In other words the high-resistance region (D_1) switches with low-resistance region (D_2) and consequently the potential is distributed in the opposite direction obtained with the previous direction of forming.

The following procedure was adopted to follow the electroforming on horosilicate triode systems and it reveals clearly the dependence of potential distribution on the direction of forming. On each substrate four triodes were deposited and alternate triodes were formed in the positive and negative forming directions. On studying the dependence of the potential distribution on the forming direction two cases are of particular interest.

(i) A triode is formed in +FD and the potential distribution is measured for different directions of applied voltage, lower than the initial forming voltage. Figure 36 shows the forming (+FD) circuit and also the form of potential distribution measured.

(ii) Triodes which were formed in -FD were biased by the application of a reverse potential. In this case for an applied voltage up to the initial forming voltage, the applied potential drops between the grid and positive electrode, i.e. in the direction of forming. Then if the reverse bias is exceeded by a few volts more than the original forming voltage, the potential drop shifts rapidly between the two distinct regions D_1 and D_2 as a result of a change in the direction of forming. Figure 37 shows the circuit used and the results in schematic form. It can be seen that the potential drop is shifted from one region to the another by changing the forming direction. Figures 38-a and 38-b show the variation of V_{GT} (voltage

between the grid and top electrode) and V_{GB} (voltage between the grid and base electrode) with forward and reverse bias voltages for the conditions shown in figure 37 .

The above results show that the initial forming process leads to a very stable structure unless somewhat higher voltages are applied to the device in the opposite direction, when the high resistance region can change to the low-resistance region and vice versa. Thus to a certain degree the resistance values of regions D_1 and D_2 are controllable.

Figure 39 shows how different stages of potential shifting between the two regions may be achieved by increasing the forming voltage and by changing the direction of its application. Shifting of the high-field region (between two regions D_1 and D_2) is limited by the dielectric breakdown strength of the devices and by the particular electrode materials used.

The form of the potential distribution in the low-resistance region of triode systems shows a similar variation with applied voltage as does the usual current-voltage characteristic of a formed triode. Figure 40 shows the variation of both circulating current (I_C) and of measured V_{GT}^+ (top electrode positive with respect to the grid) with bias voltage for an Ag-I₁-Ag-I₂-Ag triode, where I₁ and I₂ are borosilicate films. From this figure it may be noted that despite the reduction of circulating current with increasing bias voltage in the negative resistance region the conductance of the low resistance region D_2 has increased. When the bias voltage is about 8 volts most of the potential applied at the top electrode appears at the grid and the very high conductance of the top insulator region seems to be a feature of triode systems.

The analysis of this high-conductance region was made by using the circuit shown in figure 41-a. An electrometer in the grid - positive electrode circuit shows high circulating currents even for the small potential difference between these two electrodes (top and grid). These current levels are quite remarkably large in comparison with the circulating currents flowing across the whole device or between grid and top electrode if the potential is applied directly between the grid to top electrodes (see figure 41-b). Figure 41-a shows the circulating currents in the whole triode and also from grid to top electrode when the potential is applied only between the base and top electrodes. When the circulating current between the grid and top electrode is at its peak, a voltmeter in this loop indicates only one volt p.d between the grid and top electrode. In other words, a higher current flows than can be caused to flow by application of the same voltage directly between grid and top electrode. Figure 41-b shows the variation of circulating current from grid to top electrode with bias voltage applied directly between grid and top electrode, the normal diode connection. The triode has silver electrodes and $D_1 = D_2 = 5000\text{\AA}$.

Potential distribution measurements show that only a fraction of a volt of the applied bias falls in the high-resistance region as shown in figure 40. The peak current shown in figure 41-b for the grid-positive (top) electrode circuit is 130mA for a potential difference of 1 volt. In the circuit shown in figure 41-b the circulating current is only 2mA for an applied potential of 1 volt. Thus an effective current gain is seemingly observed by using the circuit of figure 41-a.

The resistance of region D_2 in figure 41-a is much lower than

that of D_2 in figure 41-b for the same voltage. This difference must arise because the grid in figure 41-b is still biased positively with respect to the base electrode. The high-field region is D_1 in this configuration and thus we shall produce a flux of hot electrons which pass through the grid (only 500 \AA thick) and add to the measured current I_3 . The additional electron current flowing upward through the grid which reduces the resistance of region D_2 will also lead to a reduction in the voltage at which the peak current occurs, since we are dealing with an essentially lower-impedance system.

It is of interest to note that, if the potential is applied between the grid and base electrodes, a voltmeter between the grid and top electrode only shows some 10 m V , arising from the electrons emitted via the grid into region D_2 and finally reaching the top electrode which, in this case, finally becomes negative with respect to the grid.

Figure 42 shows the variation of circulating current between the grid and base electrodes and the voltage ($V_{G^+ T^-}$) between the grid and top electrodes, with the bias voltage applied between grid and base electrode. The two curves are of similar form.

In the course of the measurements of potential distribution in triodes made with silver electrodes, a variation of grid polarity with respect to the electrodes was sometimes observed and a fixed bias current seems to be added to the normal current variation, as shown in figure 43.

4.2 Potential Distribution and its variation
with grid voltage in the two insulator
regions (D_1 and D_2)

Potential distribution measurements on triode systems show that applied potential between the base and top electrodes mainly drop between the grid and either the base or top electrode depending on the direction of forming (FD). By biasing the grid positively, the form of potential distribution between two distinct regions may be changed.

In the present experiments the grid voltage, V_g varied from zero to 3 V. Figures 44, 45, 46 and 47 show the variation of circulating current and the voltages V_{GB} and V_{BT} with bias voltages as the grid voltage varies. Figure 45 shows that an applied voltage of +1 V at the grid shifts the potential drop from region D_1 to region D_2 but figure 44 shows that the resistance of the region D_1 in figure 45 is still higher than the resistance of region D_2 in figure 44.

In figure 46 we see than when $V_g = +2$ V the potential distribution across the two regions assumes a different form. There is no peak voltage for V_{GT} and it simply increases slowly until at an applied voltage of about 17 volts it increases sharply at the same bias voltage value as that at which V_{GB} falls. Thus the two insulator regions seem to have switched positions.

In figure 47 (as for figure 46) the switching of potential drop between the two regions seems to occur when the bias voltage is increased to 27V. In this case aluminium was used as the top electrode since this metal needs a high forming voltage and thus gives rise, at least initially, to lower circulating currents. Thus higher voltages (up to 30V) may be applied without reaching breakdown conditions.

From figures 45, 46 and 47 it can be seen that there is a circulating current in the whole device for different values of V_g even though there is no bias voltage applied between the base and top electrodes. The current arises from the electrons emitted from the grid into region D_2 and which finally reach the top electrode and close the loop. The current varies with grid voltage from 1.5mA to 8mA. A positive grid voltage does not change the voltage at which the peak of the circulating current occurs (8V).

4.2.1. Effect of a Negatively-biased Grid

In general in triode systems, the pronounced effect of a negative grid bias voltage is to increase the circulating current and to decrease the voltage for a peak circulating current of the base-top electrode circuit.

Figure 48 shows the circuit used and the variation of circulating with bias voltage when the voltage on the grid varies from zero to -3V and it may be seen that the peak current increases from 50 mA to 65 mA for $V_g = 2V$. The voltages for peak current decreases so that for $V_g = -3V$ it is zero. Clearly the circulating current and peak voltage are controlled by controlling the negative voltage applied to the grid which amplifies the circulating current. For this experiment Ag- I_1 -Ag- I_2 -Cu triodes were used, region D_1 being about twice the thickness

of region D_2 ($D_1=5000 \text{ \AA}$, $D_2=2500 \text{ \AA}$).

4.3 General Circuit Arrangement in Triode Systems

A generalised circuit arrangement for triode systems was used in order to measure the variation of circulating current in either of the distinct regions (D_1) and (D_2) or the whole triode (D_1+D_2) with bias voltage, applied between corresponding electrodes.

The effects of applying negative and positive voltages to the grid with respect to the polarity of base electrode were studied.

In this part of the work all possible circuit arrangements have been considered. Figure 49 shows the general circuit arrangement (case a) in which the grid is biased positively with respect to the base electrode. E_1 , E_2 and E_3 refer to power supplies in circuits 1, 2 and 3. K_1 , K_2 and K_3 are keys which were used when one or two of the power supplies were required to be disconnected. Figures 50-1 to 50-8d are produced by using different parts of the general circuit as shown in figure 49. The grid voltage (E_2) is positive with respect to the base electrode. The significance of each circuit arrangement and its characteristic curve will be described separately to avoid any confusion.

Table I shows the situation of power supplies and keys in each circuit with their corresponding figures and resultant currents in MA.

Figures 50-8a to 50-8d are produced as the grid voltage is increased from +1V to +3.5V. The results obtained are very interesting to consider, especially in comparison with triodes whose grids have been biased negatively with respect to the base electrode.

Figure 50-1 shows the variation of circulating currents in circuits 1, 2 and 3 with E_1 , E_2 and E_3 when K_1 , K_2 , and K_3 are closed respectively. Table II shows the arrangement of keys and power

supplies in this case.

K_1 closed	K_2 and K_3 open	E_1 varies	I_1
K_2 closed	K_1 and K_3 open	E_2 varies	I_2
K_3 closed	K_2 and K_1 open	E_3 varies	I_3

Table II

From figure 50-1, it may be seen that the peak current in circuit 2 occurs at 3V since in this circuit the grid and base electrodes are silver, while in circuit 1 and 3 the top electrode is copper, hence higher peak voltages, 5V and 6V respectively are observed. Because of thicker insulator in circuit 1 ($D_1 + D_2 = 7500\text{\AA}$), than in circuit 3 (2500\AA) the peak current in Circuit 1 occurs at a higher voltage (6V) than in circuit 3 (5V).

Figures 50-2 and 50-3 show the variation of circulating currents in regions D_1 and D_2 with E_2 and E_3 respectively. Table III shows the arrangement of keys and power supplies in this case.

Fig. 50-2	K_1 open	K_2 and K_3 closed	E_2 varies	I_2	I_3
Fig. 50-3	K_1 open	K_2 and K_3 closed	E_3 varies	I_2	I_3

Table III

The current levels in figure 50-2 and figure 50-1 are comparable while in figure 50-3, I_3 is increased from 10mA to 30 mA varying E_3 instead of E_2 . The peak voltage for I_3 in both figures occurs at 4V while for I_2 it is increased from 3V to 4V in figure 50-3.

It may be also noted that I_2 in figure 50-3 is reduced remarkably from 80mA to about 12 mA.

Figures 50-4 and 50-5 show the variation of circulating currents in region D_2 and in $D_1 + D_2$ with E_1 and E_2 respectively. In both circuits K_2 is open while K_1 and K_3 are closed. Table IV shows the arrangements of keys and power supplies.

Fig. 50-4	K_2 open	K_1 and K_3 closed	E_1 varies	$I_1 \odot$	$I_3 \triangle$
Fig. 50-5	K_2 open	K_1 and K_3 closed	E_3 varies	$I_1 \odot$	$I_3 \triangle$

Table IV

The significance of these arrangements is in fact increasing the circulating current in circuit 3 from 22 mA (See figure 50-1.) to about 65 mA; by closing K_1 . I_1 also has been decreased from 70 mA to about 50 mA, in figure 50-5.

It may be noted that the peak voltage in circuit 3 also has been decreased from 5V to 3V while power dissipations at peak current in both arrangements are nearly equal (210 mW), i.e. as peak voltage increases the peak current decreases and vice versa.

As we shall see, any increase in peak voltage causes a reduction in the peak current in such a way that in most cases the product of $V_p \times I_p$ (peak voltage and peak current) remains constant for a particular layer.

Figures 50-6 and 50-7 show the variation of circulating currents in regions $D_1 + D_2$ and in D_1 with E_1 and E_2 respectively. K_3 is open while K_1 and K_2 are closed. Table V shows the arrangement of keys and power supplies.

Fig. 50-6	K_3 open	K_1 and K_2 closed	E_1 varies	I_1 ○	I_2 □
Fig. 50-7	K_3 open	K_1 and K_2 closed	E_2 varies	I_1 ○	I_2 □

Table V

It may be noted from figure 50-6 that current levels in circuit 1 and 2 are as high as in Figure 50-1 but the peak voltage of current I_2 is increased from 3V to 5.8V by closing K_1 . I_2 in figure 50-7 is increased nearly up to 100 A as well as its peak current from 3V to 4V. In this case it is clear that there is a current gain in this circuit arrangement. In comparison with the arrangement of figure 50-1, it can be seen that the gain is obtained by closing K_1 in circuit 1.

It is worth mentioning that in circuit 1 of figure 50-7 K_1 is closed and the circuit 1 internally is closed by emitted electrons from the grid which pass through the insulator (D_2) and reach the top electrode.

The observation of increasing and/or decreasing in either current levels or peak voltages in a particular layer of insulator by different circuit arrangements in triode systems leads to an idea that supports an electronic conduction mechanism in these devices although it is not certainly the only interpretation of the phenomena observed.

In order to study the effect of biasing the grid positively on the circulating currents of corresponding layers, the following results were obtained. Figures 50-8a, 50-8b, 50-8c and 50-8d show the variations of circulating current with E_1 in region $D_1 + D_2$ and in D_1 . The grid voltage (E_2) is fixed at +1V, +2V, +3V and +3.5 V

respectively. I_1 decreases as the grid voltage (E_2) is increased so that the peak current decreases from 70 mA (see figure 50-8a) to as low as 20 mA in figure 50-8d. It may be noted that the onset of I_1 in figures from 50-8a to 50-8d has negative value, starts from -9 mA (see figure 50-8a) and then increases slightly so that in figure 50-8d when E_2 is 3.5V, is -5 mA. Peak voltage of I_1 almost has remained constant at 7V. It may be also noted from the figures that I_2 starts with positive values and increases as E_2 is increased. The onset value of E_2 is 10mA in figure 50-8a while it is increased to 50mA in arrangement of figure 50-8d by increasing E_2 to 3.5V. I_2 , however decreases by increasing E , and reaches a minimum value at $E_1 = 6V$ (at this voltage I_1 has its highest characteristic up to $E_1 = 6V$, then starts to increase and acts as a positive resistance region. In figure 50-8a I_2 has a minimum of -9 mA, since this value is increased clear from the results obtained that currents in regions $D_1 + D_2$ and in D_1 (I_1 and I_2) are controllable by the grid voltage (E_2).

In case (b) the grid voltage (E_2) is biased negatively with respect to the base electrode. Figure 51 shows the general circuit arrangement in this case.

Table VI summarises the arrangement of keys and power supplies in each circuit with their corresponding figure number and the peak currents and peak voltages produced. Figures 52-1 to 52-8 are produced by using different parts of the general circuit arrangement shown in figure 51 and by choosing appropriate keys and power supplies in each circuit. Figures 51-8a to 51-8d are the results of

fixing the grid voltage at $-1V$, $-2V$, $-3V$ and $-3.5V$ respectively. The results for the two general cases will be considered at the end of this chapter.

Figure 52-1 shows the variation of circulating currents in circuits 1, 2 and 3 with E_1 , E_2 and E_3 when K_1 , K_2 and K_3 are closed respectively. Table VII summarises the arrangement of keys and power supplies.

K_1 closed	K_2 and K_3 open	E_1 varies	$I_1 \odot$
K_2 closed	K_1 and K_3 open	E_2 varies	$I_2 \square$
K_3 closed	K_2 and K_1 open	E_3 varies	$I_3 \triangle$

Table VII

Since D_1 is quite thin (2500\AA), the current levels in this region are higher than in regions D_2 and in $D_1 + D_2$. Peak voltage for I_1 occurs at $7V$ which is increased from $6V$ (see figure 50-1) to $7V$. Current levels in this arrangement are comparatively lower than the current levels in figure 50-1.

Figures 52-2 and 52-3 show the variation of circulating currents in regions D_1 and in D_2 with E_2 and E_3 respectively.

Table VIII summarises the arrangement of keys and power supplies.

Fig. 52-2	K_1 open	K_2 and K_3 closed	E_2 varies	$I_1 \odot$	$I_3 \triangle$
Fig. 52-3	K_1 open	K_2 and K_3 closed	E_3 varies	$I_1 \odot$	$I_3 \triangle$

Table VIII

It may be noted from figure 52-2 that I_3 decreased from 30 mA

(figure 52-1) to as low as 8 mA since only the peak current is increased from 6V to 7V, while I_2 has remained almost unchanged. In figure 52-3, I_3 has reached its original value of 30 mA since I_2 is decreased from 60 mA (see figure 52-1) to as low as 8 mA.

It is worth while to compare the arrangements of figures 50-3 and 52-3 and we see that in both cases E_3 varies in each circuit. In case a (E_2 positive with respect to the base electrode) I_2 is unchanged while in case b (E_2 negative with respect to the base electrode) it is increased from 60 mA to 8 mA. The reduction of I_2 merely is due to the injection of electrons (negative charge) to the grid which circulate in region D_2 in the opposite direction to electrons carrying current I_2 in this region and consequently lead to a reduction in I_2 . Negative charges at the grid also increase the peak voltage of I_2 to occur at 7V instead of occurring at 3V.

Figures 52-4 and 52-5 show the variation of circulating current in region D_2 and in $D_1 + D_2$ with E_1 and E_2 respectively. In both circuits K_2 is open while K_1 and K_3 are closed. Table IX summarizes the arrangements of keys and power supplies.

Fig. 52-4	K_2 open	K_1 and K_3 closed	E_1 varies	$I_1 \odot$	$I_3 \Delta$
Fig. 52-5	K_2 open	K_1 and K_3 closed	E_1 varies	$I_1 \odot$	$I_3 \Delta$

Table IX

In figure 52-4 both I_1 and I_3 are increased from 30 mA to 90 mA and 70 mA respectively. (See figure 52-1). The peak voltage for both currents also occurs at 3V. In comparison with the arrangement of figure 52-1, the products of $V_p \times I_p$ (peak voltage and peak

current) for both regions (D_2 and $D_1 + D_2$) are increased from 210 mW and 150mW to 270mW and 210mW respectively. Note that the only difference between the arrangements of figures 52-4 and 52-1 is that in the previous arrangement K_3 is open. In other words closing K_3 increases the current I_1 . Current levels and the peak voltage in figure 52-5 are similar to figure 52-4 ; note that this arrangement E_3 varies and thus I_3 is increased from 30 mA (see figure 52-1) to 80 mA. There is slight decrease for I_1 in figure 52-5 although it is still increased a great deal in comparison with its value in arrangement of figure(52-1).

Figures 52-6 and 52-7 show the variation of circulating current in regions $D_1 + D_2$ and in D_1 with E_1 and E_2 respectively. K_3 is open while K_1 and K_2 are closed. Table X summarises the arrangement of keys and power supplies.

Fig.52-6	K_3 open	K_1 and K_2 closed	E_1 varies	$I_1 \odot$	$I_3 \Delta$
Fig.52-7	K_3 open	K_1 and K_2 closed	E_2 varies	$I_1 \odot$	$I_3 \Delta$

Table X

Since in arrangements of figure 52-6, E_1 varies, the current level in region $D_1 + D_2$, (I_1) is higher than in arrangement of figure 52-7, and generally I_1 in both arrangements is lower than the arrangement of figure 52-1. Closing K_2 , however reduces I_1 .

I_2 on the other hand is decreased from 60mA (see figure 52-1) to 15 mA in figure 52-6 while in figure 52-7 it remains unchanged.

The effects of biasing the grid negatively are also studied in this case (case b). Figures 52-8a, 52-8b, 52-8c and 52-8d show the variation of circulating currents in regions D_1+D_2 and in D_1 with E_1 while the grid voltage (E_2) is fixed at $-1V$, $-2V$, $-3V$ and $-3.5V$ respectively.

It may be noted in all four figures the values of I_1 and I_2 are positive and generally current levels in region D_1 are higher than region D_1+D_2 .

I_1 and I_2 in figure 52-8a when $E_2 = -1V$ start from 14mA and 4 mA respectively, increase by increasing E_1 , having both rather broad maximum and above 6 V, both show negative resistance characteristics.

As E_2 is decreased from $-1V$ to $-2V$, the onset of I_2 starts from 20 mA, since I_1 starts almost from 0.2 mA. The peak current for both occurs at $E_1 = 4V$, and then follows a negative resistance curve. The negative resistance region in both layers is so that current levels decrease very slowly. However, the separation between two curves is increased by decreasing E_2 from $-1V$ to $-2V$ (see figure 52-8b).

It is interesting to note that on figure 52-8c the onset of I_2 again is increased to 50 mA as E_1 is decreased from $-2V$ to $-3V$ although when E_1 is increased to 2 V, there is a sharp fall for I_2 from 50 mA to 30 mA. At $E_1 = 3V$, I_2 increases to 35 mA and almost keeps this level up to $E_1 = 16V$.

I_1 on the other hand, shows a broad maximum between $E_1 = 4V$ and $E_1 = 7V$, although like I_2 , after $E_1 = 9V$, it varies very little with E_1 , and remains almost constant at the level of 7mA.

It may be noted that the separation between two curves, however, is increased (figure 52-8c).

Figure 52-8d shows the current variation in the same regions, when $E_2 = -3.5$ V., with E_1 .

The onset of I_2 again is increased, now is about 57 mA, having a maximum value of 60 mA at $E_1=1$ V. and then decreases very slowly with E_1 . I_1 also starts from 6 mA with a maximum value of 10mA at $E_1=1$ V the same as for I_2 , then decreases to a minimum value of about 6mA at $E_1 = 3$ V .

At $E_1=4$ V. there is a little rise from 6mA to 8mA as a second maximum which then decreases slowly. Similarly to I_2 , and almost parallel to it with increasing E_1 . The separation between the two curves however, in this case ($E_2 = -3.5$ V) has its highest value.

In order to study the effects of different electrode materials, in particular Al, Ag and Cu on the electroforming process, circulating current (and consequently on the emission current), peak voltage and potential distribution, all possible combinations of the above materials were used. The use of different electrode materials for base, grid and top electrodes even using only Al, Ag and Cu produces large numbers of different triode structures. The preparation of such a range of possible devices and comparison of the obtained results, however, involved a very long programme of work. Giving only even one example of each different set requires presenting of at least hundred graphs especially if the circuit arrangement and potential distribution measurements are added. In this thesis only the results of triodes with Al electrodes will be reported. The rest of the results may be published later.

Triodes with Al electrodes similar to diode systems with Al electrodes were formed. To form the devices a potential of 20 V for 15 minutes was applied in + FD. Most of the triodes were formed successfully. The following results are obtained from triodes where region D_1 is twice as thick as region D_2 . All formed triodes show VCNR. Connection of the grid to base electrode in the circuit shown in figure '53' by key K decreases the circulating current at the negative resistance region while in the positive resistance region it increases the circulating current. Current levels are quite low (in the range of a few mA). The peak voltage occurs at 5 V which is indicative of perfect forming and the circulating current when the bias voltage is more than 10 V, increases; so that a second maximum at 11 V and a third maximum higher than second maximum occurs at = 14 V. Figure 54 shows the variation of circulating current in region $D_1 + D_2$ when K is closed with bias voltages E_1 and E_3 respectively. The reasons for this arrangement is that, although it seems that when K is closed, the region D_1 is out of circuit, in other words current passes through the connection wire rather than passing through the region D_1 , this is not so, since direct application of bias voltage across the region D_2 shows lower current levels at equal bias voltages than in region D_1 and D_2 . However, closing K in the first circuit of figure 54 : certainly increases the current level in region D_1 and D_2 .

Figure 55 shows the potential distribution in region $D_1 + D_2$ with bias voltage for forward bias (up to 18 V) and to reverse bias up to 30 V . It may be noted that even though reverse bias is

applied, up to 18V (initial forming voltage) the potential distribution is similar to the case of forward bias application. As reverse bias is increased beyond 18V, the potential drop in region D_2 (previously low-resistance region) starts to increase (instead of decreasing) indicative of the fact that the forming direction is changing. It can be seen that at $V_b = 30V$ still the potential drop in region D_2 increases rapidly while the potential drop in region D_1 increases very slowly. Further application of reverse voltage causes switching of low and high resistances between the regions D_1 and D_2 .

Figure 56 shows the variation of circulating and emission current with bias voltage in an Al- I_1 -Al- I_2 -Al triode, where I_1 and I_2 are borosilicate glass films (SiO_x/B_2O_3) and $D_1 = 2D_2 = 5000 \text{ \AA}$. Emission current effectively starts from $V_b = 18V$ (see figure 56) where at $V_b = 26V$ is the highest and then decreases to as low as 10^{-9} A at $V_b = 34V$.

Figure 57 shows the variation of circulating current in regions D_1 , D_2 and in D_1+D_2 with bias voltage. The electrodes are aluminium and $D_2 = 1500 \text{ \AA}$ and $D_1 = 6000 \text{ \AA}$ ($D_1 = 4D_2$). It may be noted from figure 57 that the triode is formed perfectly, showing currents as high as 42 mA. This is indeed a very high current with Al electrodes. Since the peak currents are high the peak voltage is reduced to 4V. Since region D_2 is four times thinner than region D_1 , the circulating current in this region is nearly four times higher than in region D_1 although this is not a general rule for variation of circulating current with insulator thickness. The circulating current in the whole triode (region D_1+D_2) is much higher than region D_2 , this is due to the contribution of emitted

electrons from the base electrode to the conducting electrons in region D_2 . In other words, the emitted electrons from the base electron are accelerated by the grid which is positive with respect to the cathode, since the region is very thin (1500 \AA) the field also is strong and contributes to their motion towards the grid. Figure 58 shows the potential distribution in regions D_1 and D_2 of the same triode. Note that V_{GT} has a maximum at 4 V , similar to the circulating current in either regions of the device.

4.4. Discussion of the results on triode systems

As pointed out earlier, M-I-M-I-M structures are very suitable devices to study the common phenomena happening in the thin oxide films. The advantage of employing triode as opposed to diode systems is in having two distinct regions D_1 and D_2 as well as having a third electrode (the grid) and in consequent a choice of application of bias voltage between any two of these three electrodes.

By means of the third electrode (the grid) the experiments of electroforming process, potential distribution and in particular the concept of forming direction (FD) are much more informative.

Special phenomena such as controlling the circulating and consequently the emission current by means of the grid potential distinguishes the great advantage of using triode to diode systems.

In the experiments of section 4.4., the grid voltage was employed as an effective tool to make the triode structure much more useful devices in application of thin insulating films. Having choice of different circuit arrangements in triode systems, however, indicates the possibility of these structures being used as new electronic components in the future.

The experiments on M-I-M-I-M triodes, using borosilicate glass as the insulator material, however, showed some new results.

Electroforming process in triode systems is found to be similar to diode systems. In this section by referring frequently to the number of previous figures in section 4.4. and related phenomena observed, more possible and likely interpretations will be given.

As has been mentioned above, a triode structure in fact can be considered as a set of three diodes, (i) base - D_1 - grid,

(ii) grid - D_2 - top, (iii) base - D_1 + grid + D_2 - top.

The electroforming process is developed in the whole triode by application of forming voltage, V_F between the base and top electrodes. Formation of the individual layers (D_1 and D_2) is not then found to be necessary. Circulating current levels in regions D_1 , D_2 and in $D_1 + D_2$ (I_2 , I_3 , and I_1 respectively) vary due to their thicknesses, the polarity of the grid voltages, the circuit arrangements and electrode materials. In fact the existence of positive or negative charges at the grid either slows down or accelerates the circulating electrons in the devices when the bias voltage is applied. The existence of the charges will show that to a certain extent, the role of this electrode is quite similar to the role of the grid in triode vacuum tubes.

Potential distribution measurements showed dependence of this characteristic on the forming direction (FD). It has been reported by Hickmott¹³ that reversing the polarity of the bias voltage can change the direction of the potential distribution in the two distinct regions. In fact we consider that the application of the reversed polarity does not change the order (direction) of the potential distribution in triode systems unless the forming direction (FD) is changed completely⁶².

Switching of low and high resistances in the two distinct regions by reversing the forming direction is indicative of the fact that the forming direction is a dominant condition responsible for the distribution of potential in the insulating layers of the device.

One possible explanation of the observed phenomena is that the

structure of the conducting filaments, as postulated by Dearnaley, is not 'uniform' in other words, their resistance increases in a certain direction which is totally dependent on their forming direction. Therefore, the polarity and the magnitude of the applied potential and in consequence the forming direction change the direction of filament resistance. Experiments of the reversing the bias voltage polarity and potential distribution measurements are indicative to the nonuniformity of filament resistance. Figure 59 shows a schematic diagram of a non-uniform filament in a triode structure.

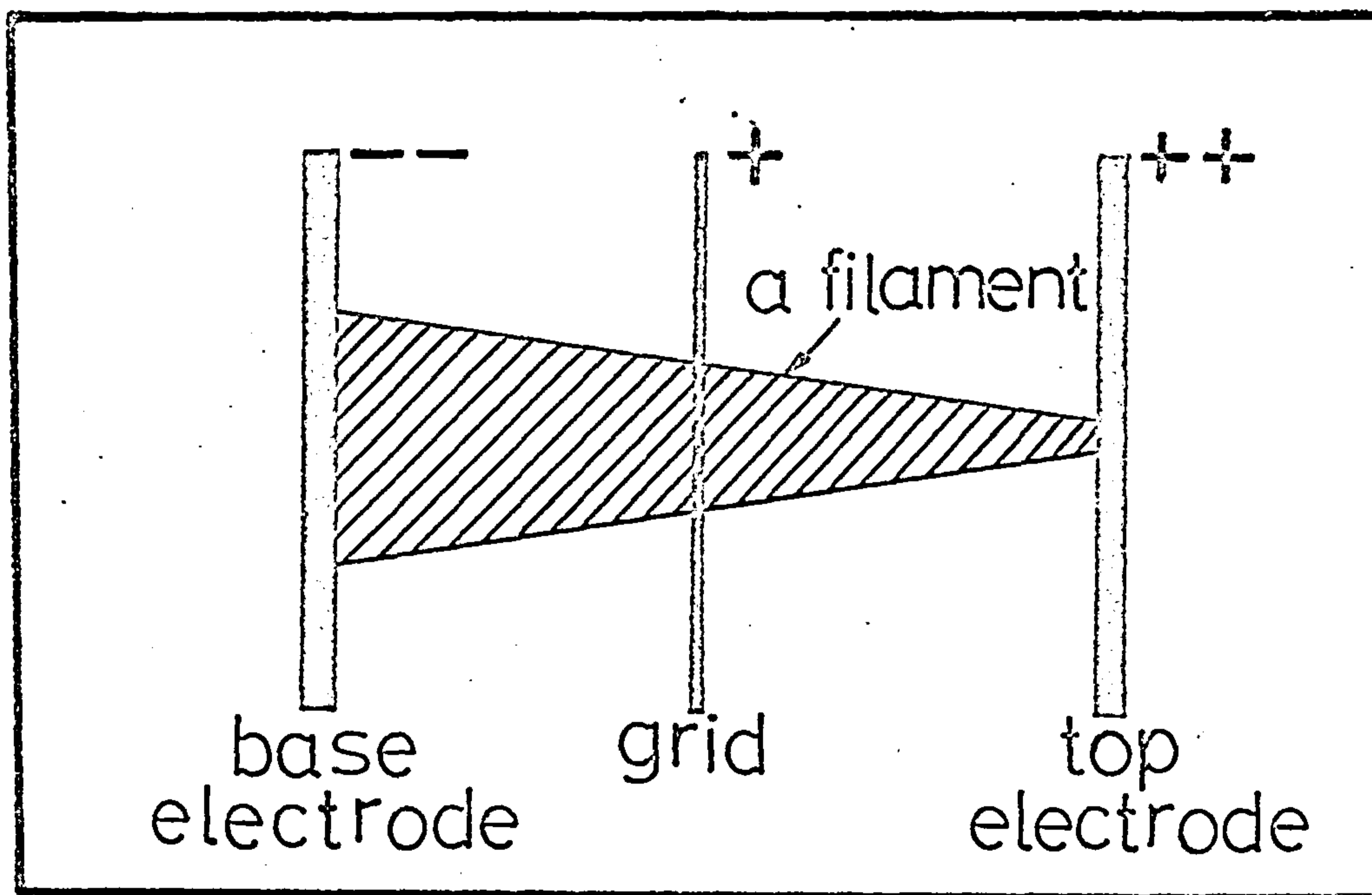


Figure 59. "Resistance of the conducting filament is not uniform along itself".

Exceeding the reverse bias more than was needed for initial electroforming to take place, changes the direction of initial forming rapidly and consequently changes the direction of potential distribution. An example of such a rapid change is given in figures 38- a and 38- b .

The form of the potential distribution in the low resistance region always follows the shape of I-V characteristics of the devices. In figure 40 it has been shown that especially the both curves ($V_{GT} - V_b$) and ($I_c - V_b$) have the identical peak voltage. This is found an unchanged phenomena in triode structures as long as no external potential is applied to the grid.

Circulating currents in the low-resistance region (say for example D_2) are usually much higher than the circulating currents that can be caused to flow in this region by application of bias voltage directly between the grid and top electrode (D_2). Having higher current levels in region D_2 , when the potential is applied between the base and top electrodes is due to existence of two particular conditions in this case.

(a) Fast emitted electrons from the base electrode and with high energy, are being accelerated by the small amount of potential difference between the grid and top electrode in D_2 region.

(b) The existence of a quite high field (about $10^5 - 10^6$ V cm⁻¹) between the base and top electrodes caused by the application of bias voltage between these electrodes, contributes to the acceleration of circulating electrons (emitted from the base electrode) in D_2 region. The above expression is illustrated schematically in figure 60.

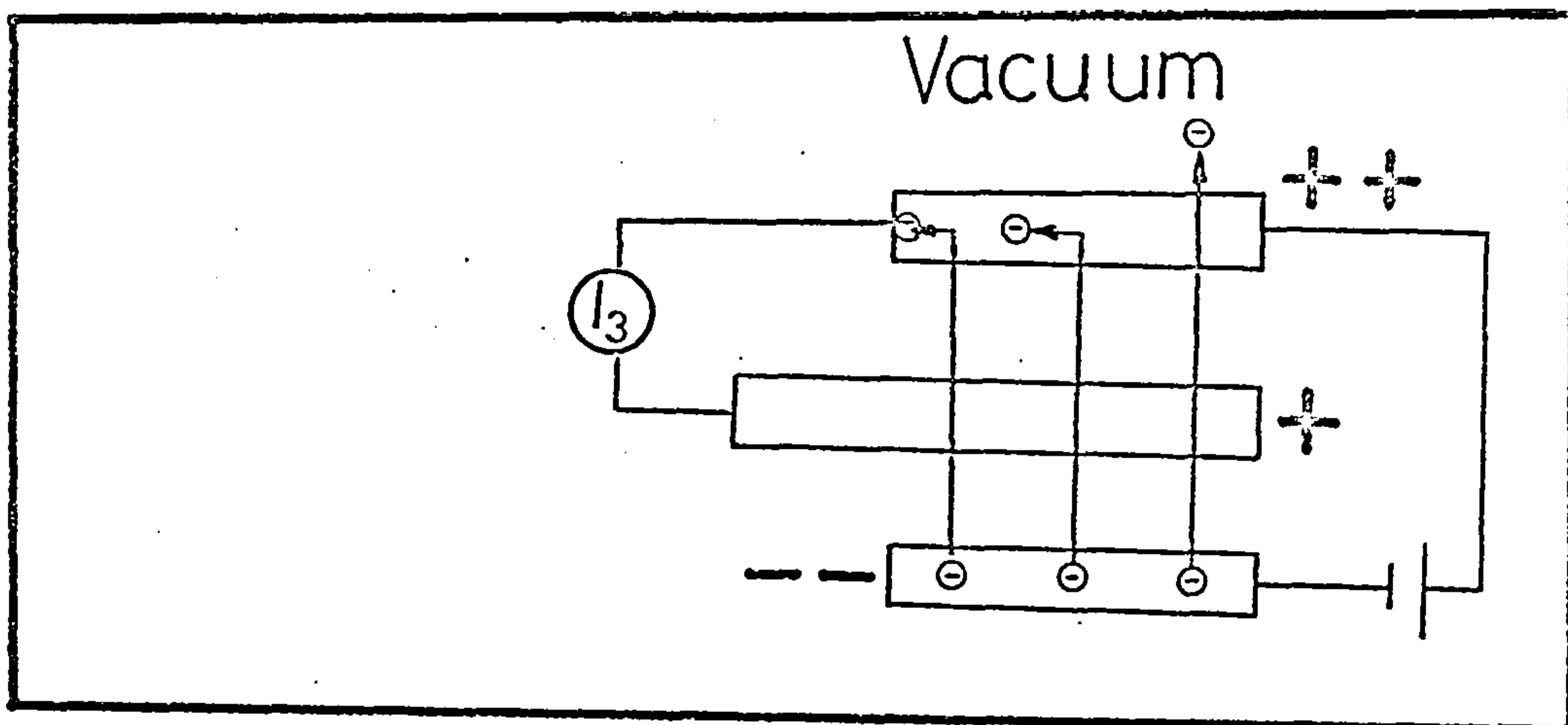


Fig. 60 Schematic diagram, illustration of the expression for acceleration of the emitted electrons from the base electrode in the presence of the high field induced between base and top electrodes of a triode system.

In the case of direct application of a bias voltage between the grid and top electrode, the two conditions mentioned, do not exist, since to produce such a high field in that region requires application of more than 5V . In the former case, however, the emitted electrons passes higher energy than the case of application of 1 V directly between the grid and top electrode as well as the fact that the high field in the previous case was already established. The above discussion fits the experimental results whown in figures 41 - a and 41 - b

In the experiments of figure 42 a bias voltage was applied between the grid and base electrodes. The emitted electrons from the cathode have enough energy to pass through the grid and region D_2 . Some of them emit into the vacuum and some are being stopped (attenuate) in the top electrode. Since the number of electrons emitted from the cathode is much more

than the number of electrons reaching the top electrode, this electrode (top) becomes positive with respect to the cathode (base). A voltmeter between the grid and top electrode, which is negative with respect to the grid, reads the potential difference between these electrodes. The potential distribution in region D_2 , however, generally follows the shape of the circulating current in region D_1 . The above expression is illustrated schematically in figure 61.

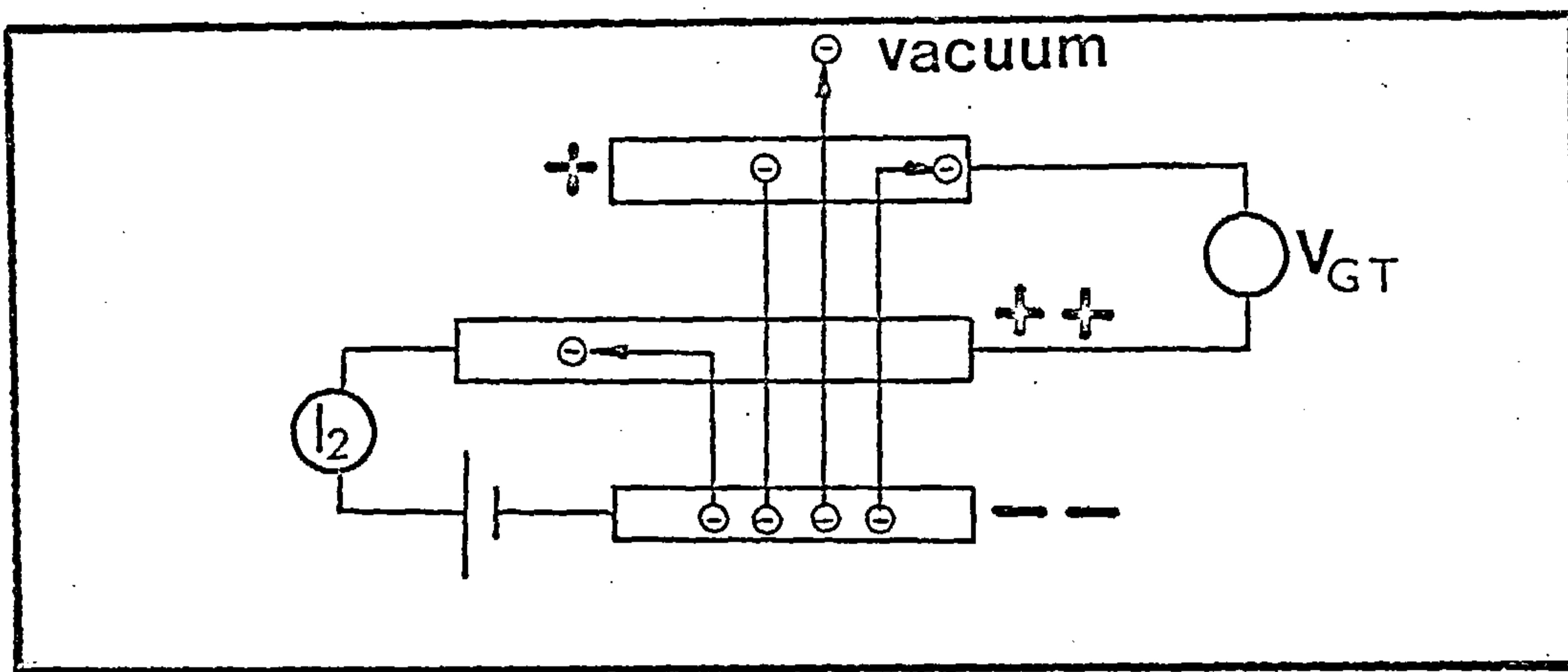


Figure 61. Schematic diagram illustrating the emitted electrons from the base electrode.

The polarity of the distributed potential in the low-resistance region of some triodes changes with bias voltage. Figure 43 was a typical example of this anomalous phenomenon. As has been shown the grid becomes twice positive with respect to the top electrode for the bias voltage values of 0 V to 2.3 V and more than 5.2 V. It is negative with respect to the top electrode between 2.3 V to 5.2 V.

Application of negative or positive potential at the grid has a great effect on the circulating current as well as on potential

distribution in triode systems.

If no bias is applied to the grid, the form of potential distribution in the low-resistance region follows the shape of I-V characteristic. Application of bias voltage to the grid changes the form of potential distribution in the both low and high resistance regions. Positive potential at the grid in fact accelerates the emitted electrons from the base electrode and as a result decreases the resistance of high resistance region. The resistance of the low-resistance region increases at the same time, so that the potential drop in this region also increases. The results shown in figures 45. and 46. were typical examples for the biasing the grid positively and its effect on the potential distribution. For example, in figure 45 when the grid voltage is 2 V , the potential drop is increased from 2 V to 4 V .

Finally, the two main tables (I and VI) in which the arrangements of keys and power supplied together with peak current and peak voltage of each circuit are given, summarise the general circuit arrangements in base (a) and base (b). It may be noted from the tables (I and VI) that in most cases wherever a peak current decreases, the peak voltage is increased and vice versa.

It is worth to mention that at low voltages the potential distribution was essentially uniform and divided over the insulating layers in proportion to their thicknesses. As the voltage increased the potential distribution became increasingly non-linear, until after forming almost the entire voltage was dropped over one region.

Observation of the behaviour of M-I-M structure
in the scanning electron microscope during the
dynamic operation of the devices

5.1. Introduction

Thin film sandwich structures of the form M-I-M have been shown to exhibit a variety of interesting phenomena after electroforming. Electroforming is believed to take place by means of the production of filaments of electrode material introduced by a metal/vacancy diffusion process from the electrode as postulated by Dearnaley, Morgan and Stoneham³⁶, and such evidence as pitting of the electrode material is consistent with this model. The spots formed on the metal electrode surface (top electrode) are believed to be related to the discrete spatial pattern of electron emission which is inferred from the individual scintillations observed when a fluorescent screen is used to study the electron emission pattern,^{40,40,55}

Previous discussions have suggested that a single filament is unlikely to form and ~~than~~ in view of the excess currents which may be carried by them after forming of the devices, they are probably at least several atomic spacings in diameter.

Clearly the use of the scanning electron microscope will be of value in observation of localised effects at the electrode surfaces while the sandwich structures are being operated as

electron emitters.

Park and Basavaiah⁸⁹ have studied the superstructure during emission from sandwich structures in which the insulator was ZrO_2 .

Emmer⁸⁷ has studied the defects which were observed after the electrical measurements in formed Al - Al_2O_3 -Au structures. Two kinds of local defects were found on the surface of the active area. The first kind which are holes of typically $10 \mu m$ in diameter, are described in agreement with Klein,⁹⁰ as single hole non-shortening breakdown of the dielectric layer. Such breakdown spots were usually found in samples which had been operated at higher voltages during the electrical measurements.

Defects of the second kind which occur in all cases of successfully formed samples, i.e. whose I-V characteristics show VCNR, have a remarkable circular shape, which implies that their formation is accompanied by strong local heating. However, this is not the general case, since formed devices of borosilicate glass films with different electrode material show different shapes of defect pattern at their surfaces.

The observation on sandwich structures of borosilicate films in the forms of $Ag-SiO_x/B_2O_3 - Ag$ and $Cu-SiO_x/B_2O_3-Cu$ prepared by co-evaporation made in studies of surface topography both before and after the application of an electroforming voltage

to the specimens during the operation, have recently been reported by Taheri and Hogarth.³⁹

5.2. Results of topography of the device surfaces during the dynamic operation

Using a co-evaporation technique, thin amorphous films of borosilicate material were formed from B_2O_3 (30%) and SiO_x (70%). The electrode materials were copper for some devices and silver for others, and previous work had shown that these high-conductivity metals led to efficient and well-characterised devices. Electrode thicknesses were in the range of 3 to 6×10^{-6} cm and the insulator thickness in the range 3 to 5×10^{-5} cm. The substrate material was well-cleaned Corning glass 7059 as for previous devices.

The M-I-M devices after preparation were then transferred to a scanning electron microscope (Cambridge Stereoscan 54) at a pressure of 10^{-5} torr and electroformed.

The magnification available in the scanning electron microscope was up to 20,000 but most of the experiments used a much lower value of magnification than this, since the high field through the devices caused high disturbances on the electron beam and consequently observation on the screen was impossible. Thus the acceleration voltage of the electron beam was kept in the range 5 - 10 kV to reduce the tendency for specimens to charge up and thus to achieve clear observations on the screen of the scanning electron microscope.

The normal circulating current through the specimen and substrate arising from the incident electrons was measured and found to be less than 10^{-12} A during the experiments.

It was found possible to observe the local phenomena at a point on the counter-electrode surface before the maximum in the voltage - current characteristic and beyond it, but at the peak applied voltage, where the current through the device is the highest, clear observation of the surface was not possible.

The main observations made were of local apparent hot spots, believed to be the terminations of filaments, and evidence of disturbances to the surface region around them. There is also evidence of tracks developing on or near the surface.

The results for specimens having copper or silver electrodes show similarities but also dissimilarities, and these differences will be ascribed to differences in diffusivities of copper and silver and in their different affinities for oxygen.

All the evidence points to considerable power dissipation at the ends of the filaments. However, devices were electroformed inside the scanning electron microscope and the top electrodes (positively biased) were observed. Typical voltage-current characteristics for both formed $\text{Ag-SiO}_x/\text{B}_2\text{O}_3-\text{Ag}$ and $\text{Ag-SiO}_x-\text{Cu}$ sandwich structures were observed.

The measured circulating currents were many orders of magnitude greater than the standing current resulting from the incident electron beam.

Before forming no special features were observed on the counter-electrodes of the devices. In view of the very smooth nature of the amorphous oxide films and of the similar nature of the metal electrode, a smooth and featureless image would be expected. Whilst the applied voltage was gradually increased the active area under the electron beam was moved from point to point in order to search for any local changes. Having established that there were no special surface features, the devices were formed by the application of 7V (devices with silver electrodes) or 9 V (devices with silver and copper electrodes).

During the electroforming process a number of spots ranging in diameter from 7 to 15×10^{-4} cm were observed. Observation of such spots was fairly straightforward since there was evidence of pitting of the material in some cases and of deposits above the surface in others.

The observations suggest that the temperature in the vicinity of the localised filamentary regions is high, since the density of filaments at any time is quite low (between 1 and 10 in a typical 3mm x 3mm active area) and if the excess current (over the normal bulk dielectric current) is mostly carried by the filaments, the power dissipation in very localised regions will be high and

a high temperature will result. The localised regions where filaments are observed vary from time to time, being formed, re-formed and destroyed and a typical density of such regions at a given time is 5 in 9 mm^2 . If, in the simplest case, there were only one filament in such a section having an area of 10^{-6} cm^2 then for a peak current of 100 mA the effective current density would be 10^5 A cm^{-2} . This would be reduced to 10^4 A cm^{-2} if as many as 10 filaments were operating at any given time, but in any case considerable localised heating is inevitable and melting of the counter-electrode highly probable.

Some filaments remain active for a few seconds and then break down and another filamentary region is formed. The traces of this process cause tracks on the surface of the counter electrode. The high power dissipation in the vicinity of the filament leads to an evolution of energy and the patterns resulting from this are shown in the photographs.

Figure 62 for a $\text{Ag} - \text{SiO}_x/\text{B}_2\text{O}_3 - \text{Ag}$ device operating near the peak current, shows the origin where a filament terminates at a Ag counter electrode surface and clearly a disturbance has spread outward from it. The bright spots in the tracks are all believed to be electron emission sources and it may be observed that the tracks have a discrete character and this is consistent with a metal/vacancy diffusion process or, more probably, with a local electrolysis giving rise to regions deficient in oxygen. The spread of disturbance is approximately circular in shape.

In this figure the central filament is in the size range $10 - 12\mu\text{m}$.

Figure 63 shows another region on the same device and the damage to the counter electrode, which can be caused after considerable power dissipation, is clearly observable. The bright spots are believed to be the regions of electron emission and it may be noted that they are all near the edge of the hole in the counter-electrode, causing further erosion. Figure 63 was taken for a voltage lower than that at which the peak circulating current occurred V_p .

Figure 64 shows the same region shown in figure 63 where the device is being operated at voltages beyond V_m . In figure 64 the emitting regions are smaller and the odd emission spots in the tracks outside the main filamentary region are no longer visible. Some spots are seen even where the counter electrode has been locally removed. In fact the device is operating at the negative resistance region.

Figure 65 shows a more magnified (x800) part of the specimen seen in figures 63 and 64, and changes on the smooth surface of the insulator in places where the electrode has been peeled off may be seen. The tracks which spread from the active emission spots are seen to be operating in the metal counter-electrode and have not caused this to be stopped from the insulator below it.

With all the above photographs the dissipation of heat and the consequent deformation of the counter electrode and the production of local tracks is characteristic of devices carrying silver counter-electrodes.

With devices carrying copper counter-electrodes the central filamentary region is observed but in this case the tracks formed seem to spread more on the surface as shown in figure 66 where considerable debris results from the passage of high current densities through a nearby filament. This is mostly due to the relatively easy oxidation of copper in relation to that of silver.

Figure 67 shows a magnified ($\times 1600$) view of the tracks running through the silver counter electrode of a device and the smaller emitting filamentary regions in these tracks may be clearly observed. These regions are of linear dimension from 5×10^{-5} to 2×10^{-4} cm and seem to be more stable than the large filamentary cores which are formed in a destructive manner.

The scanning electron microscope provides a useful method for observing localised effects in M-I-M cathodes during their operation.

The main features of the filamentary conduction model seem to be confirmed by the observations mentioned in this chapter.

Breakdown in fact is a continuous process of electroforming, in other words the observed spots on the counter electrode (see figures 62 , 63 , and 66) are the origin of the breakdown processes. As the devices are operated at high voltages, these spots grow in size so that they effect the peak current. Since the area of the counter-electrode is reduced, the circulating current also decreases. However, complete breakdown never occurred because there is always a little undamaged area left on the active part which conducts although in this case the current levels are reduced a great deal.

Nevertheless it is clear that levels of circulating and emission currents depend on the size and the number of the conducting filaments at the time. The number of filaments are reduced as the devices are operated frequently at high levels of current and voltage.

As pointed out, the borosilicate glass films show remarkably strong dielectric properties and surprisingly withstand very high voltages, sometimes even up to 800°C , without suffering destructive breakdown. Since the temperature of the filaments at the time of growth and while conducting electricity is very high, perhaps more than 800°C when they grow, the power dissipations in these films are also high. The high temperature normally evaporates or peels off some part of the counter electrode, so that the active area is reduced. By reduction of the counter electrode-area most of the unbroken filaments effectively will be out of the device circuit, since any filament needs the counter-electrode to be in the circuit and consequently contributes to the circulating and emission current.

Chapter 6

Summary and Conclusions

A co-evaporation technique was used to prepare thin amorphous films of borosilicate material from B_2O_3 and SiO_x .

Electrical properties of 3000 Å - 6000 Å thick borosilicate glass films, sandwiched between Al electrodes were studied.

The observation of electroforming phenomena and the appearance of a negative resistance region suggested that the SiO_x/B_2O_3 films might act as electron emitters. Consequently the relevant properties of electro formed devices were investigated using this complex.

Electron emission into a vacuum was detected from these devices as well as observation of clear negative resistance region, although the forming voltage V_F , and peak voltage, V_m occurred at quite high voltages.

The very high dielectric strength of the mixture of 30% B_2O_3 and 70% SiO_x allowed higher voltages to be applied across the insulator (up to 600 V) without breakdown occurring. Although current levels were low the high applied voltage meant that considerable power was being dissipated in the devices.

Electron emission into a vacuum starts at about 10 - 20 V depending on the dielectric thickness and the degree of formation

of the devices, while at lower voltages emission current is as low as 10^{-12} A.

The emission current densities were of the order of 10^{-5} A cm⁻² and since the circulating currents through the sandwiches were lower than in similar films of SiO_x, the transmission efficiency was high.

In order to test whether any appreciable quantity of heat was dissipated in the devices, especially at the very high voltage level, a thermocouple was attached to the top of some devices and the temperature monitored. The T - V_b curve, in general, follows the I_c - V_b curve and the maximum temperature occurs when the current flow is highest.

The model of Dearnaley et al, was supported by the temperature measurements which showed that the temperature was a maximum before the onset of negative resistance. Beyond this region the temperature falls and there is no evidence of thermally-induced breakdown. This poses the question of the failure of emission at voltages of the order of 100 V .

Further work on the electrical and electron emission behaviour of metal-borosilicate glass - metal (M-I-M) structures continued. Differences in the behaviour of the samples were formed for different electrode materials and a systematic variation of properties with insulator thicknesses was observed.

By means of the technique of coating with a SiO_2 layer, the behaviour of samples containing more than 50% B_2O_3 could be studied. This technique prevents the absorption of water vapour by complexes containing more than 40 - 50 % B_2O_3 and also enables certain novel results to be obtained.

The variation of the properties of M-I-M structures with temperature was discussed and related to the general problems of electronic conduction and emission.

In an attempt to establish a more definite variation of voltage-current characteristics with thickness, specimens were made in the form of successive steps of different dielectric thickness during the evaporation process. This procedure was superior to earlier results using a wedge-shaped layer carrying several electrodes, defining specimens of only an 'average' thickness.

The variation of circulating currents with time for the initial application of forming voltage was studied. The forming process using Al electrodes was found to be slow and may last from 5 minutes to 2 hours, depending on the applied voltage, dielectric thickness and temperature. For the higher conductivity electrodes (Ag, Au, Cu,) forming takes place much more quickly, typically in from 1 to 30 seconds.

The peak voltage V_m with Ag, Au and Cu electrodes is much lower and current levels are higher than for samples with Al electrodes.

The current levels increase symmetrically with decreasing thickness of insulator in formed specimens made in steps on one substrate as described in Chapter 3. The characteristics of coated and uncoated samples are generally of the same form, but the peak voltage increases and the peak current decreases for the covered films.

The emission current density is lower for samples with Al electrodes (about 10^{-5} A cm⁻² or higher). The electron emission also depends on the dielectric thickness and the top electrode materials due to the attenuation of electrons in these regions.

From a study of the curves of circulating current as a function of applied bias voltage the power dissipation at the peak has been calculated and a pattern of behaviour identified. Power dissipation calculated for the devices with Ag and Cu electrodes is higher than the specimens carrying Al electrodes. This suggested that the diffusion of Al only leads to the formation of thin filamentary paths which pass lower excess currents and thus are only capable of dissipating a smaller amount of energy before the voltage at which they are ruptured, is applied. The diffusion of Cu or Ag is more favourable and higher currents are passed and a higher power can be dissipated before rupture of the filaments.

The higher power dissipation at the peak voltage was observed for the thinner films and thus as a consequence, more energy would be available for communication to the electrons. Consequently a high electron emission for a given bias voltage would be expected.

The temperature measurement of the devices with well-conducting metal electrodes showed a rise in temperature to 300°C or so at peak voltage.

In a further study of the potential distribution across the insulating layers, M-I-M-I-M (triode) systems were employed. By using different circuit arrangements and by controlling the grid voltage, the circulating and emission currents were controlled.

VCNR and electron emission from triode structures were observed. The electroforming process was studied. The potential distribution in the distinct regions of triode systems was found to be dependent on forming direction and grid voltage. Effects of applying a negative or positive voltage at the grid on circulating and emission currents were also studied.

Switching of the low and high resistances in the two distinct regions, by reversing the forming direction, was indicative of the fact that the forming direction is a dominant condition responsible for the distribution of potential in the insulating layers of the device. One possible explanation of the observed phenomena was to propose that the structure of the conducting filaments is not uniform i.e. their resistance increases in a certain direction which is totally dependent on their forming direction. The form of the potential distribution in the low-resistance region always follows the shapes of the $I_c - V_b$ characteristics of the devices.

Electroforming is believed to take place by means of the production

of filaments of electrode material introduced by a metal/vacancy diffusion process from the electrode.

The use of the scanning electron microscope produced valuable photographs of localised effects at the electrode surfaces while the structures were being operated as electron emitters.

The main observations made were of local apparent hot spots, believed to be the terminations of filaments and evidence of disturbances to the surface region around them.

The results of specimens having Cu or Ag electrodes showed similarities but also dissimilarities. These differences were described to differences in diffusivities of Cu and Ag and in their different affinities for oxygen.

All the evidence pointed to considerable power dissipation at the end of the filaments.

During the electroforming process a number of spots ranging in diameter from $7 - 15 \times 10^{-4}$ cm were observed. The observations also suggested that the temperature in the vicinity of the localised filamentary region was high, since the density of filaments at time was quite low (between 1 - 10 in a typical 3mm x 3mm area). In the simplest case, when only one filament was considered the current density through this filament would be as high as 10^5 A cm⁻². This would be reduced to 10^4 A cm⁻² if as many as ten filaments were operating at any given time, but, in any case, considerable localised heating was inevitable and melting of the counter-electrode was highly probable.

The main features of the filamentary conduction model seem to be confirmed by the observations mentioned in Chapter 5.

Breakdown in these devices was found to be dependent on both the electrode and insulating material and on the insulator thickness.

Since the circulating current in the films, which carry noble metal electrodes, is much higher than those which carry reactive electrode materials such as Al, the device temperature is very high and these have led us to the conclusion that this type of breakdown is very likely to be thermal in origin.

REFERENCES.

1. J.G. Simmons, D.C. Conduction in thin films, published by Mills and Boon Ltd. 1971.
2. N.F. Mott, Phil. Mag. 19 (1969) 835.
3. J.G. Simmons and R.R. Verderber, Proc. Roy. Soc. A 301 (1967) 77.
4. N.F. Mott, Adv. Phys. 16 (1967) 49.
5. J.G. Simmons, Phys. Rev. 166 (1968) 912.
6. J.G. Simmons, Phys. Rev. 32 (1971) 1987.
7. P.J. Price and J.M. Radcliffe, IBM J. Res. Dev. 3 (1959) 364.
8. R. Stratton, J. Phys. Chem. Sol. 23 (1962) 1172.
9. J.G. Simmons, J. Phys. D. Appl. Phys. 4 (1971) 613.
10. K.H. Grundlach and Heldman, Phys. Stat. Sol. 21 (1967) 575.
11. N.F. Mott and R.W. Gurney, Electronic Process in solids (Oxford, 1948).
12. C.A. Mead, J. Appl. Phys. 32 (1961) 646.
13. T.W. Hickmott, J. Appl. Phys. 35 (1964) 2679.
14. G. Dearnaley, A.M. Stoneham and D.V. Morgan, Rep. Prog. Phys. 33 (1970) 1129.
15. S.R. Pollack, J. Appl. Phys. 34 (1963) 877.
16. S.R. Pollack, W.O. Freitag and G.E. Morris, Electrochem. Technol. 1 (1963) 96.
17. T.W. Hickmott, J. Appl. Phys. 33 (1966) 2669.
18. G.A. Filarentou, V.I. Stafeyev, G.A. Cherkashin, M.S. Lure, i/u. Z. Bubnov and Zh. S. Asina, Radio Engng. Elec. Phys. 11 (1966) 246.
19. C. Barriac, F. Giraud-Heraud, P. Pinnard and F. Davoine, C.R. Acad. Sci. 262 (1966) 900.
20. R.R. Verderber, J.G. Simmons and B. Eales, Phil. Mag. 16 (1967) 1049.

21. G.Dearnaley, Phys. Letters 25A (1967) 760.
22. P.D. Greene, E.L. Bush and I.R. Rawlings, Proc. Symp. on deposited thin film dielectric materials, Ed. F. Vratny (New York: The Electrical Society, 1968).
23. C. Barriac, P. Pinard and F. Davoine, Phys. Stat. Solidi 34 (1969) 621.
24. S.R. Jawalekar, Indian J. Pure App. Phys. 8 (1970) 36.
25. G. Doucas and D. Walsh, thin solid films 9 (1971) 25.
26. R.A. Collins, thin solid films 11 (1972) 187.
27. R.R. Sutherland, J. Phys. D: Appl. Phys. 4 (1971) 468.
28. T.W. Hickmott, thin solid films 9 (1972) 431.
29. R.R. Sutherland, J.P.A. Williamson and R.A. Collins, J. Phys. D: Appl. Phys. 5 (1972) 1686.
30. R.R. Sutherland, Ph.D. Thesis, University of Lancaster (1972).
31. L. Pauling, The nature of the Chemical Bond, 3rd Ed. (New York: Cornell Univ. Press, 1960) P. 98.
32. K.M. Gundlach and J. Kadlec, Thin solid films 13 (1972) 225.
33. R.E. Thurstans, P.C. Wild and D.P. Oxley, Thin Solid Films 20 (1974) 281.
34. C.A. Hogarth and E.H.Z. Taheri, Thin Solid Films 10 (1972) 455.
35. E.H.Z. Taheri, C.A. Hogarth and R.D. Gould, Phys. Stat. Solidi (a) 12 (1972) 563.
36. G. Dearnaley, D.V. Morgan and A.M. Stoneham, J. Non-Crystalline Solids 4 (1970) 593.
37. C.A. Hogarth and E.H.Z. Taheri
Int. J. Electronics, 1974 (under publication).
38. C.A. Hogarth and H. Bidadi, Thin Solid Films 13 (1972) S27.

39. E.H.Z. Taheri and C.A. Hogarth, J.Non-Crystalline Solids 1974 (under publication).
40. R.D. Gould and R.A. Collins, App.Phys.Letters 16 (1970)893.
41. J.G. Simmons, R.R. Verderber, J.Lytollis and R.Lomax, Phys.Rev.Letters 17 (1966) 675.
42. K.H. Henisch, Scientific American 221, 5 (1969) 30.
43. J.F. Gibbons and W.E. Beadle, Sol.State Electronics 7 (1964) 785.
44. S.R. Ovshinsky, Phys. Rev. Letters 21 (1968) 1450.
45. C.F. Drake, I.F. Scanlan and A. Engel, Phys.Stat.Solid. 32 (1969) 193.
46. K.L. Chopra, J. Appl. Phys. 36 (1965) 184.
47. N.B. Hanney, D. Mac Nair and A.M. White, J. Appl.Phys. 20 (1949) 669.
48. W.Heinze and S.Wagener, Z. Tech.Phys. 20 (1939) 17.
49. T.W. Hickmott, J.Appl. Phys. 37 (1966) 4380.
50. T.W. Hickmott, J. Appl. Phys. 3 (1969) 85.
51. G. Dearnaley, Thin Solid Films 3 (1969) 161.
52. H. Kanter and W.A. Feibelman. J. App.Phys. 33 (1962) 3580.
53. R.R. Verderber and J.G. Simmons, Radio Electr.Eng. 33 (1967) 347.
54. T.W.. Hickmott, J. Appl. Phys. 36 (1965) 1885.
55. R.W. Lomax and J.G. Simmons, Radio Electr. Eng. 35(1968)265.
56. P. Hartmann, G. Niquet and P. Vernier, J.Vac.Technol. 6 (1969) 719.
57. R.A. Collins and R.D. Gould, Solid State Electronics 14 (1971) 805.
58. P.P. Budenstein and P.J. Hayes, J. Appl.Phys. 38 (1967)2837.

59. C.A. Mead, J.Appl.Phys. 36 (1965) 1885.
60. O.C. Nelson and D.E. Anderson, J. Appl.Phys. 37 (1966) 66.
61. J. Antula, J.Appl.Phys. 43 (1972) 1830.
62. E.H.Z. Taheri and C.A. Hogarth 1974 (to be published).
63. J. Raby and R.A. Collins, Thin Solid Films 20 (1974) 227.
64. A.A. Abidi and C.A. Hogarth Thin Solid Films 22 (1974)203.
65. C.Barriac, P.Pinard and F.Davoine, C.R.Acad.Sci. 266
(1968) 423.
66. J.E. Ralph and J.M. Woodcock, J.Non-Crystalline Solids 7
(1972) 236.
67. N.F. Mott, Phil.Mag. 17 (1968) 1259.
68. J.M. Ziman, J. Phys.C. Solid State Phys.2 (1969) 1230.
69. P.W. Anderson, Phys. Rev. 109 (1958) 1492.
70. G.S. Kreynina, L.N. Selivanov and T.I. Shinskaiã-Radio Eng.
Elec.Phys. 5 (1960) 219.
71. K.H. Gundlach and J. Kadlec, Phys.Stat.Solidi (a) 10
(1972) 371.
72. J.G. Simmons and R.R. Verderber, Appl.Phys.Letters 10
(1967) 197.
73. S. Whitehead, Dielectric Breakdown in Solids Oxford Univ.
Press. (1951).
74. J.J. O'Dwyer, Theory of Electronic Conduction and Breakdown
in Solid Dielectrics, O.V.P. (1973).
75. F. Forlani and N. Minnaja, Phys.Stat.Sol. 4 (1964) 311.
76. F. Seitz, Phys.Rev. 79 (1949) 1376.
77. L.A. Wright, Ph.D. Thesis, Brunel University (1967).
78. P.A. Timson, Ph.D.Thesis, Brunel University (1971).
79. C.A. Hogarth and L.A. Wright Proc.Intern.Conf.Physics

Semiconductors, Moscow, 1968, P. 1274.

80. L.Holland (Ch.5. Steckelmacher), Thin Film Microelectronics Chapman-Hall; London, 1965) P. 204.
81. P.A. Timson and C.A. Hogarth Thin Solid Films 10 (1972) 321.
82. J. Pivot, M. Boudeulle, A.Cachard and C.H. Dupley, Phys. Stat. Solidi (a) 2 (1970) 3K.
83. R.D. Gould, C.A. Hogarth and R.A. Collins, J. Non-Cryst. Solids 12 (1973) 131.
84. P.A. Timson and C.A. Hogarth, Thin Solid Films 10 (1972) 321.
85. G.S. Kreynina, Radio Engng.Elec.Phys. 7 (1962) 166.
86. C. Barriac, F.Giraud-Heraud, P.Pinard & F. Lomax.Phys. Rev. Letters 17 (1966) 675.
87. I. Emmer Thin Solid Films, 20 (1974) 43.
88. R.D. Gould & C.A. Hogarth J. Non-Cryst Solids 12 (1973) 131.
89. K.C.Pork and S. Basavaiah, J.Non-Cryst. Solids 2 (1970) 284.
90. N. Klein. Thin Solid Films 7 (1971) 149.
91. R.A. Collins, G. Bowman and R.R. Sutherland, J. Phys. D: Phys. 4 (1971) L 49

FIGURES

1. Properties of formed devices
2. Band diagram of un-formed and formed diodes (after Hickmott)
3. Band diagram of un-formed device (after Simmons)
4. Band of formed device (after Simmons)
5. The simple triangular distribution of filament resistance (after Dearnaley)
6. Model of Ralph and Woodcock
7. Schematic diagram of solution to fundamental equation of thermal breakdown
8. Masks used for Diode Systems
9. Masks used for Triode Systems
10. Design of boats and spiral used for evaporation of SiO , B_2O_3 , Au, Ag, Cu, and Al.
11. Device arrangement a) diode, b) triode
12. Typical Talystep traces and schematic diagram of the instrument
13. Photograph of the cooling part of the test system
14. Circuit used for the electrical measurements
a) diode, b) triode
15. Typical I-V characteristic of an Al-borosilicate (3000\AA) -Al film
16. I-V characteristic of a 6000\AA borosilicate film carrying Al electrodes
17. Variation of circulating current with bias voltage, Al electrodes, perfectly formed

18. Variation of emission current with bias voltage, Al electrodes
19. Variation of transmission ratio ($\alpha = I_e / I_c$) with bias voltage, Al electrodes
- 20a. Vertical section of specimen used to determine thickness variation of circulating current
- 20b. Vertical section of specimen protected by silica later
21. Circulating current as a function of bias voltage in borosilicate thin films (3×10^{-5} cm thick) using three electrode materials
22. Circulating current as a function of bias voltage for a borosilicate specimen as shown in Fig. 20a and carrying Al electrodes
23. Circulating current as a function of bias voltage for two specimens, one with a protective silica coating
24. Emission current as a function of bias voltage for an Al-borosilicate specimen
25. Emission current as a function of bias voltage for borosilicate films carrying Ag and Cu electrodes
26. Emission current as a function of bias voltage for a specimen of the form shown in Fig. 20a
27. Emission current as a function of bias voltage for uncovered and covered borosilicate specimens carrying Al electrodes
28. Variation of temperature with bias voltage for a borosilicate film carrying Al electrodes
29. Circulating current and local specimen temperature as a function of bias voltage for a borosilicate sample carrying Cu electrodes

30. Variation with time of the circulating current for the initial application of forming voltage carrying Al electrodes
31. Variation with time of the circulating current for the initial application of forming voltage for a specimen carrying Ag electrodes
32. Dependence of V on insulator thickness for specimens carrying Al electrodes
33. Dependence of V on insulator thickness for specimens carrying Ag electrodes
34. I-V characteristics of a formed Ag-borosilicate structures at various temperatures
- 35a. Triode configuration
- 35b. Symbols used for triode in this thesis
36. Schematic diagram of potential distribution in a triode biased in two different directions
37. Schematic diagram of potential distribution in a triode biased in three different voltages
- 38a. Variation of V_{GT} and V_{GB} with forward bias voltage for conditions shown in Fig. 37 (a)
- 38b. Variation of V_{GT} and V_{GB} with reverse bias voltage for condition shown in Fig. 37 (b)
39. Schematic potential profiles across triode systems under different conditions of applied voltage
40. Variation of both circulating current and V_{GT} with bias voltage
- 41a. Variation of both I_1 and I_3 with bias voltage
- 41b. Variation of I_3 with V_{GT}

42. Variation of both I_c and V_{GT} with V_{GB}
43. Variation of both I_1 and V_{GT} with bias voltage
44. Variation of both I_1 and potential drop in regions D_1 and D_2 with bias voltage when $V_g = 0V$
45. Variation of both I_1 and potential drop in regions D_1 and D_2 with bias voltage when $V_g = +1V$
46. Variation of both I_1 and potential drop in regions D_1 and D_2 with bias voltage when $V_g = +2V$
47. Variation of both I_1 and potential drop in regions D_1 and D_2 with bias voltage when $V_g = +3V$
48. Variation of I_1 with bias voltage when $V_g = 0, -1, -2$ and $-3V$
49. General circuit arrangement (Case a)
- 50-1. Variation of I_1, I_2 and I_3 with E_1, E_2 and E_3 respectively
- 50-2. Variation of I_2 and I_3 with E_2
- 50-3. Variation of I_2 and I_3 with E_3
- 50-4. Variation of I_1 and I_3 with E_1
- 50-5. Variation of I_1 and I_3 with E_3
- 50-6. Variation of I_1 and I_2 with E_1
- 50-7. Variation of I_1 and I_2 with E_2
- 50-8a. Variation of I_1 and I_2 with E_1 when $E_2 = +1V$
- 50-8b. Variation of I_1 and I_2 with E_1 when $E_2 = +2V$
- 50-8c. Variation of I_1 and I_2 with E_1 when $E_2 = +3V$
- 50-8d. Variation of I_1 and I_2 with E_1 when $E_2 = +3.5V$
51. General circuit arrangement (Case b)
- 52-1. Variation of I_1, I_2 and I_3 with E_1, E_2 and E_3 respectively

- 52-2. Variation of I_2 and I_3 with E_2
- 52-3. Variation of I_2 and I_3 with E_3
- 52-4. Variation of I_1 and I_3 with E_1
- 52-5. Variation of I_1 and I_3 with E_3
- 52-6. Variation of I_1 and I_2 with E_1
- 52-7. Variation of I_1 and I_2 with E_2
- 52-8a. Variation of I_1 and I_2 with E_1 when $E_2 = -1V$
- 52-8b. Variation of I_1 and I_2 with E_1 when $E_2 = -2V$
- 52-8c. Variation of I_1 and I_2 with E_1 when $E_2 = -3V$
- 52-8d. Variation of I_1 and I_2 with E_1 when $E_2 = -3.5V$
53. Variation of I_1 with bias voltage in a triode with Al electrodes
54. Variation of I_1 with E_1 and E_3 in a triode with Al electrodes
55. Variation of V_{GT} and V_{GB} with V_b biased in two different directions
56. Variation of I_c and I_e in a triode carrying Al electrodes
57. Variation of I_1 , I_2 and I_3 with E_1 , E_2 and E_3 respectively in a triode carrying Al electrodes (Case a)
58. Potential distribution of V_{GT} and V_{GB} with bias voltage in a triode carrying Al electrodes ($D_1 = 4D_2$)
59. Schematic diagram of a non-uniform filament in a triode structure
60. Schematic diagram: illustration of the expression for acceleration of the emitted electrons from the base electrode in the presence of the high field induced between base and top electrode of a triode system

61. Schematic diagram illustrating the emitted electrons from the base electrode
62. S.E.M. picture of a counter-electrode of a Ag-borosilicate-Ag structure, operating near the peak current (x800)
63. Another region on the same counter-electrode as shown in Fig. 62 and the damage to the counter-electrode (x160)
The picture was taken at a voltage less than that at which the peak current occurred (V_m)
64. The same region as shown in Fig. 63 when the device was operated at a voltage greater than V_m
65. A more magnified (x800) part of the counter-electrode shown in Figs. 63 and 64
66. A counter-electrode of a Cu-borosilicate-Cu structure operating near the peak current (x240)
67. A magnified (x1600) view of the tracks running through the Ag counter-electrode of a Ag-borosilicate-Ag structure

Properties of formed device

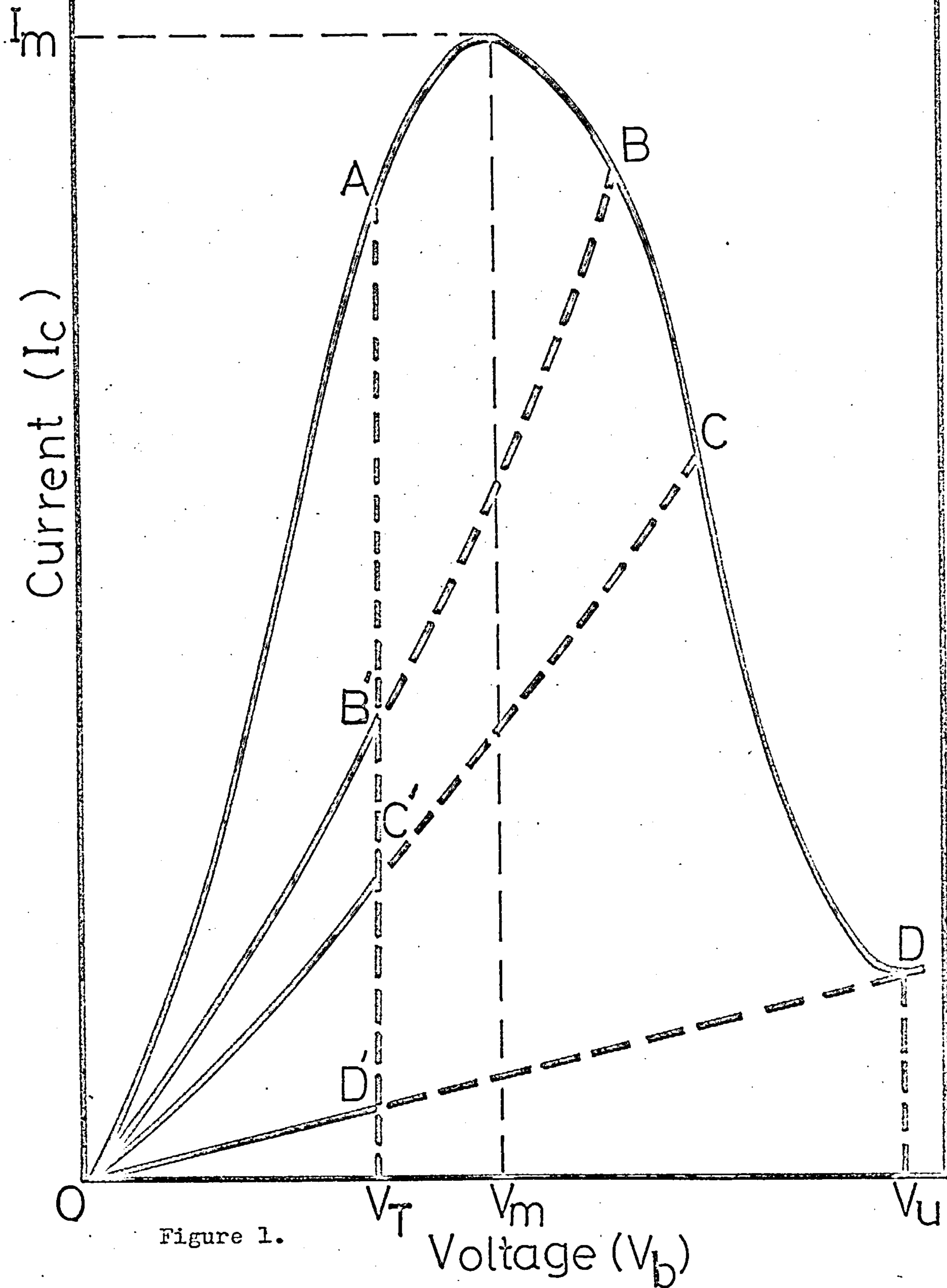


Figure 1.

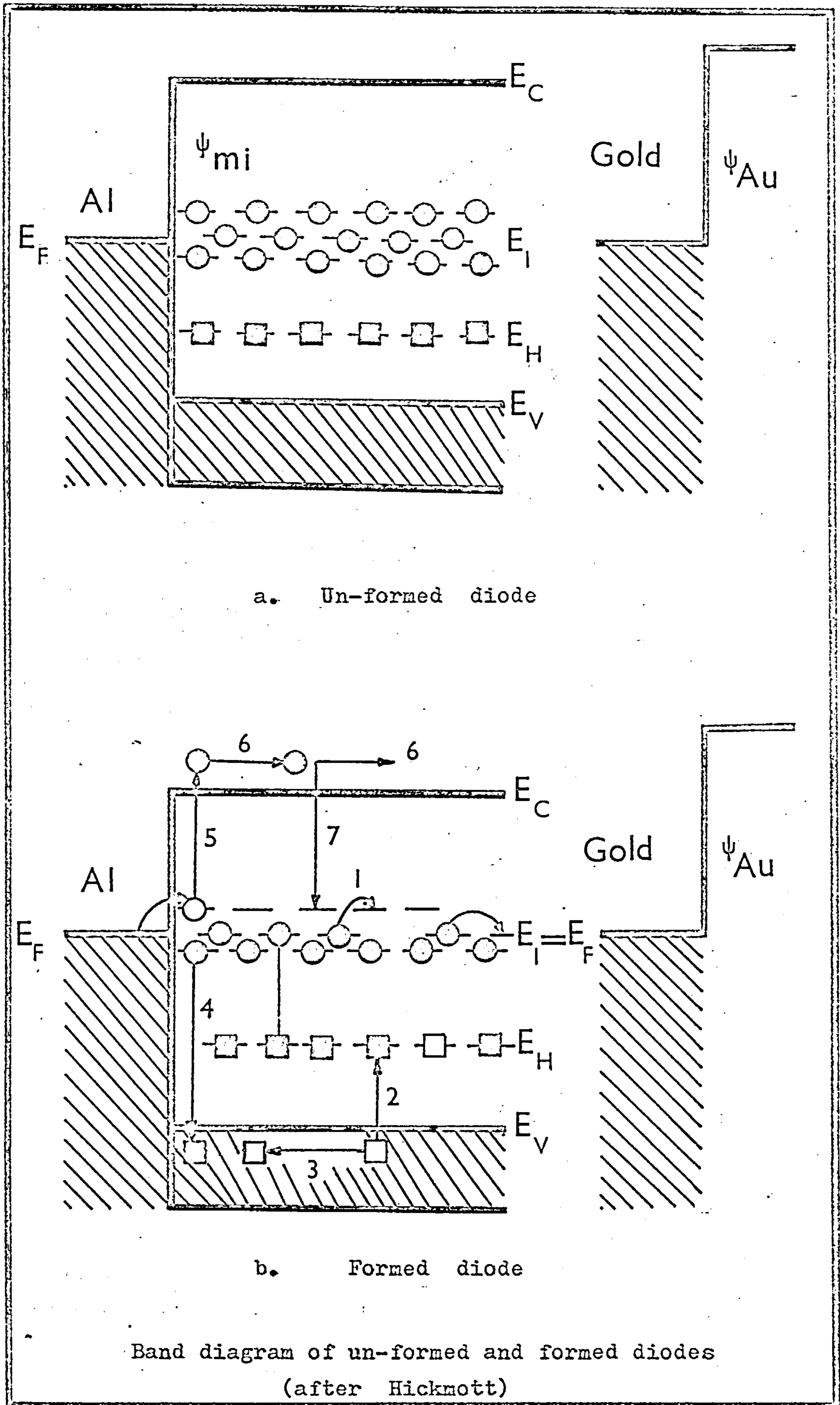


Figure 2.

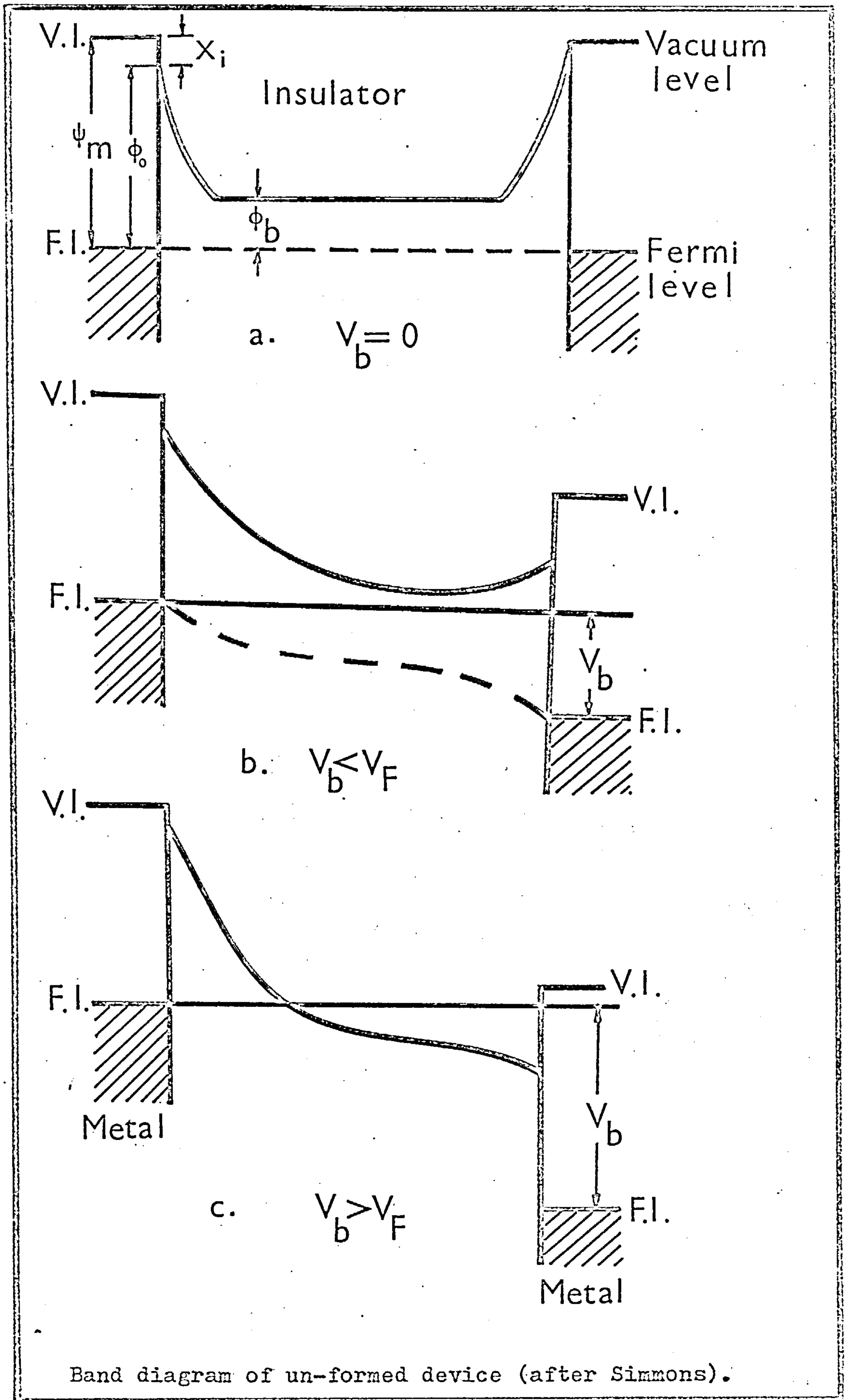
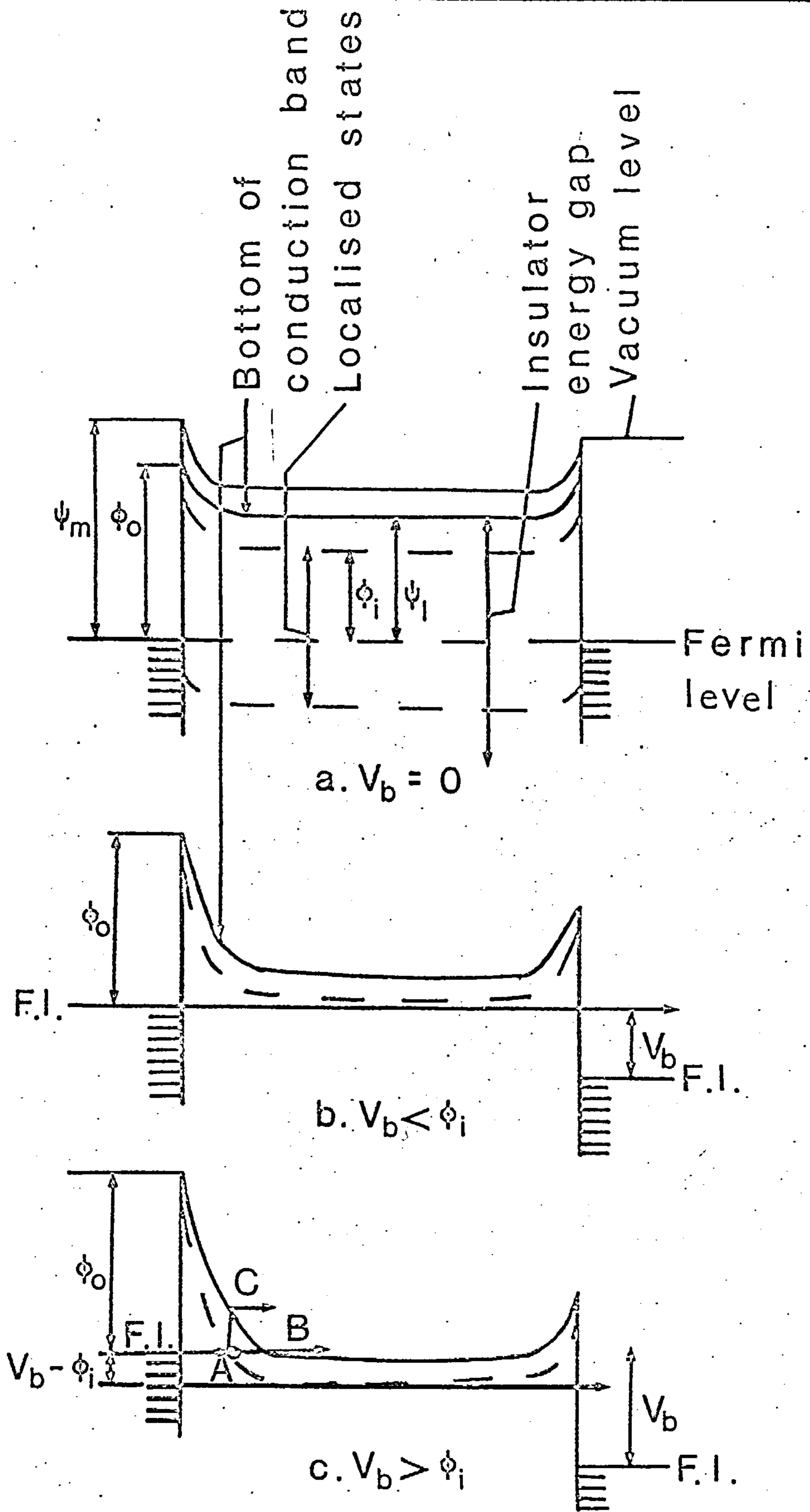
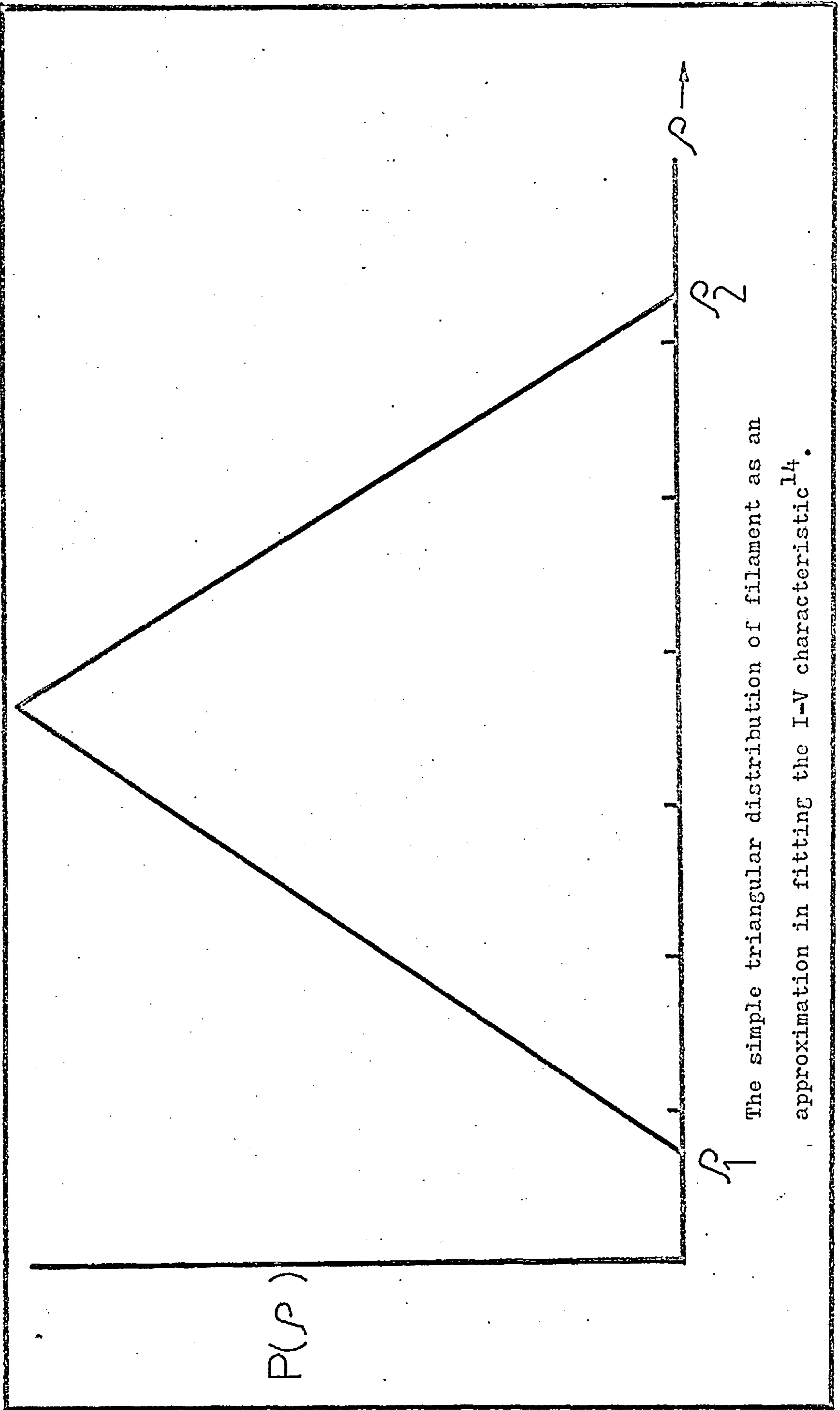


Figure 3.



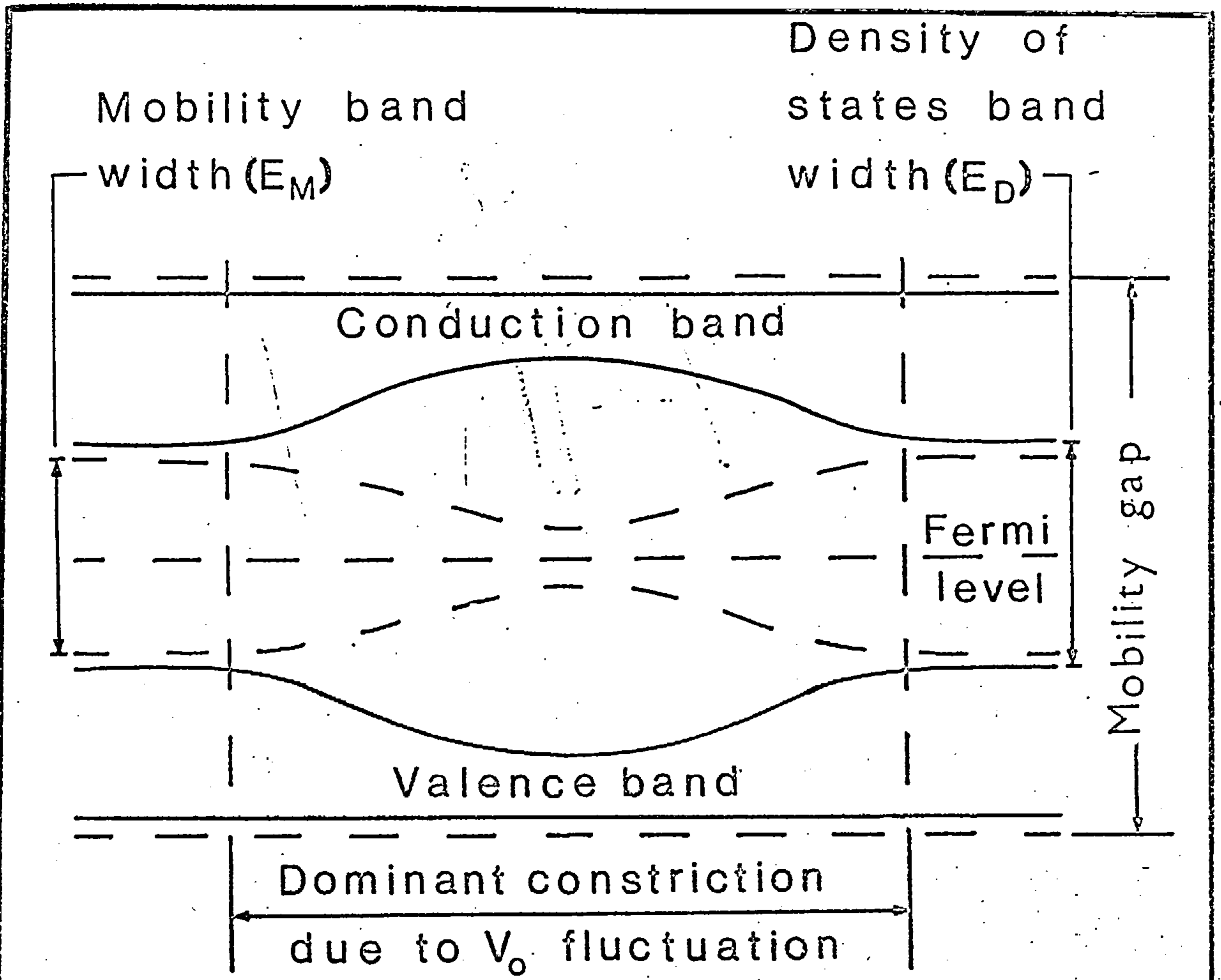
Band diagram of formed device (after Simmons)

Figure 4.

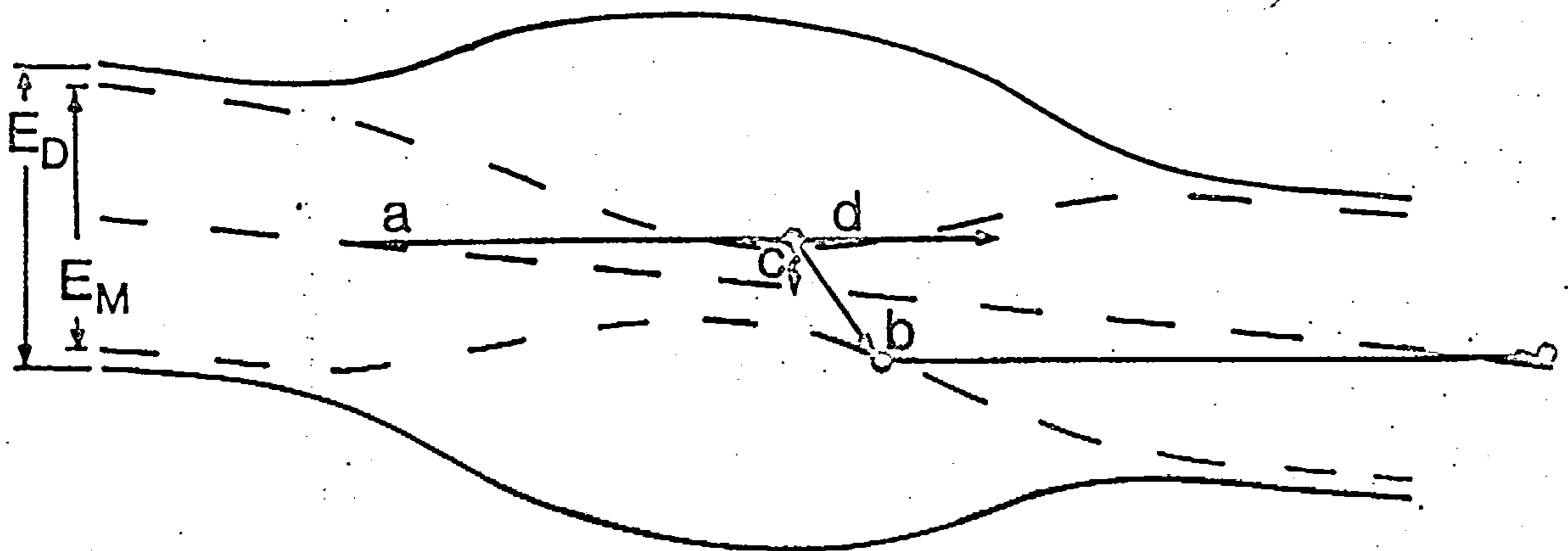


The simple triangular distribution of filament as an approximation in fitting the I-V characteristic¹⁴.

Figure 5.



a) Band model of filamentary constriction at zero bias



b) Conduction process at low bias

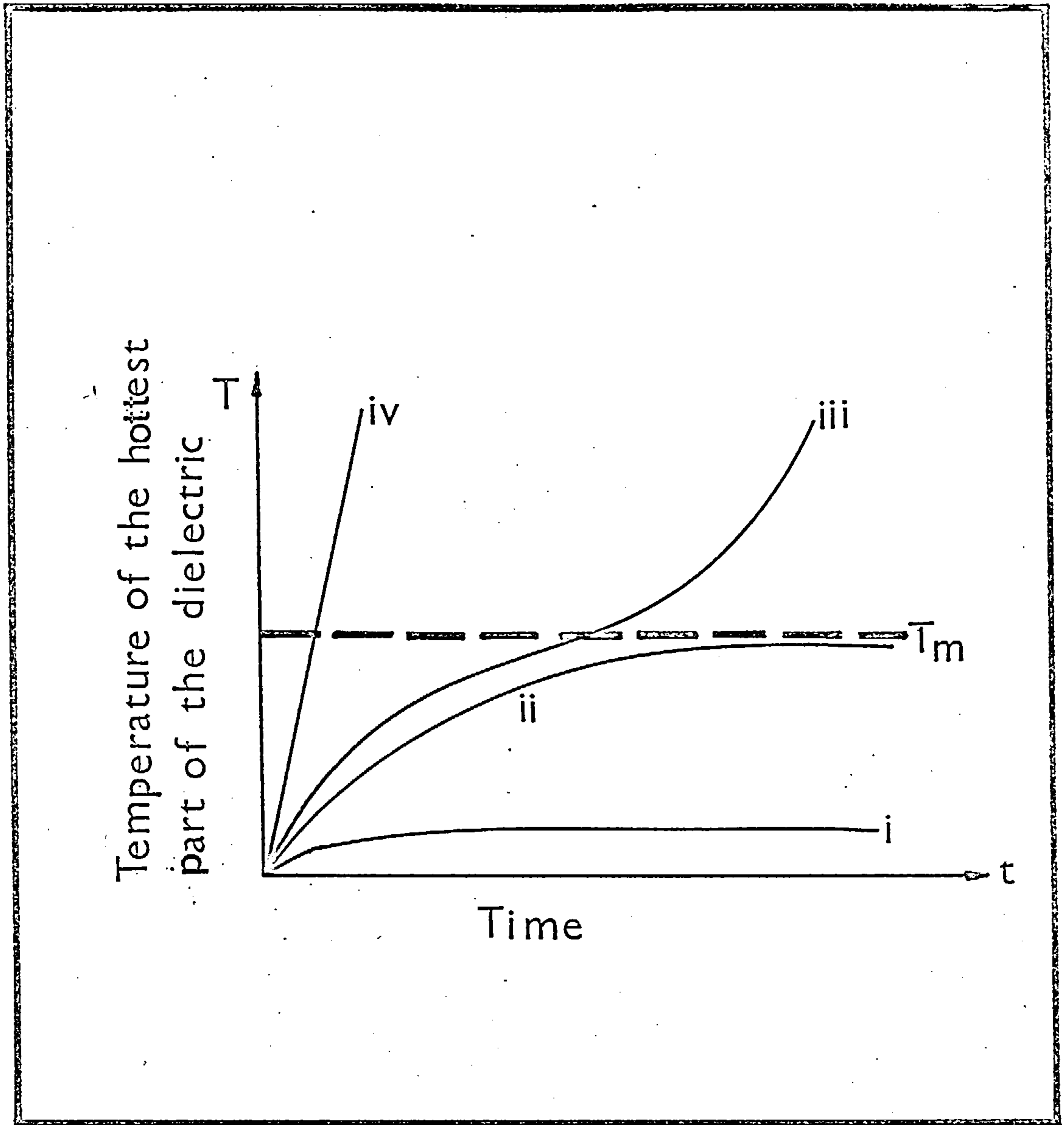
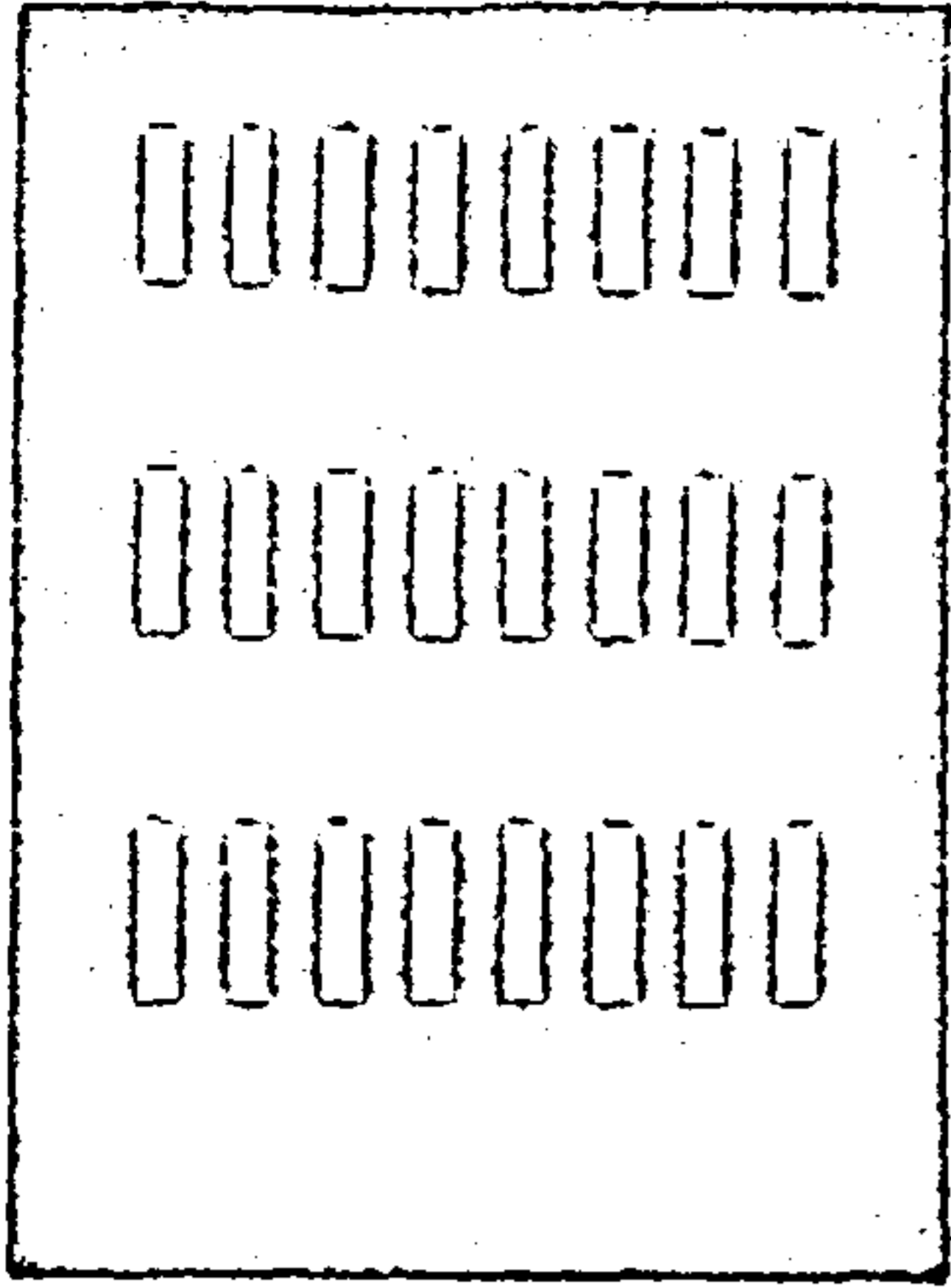
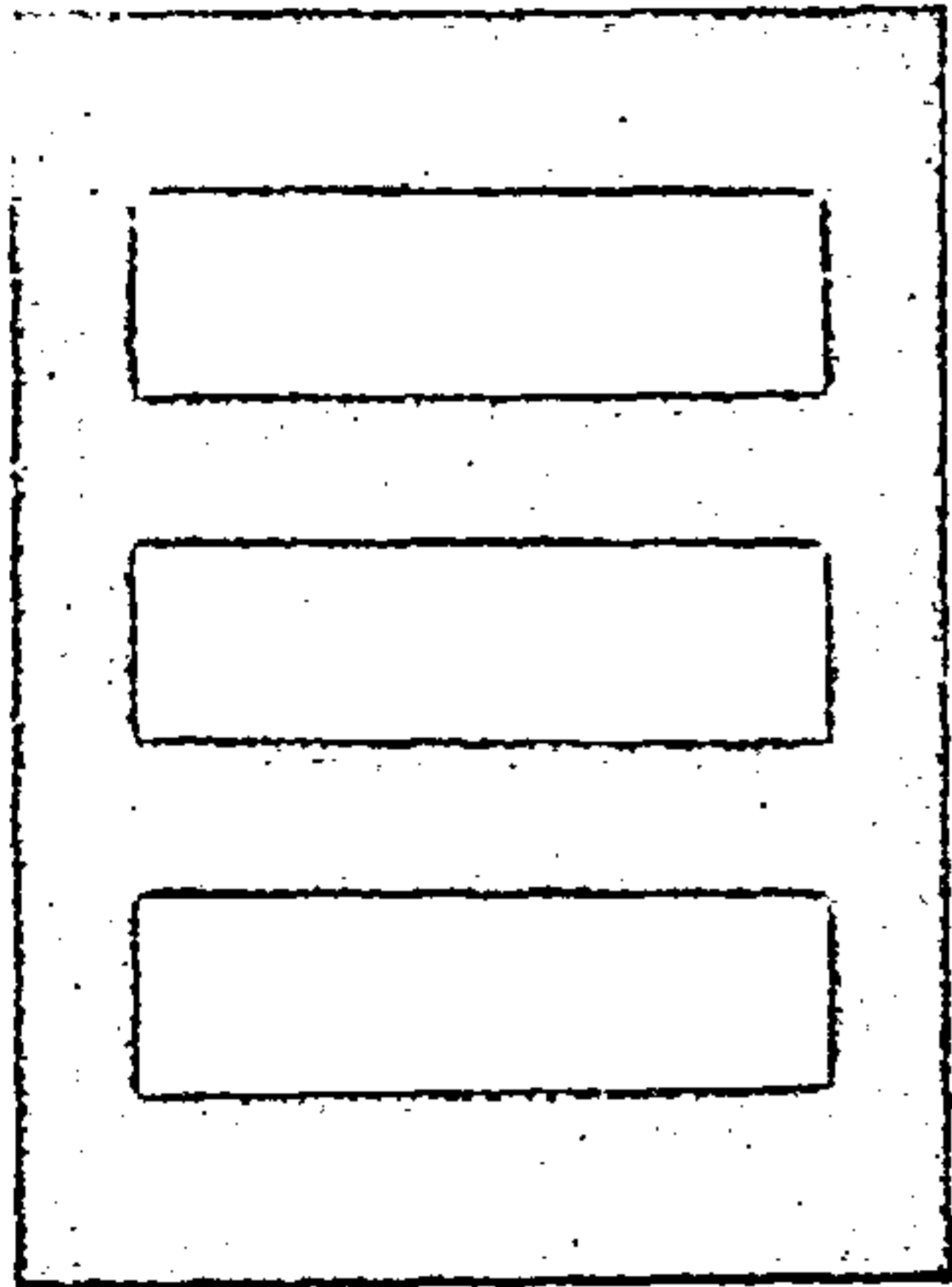


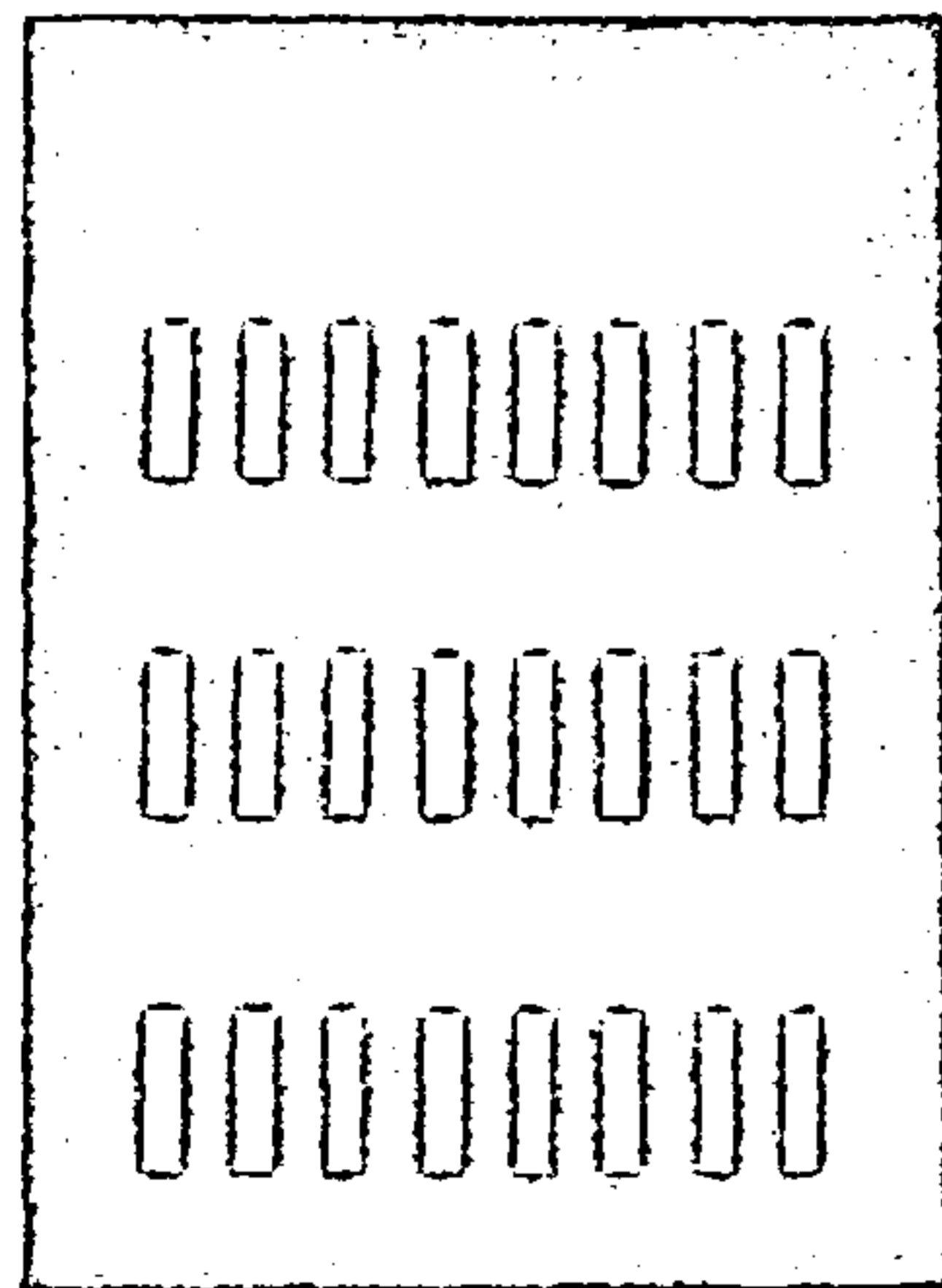
Figure 7. Schematic diagram of solution to fundamental equation of thermal breakdown.



Base
electrode

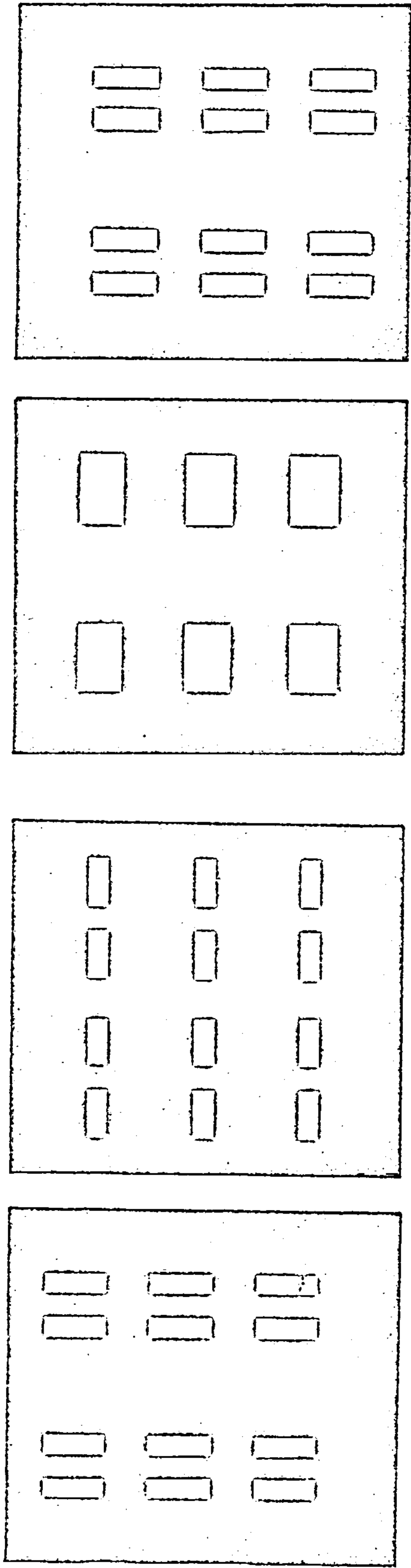


Dielectric



Counter
electrode

Fig. 8 : Masks used for Diode Systems



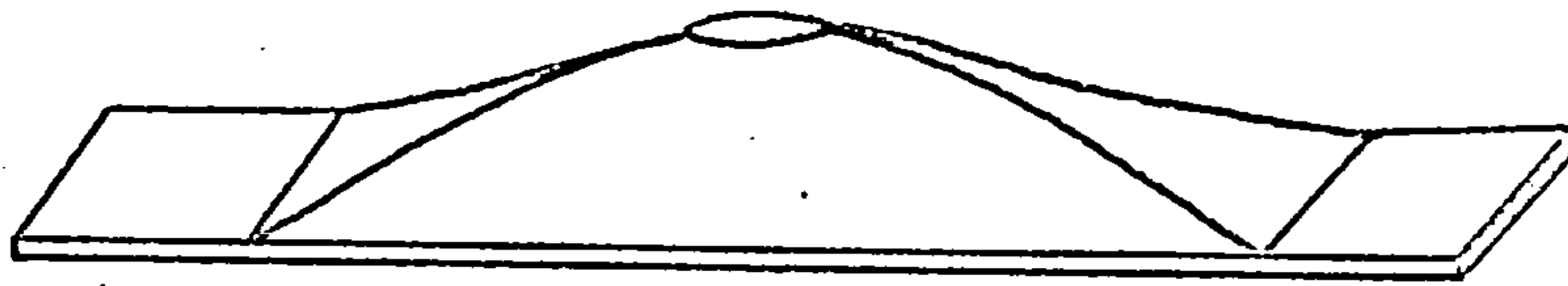
Base
electrode

Grid

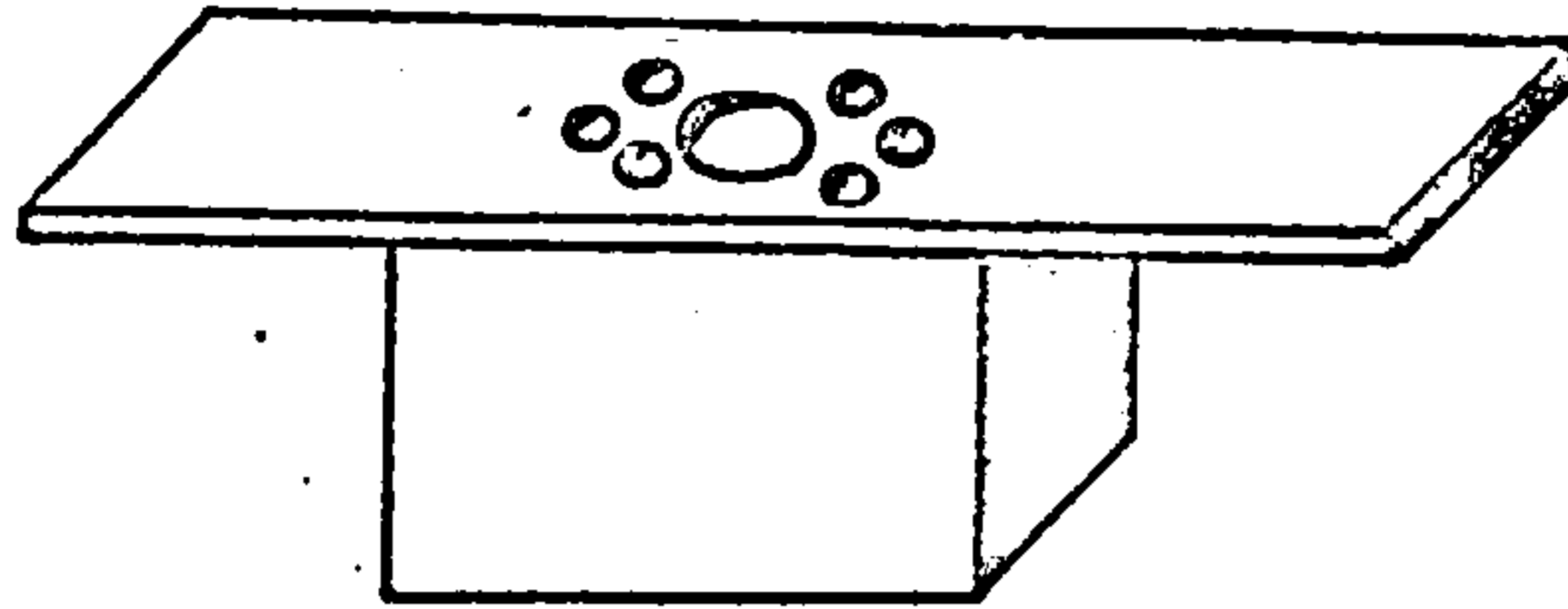
Dielectric

Counter
electrode

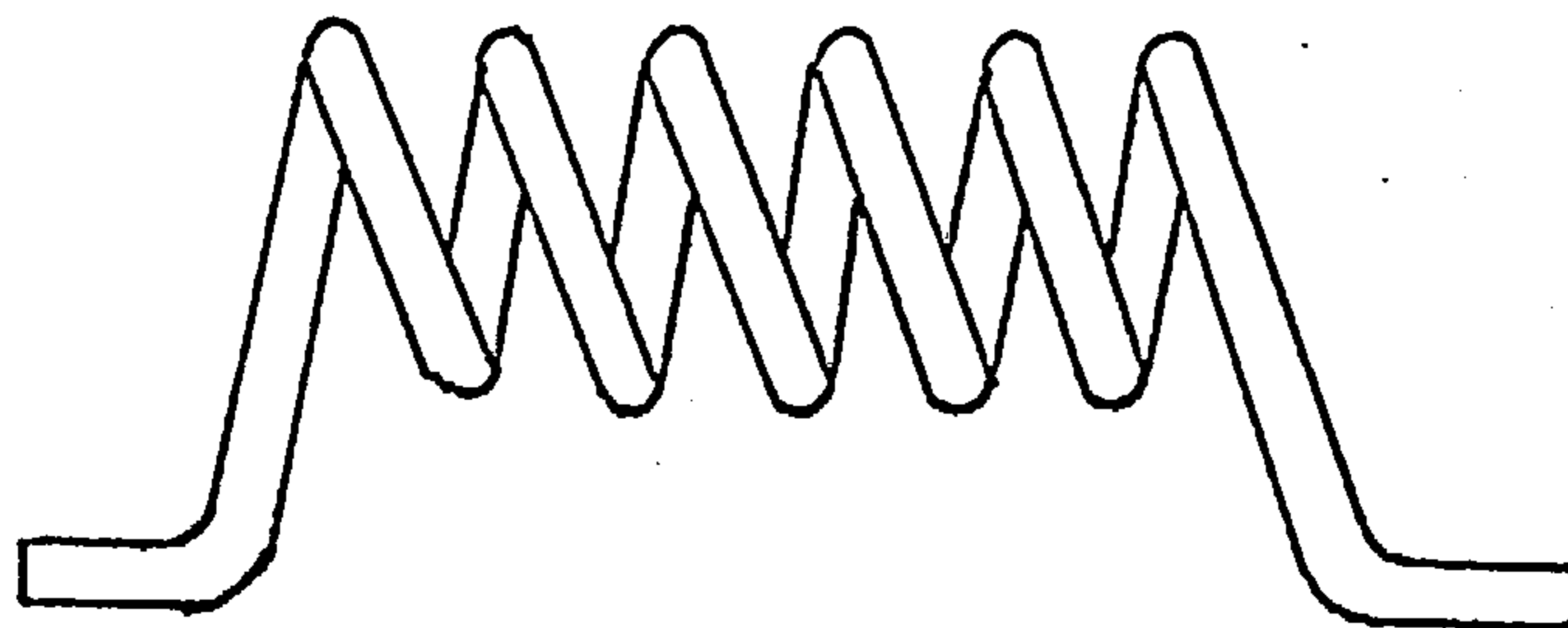
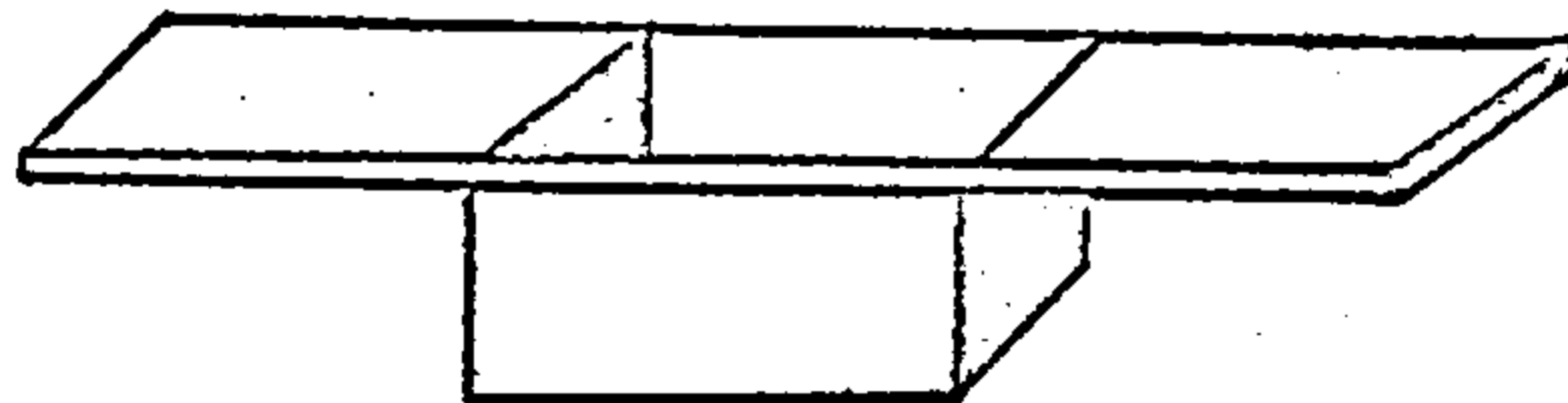
Fig. 9 : Masks used for Triode Systems



a) Molybdenum, or tantalum boats
for SiO_2 and B_2O_3 ,



b) for Au, Ag, and Cu



c) Tungsten spiral for Al

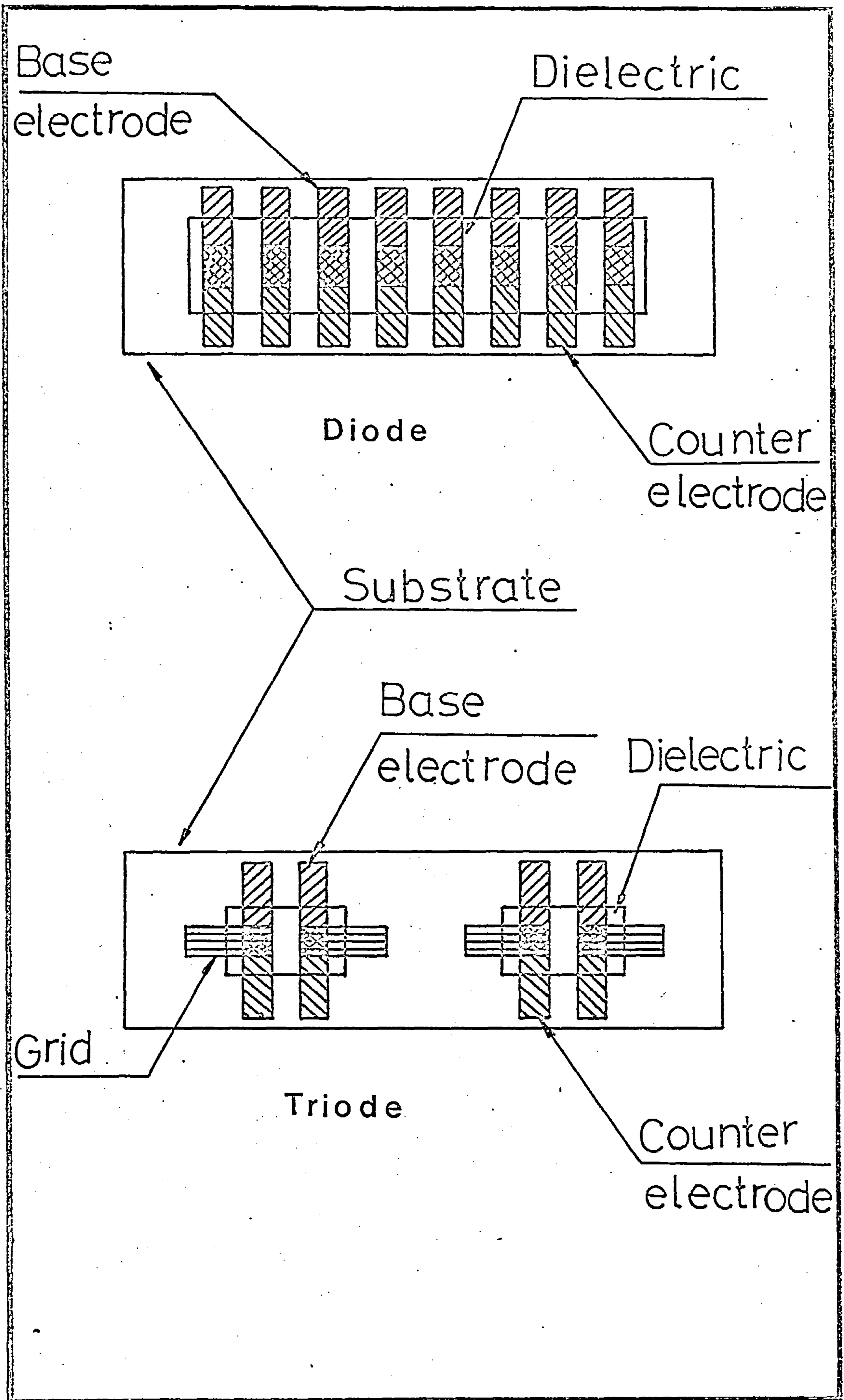
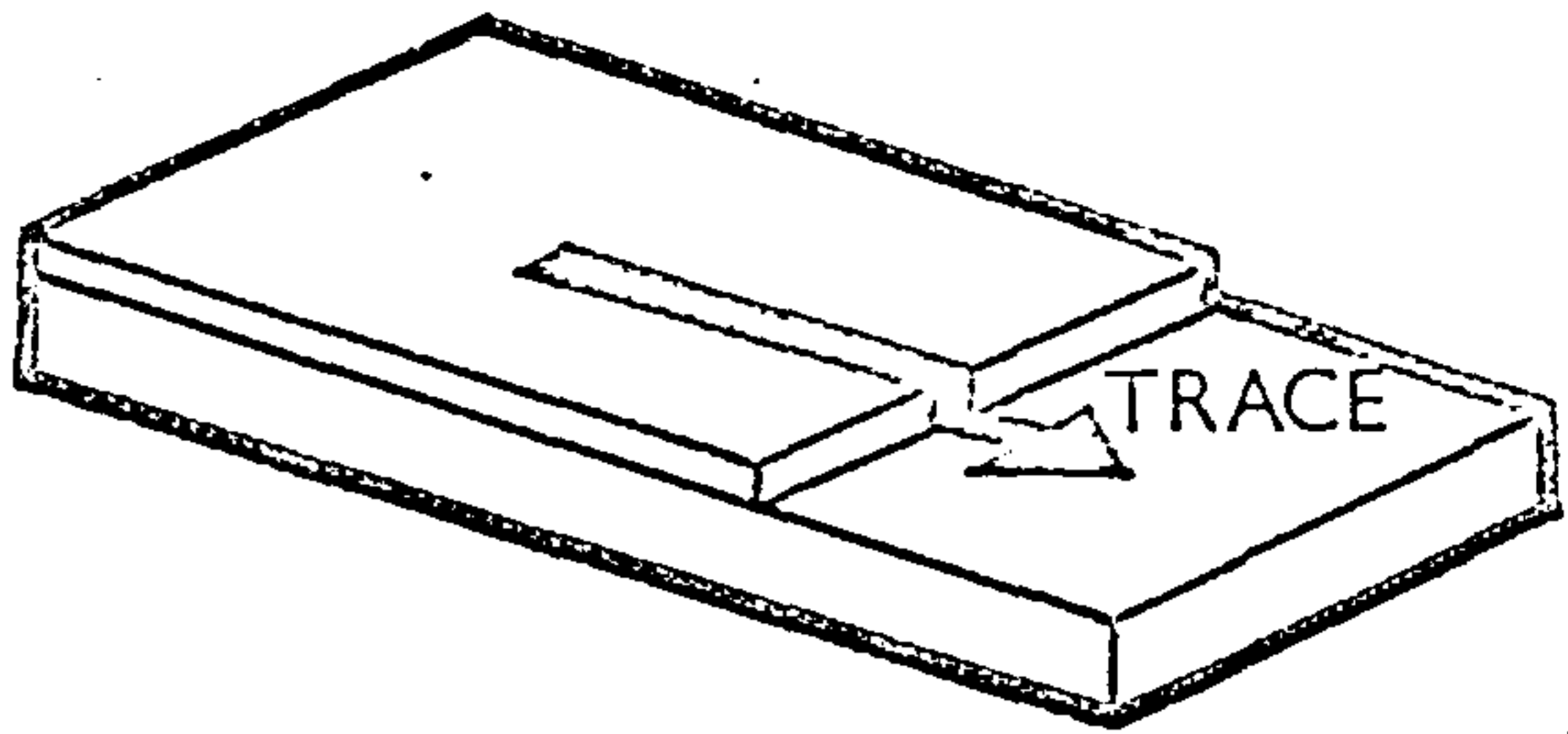
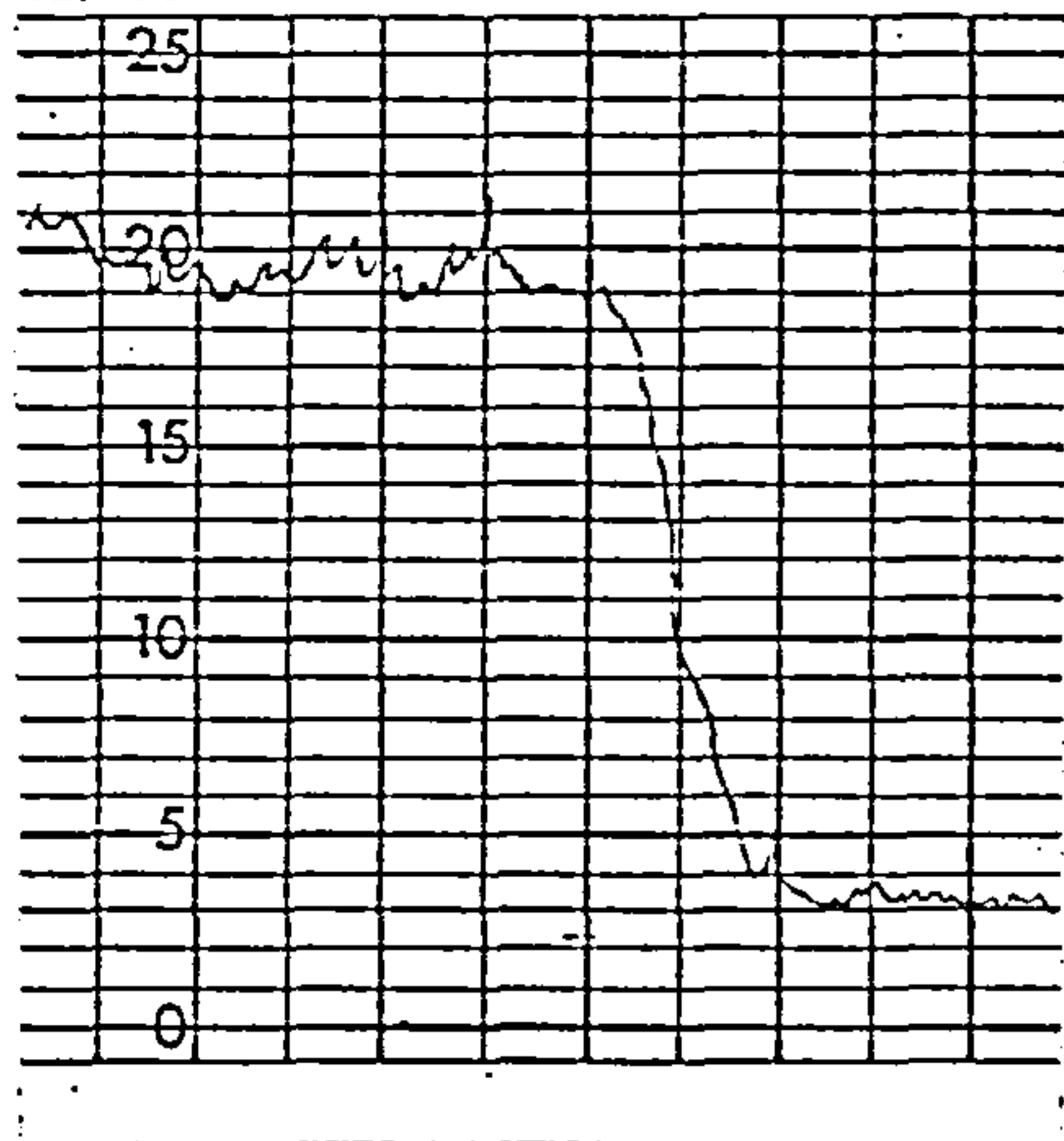


Figure 11. Device arrangement a) diode b) triode

112/338



Silver deposit on glass substrate. Step left by removal of masking. Graph details:
Vertical Magnification $\times 1\,000\,000$
1 Small Division = 20 angstroms
Horizontal Magnification $\times 200$
1 Small Division = 0,025 mm
Thickness of deposit measured between mean lines = approximately 300 angstroms (30 mm on chart)

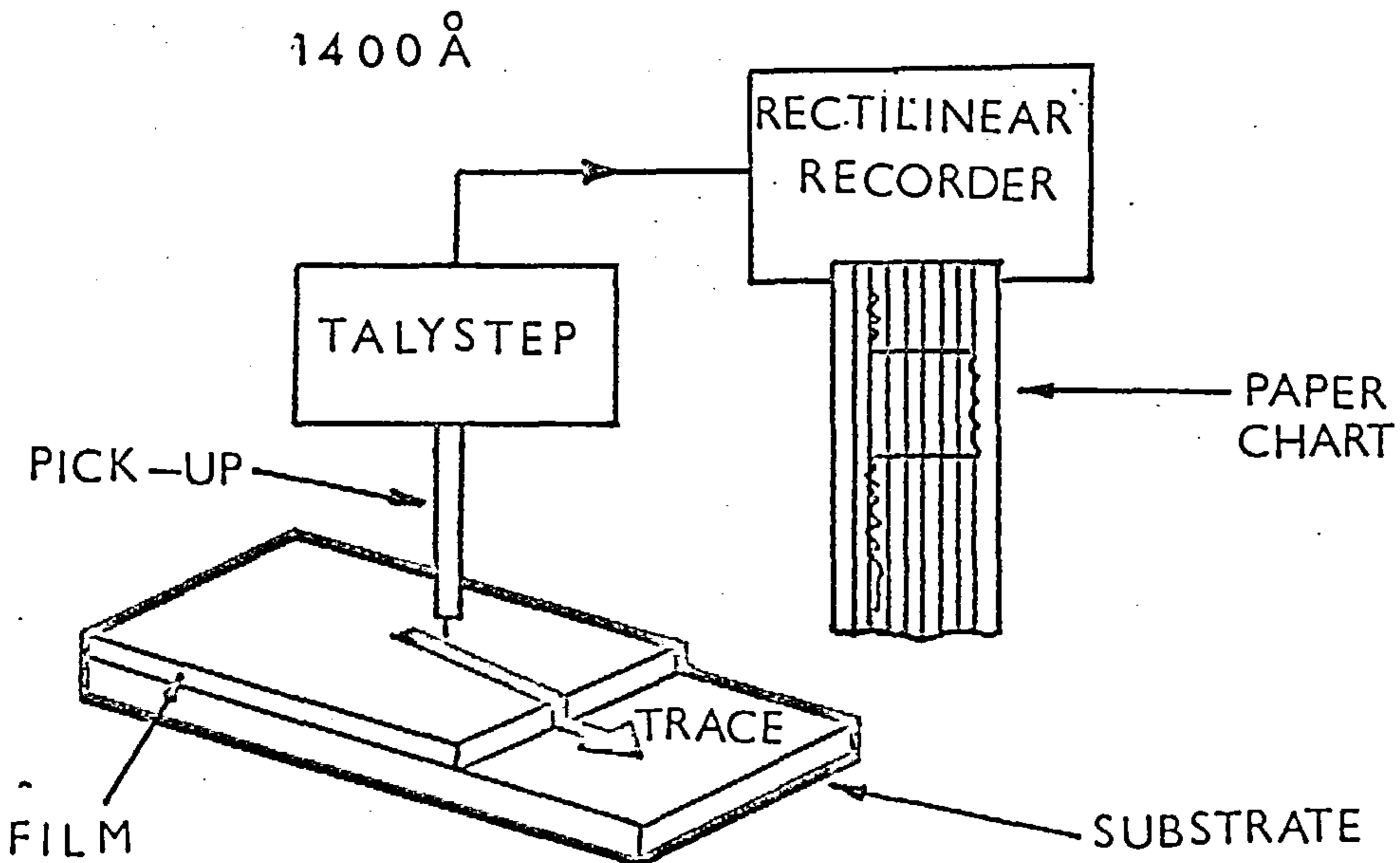
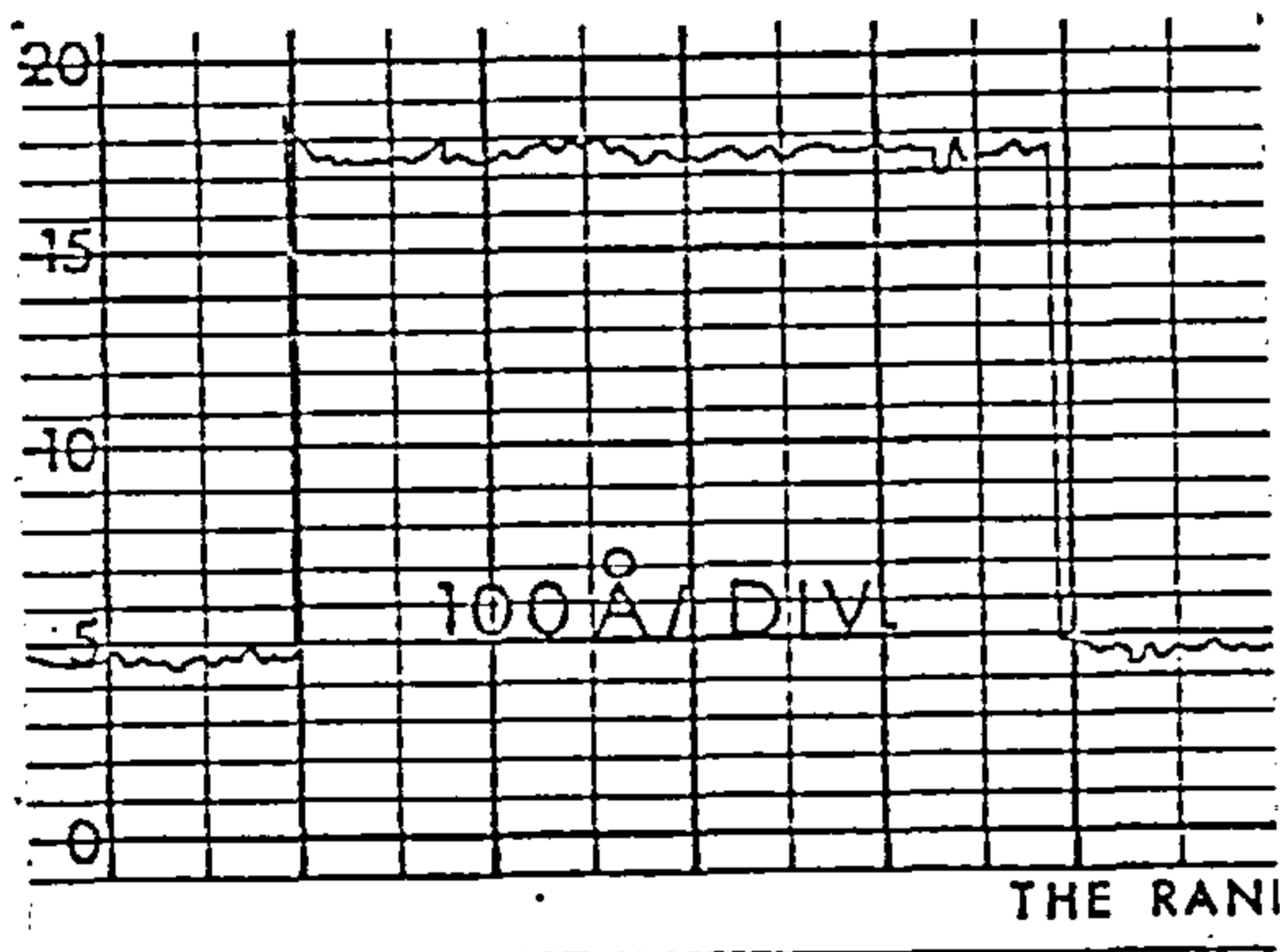


Figure 12. Typical Talystep traces and schematic diagram of the instrument.

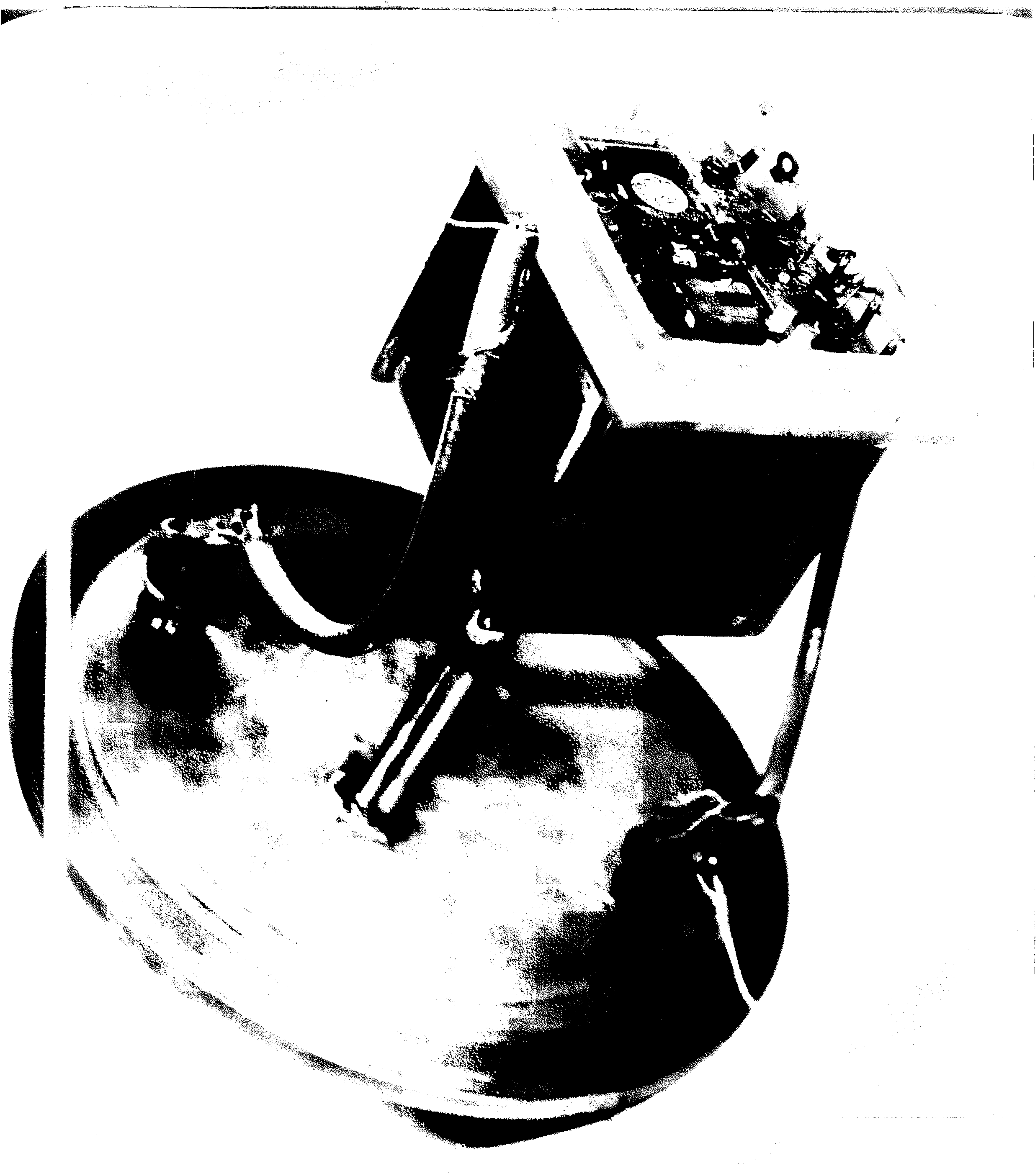


Fig. 13

Cooling part of the test
system

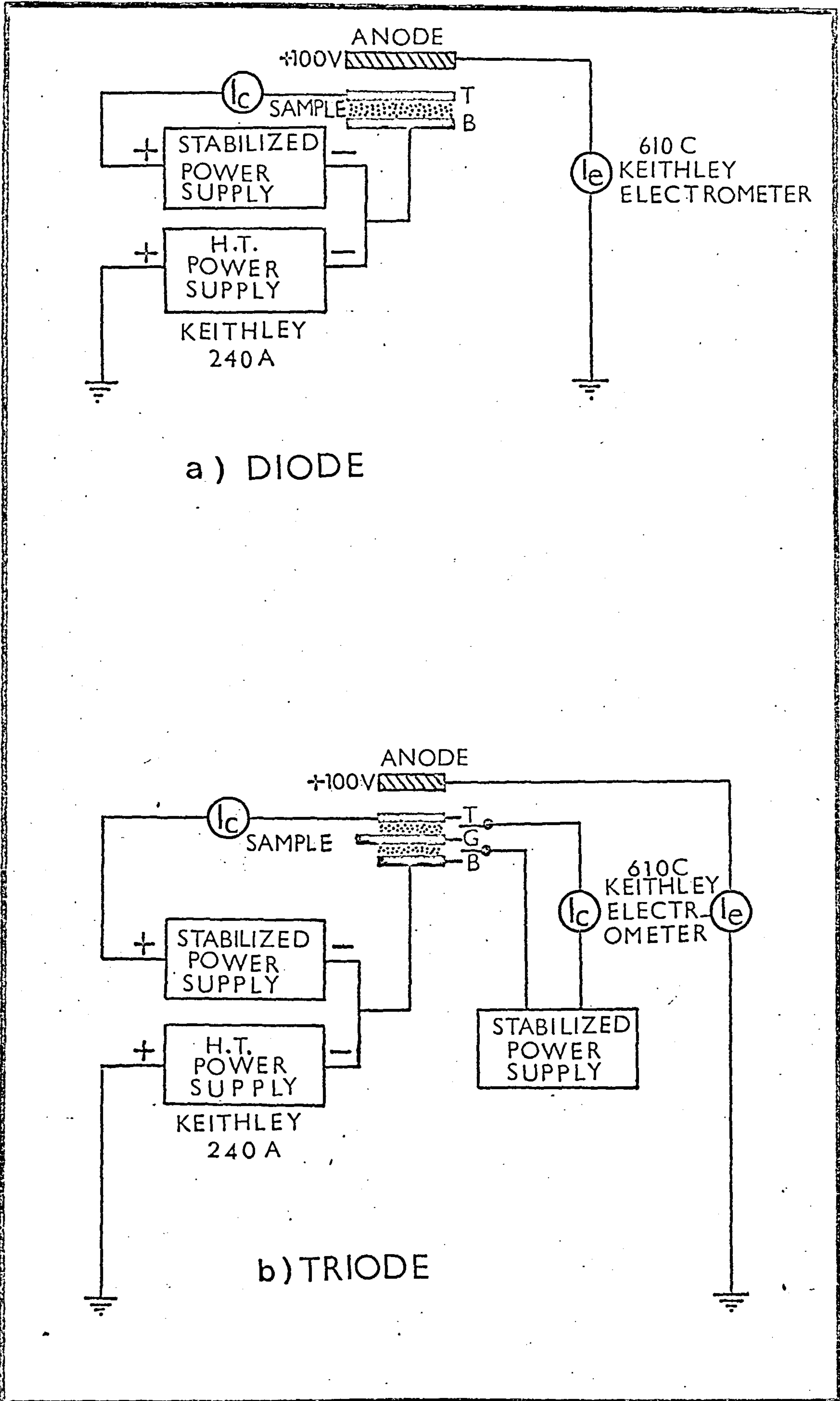


Figure 14. Circuit for electrical measurements a) diode
b) triode.

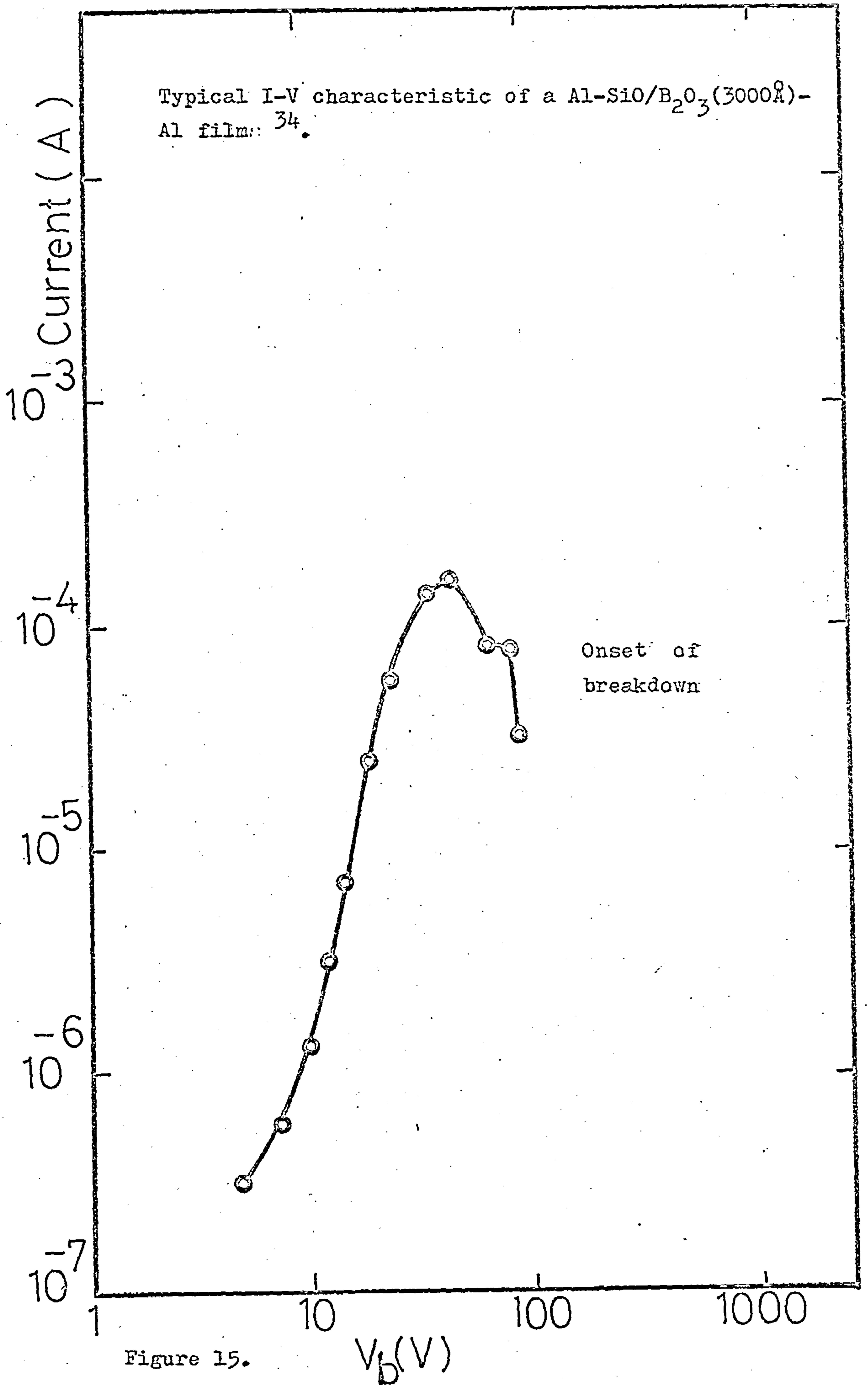
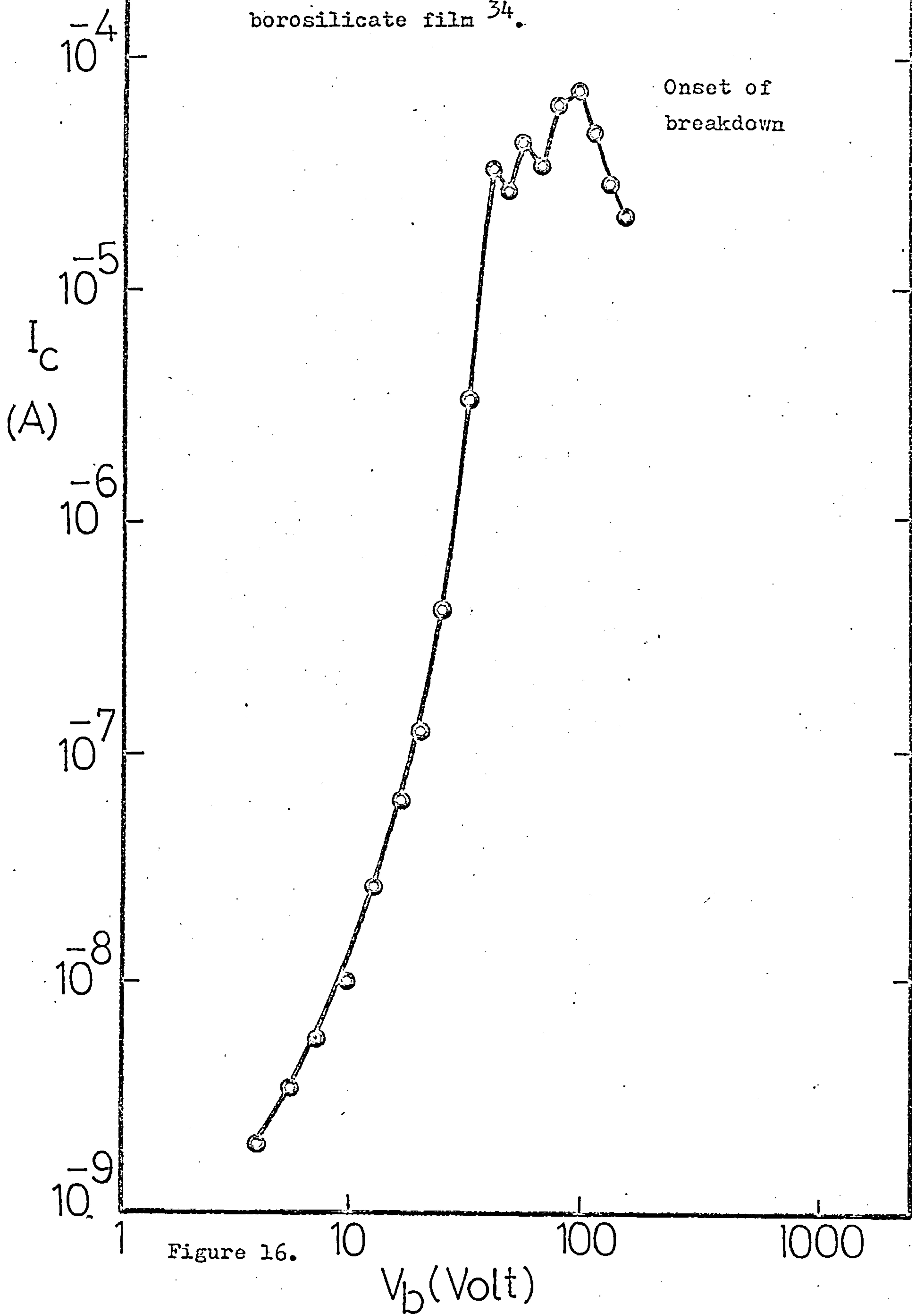


Figure 15.

V_b(V)

Current-voltage characteristic of a 6000Å borosilicate film ³⁴.



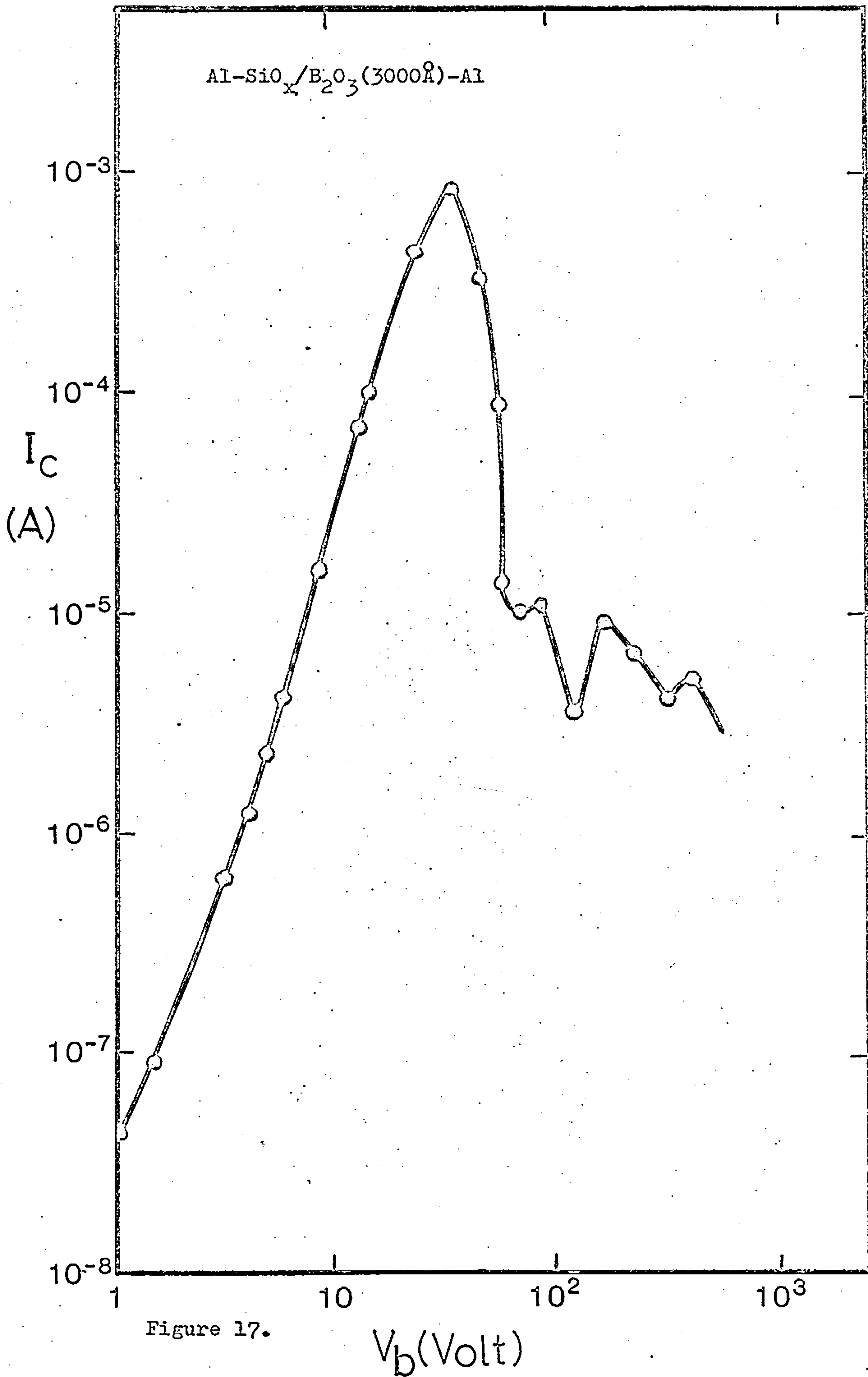


Figure 17.

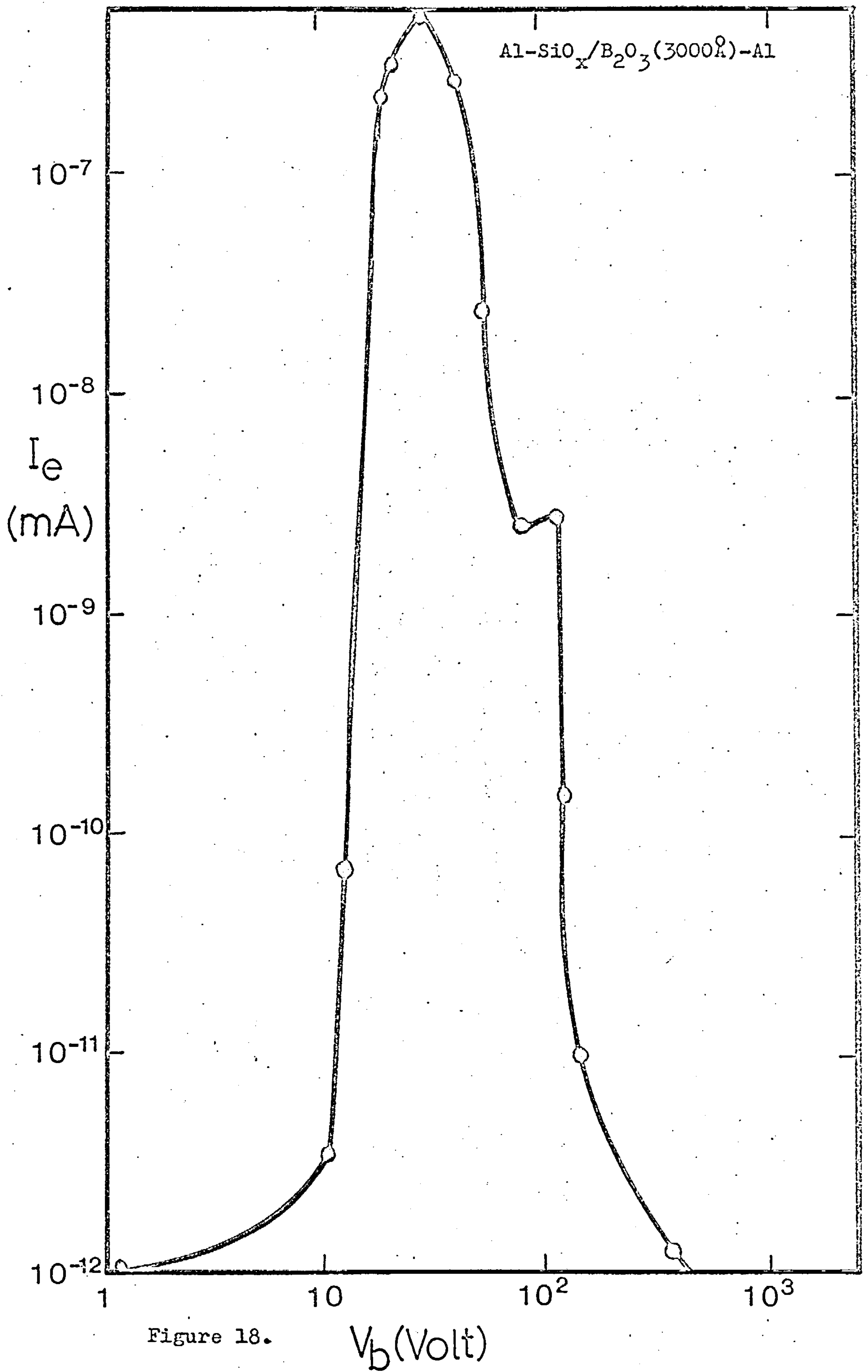


Figure 18.

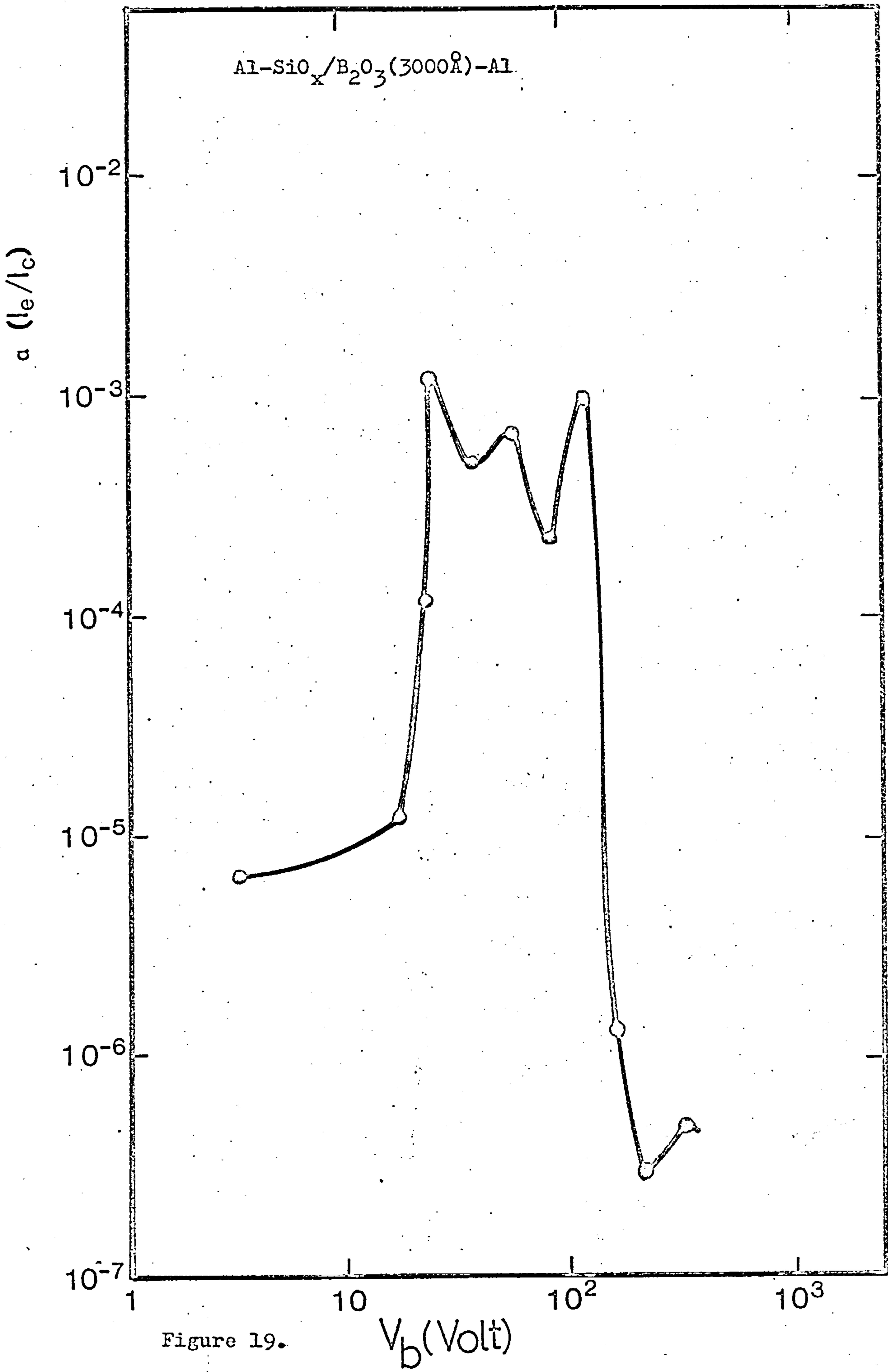
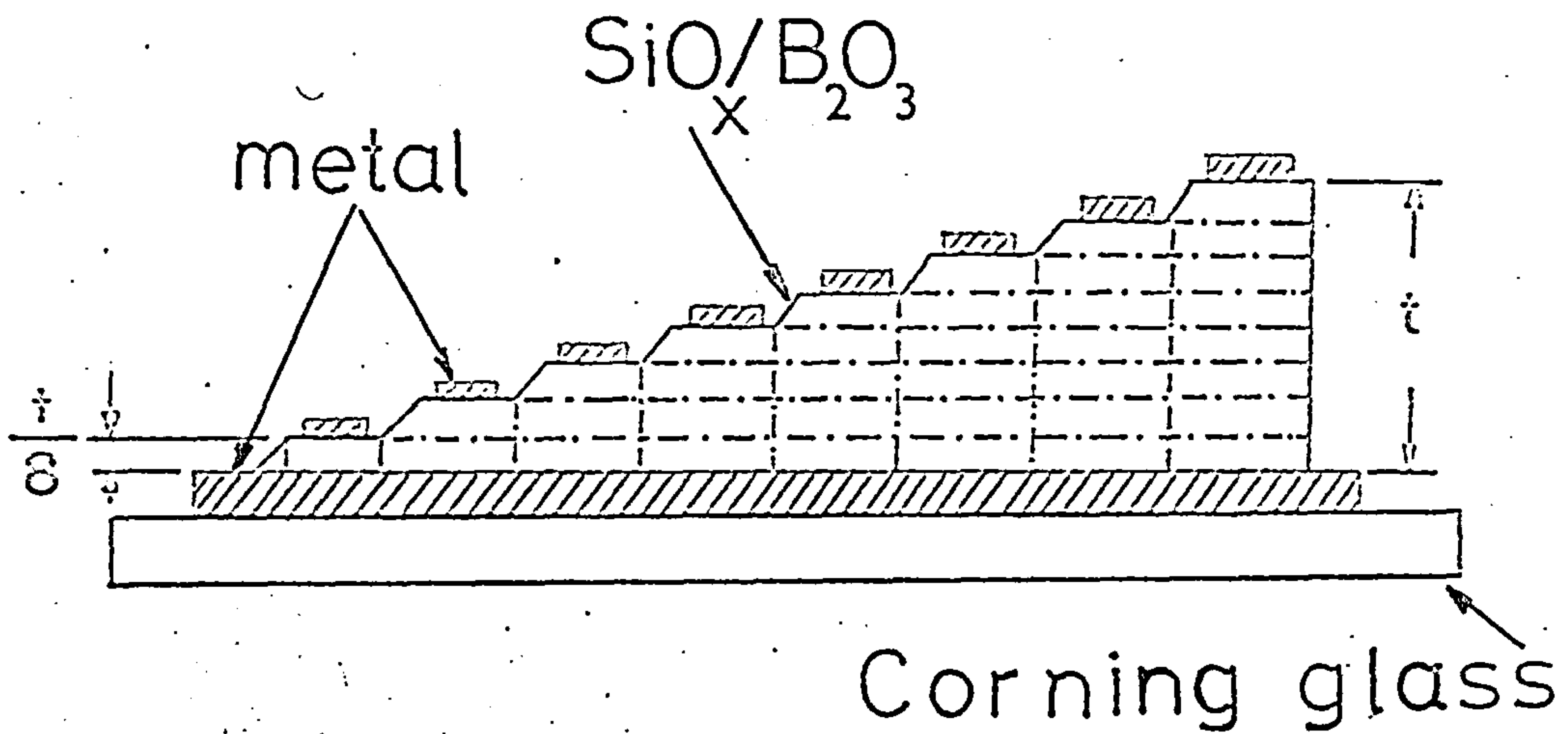
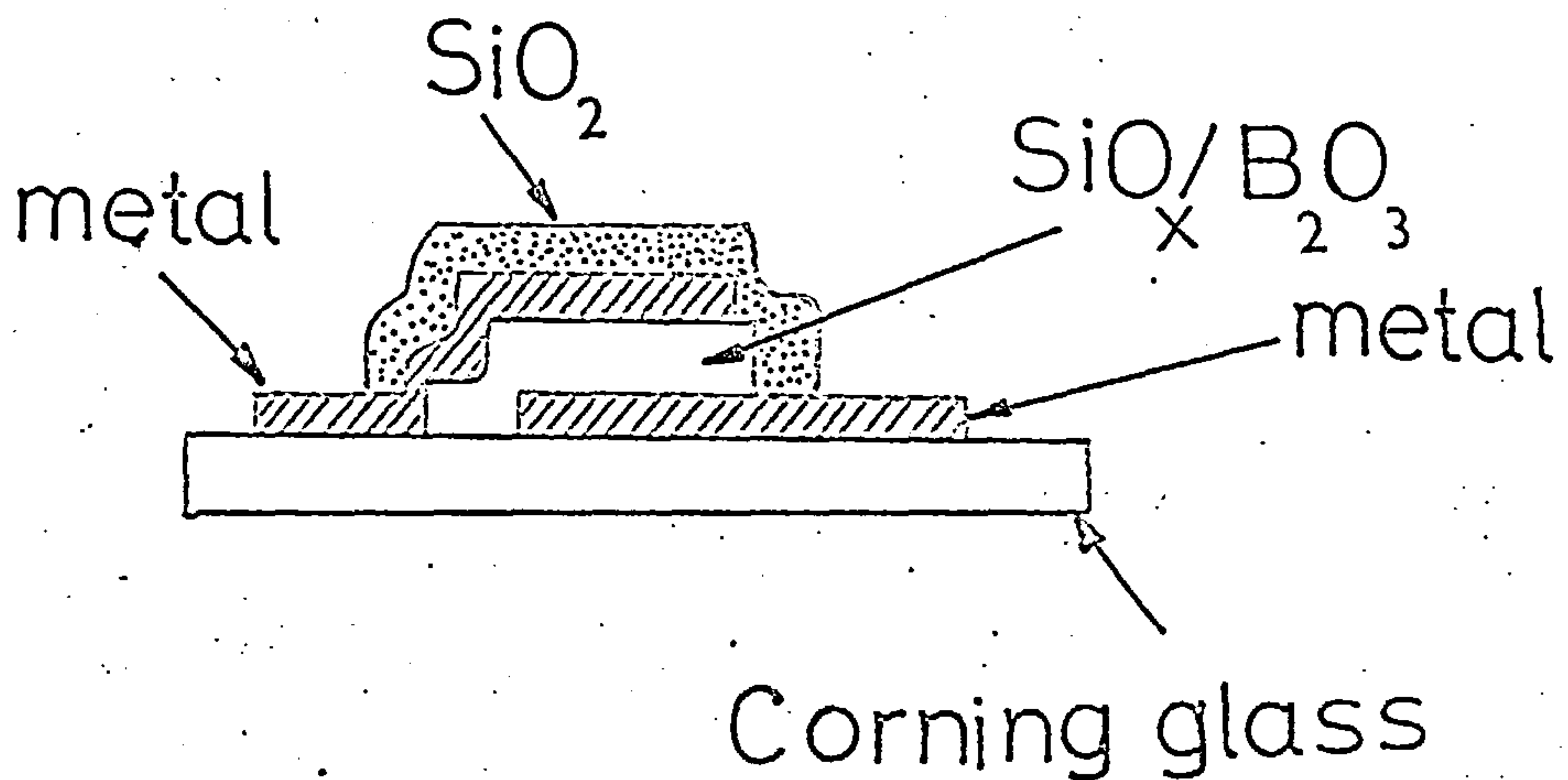


Figure 19.

V_b (Volt)



a) Vertical section of specimen used to determine thickness variation of circulating current (t is insulator thickness).



b) Vertical section of specimen protected by silica layer.

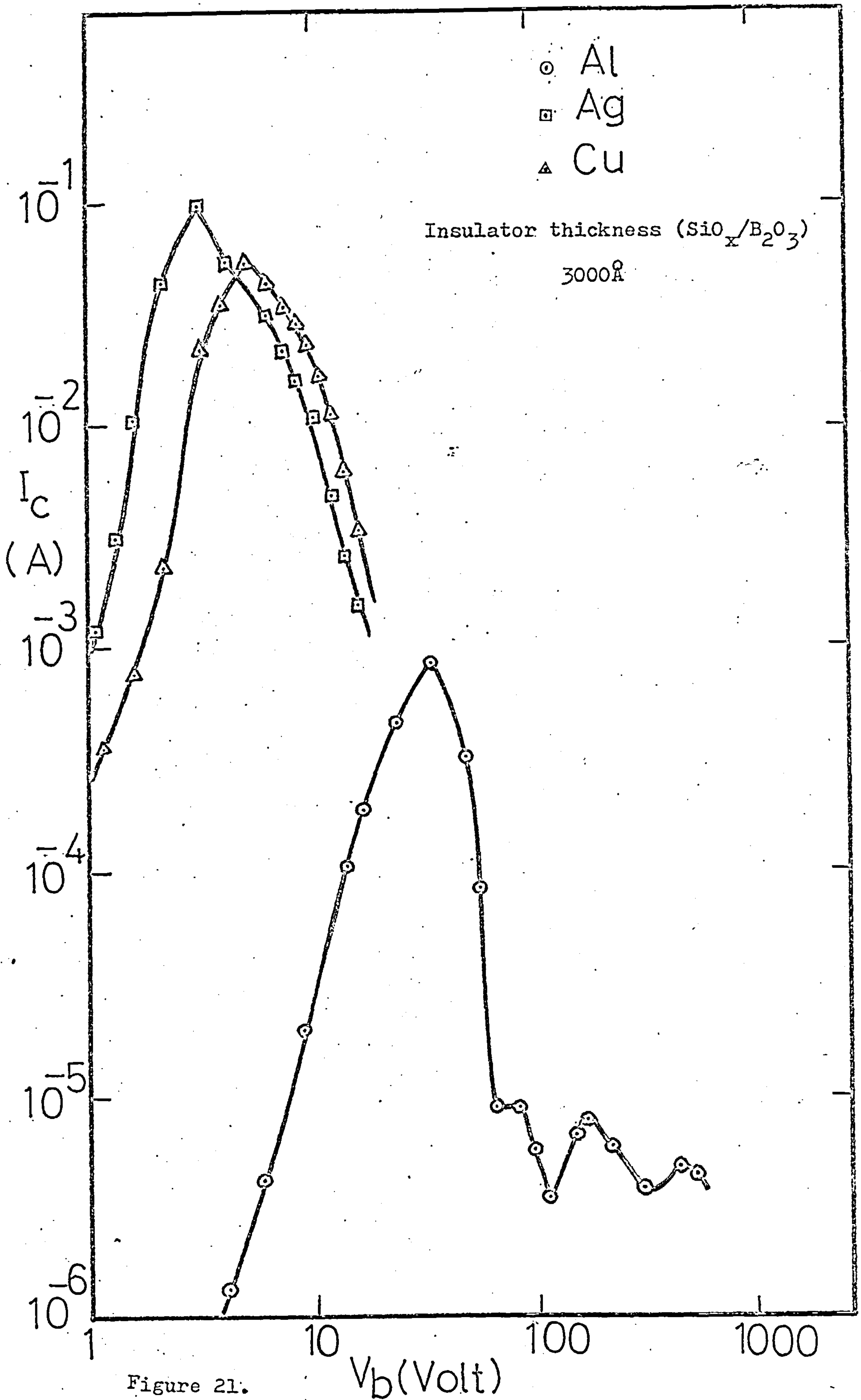


Figure 21.

Al-SiO_x/B₂O₃-Al

- 1 ○ 3000 Å
- 2 △ 5000 Å
- 3 □ 7000 Å
- 4 ○ 10000 Å
- 5 △ 12000 Å
- 6 □ 15000 Å

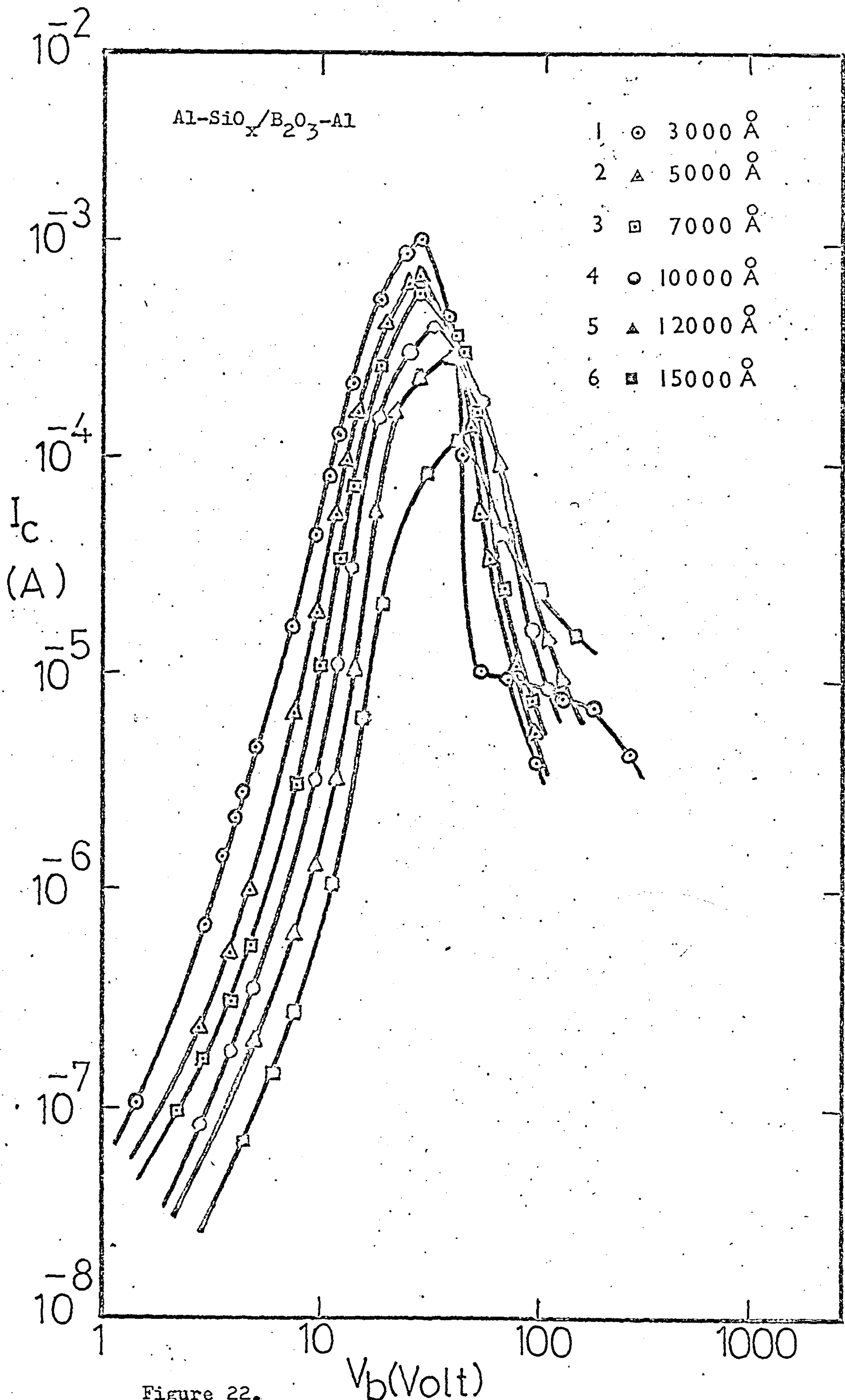


Figure 22.

V_b (Volt)

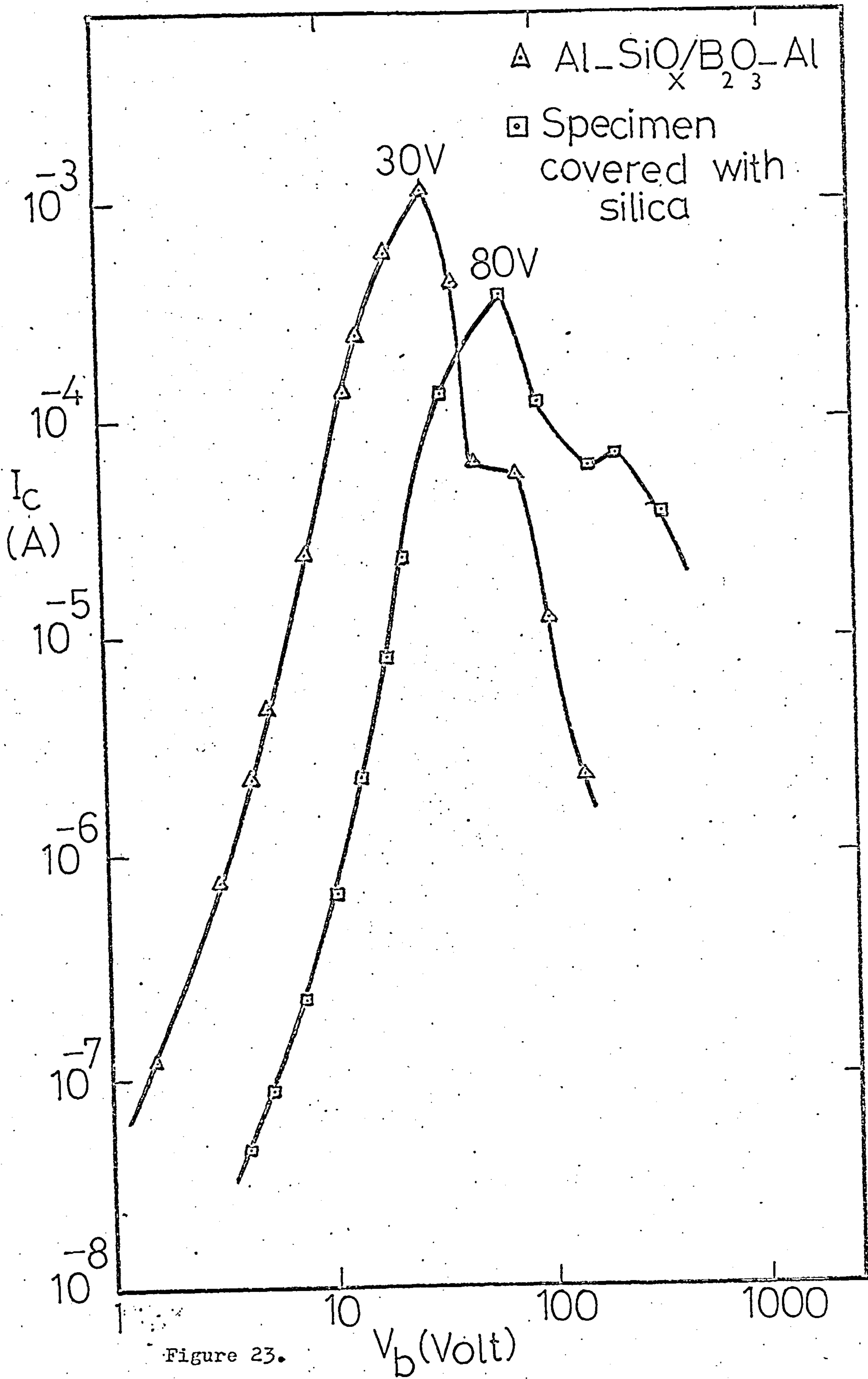


Figure 23.

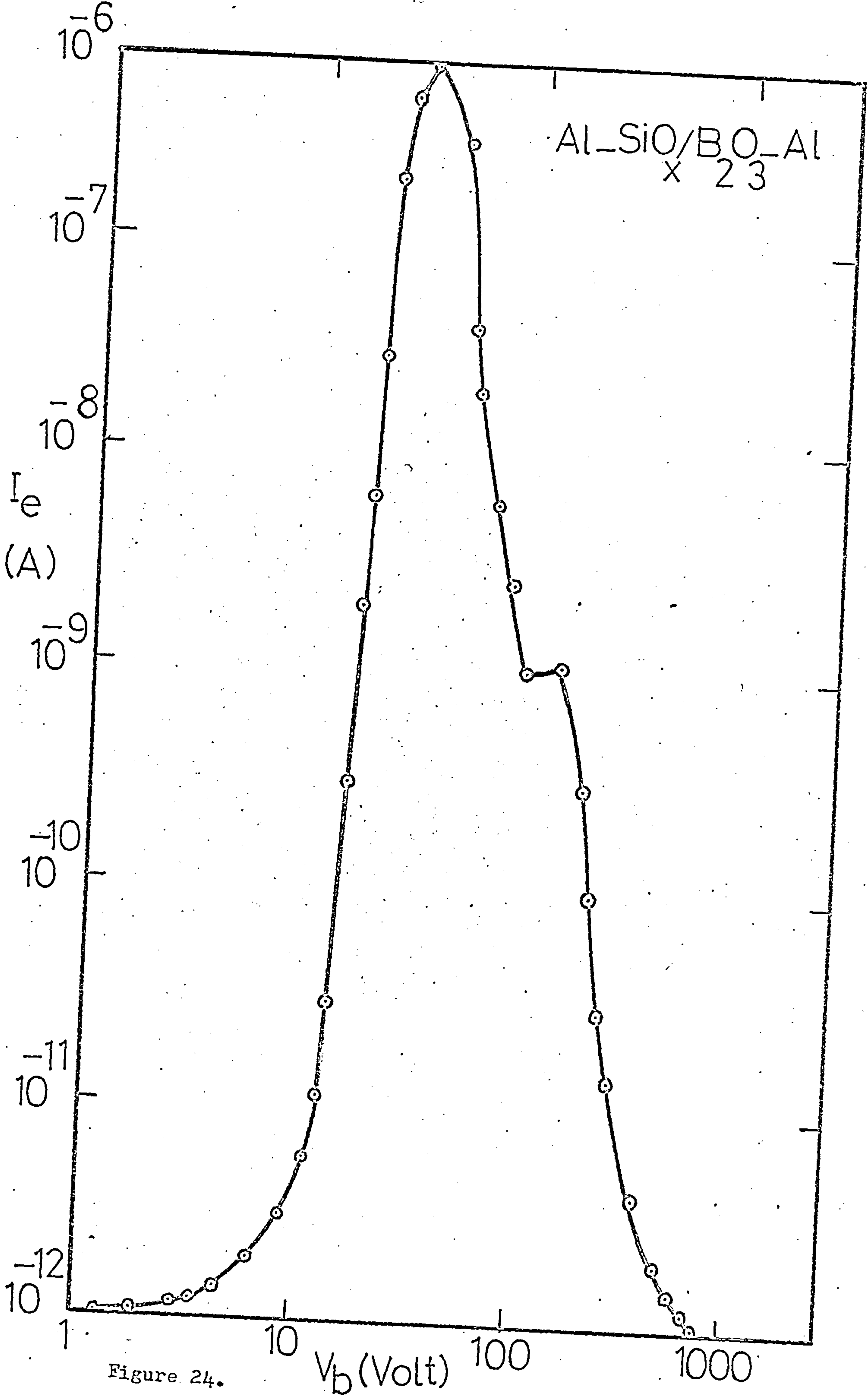


Figure 24.

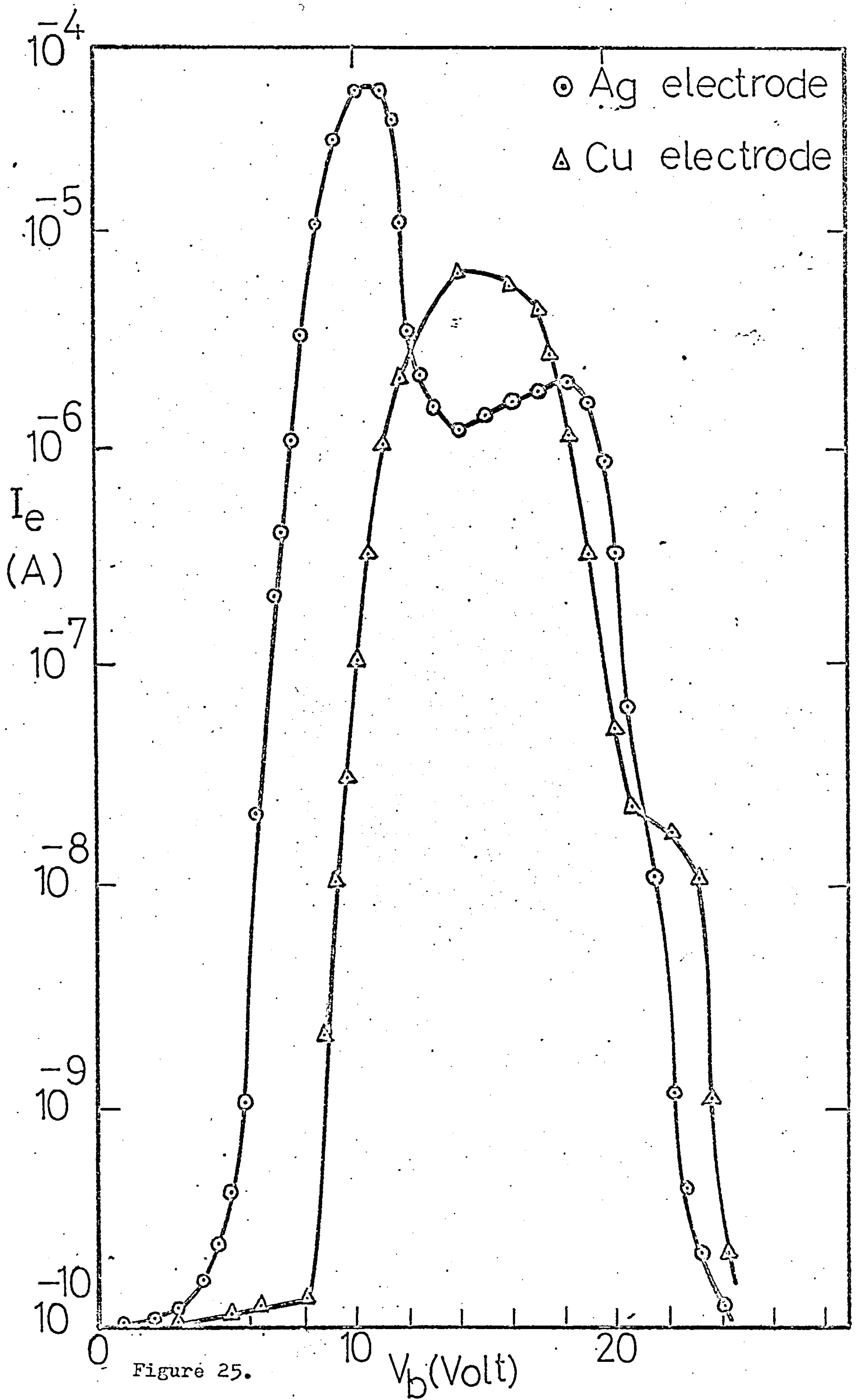


Figure 25.

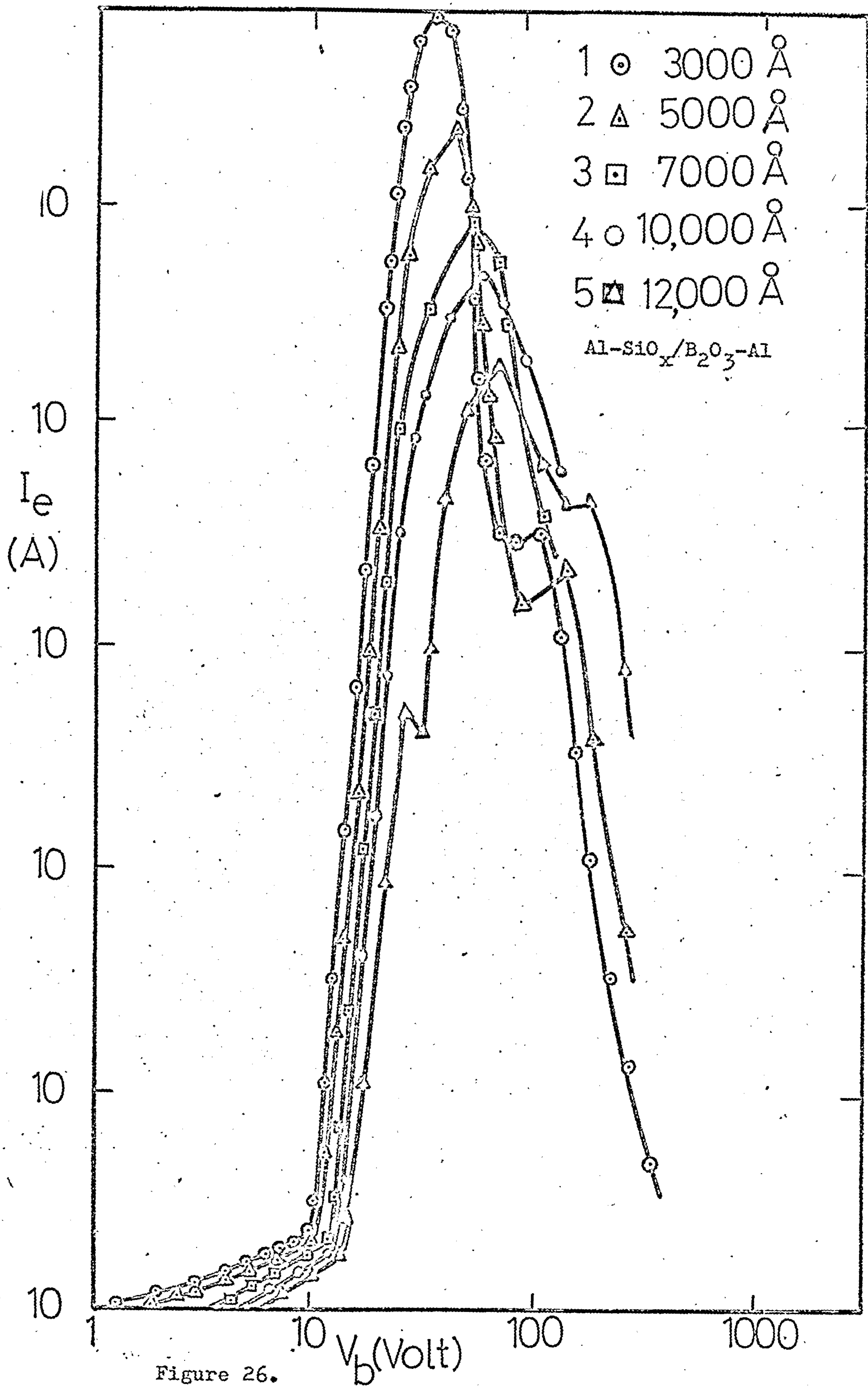


Figure 26.

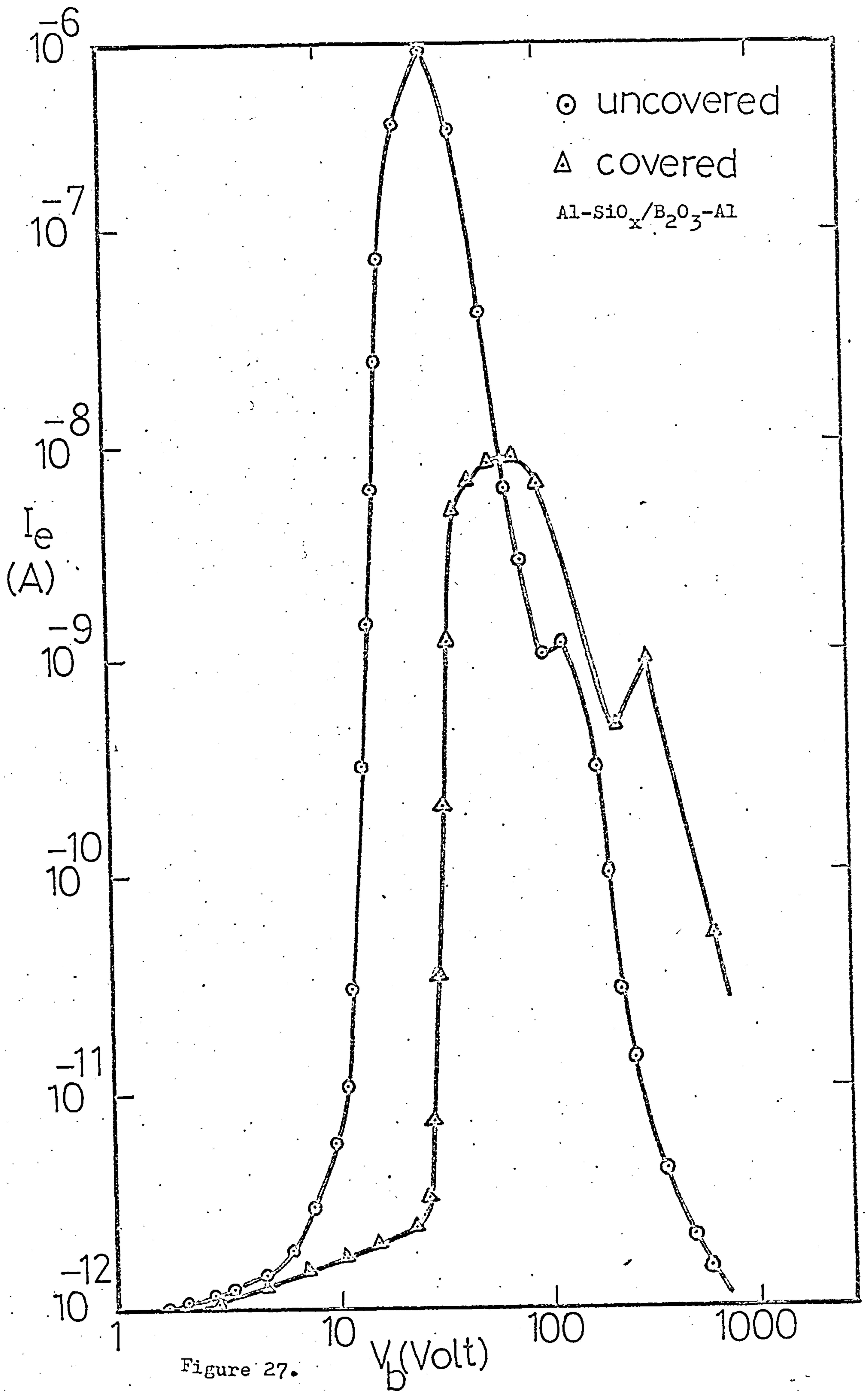


Figure 27.

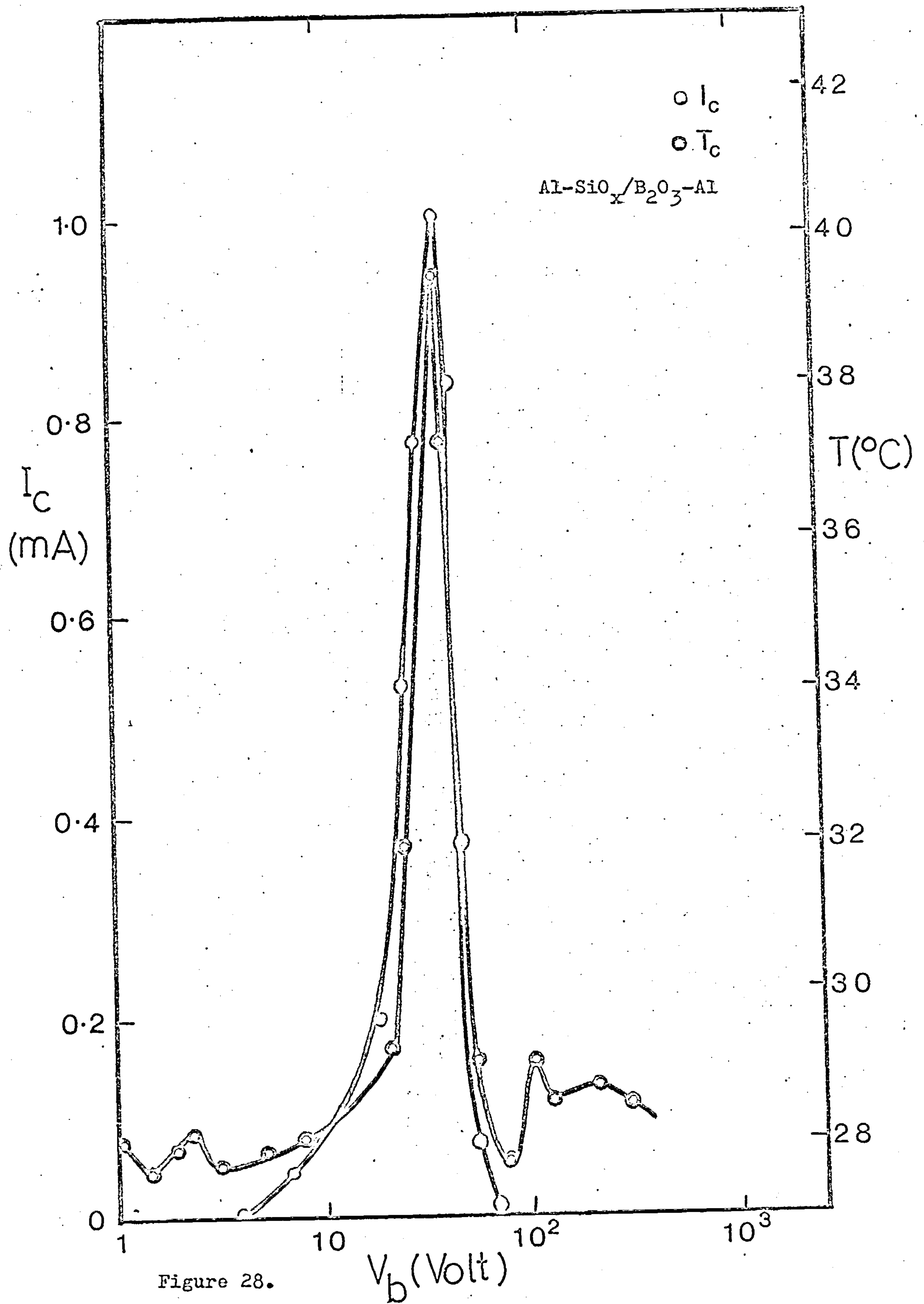


Figure 28.

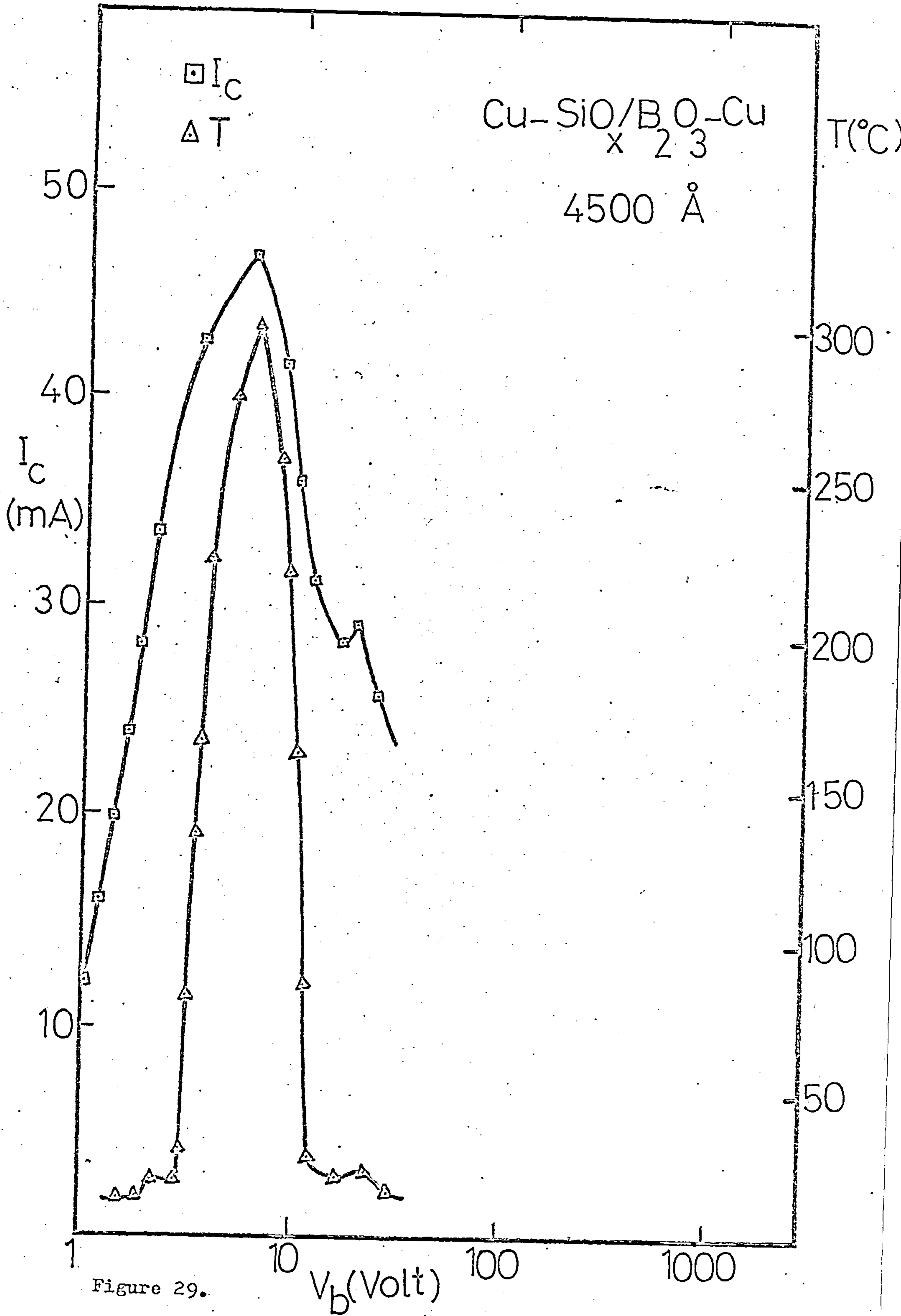


Figure 29.

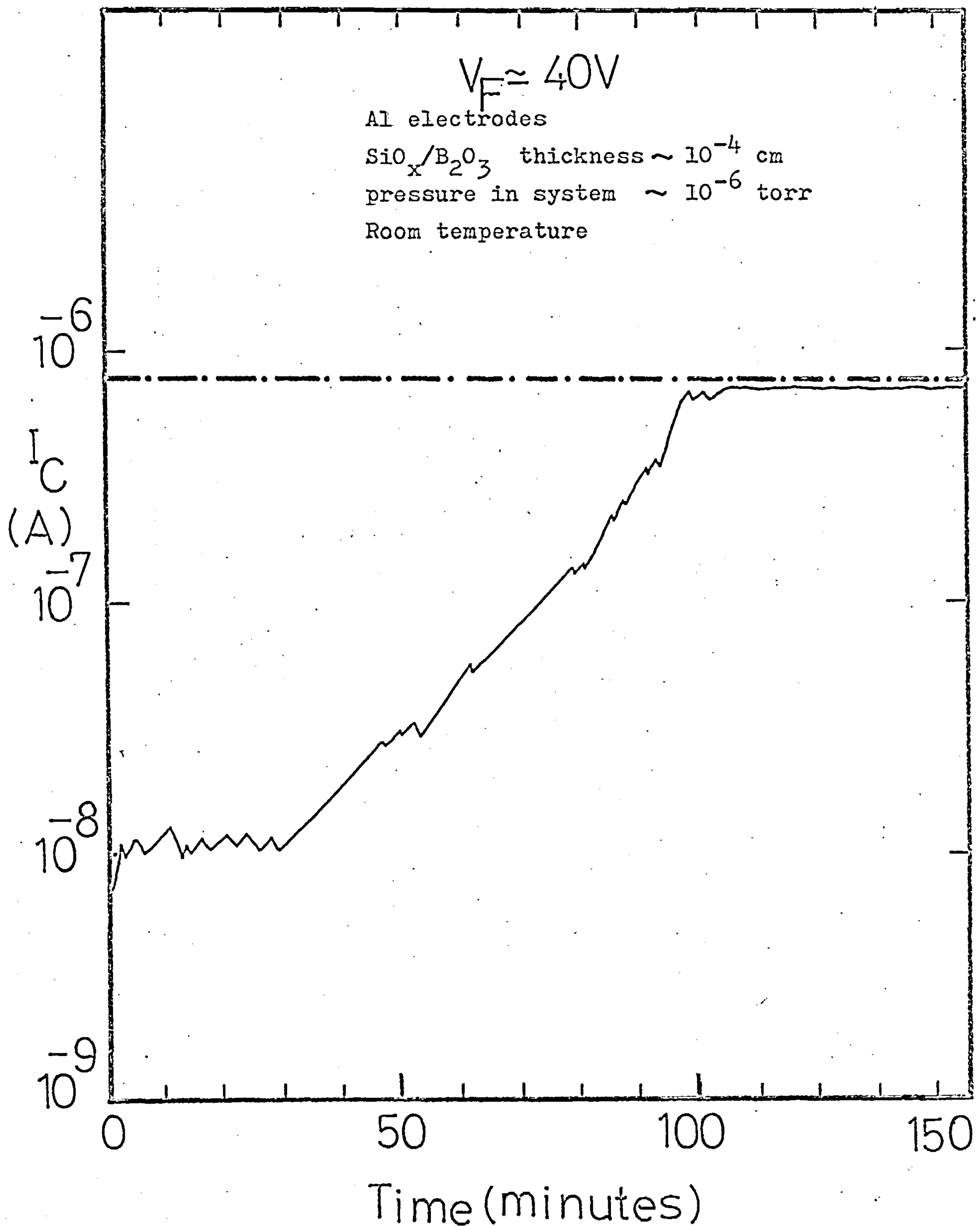


Figure 30. Variation with time of the circulating current for the initial application of forming voltage.

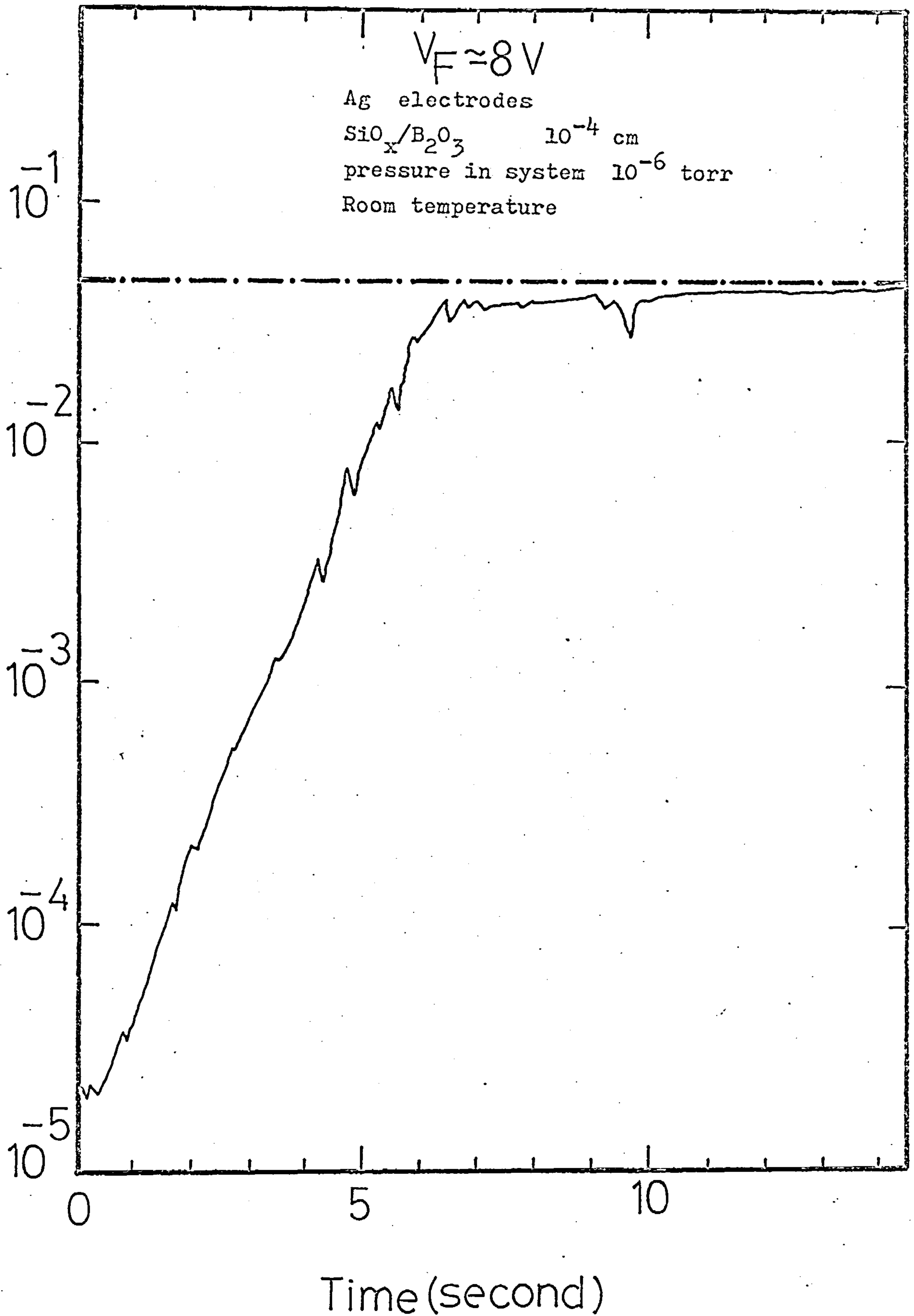


Figure 31. Variation with time of the circulating current for the initial application of forming voltage.

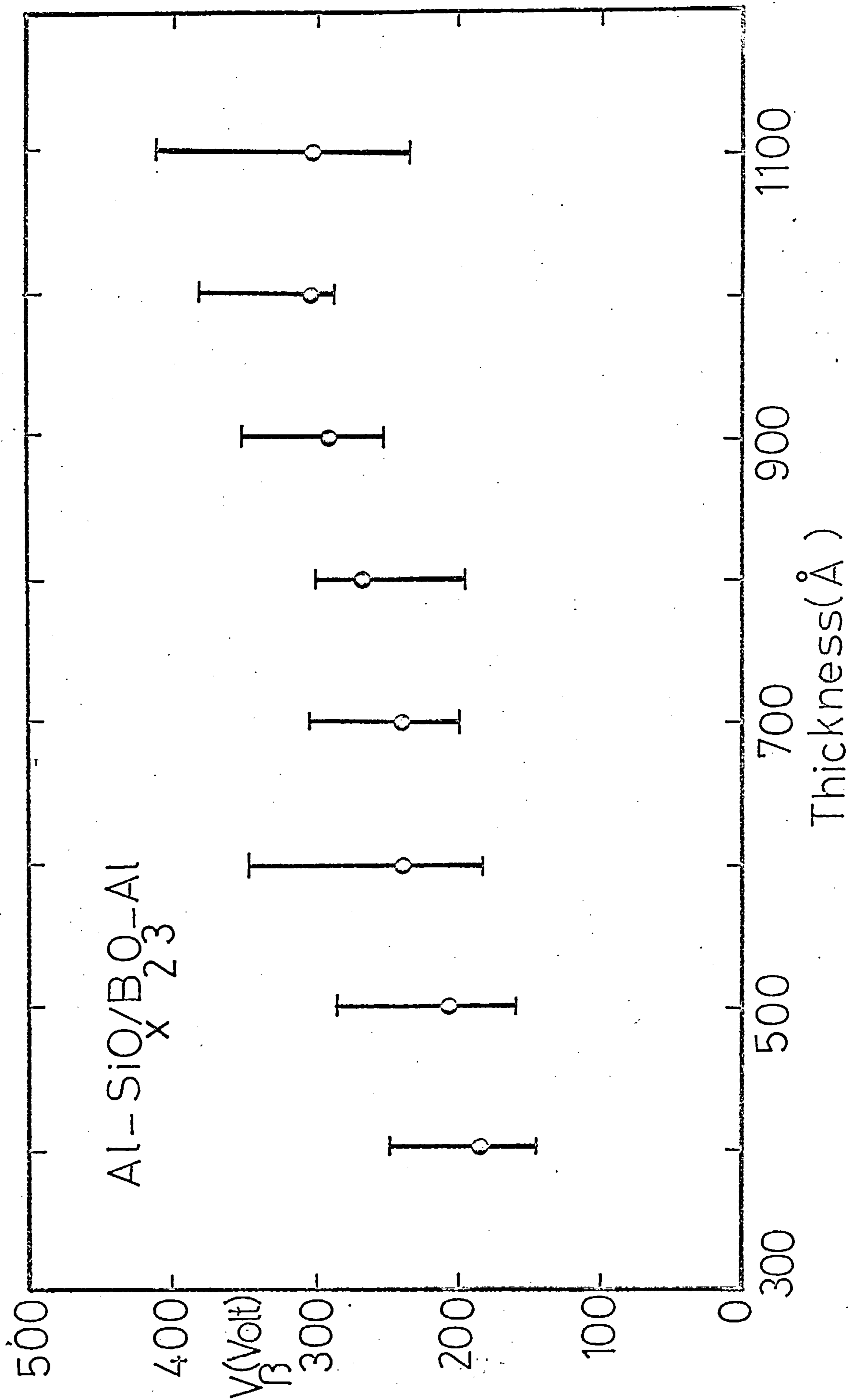


Figure 32. Dependence of V_B on insulator thickness.

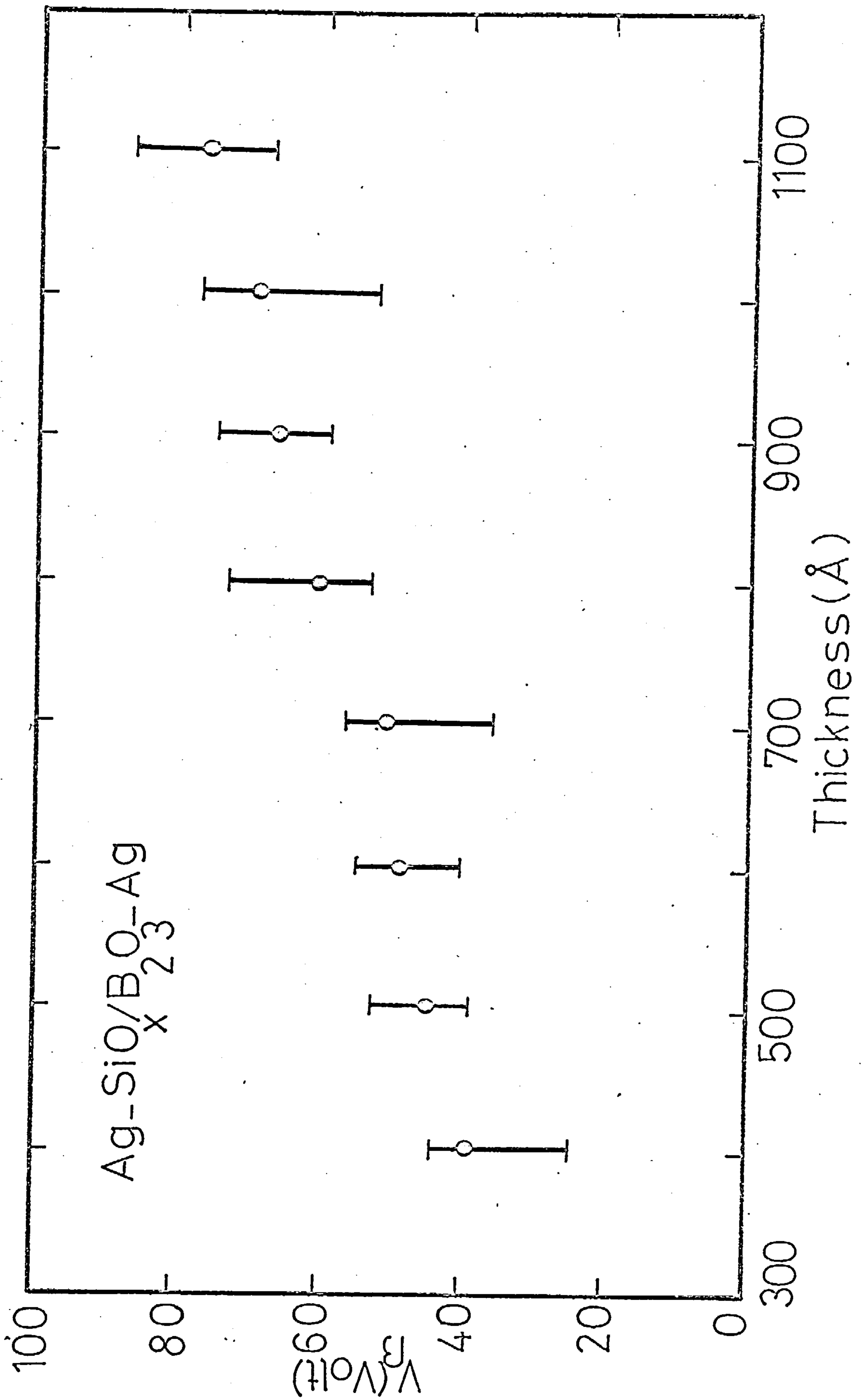


Figure 33. Dependence of V_B on insulator thickness.

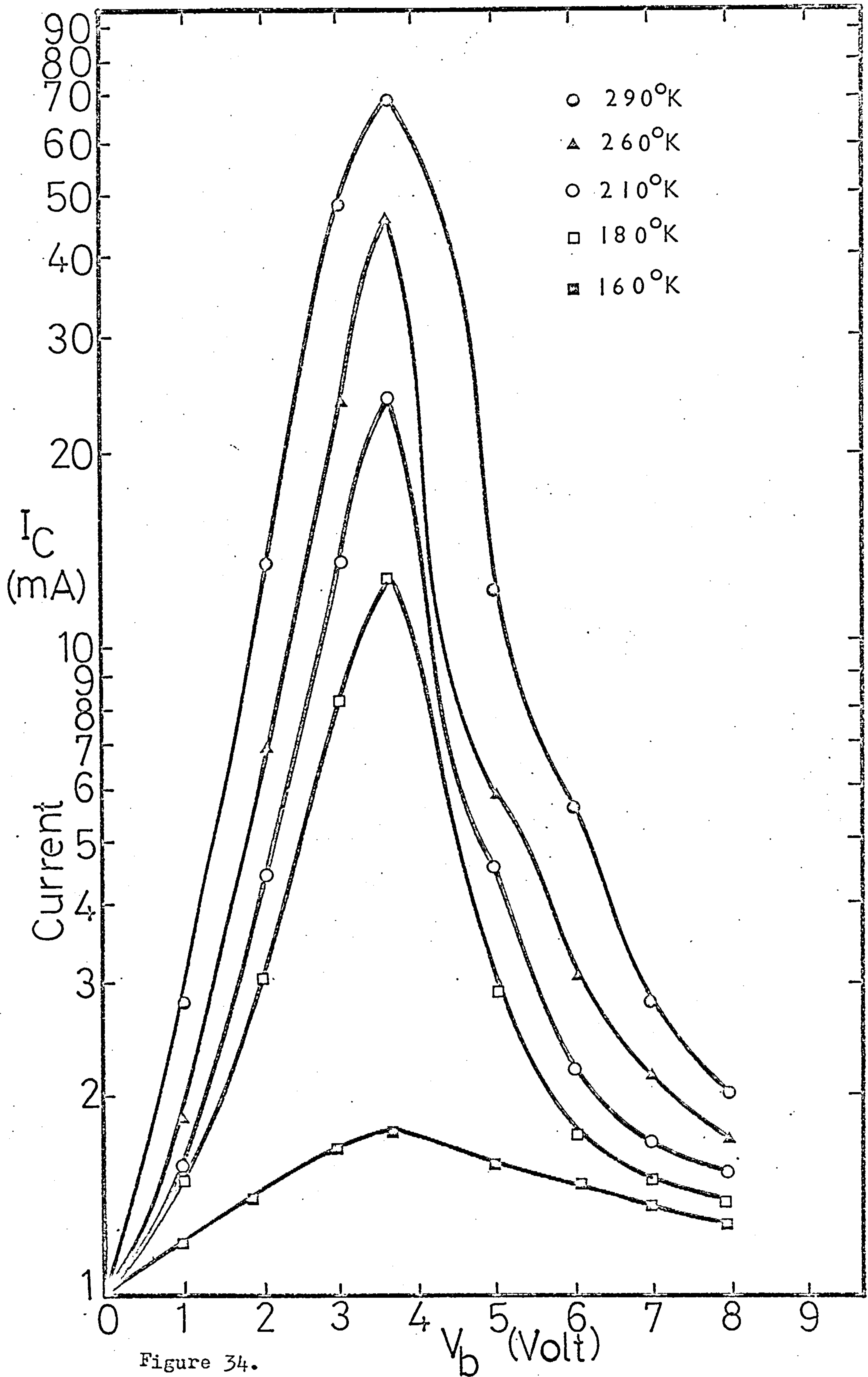
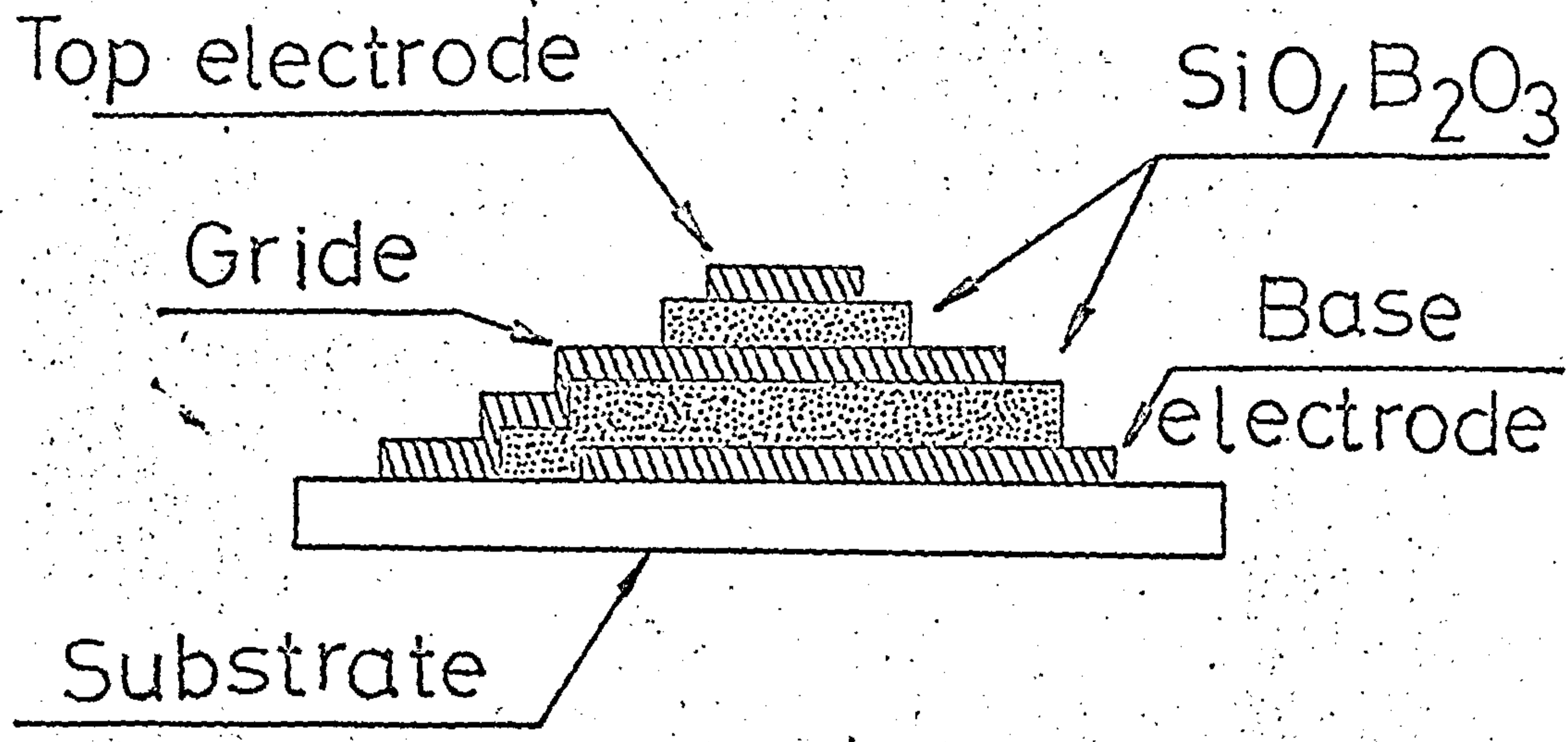
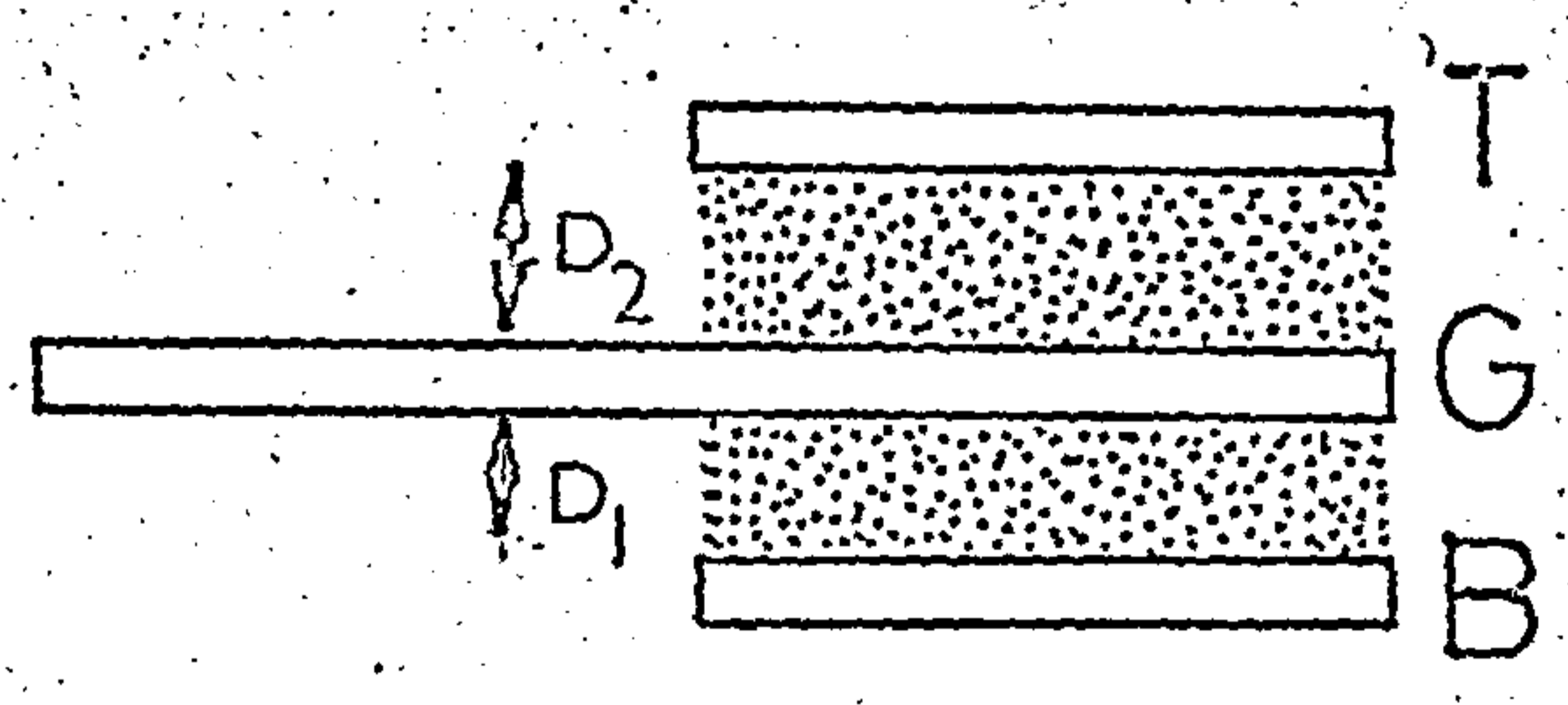


Figure 34.

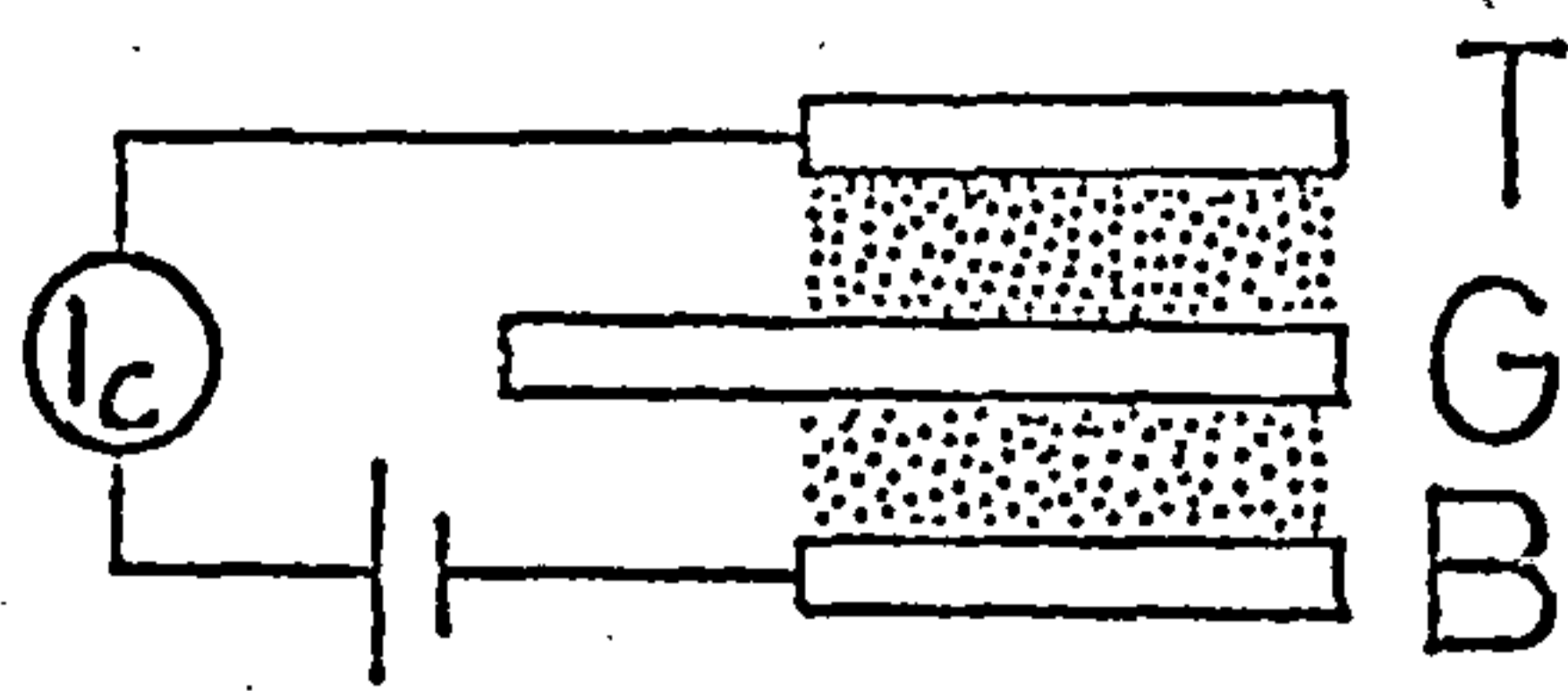


a) Triode configuration

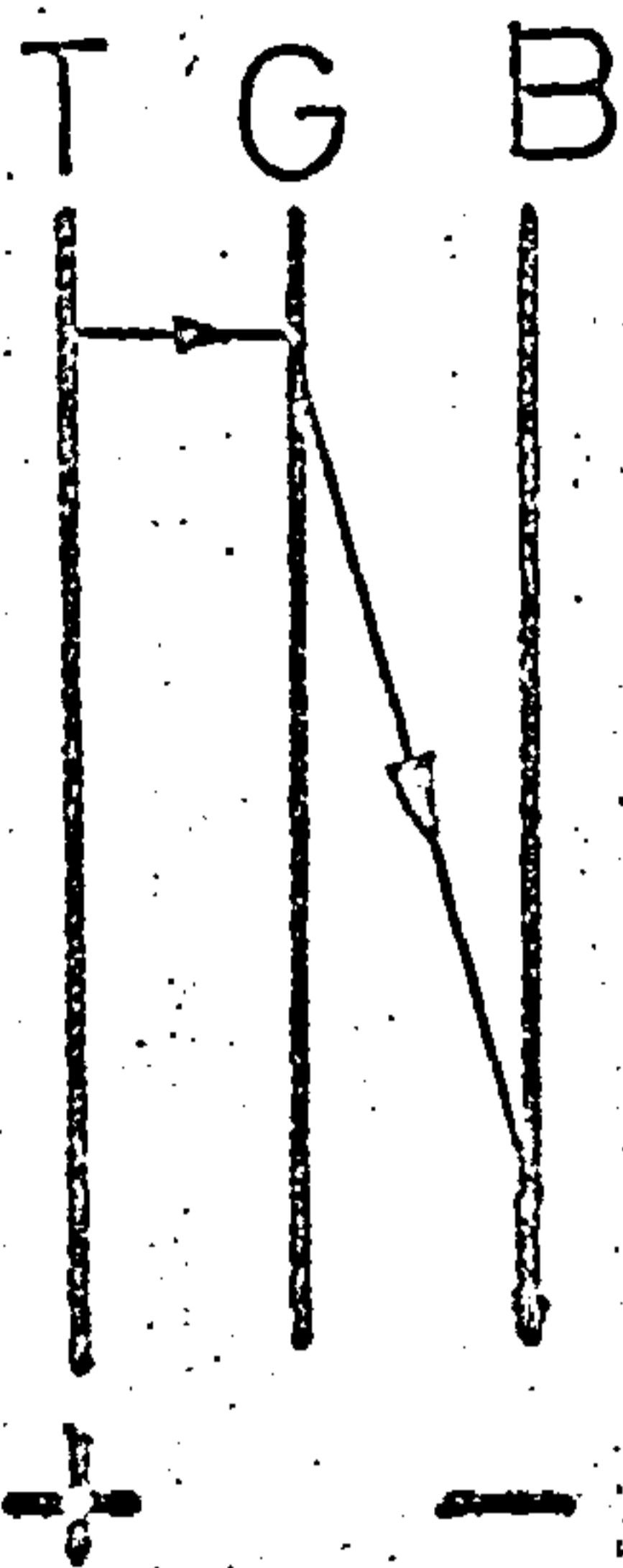


b) The symbols

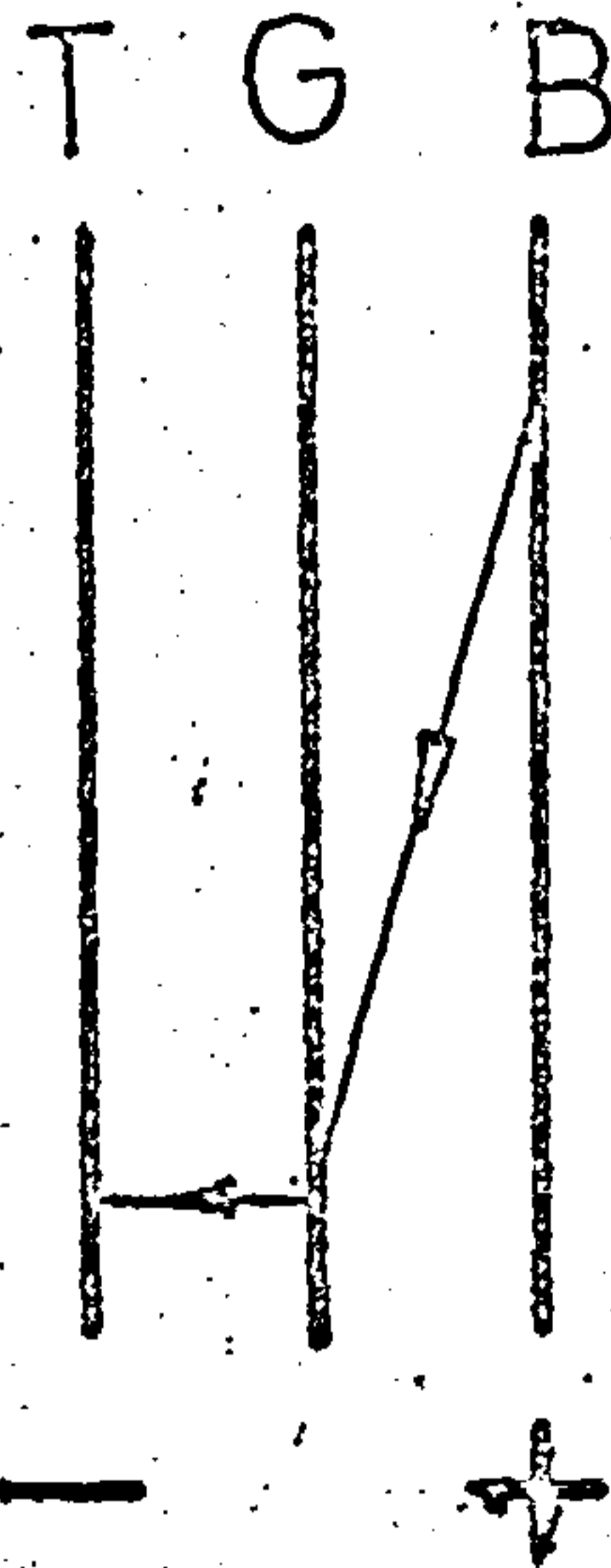
Figure 35, (a) Triode configuration and (b) symbols used in this thesis.



+FD Circuit

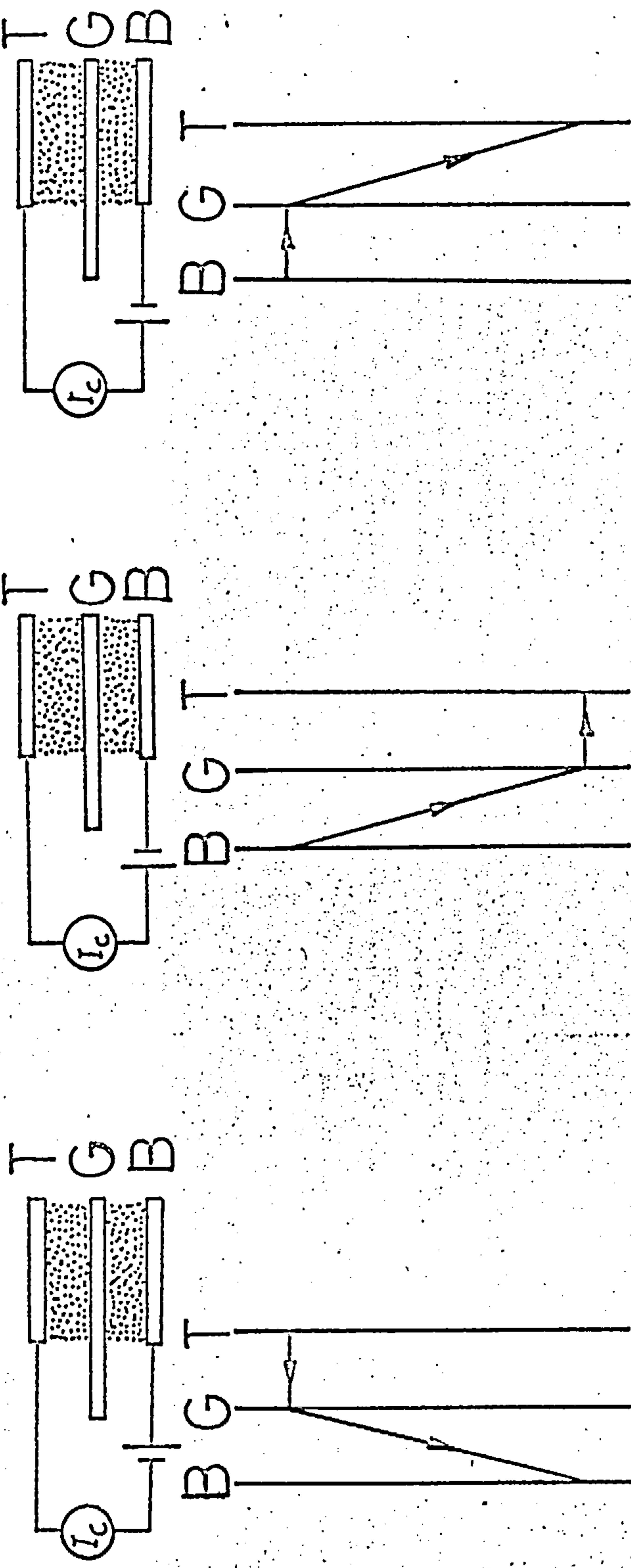


Biased in the direction
of forming; $V_b = 10$ V.



Biased in the opposite
direction of forming;
 $V_b < 10$ V.

Figure 36. Potential distribution shown schematically for a triode structure biased in two different directions and with the applied voltage lower than the voltage used for the initial electroforming.



a)

b)

c)

Biased in the direction of forming(-FD); $V_b = 10$ V.

Biased as in (b) to that for forming; $V_b \leq 10$ V $V_b > 14$ V.

Applied potential drops between grid and base electrode independent of top electrode polarity [for(a) and(b)] . Excess reverse voltages shifts the high-field region, (c) to the region between B and G.

Figure 37.

$\triangle V_{GT}$

$\square V_{GB}$

$Ag-SiO_x/B_2O_3-Ag-SiO_x/B_2O_3-Ag$

$D_1=D_2=5000 \text{ \AA}$

20

15

10

5

0

5

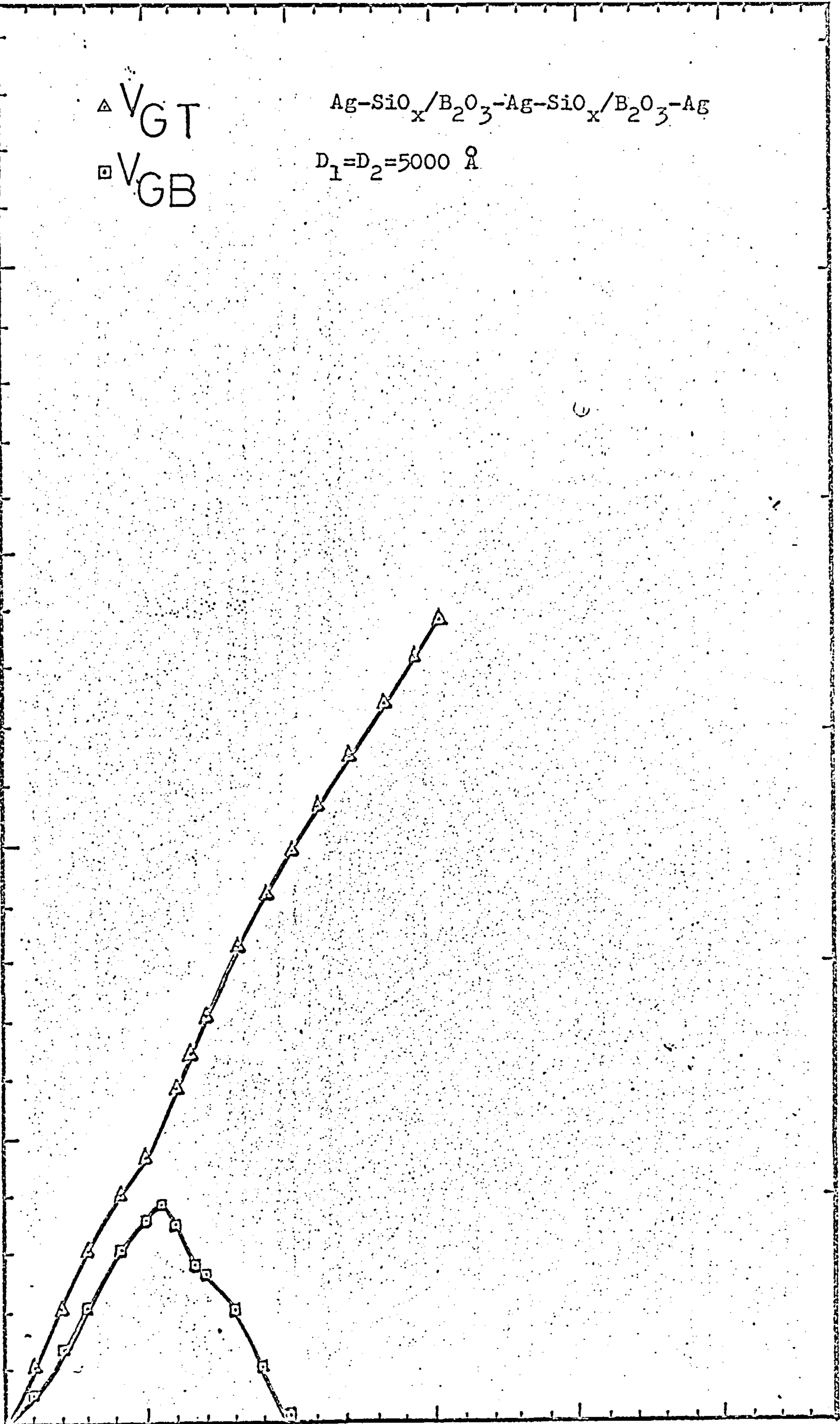
10

15

20

25

Figure 38-a.



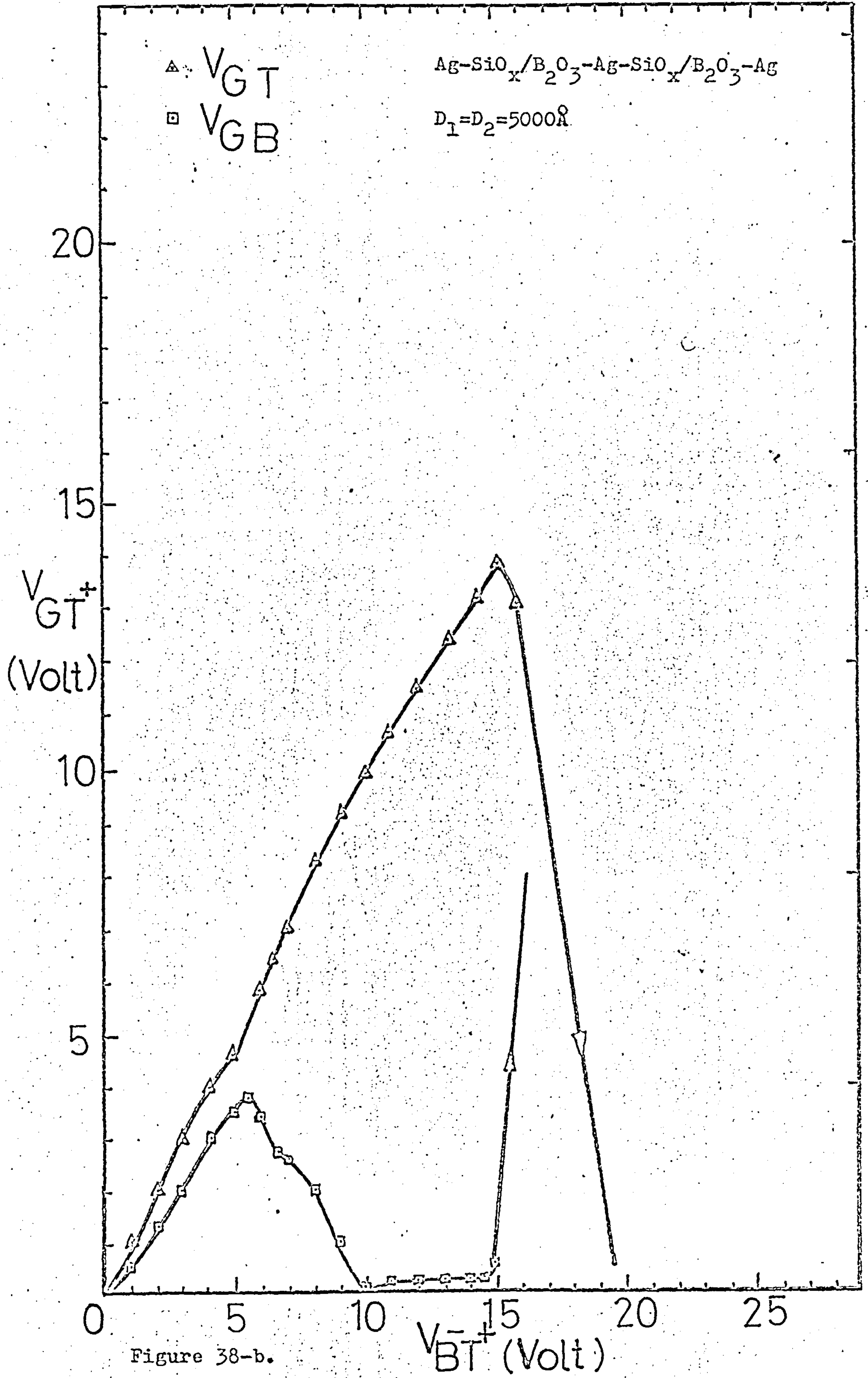
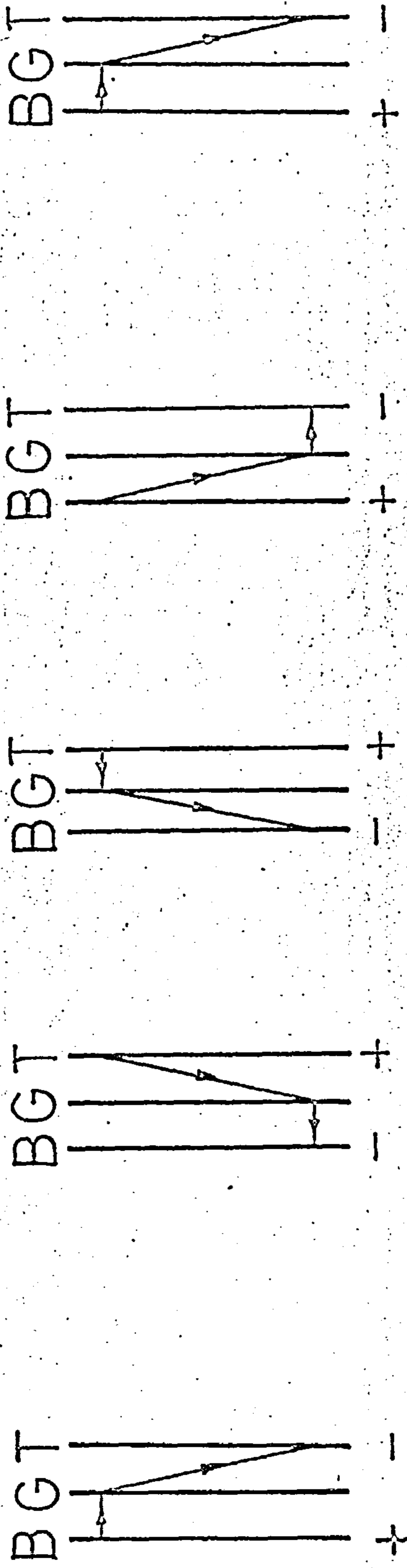
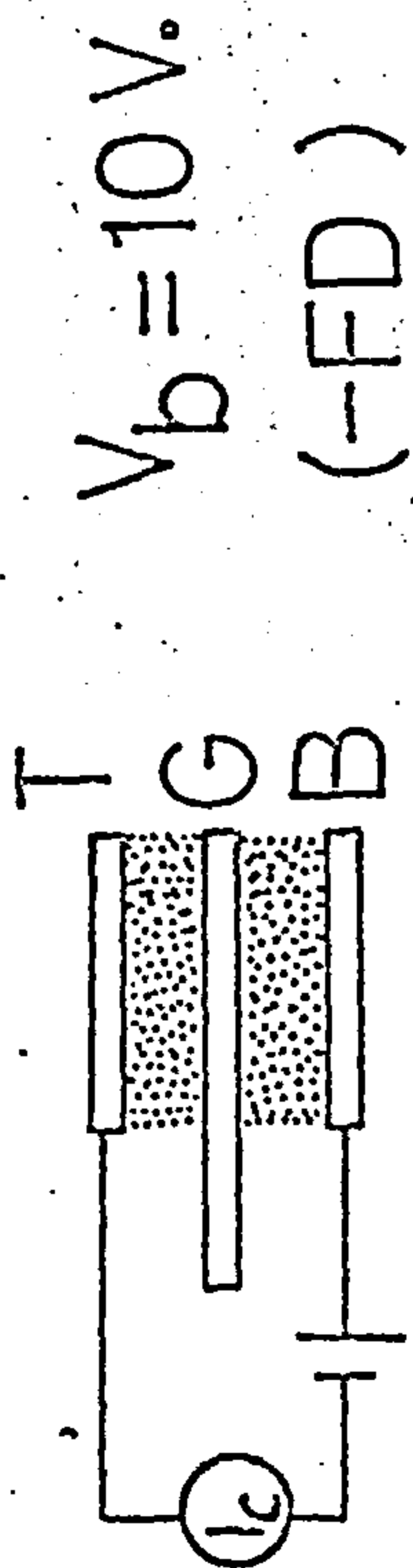


Figure 38-b.



$V_b = 10V$
 a b

Biased in the direction of forming.

$V_b \leq 10V$
 b

Biased in the opposite direction (high-resistance region remains D_2).

$V_b = 14V$
 c b

Biased in the same direction as (b). High-resistance removes to D_1 . Direction of forming now is changed.

$V_b \geq 14V$
 d b

Biased in the same direction as (a). High-resistance region remains D_1 .

$V_b = 18V$
 e b

Biased in the same direction as (a). High-resistance region shifts to D_2 . Forming direction has changed.

Figure 39.

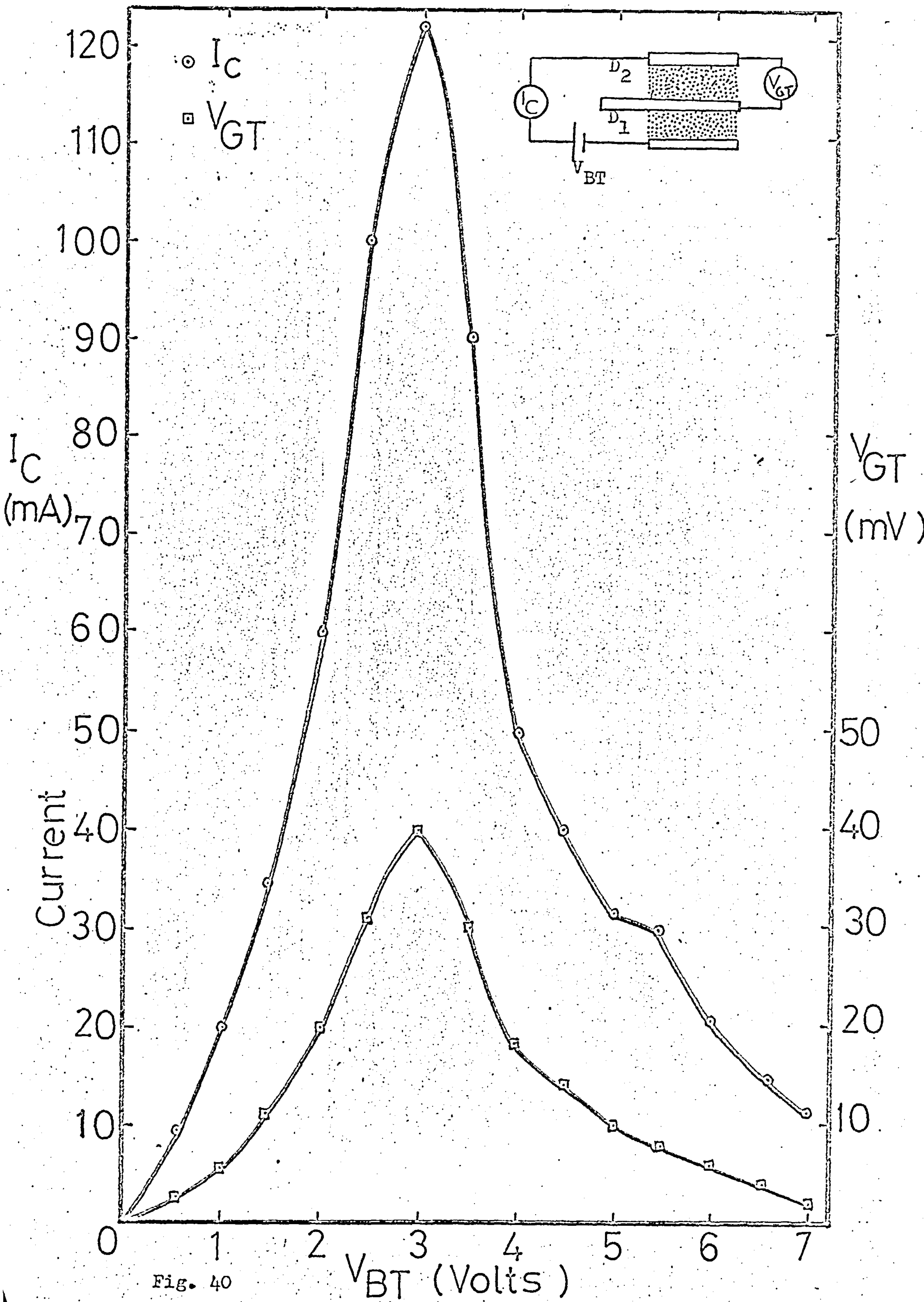


Fig. 40

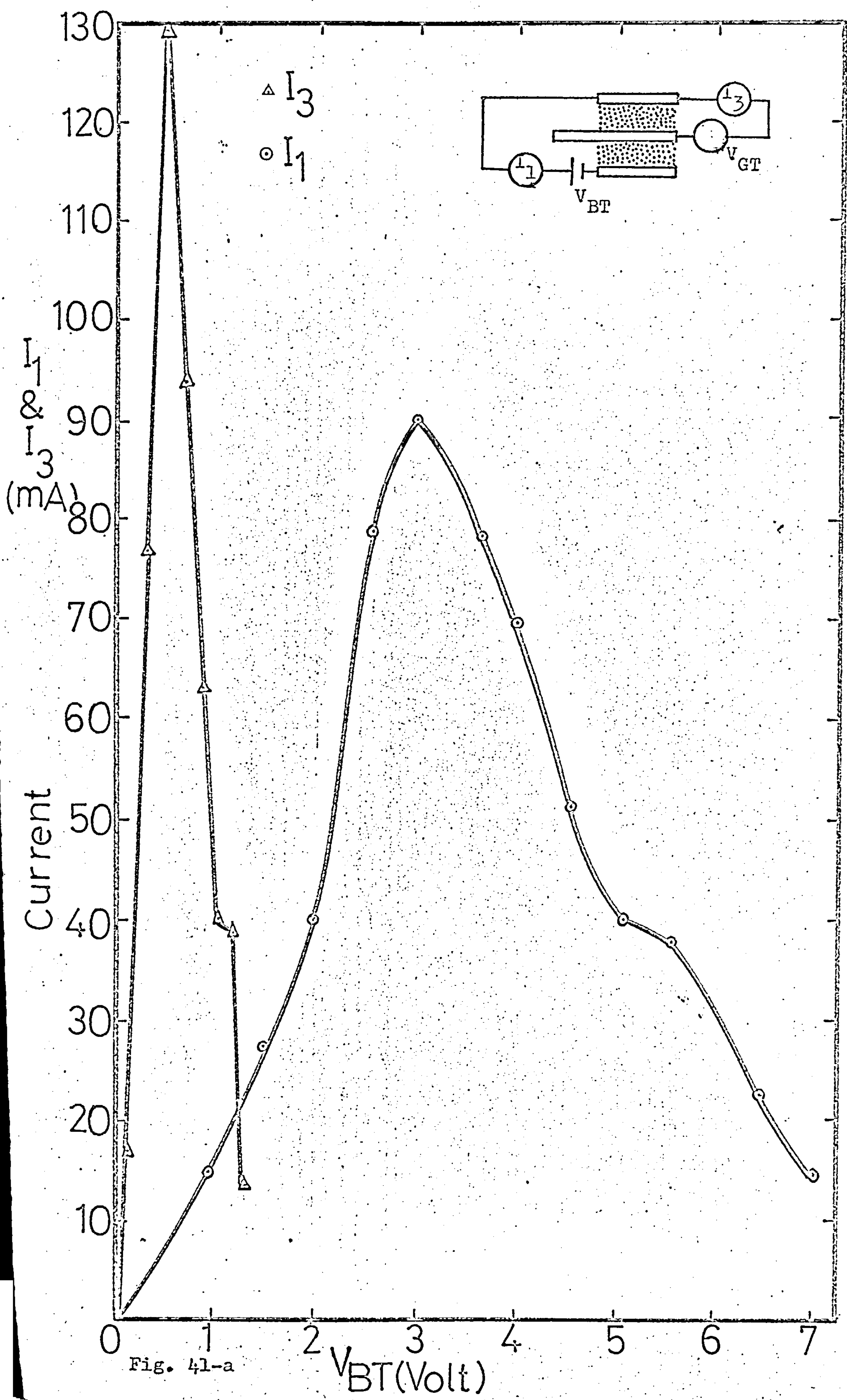


Fig. 41-a

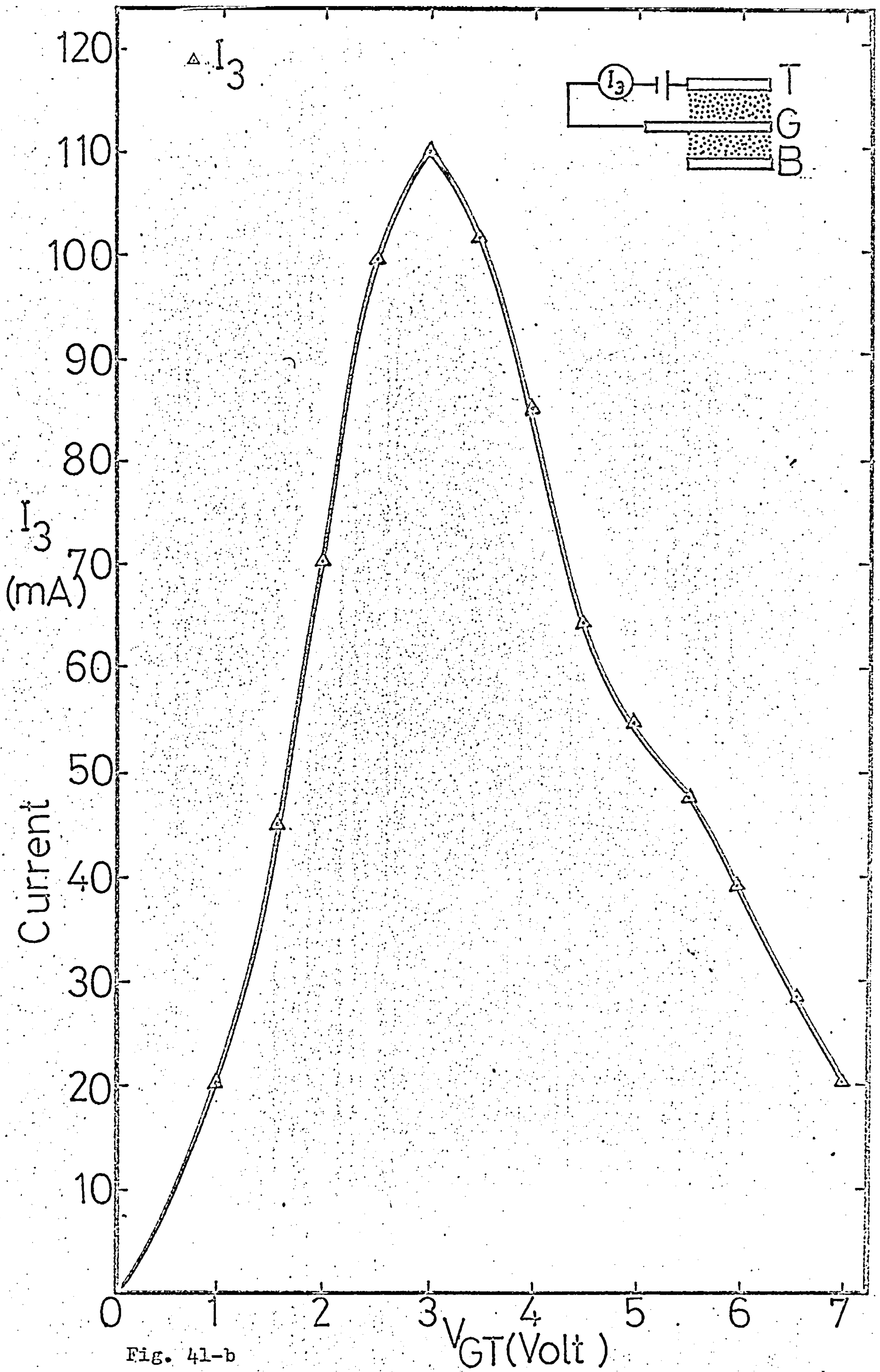


Fig. 41-b

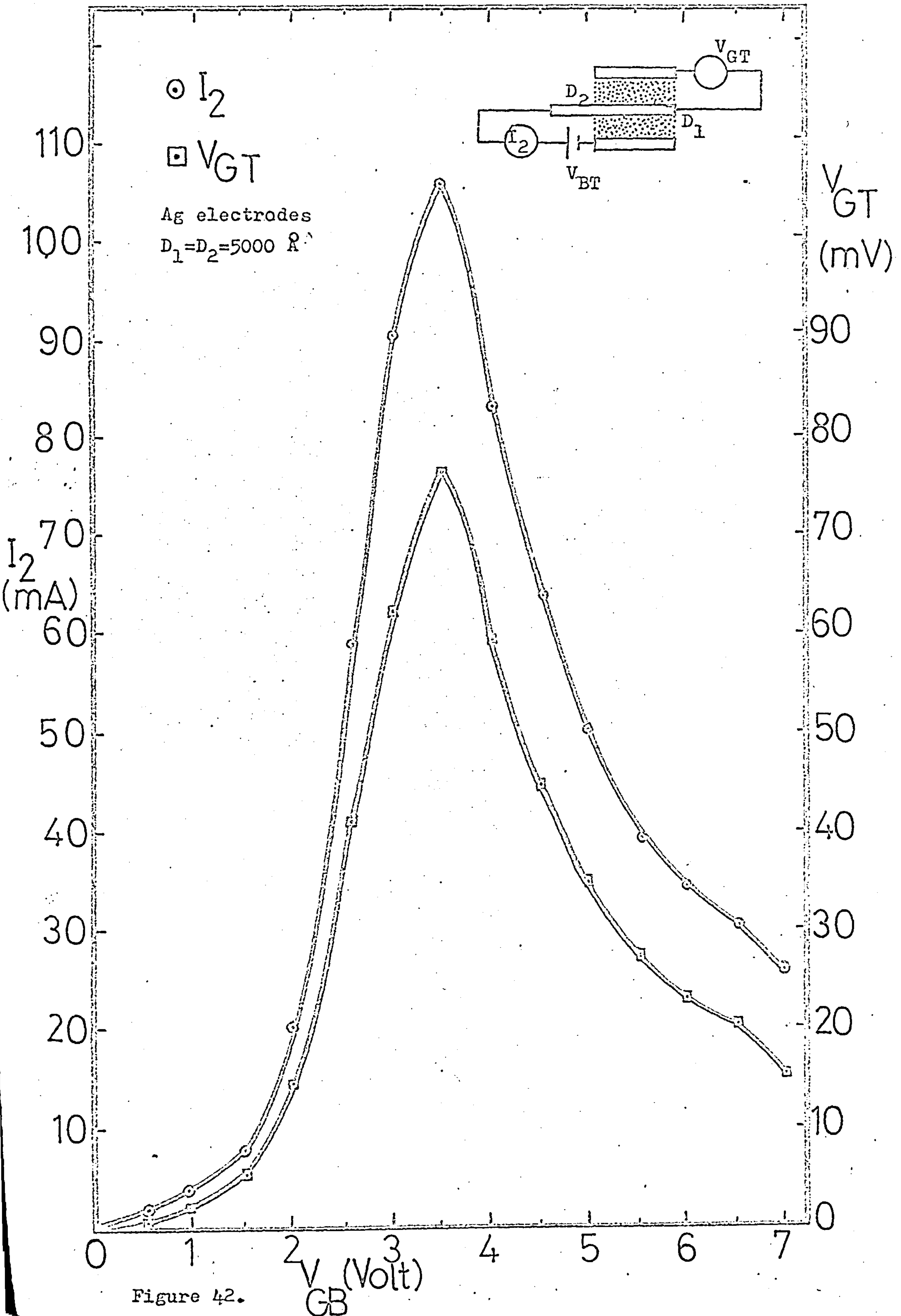


Figure 42.

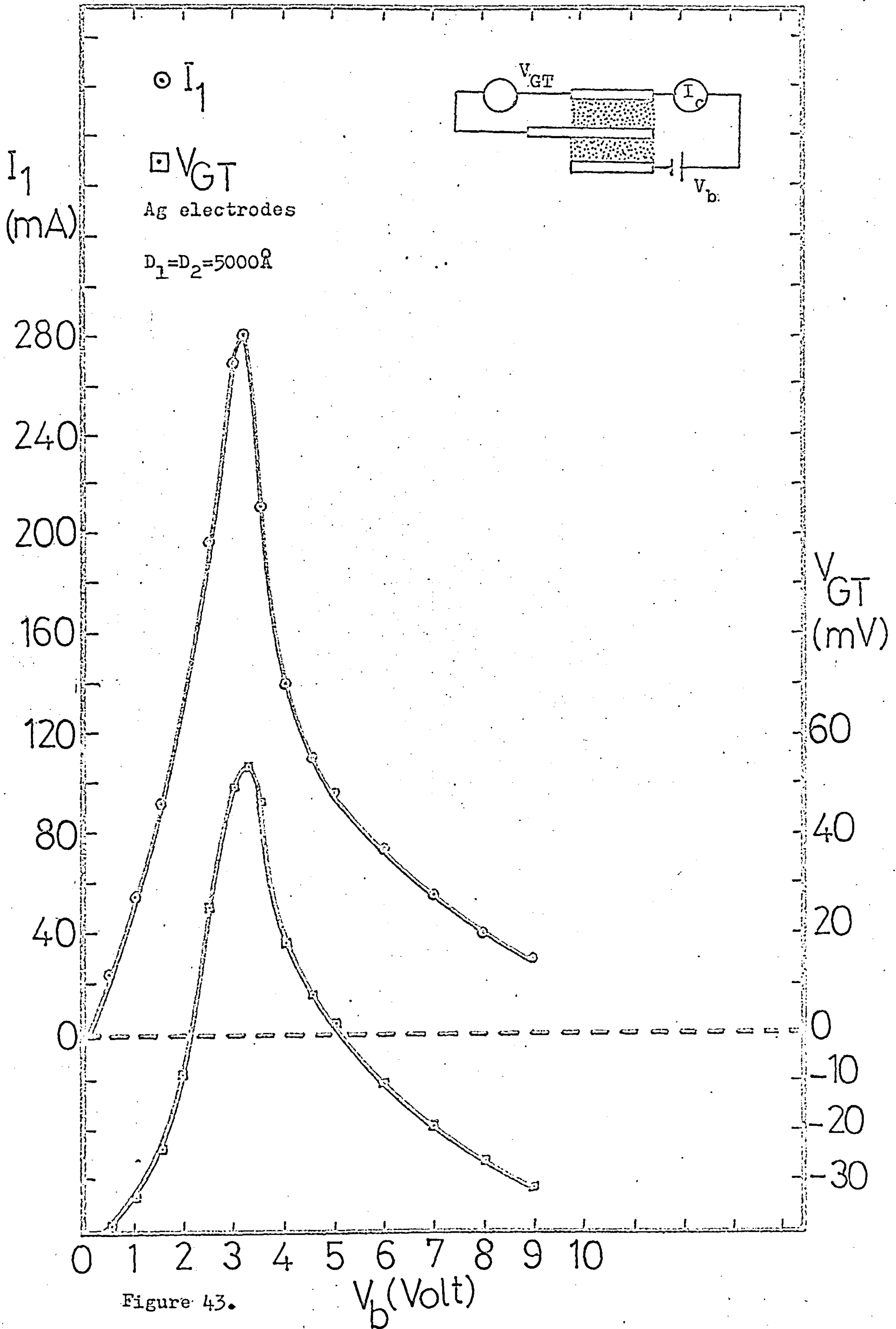


Figure 43.

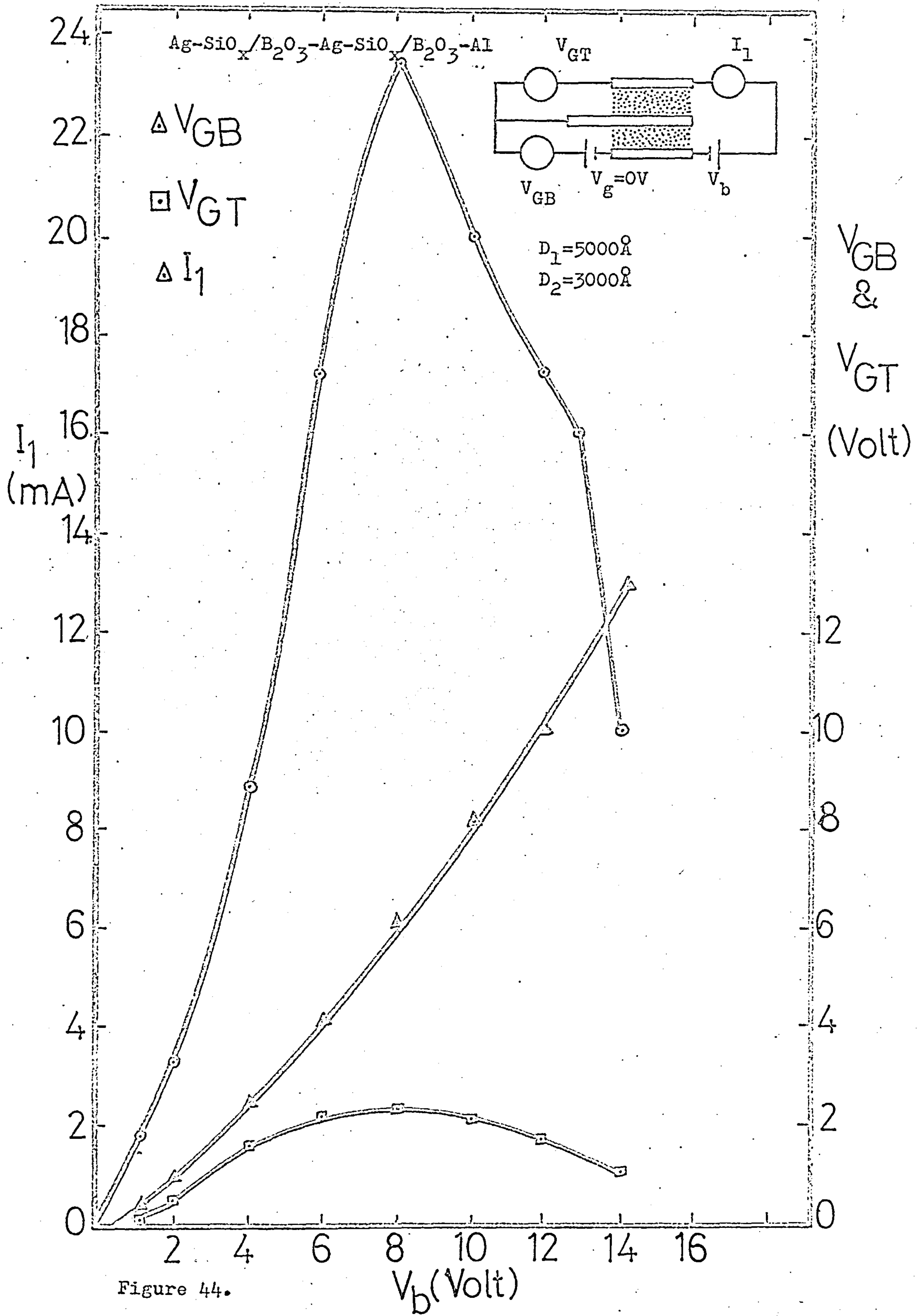


Figure 44.

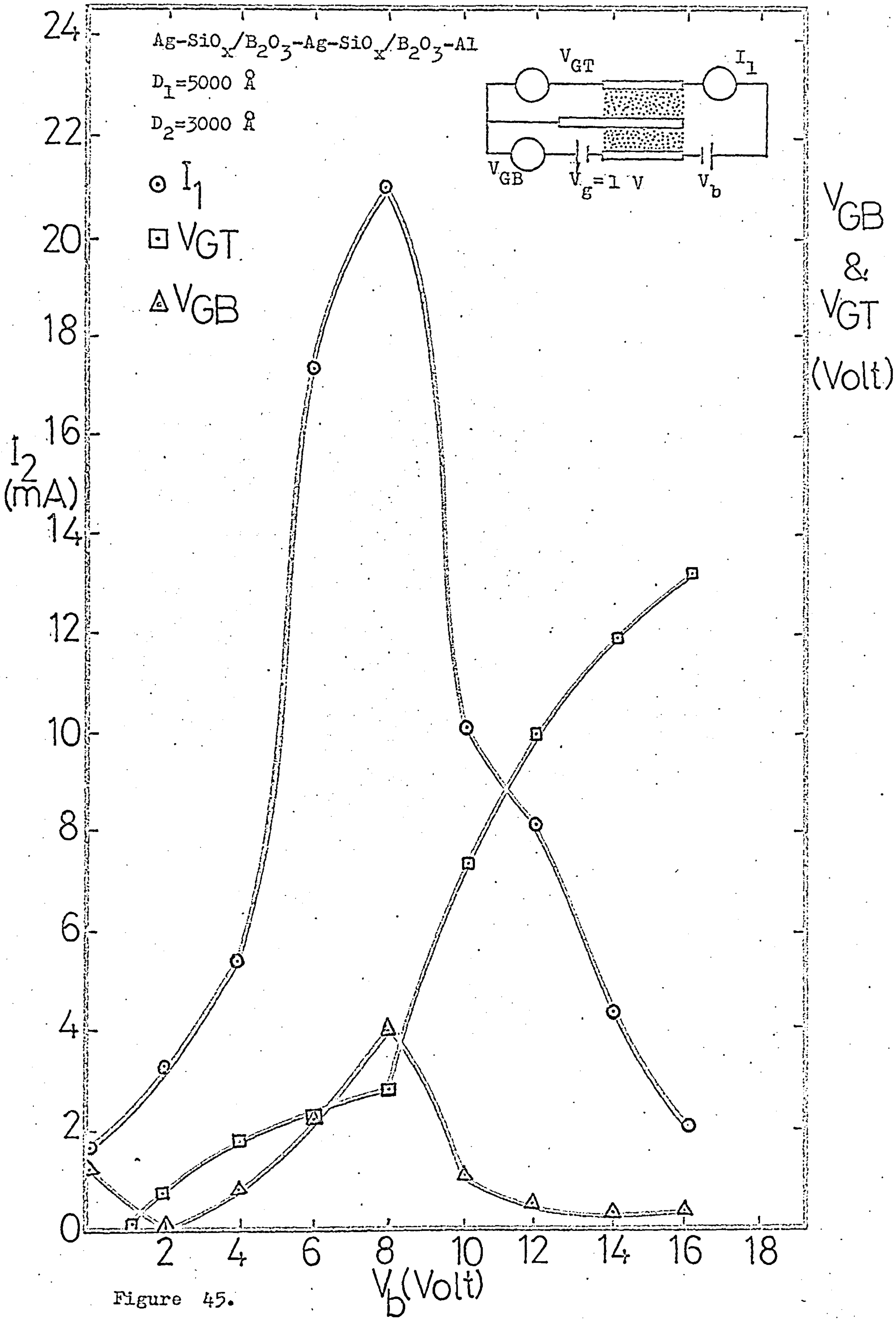


Figure 45.

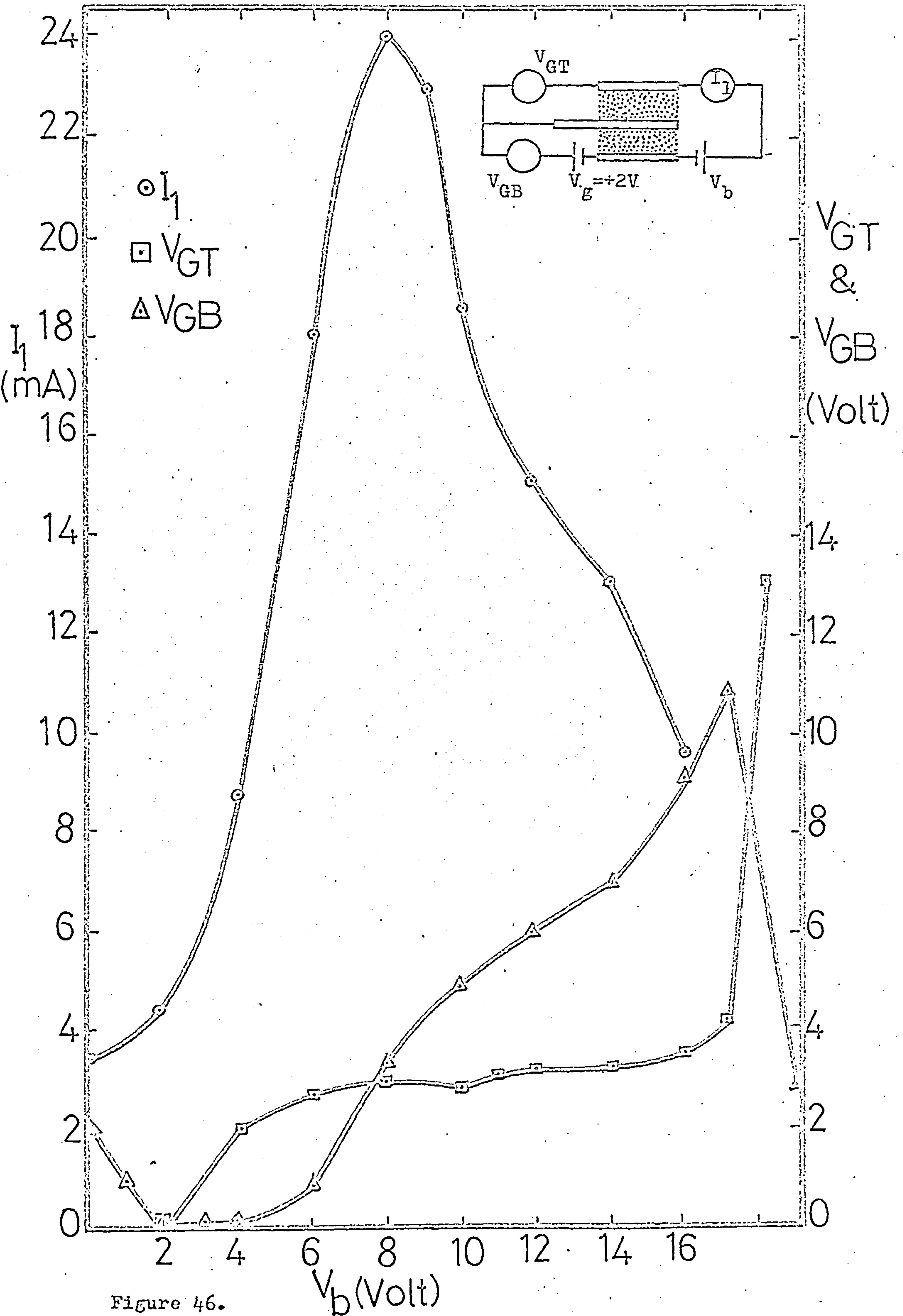
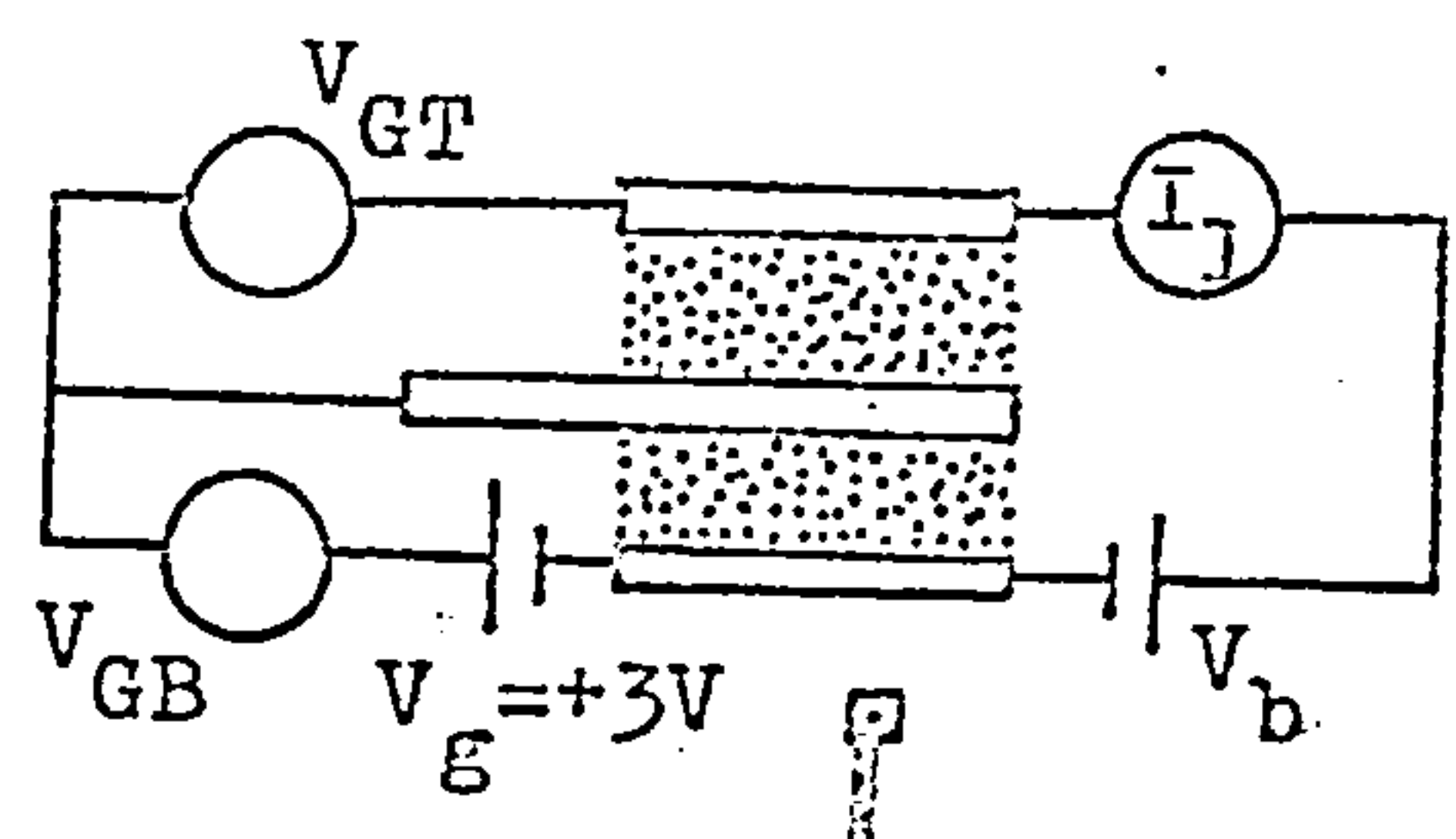


Figure 46.

Ag-SiO_x/B₂O₃-Ag-SiO_x/B₂O₃-Al
 $D_1 = 5000\text{\AA}$ $D_2 = 5000\text{\AA}$



I_1
(mA)

○ I_1
 □ V_{GT}
 △ V_{GB}

V_{GT}
&
 V_{GB}
(Volt)

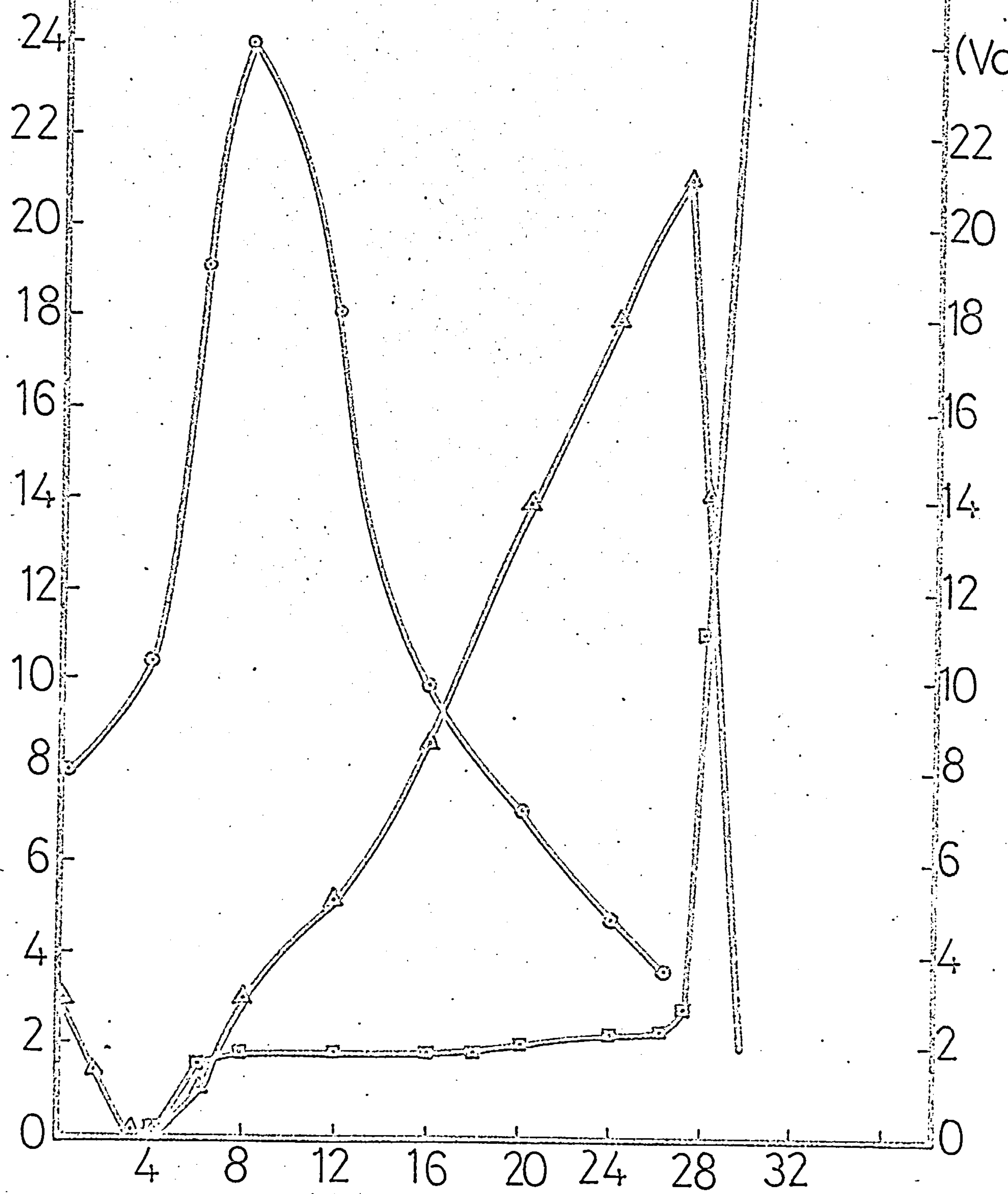


Figure 47.

V_b (Volt)

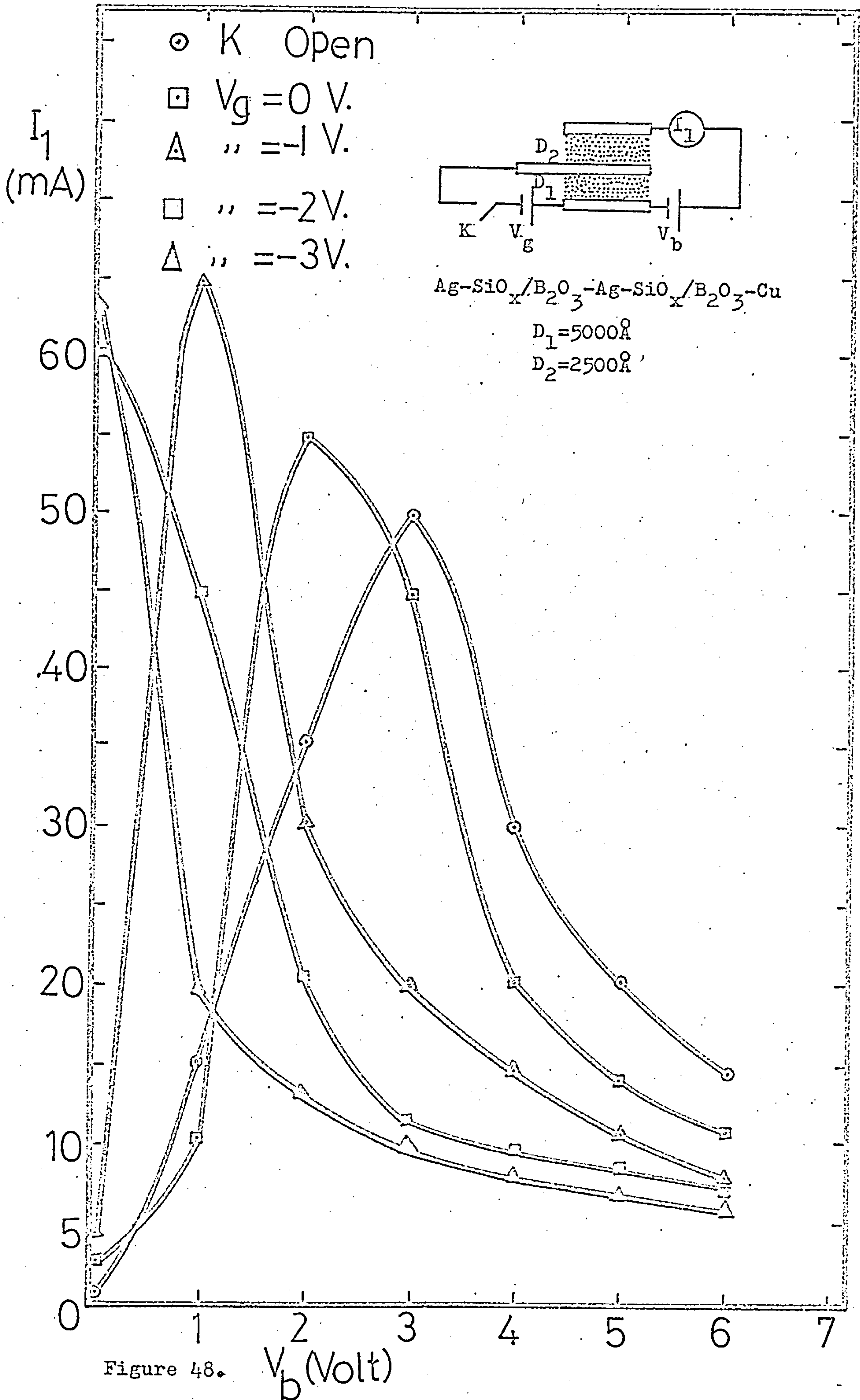


Figure 48.

E_1	E_2	E_3	K_1	K_2	K_3	I_1	I_2	I_3	V_1	V_2	V_3	Fig.
E_1	-	-	C	O	O	70	-	-	6	-	-	50-1
-	E_2	-	O	C	O	-	75	-	-	3	-	50-1
-	-	E_3	O	O	C	-	-	24	-	-	5	50-1
E_1	-	-	C	O	C	80	-	65	3	-	3	50-4
-	E_2	-	O	C	C	-	80	12	-	3	5	50-2
-	-	E_3	O	C	C	-	12	30	-	4	4	50-3
E_1	-	-	C	C	O	70	55	-	5.5	5.5	-	50-6
-	E_2	-	C	C	O	55	95	-	5	4	-	50-7
-	-	E_3	C	O	C	50	-	65	3	-	3	50-5

Table I. Experimental conditions for measurements on different parts of the generalised circuit (case a).

(O=Open; C=Closed ; I=peak current ; V=peak voltage.)

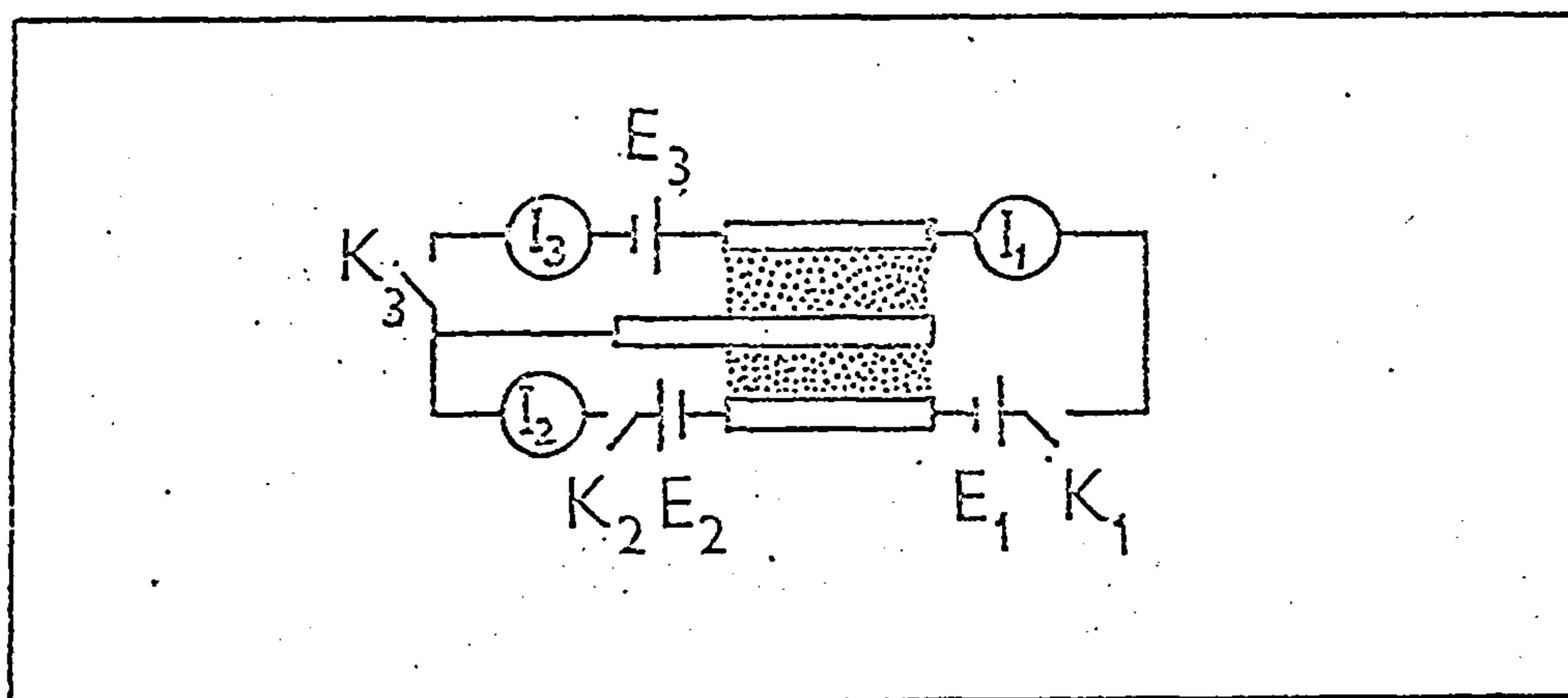


Figure 49. General circuit arrangement. Case(a) .

Grid voltage(E_2) is biased positively with respect to the base electrode.

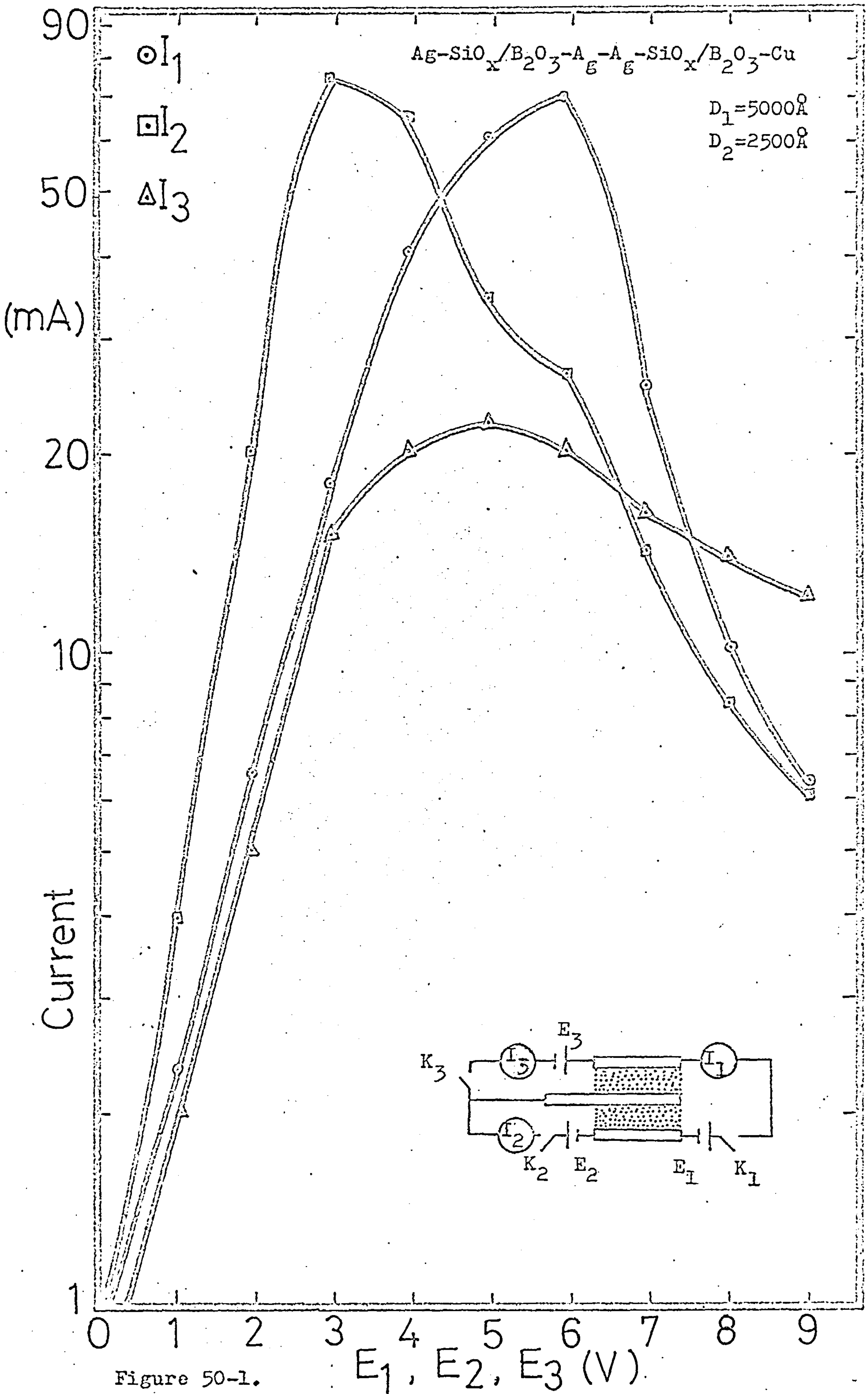
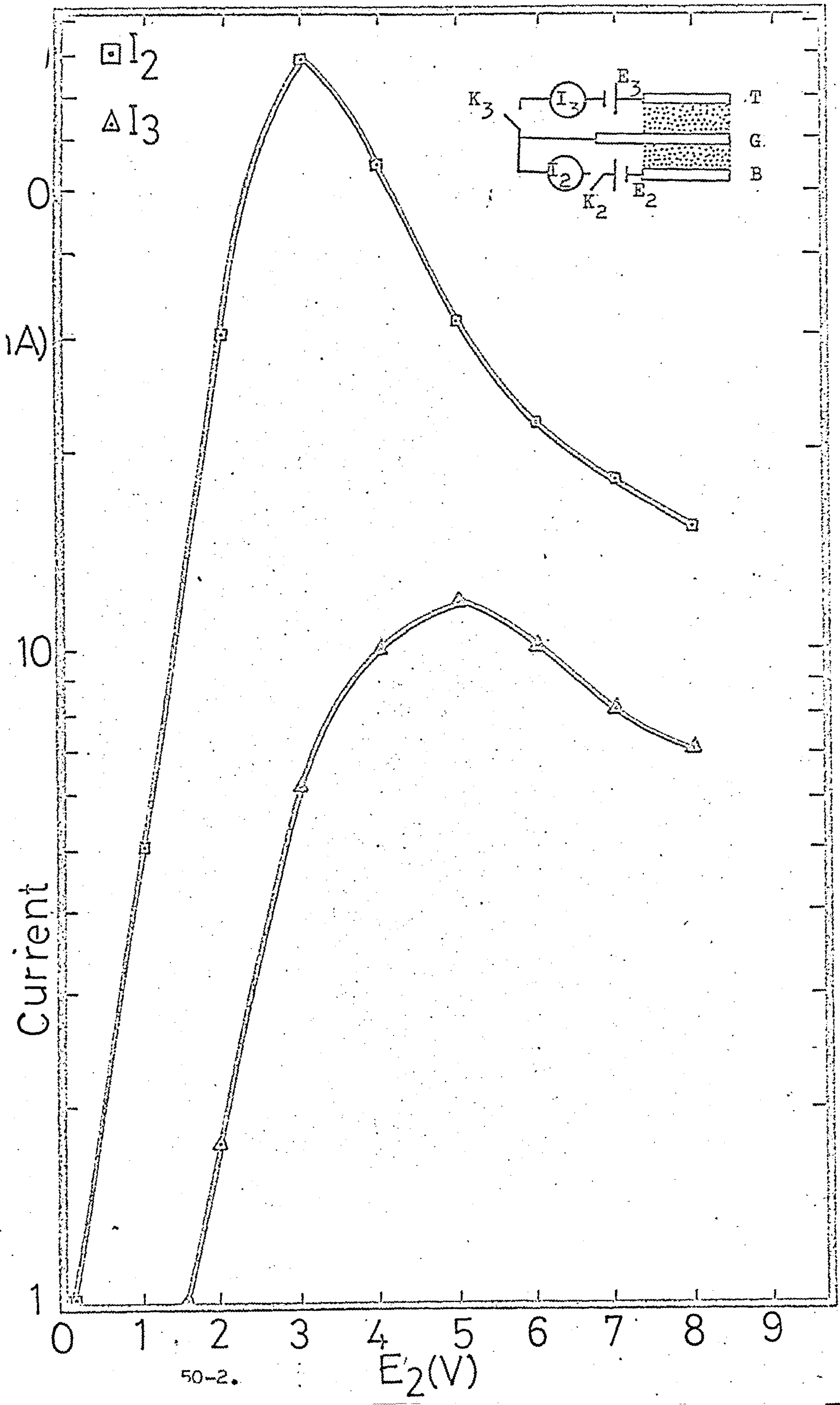


Figure 50-1.



50-2.

E_2 (V)

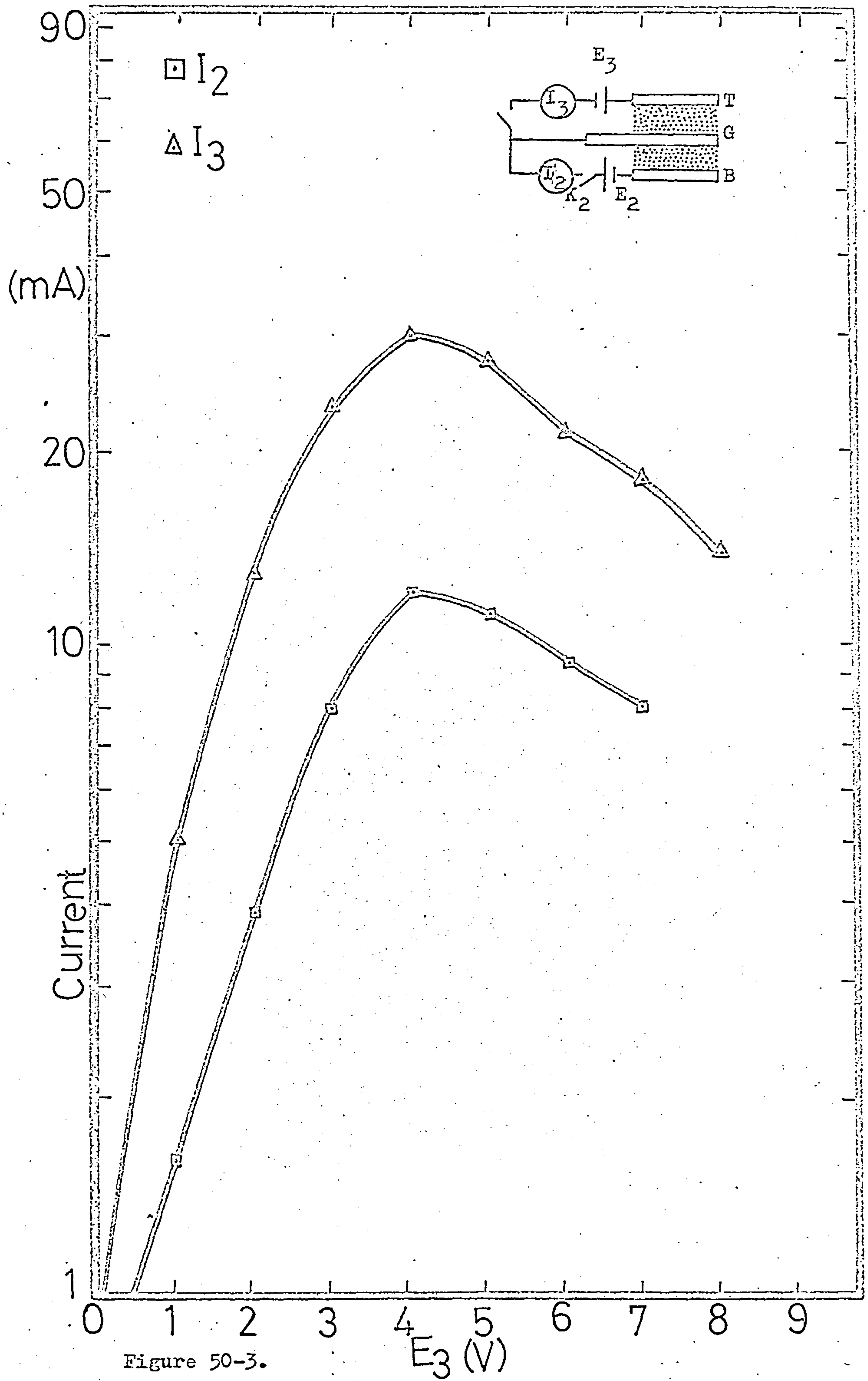


Figure 50-3.

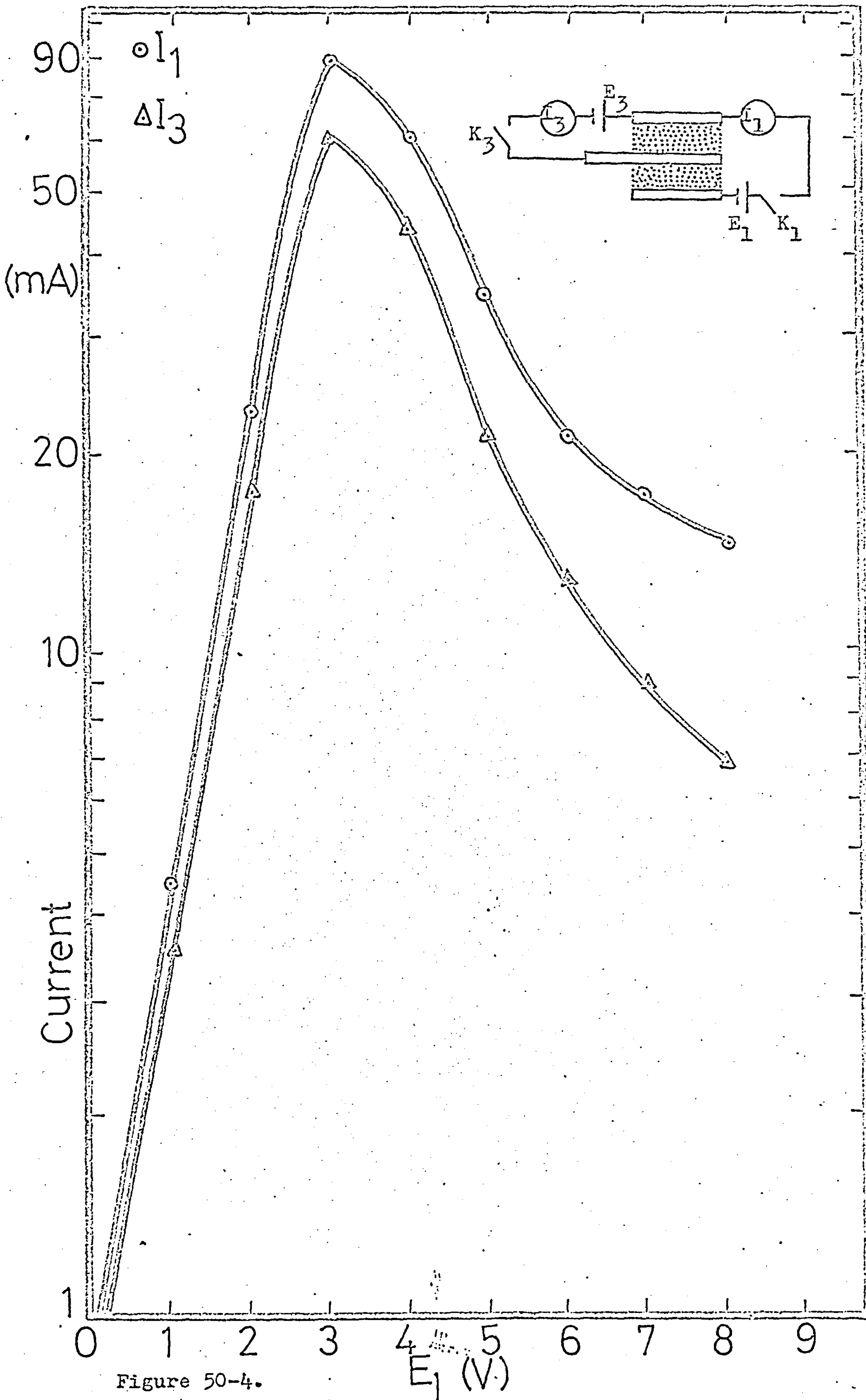


Figure 50-4.

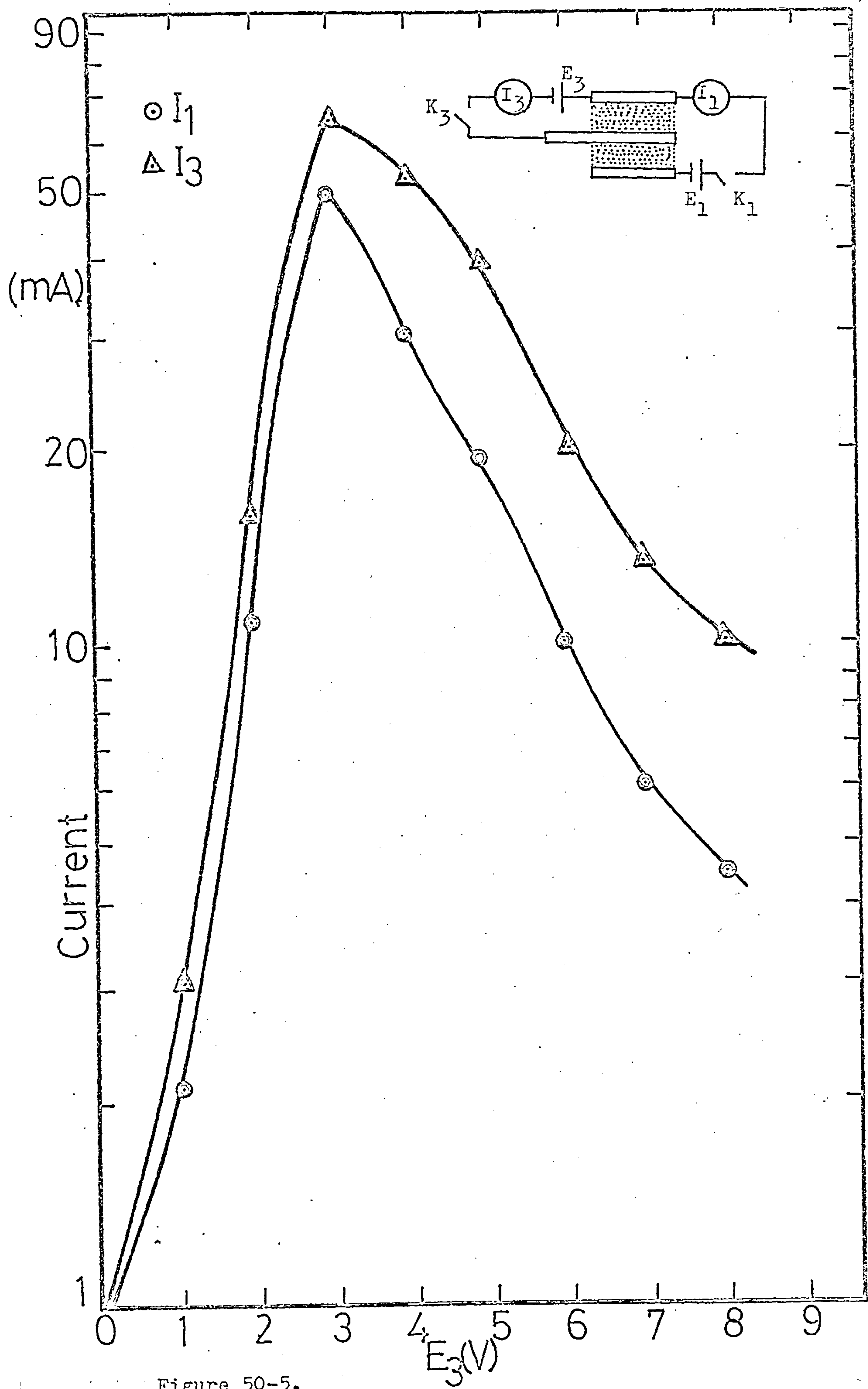


Figure 50-5.

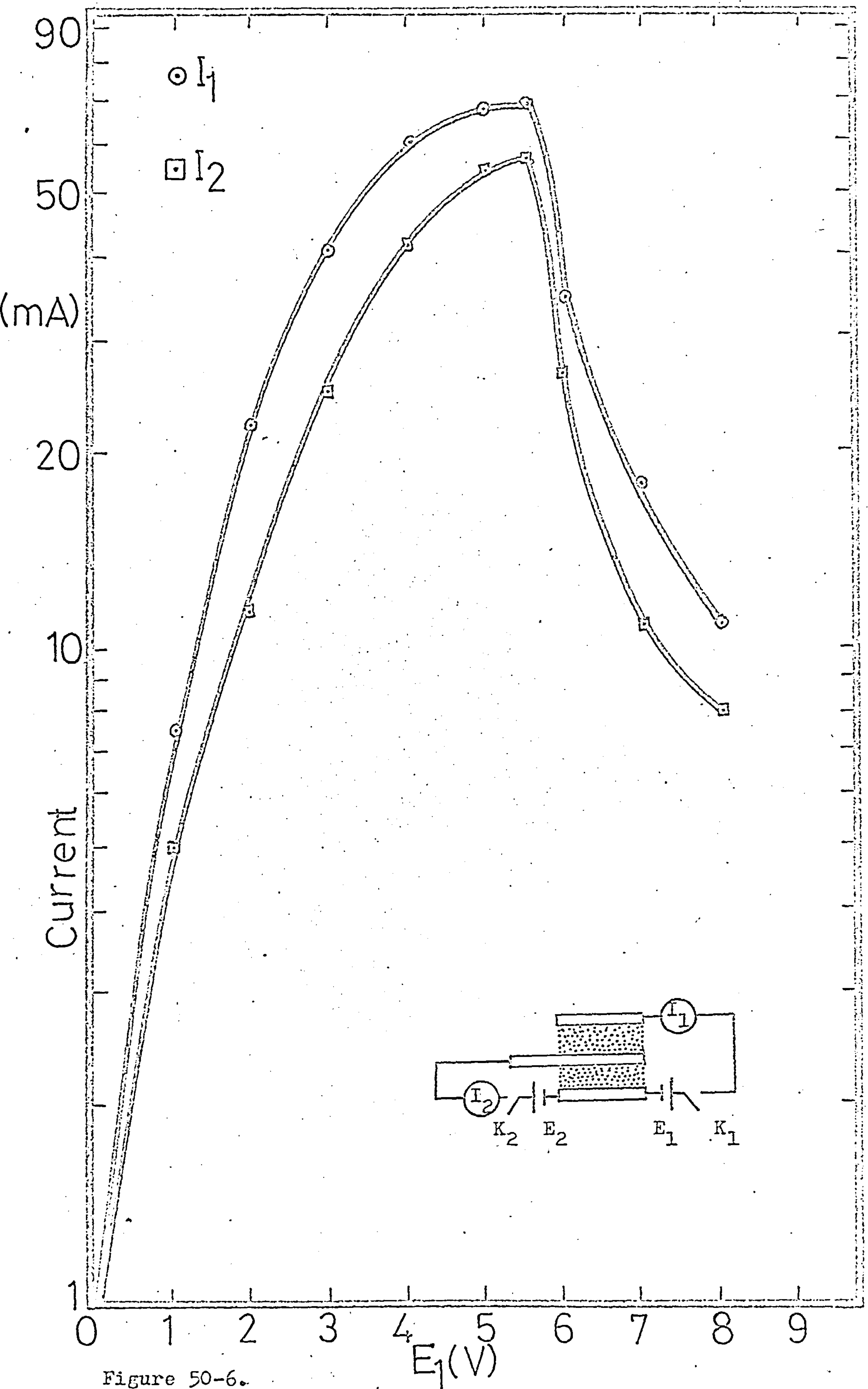


Figure 50-6.

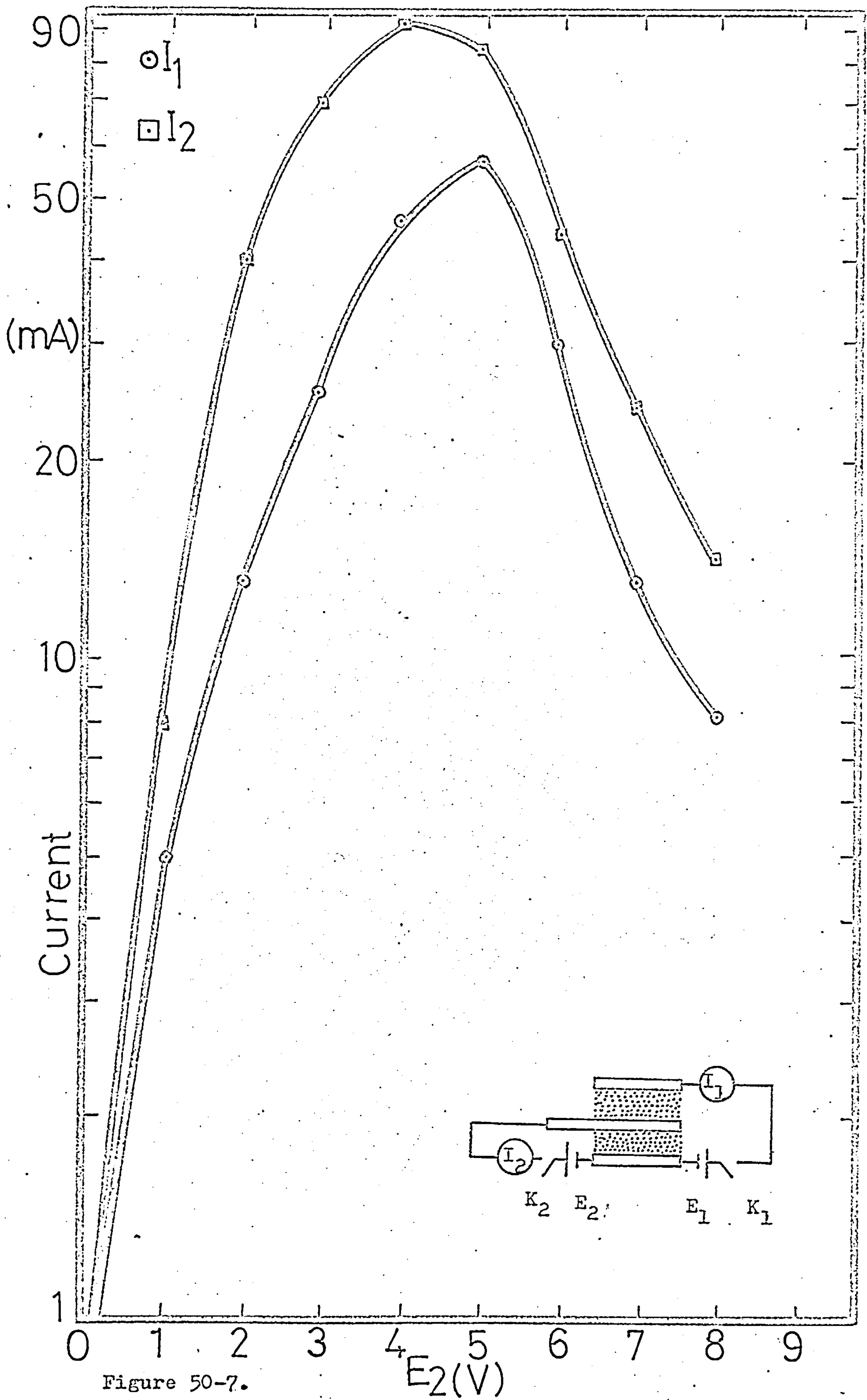


Figure 50-7.

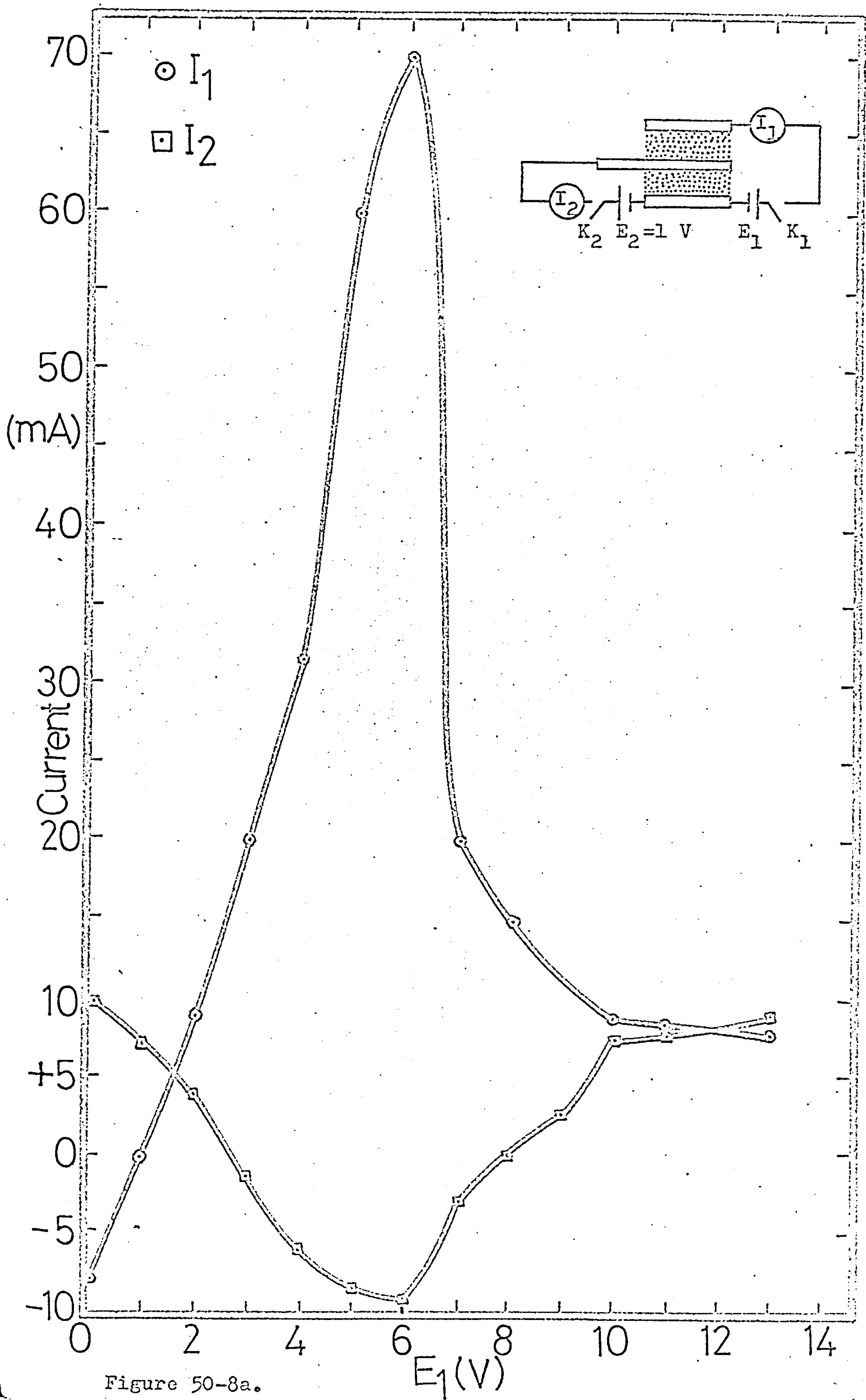


Figure 50-8a.

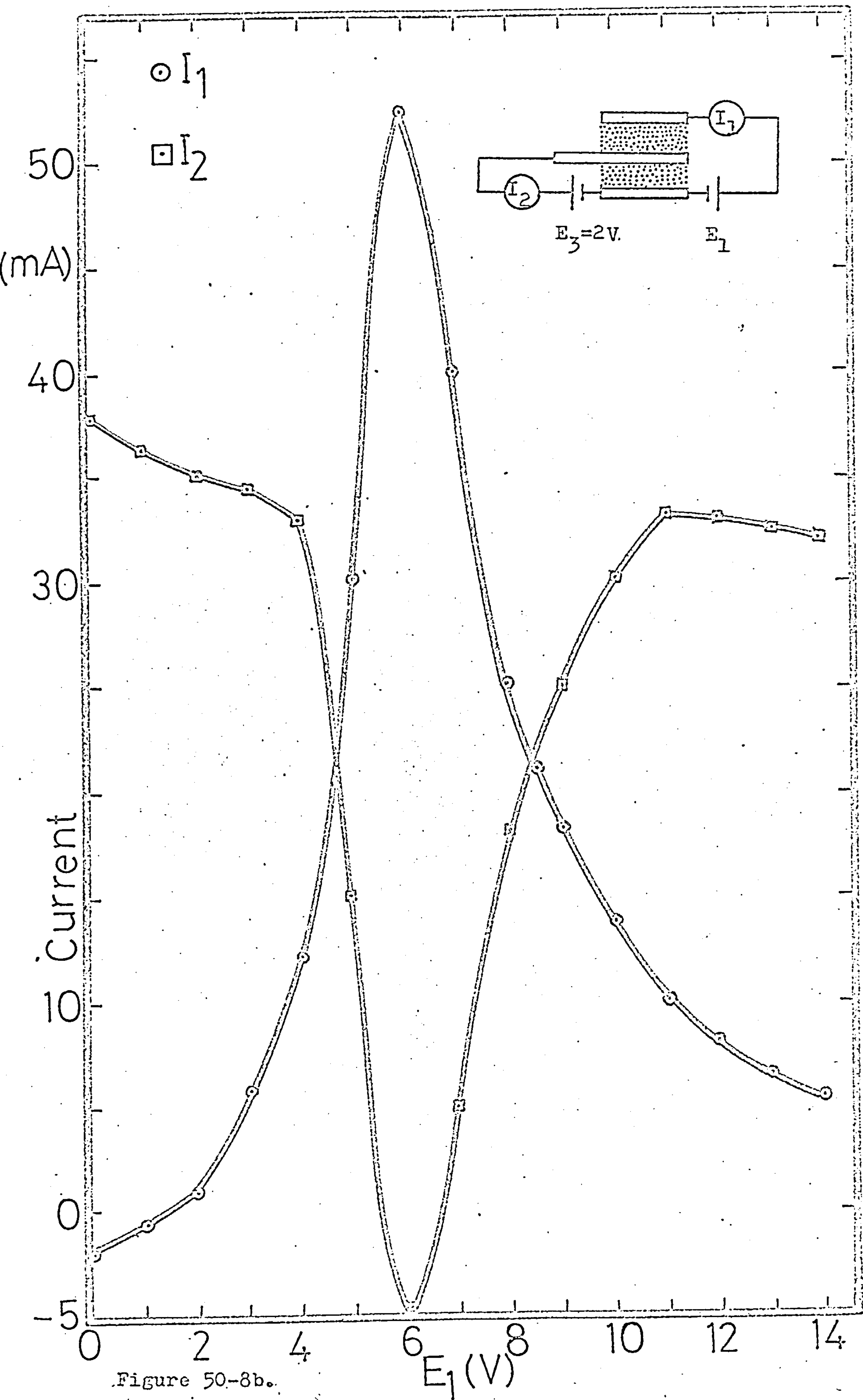


Figure 50-8b.

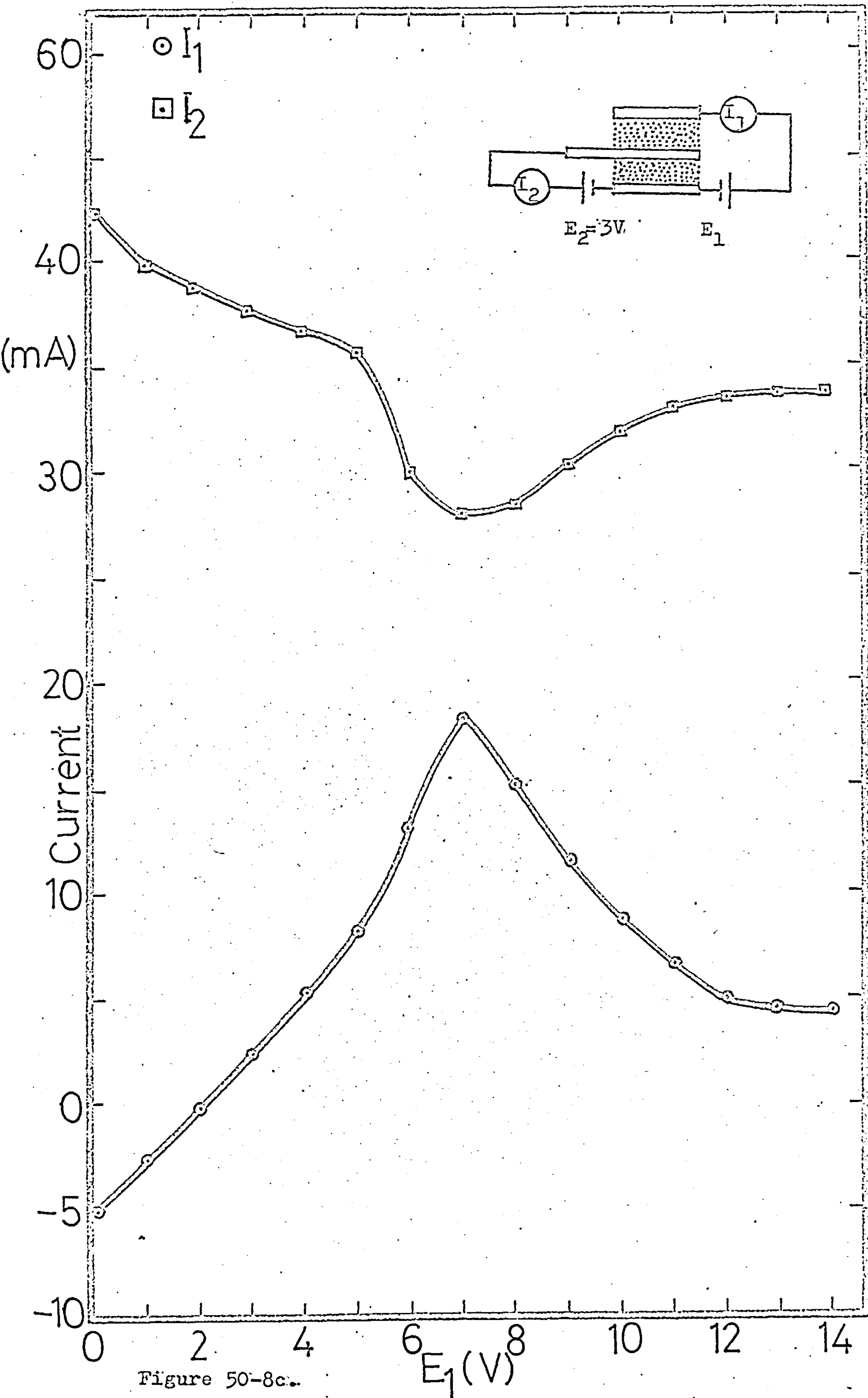


Figure 50-8c.

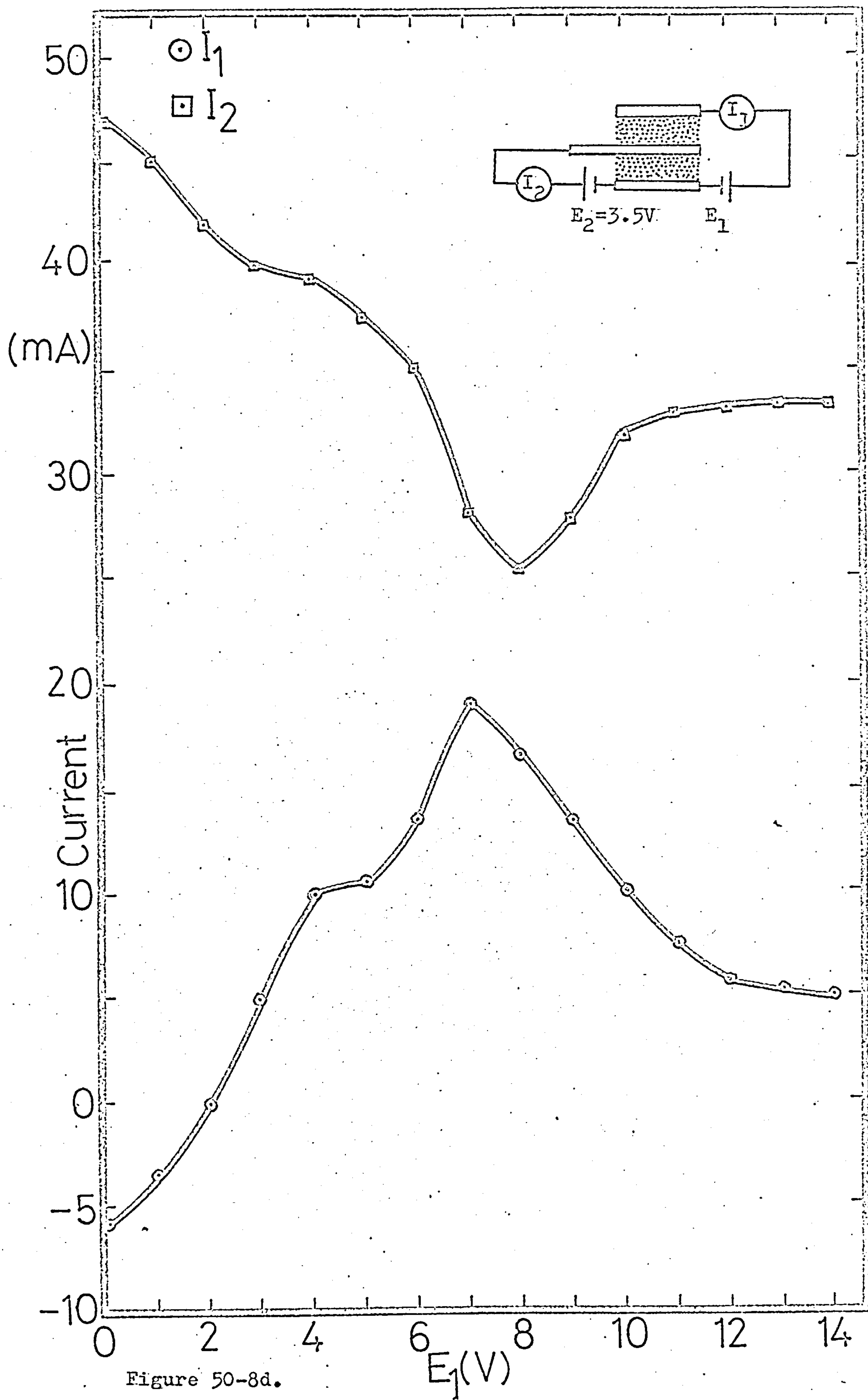


Figure 50-8d.

E_1	E_2	E_3	K_1	K_2	K_3	I_1	I_2	I_3	V	V	V	Fig.
E_1	-	-	C	O	O	30	-	-	7	-	-	52-1
-	E_2	-	O	C	O	-	60	-	-	3	-	52-1
-	-	E_3	O	O	C	-	-	30	-	-	5	52-1
E_1	-	-	C	O	C	85	-	70	3	-	3	52-4
-	E_2	-	O	C	C	-	65	8	-	3		52-2
-	-	E_3	O	C	C	-	8	28	-	7	5	52-3
E_1	-	-	C	C	O	25	15	-	5	5	-	52-6
-	E_2	-	C	C	O	17	70	-	5	3.5	-	52-7
-	-	E_3	C	O	C	65	-	80	3	-	3	52-5

Table VI. Experimental conditions for measurements on different parts of the generalised circuit (case b).

(O=Open; C=Closed; I=peak current; V=peak voltage.)

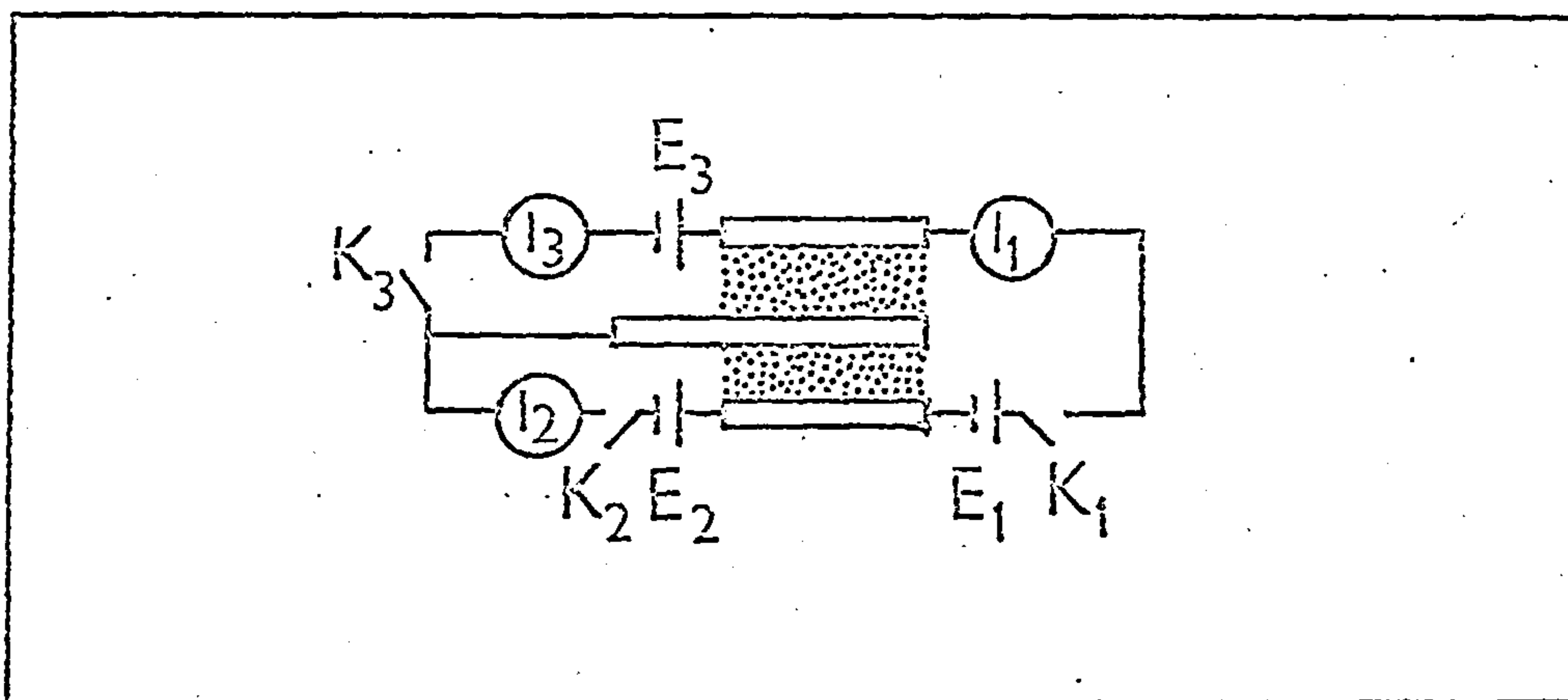


Figure 51. General circuit arrangement. Case(b)

Grid voltage(E_2) is biased negatively with respect to the base electrode.

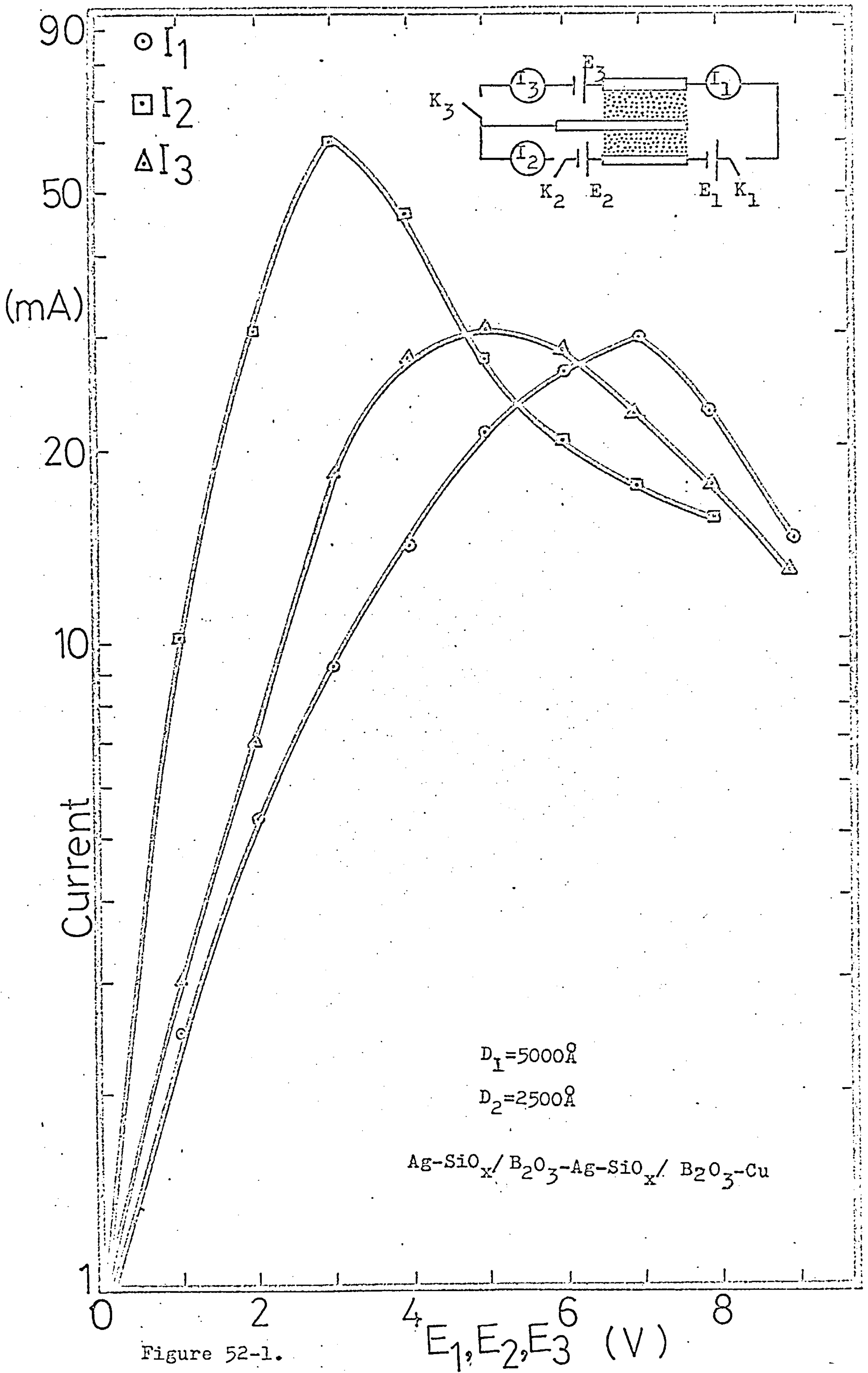


Figure 52-1.

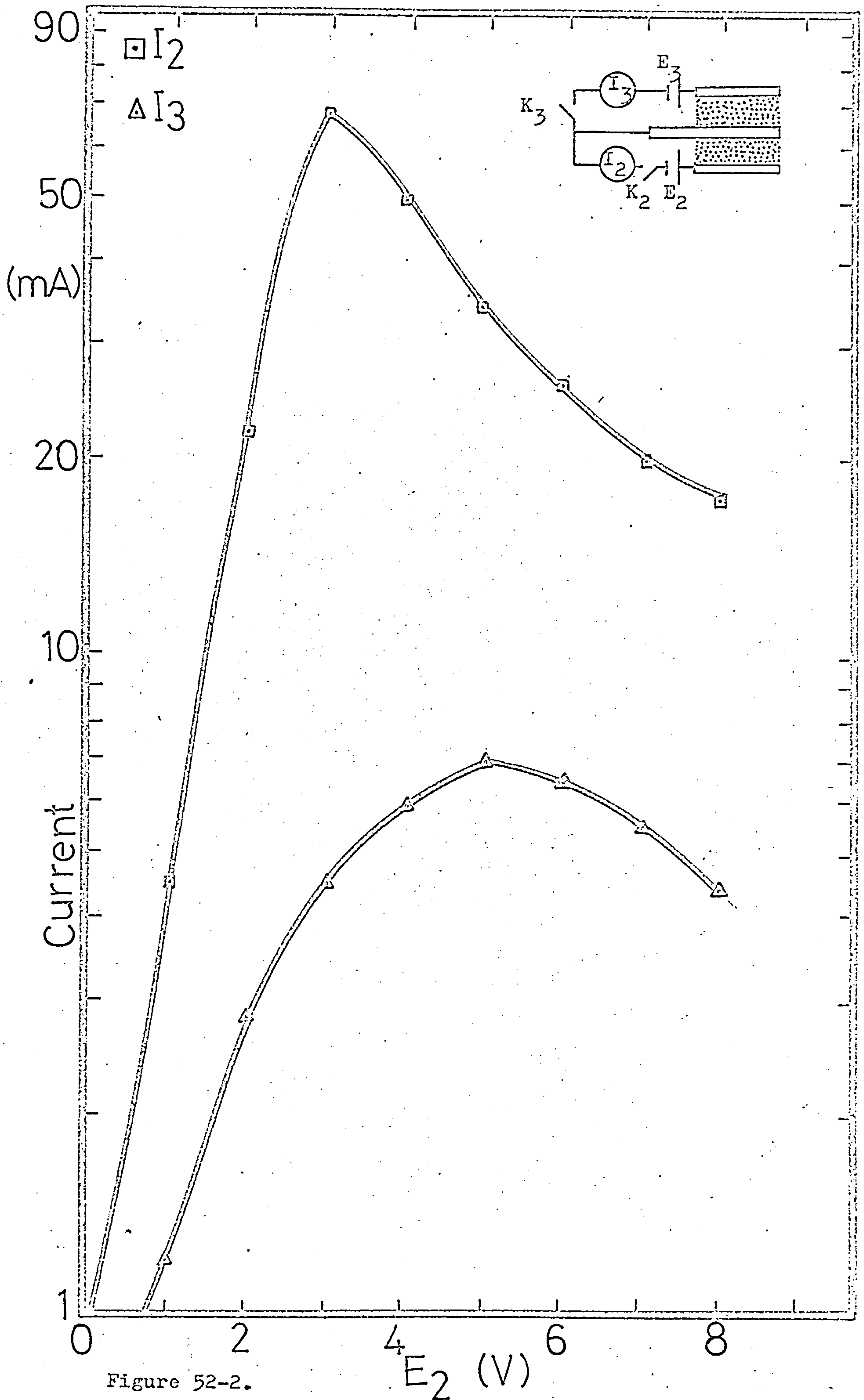


Figure 52-2.

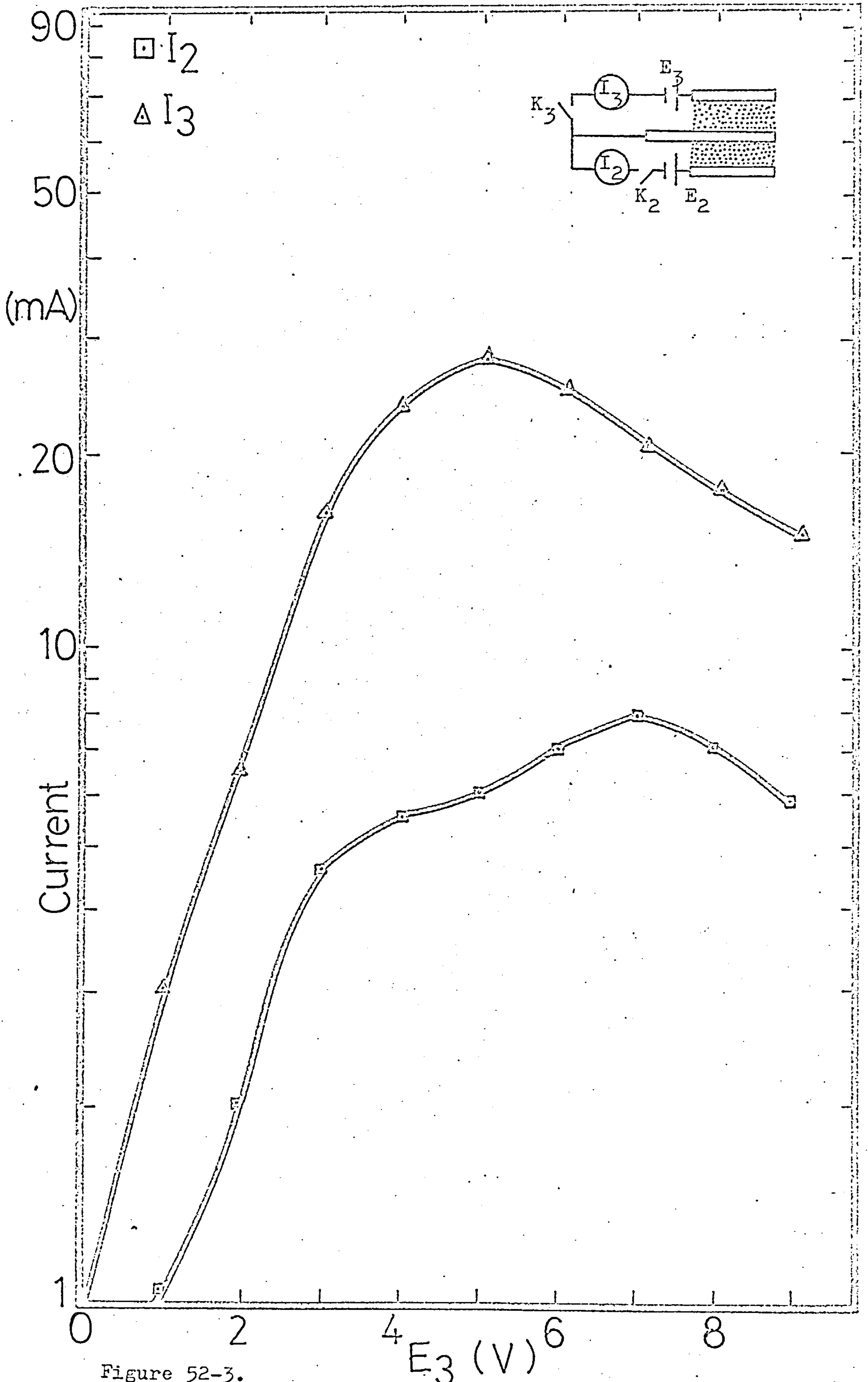


Figure 52-3.

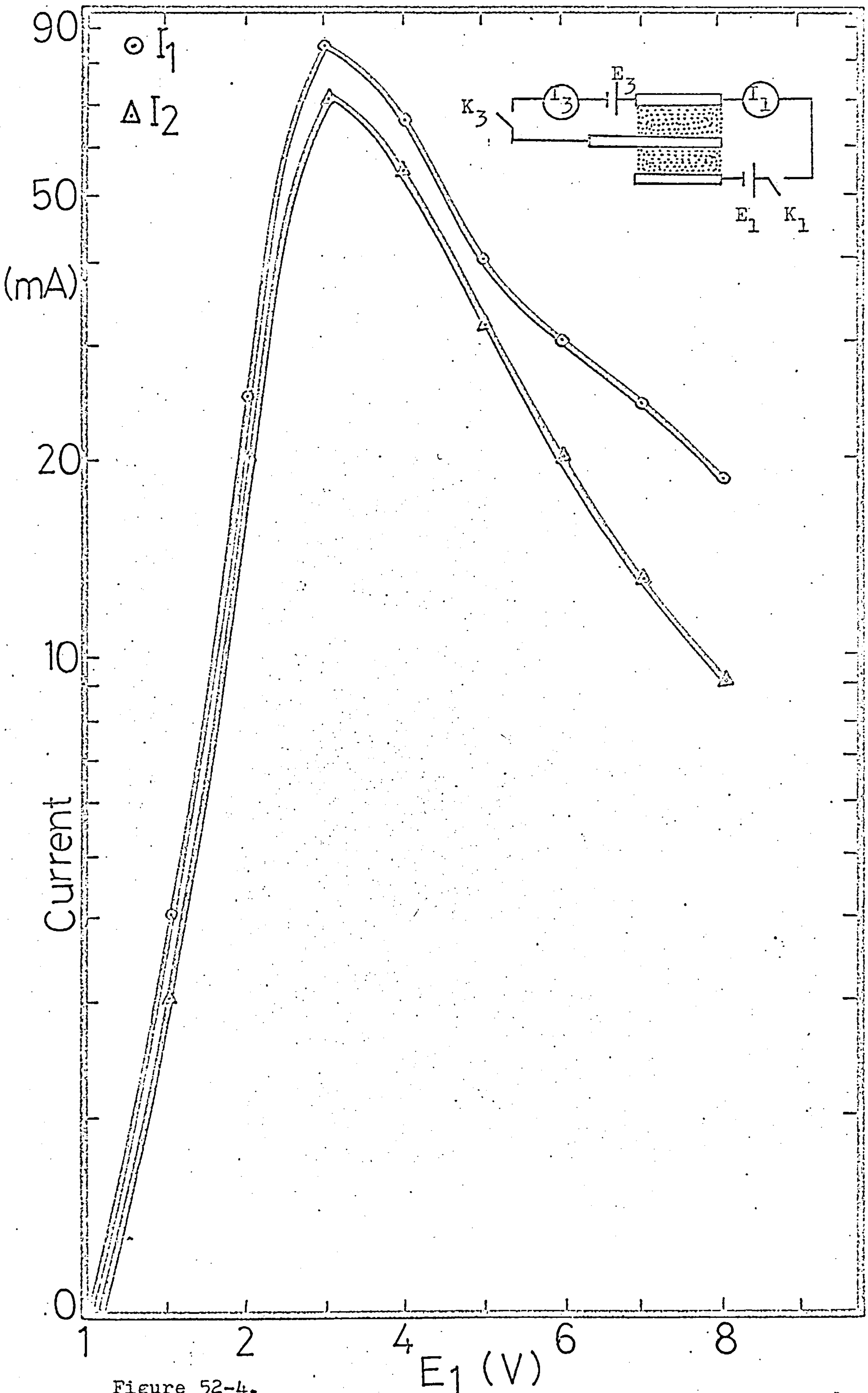


Figure 52-4.

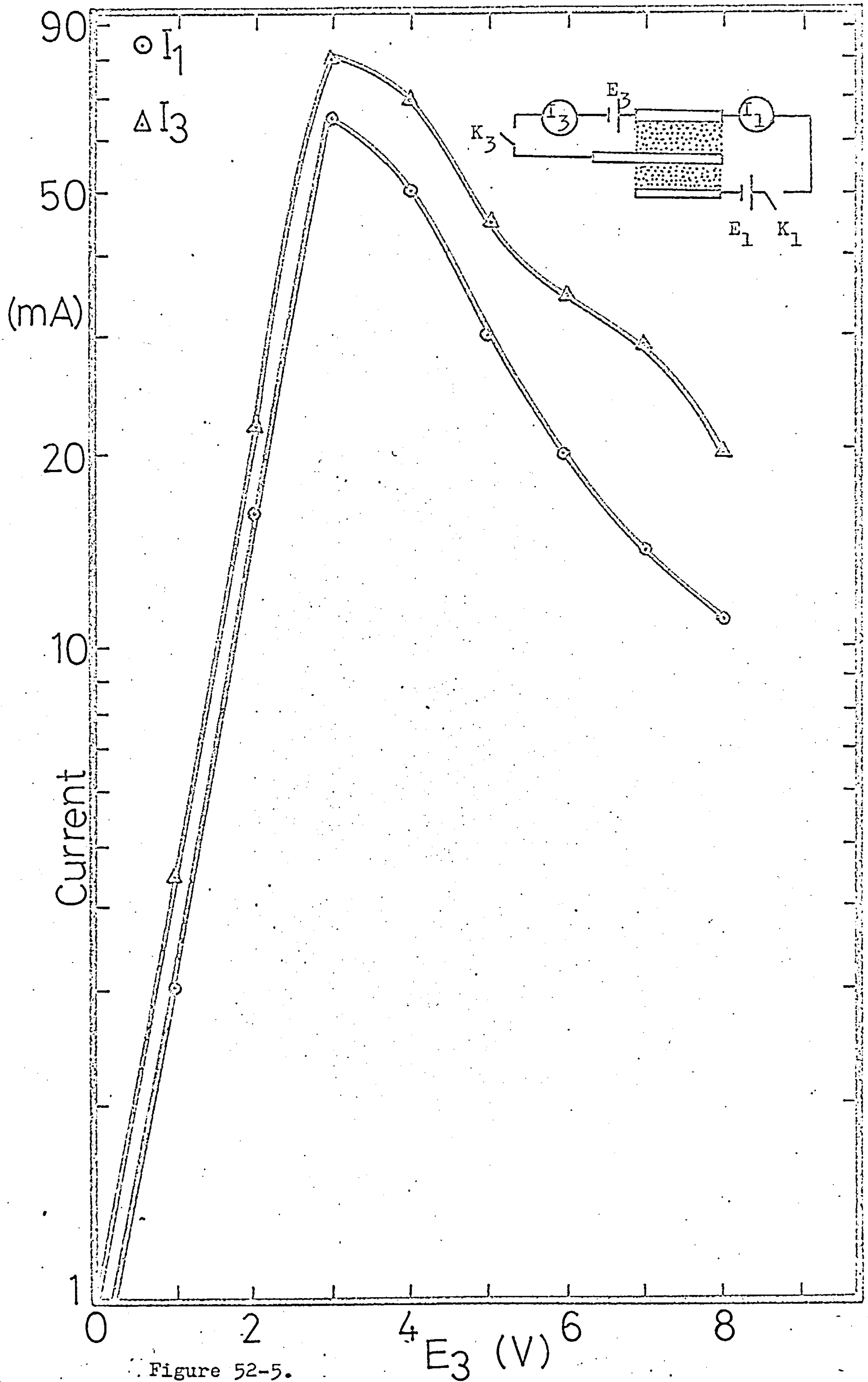


Figure 52-5.

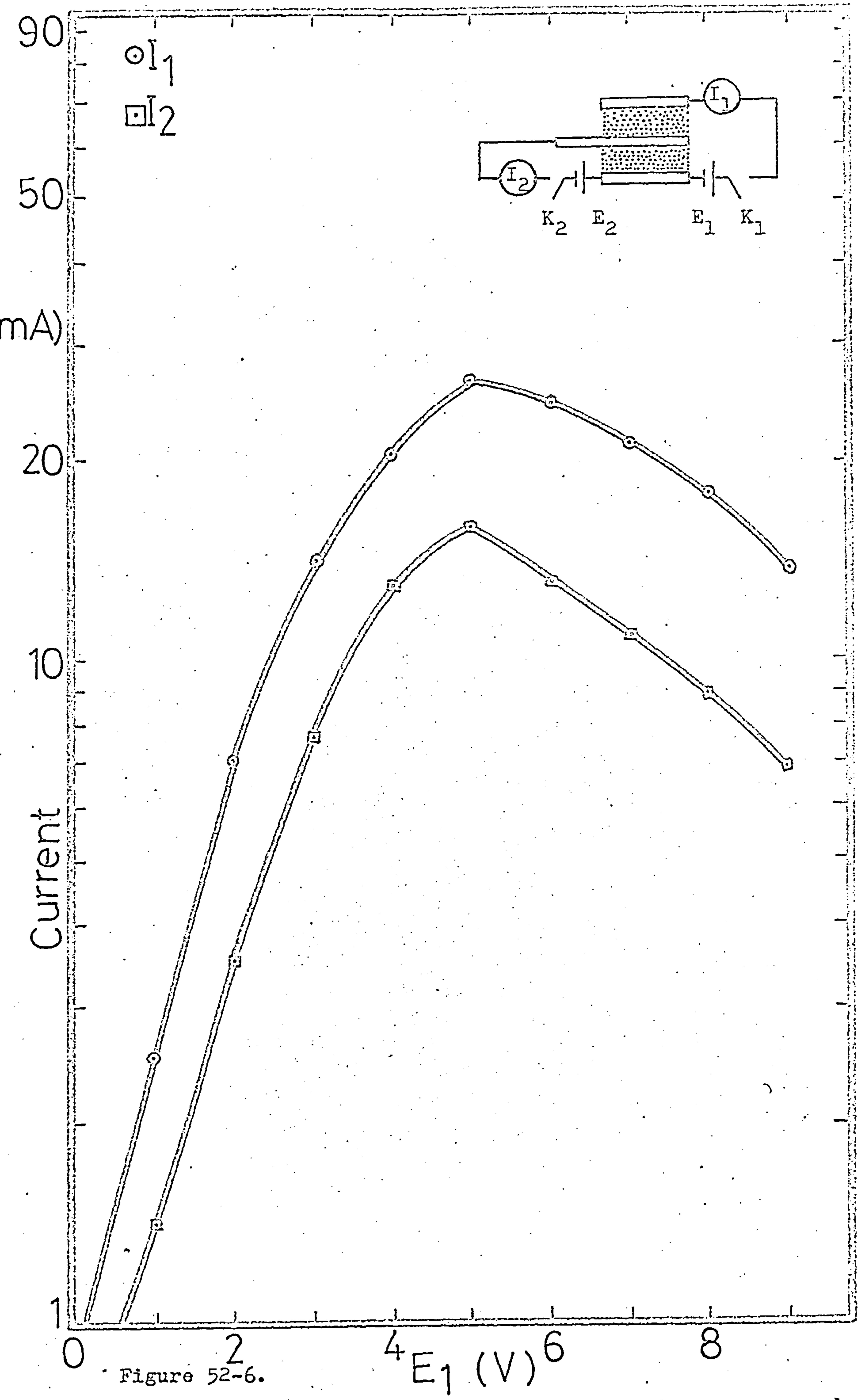


Figure 52-6.

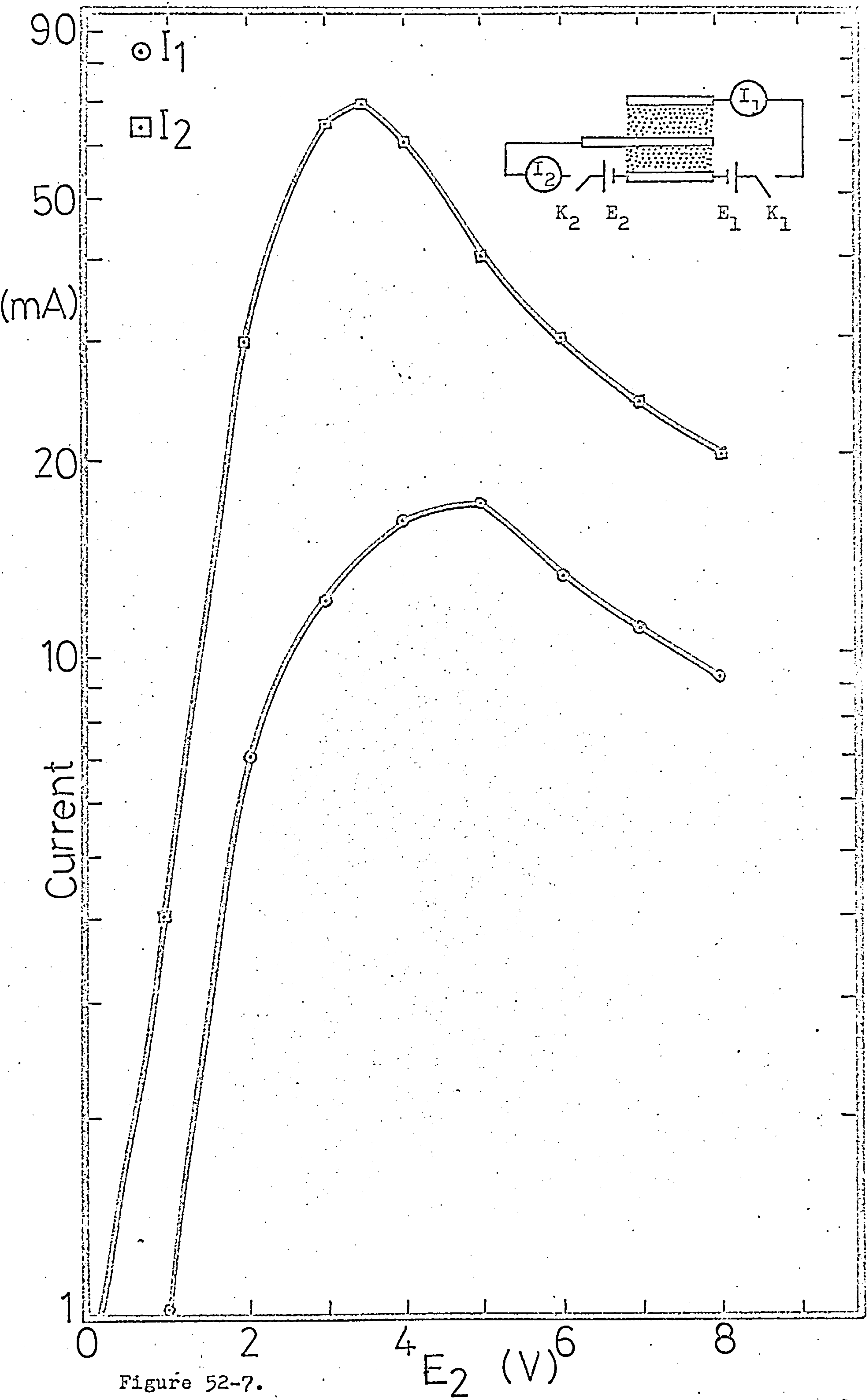


Figure 52-7.

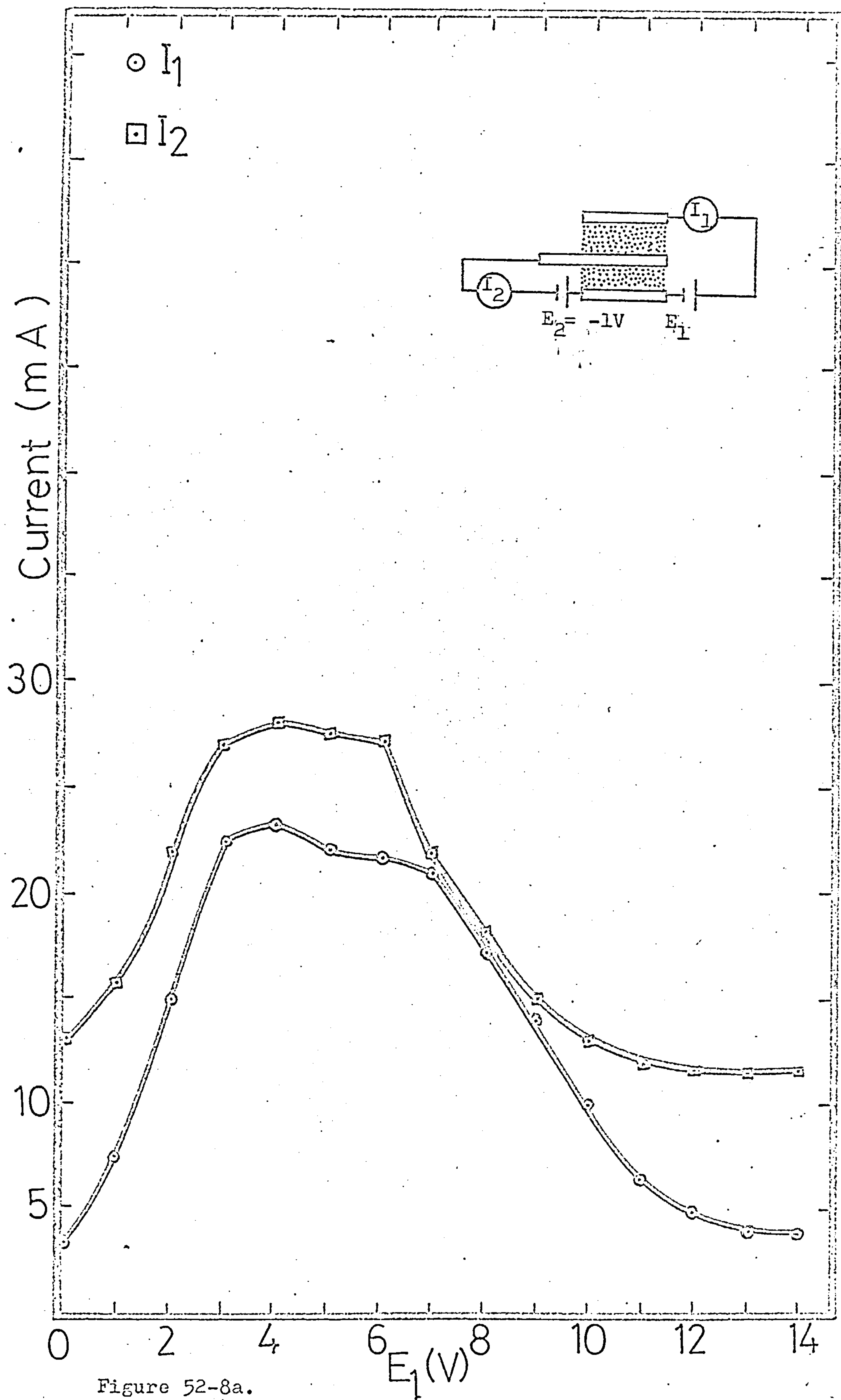


Figure 52-8a.

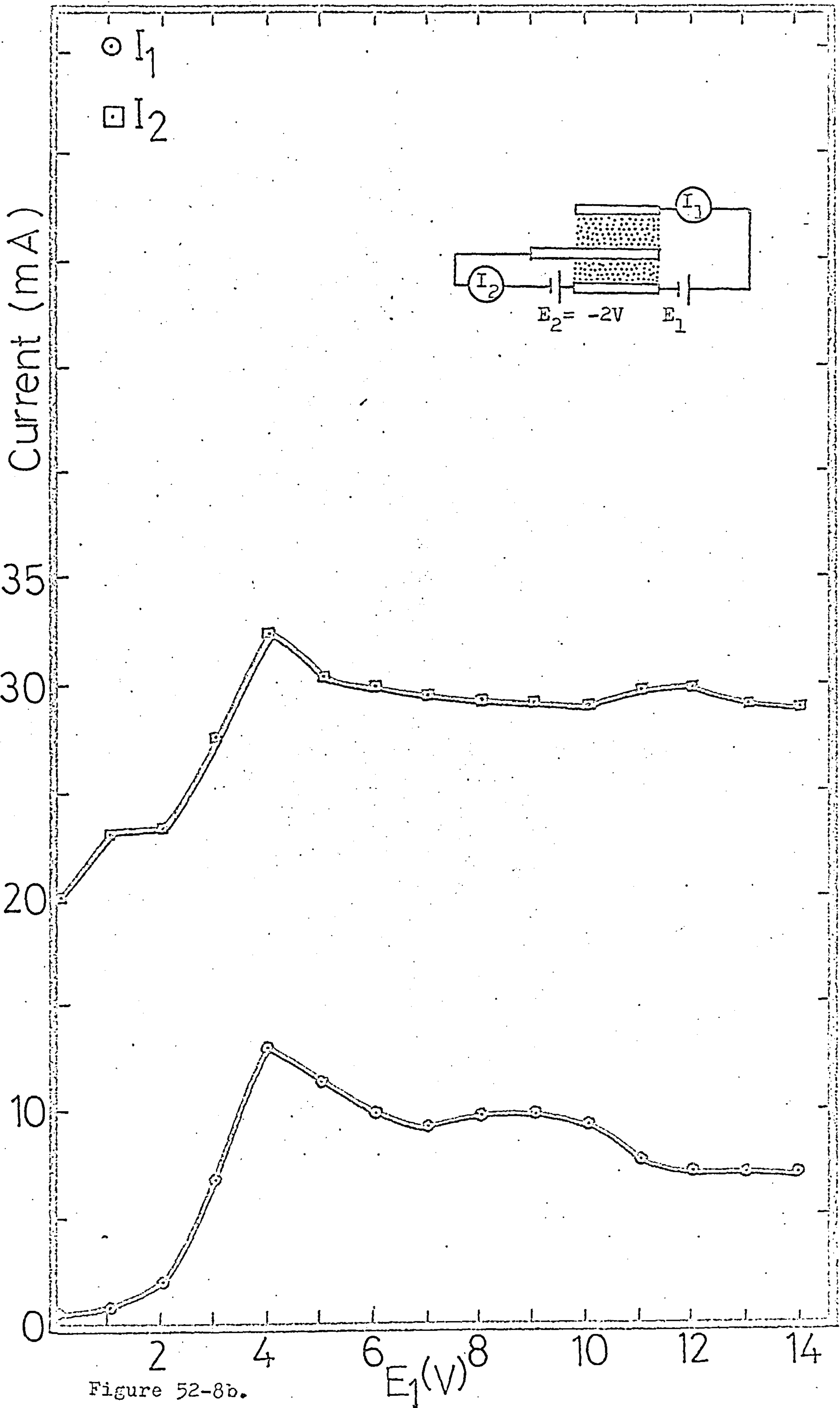


Figure 52-8b.

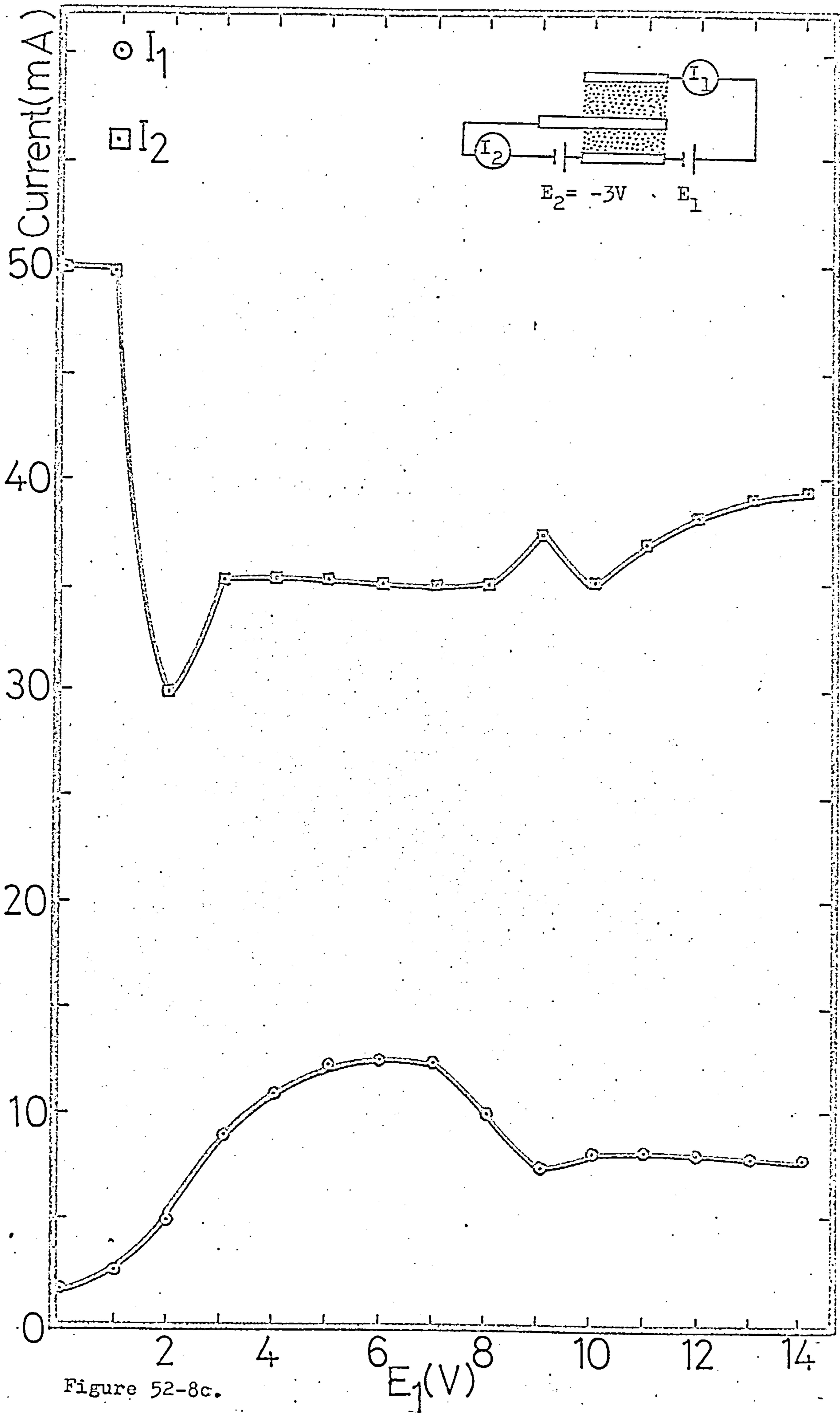


Figure 52-8c.

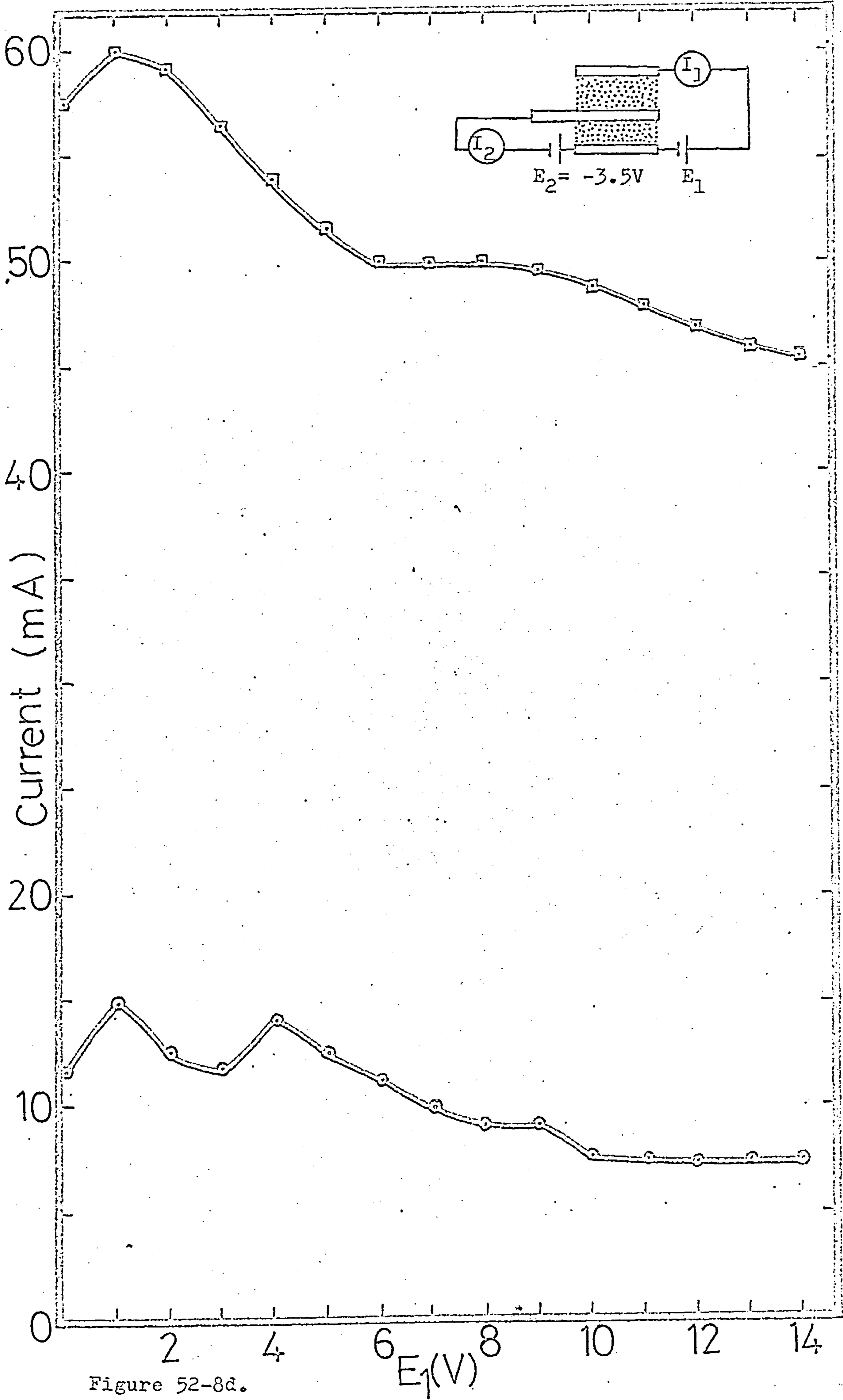


Figure 52-8d.

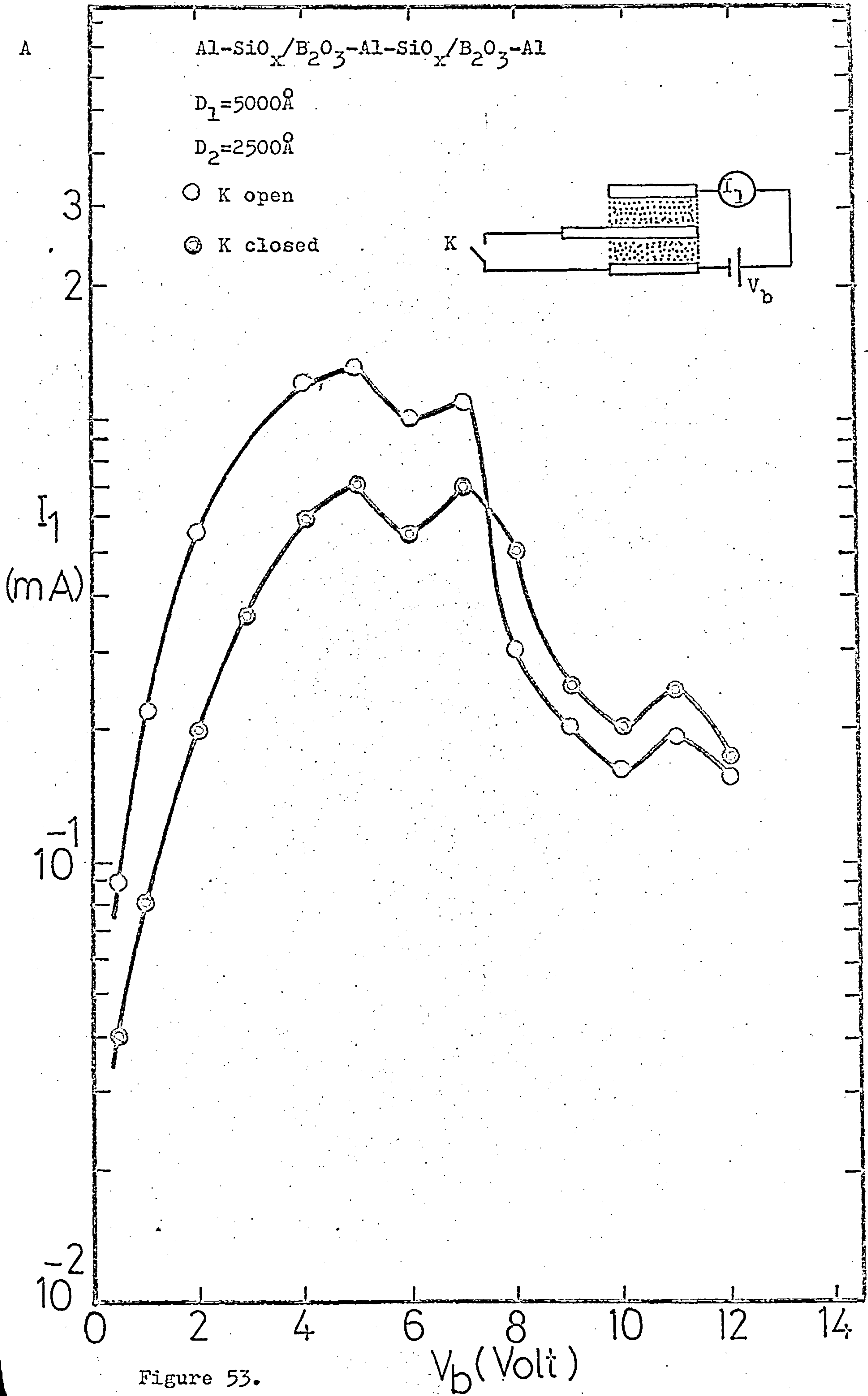


Figure 53.

V_b (Volt)

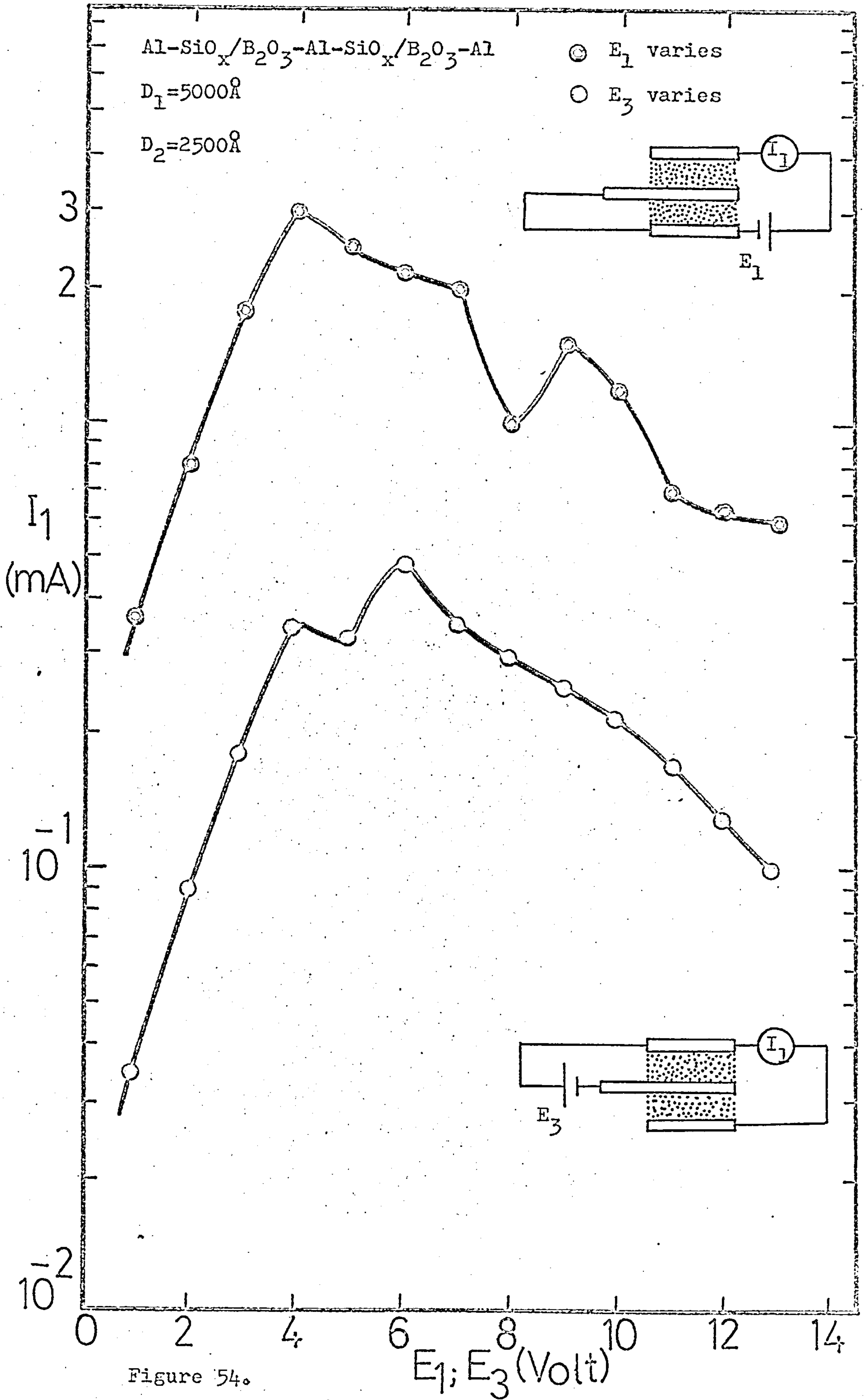


Figure 54.

Al-SiO_x/B₂O₃-Al-SiO_x/B₂O₃-Al

D₁=5000 Å

D₂=2500 Å

□ V_{GB} when B⁻, T⁺

□ V_{GB} when B⁻, T⁺

△ V_{GT} when B⁻, T⁺

△ V_{GT} when B⁻, T⁺

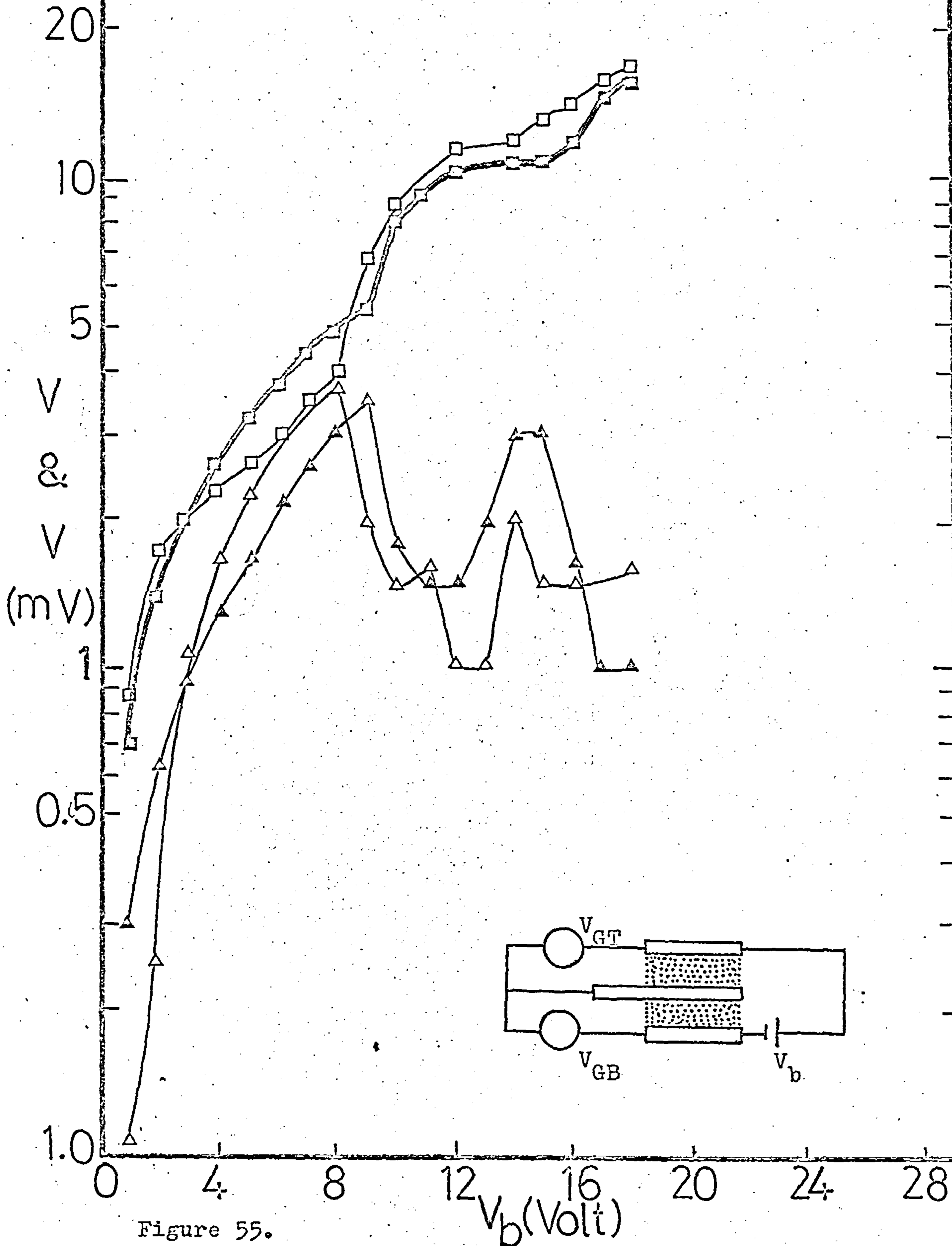


Figure 55.

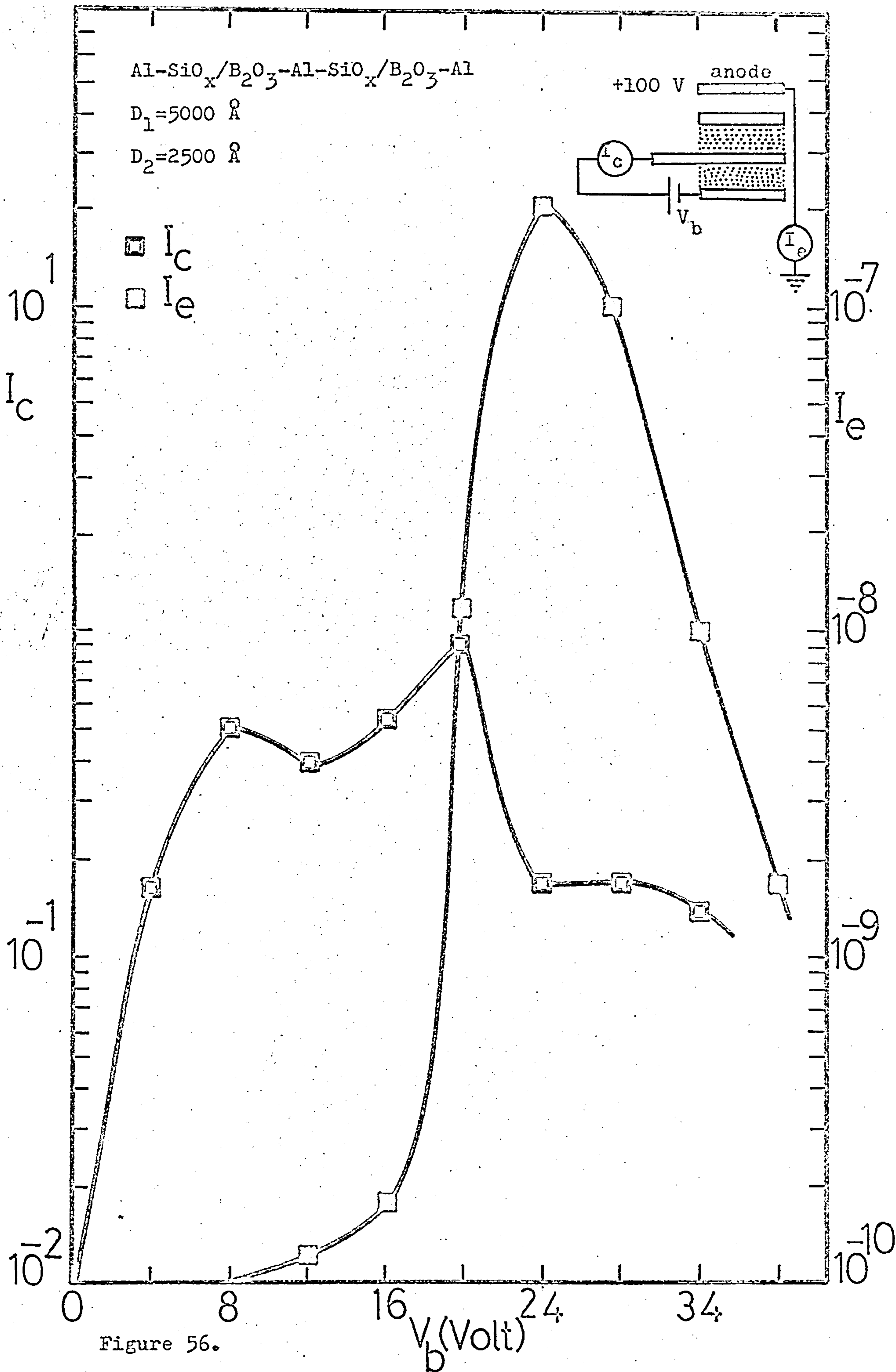


Figure 56.

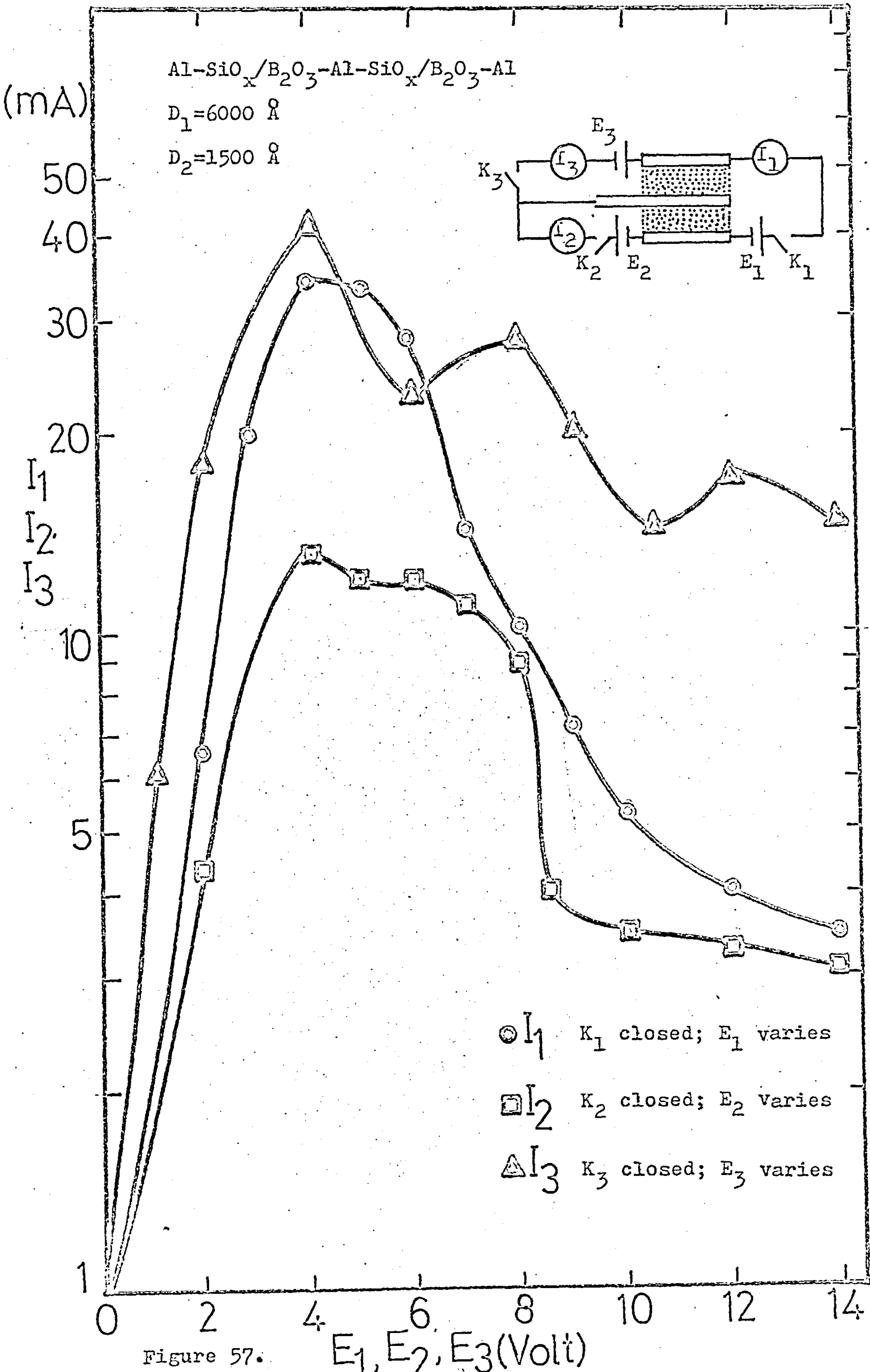


Figure 57.

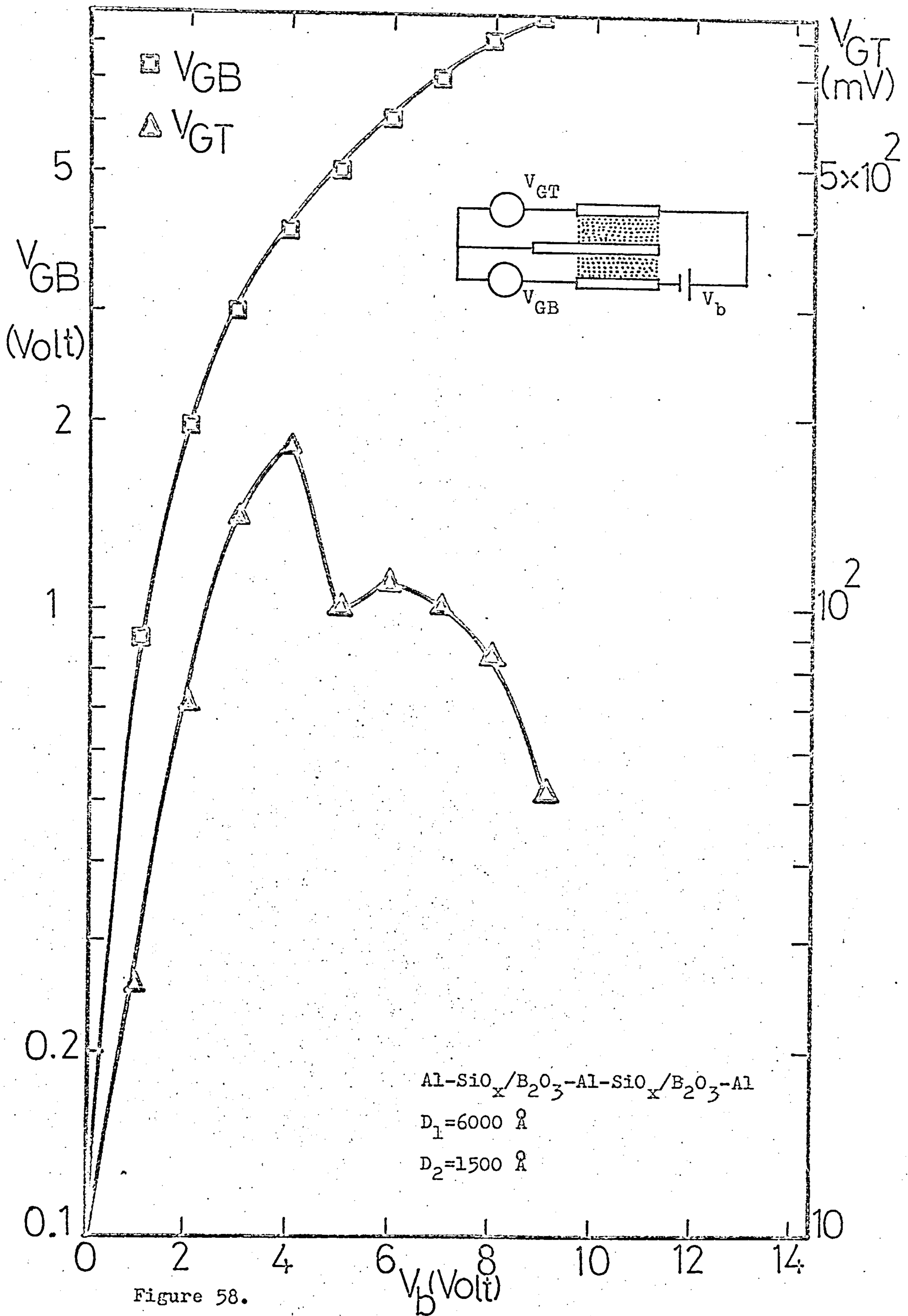


Figure 58.

┌
12.5 μ

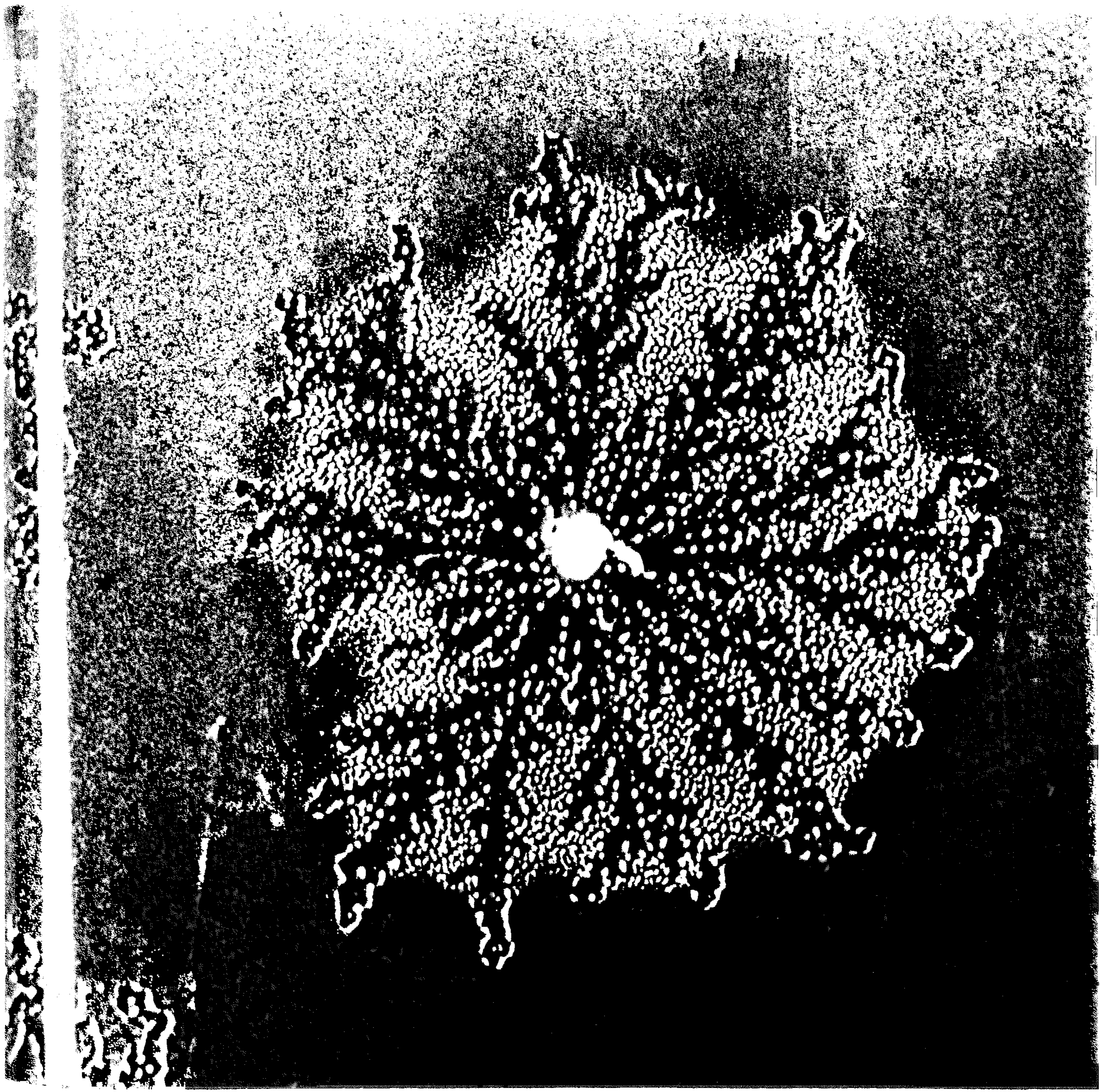


Fig. 62

Ag. electrode ($\times 300$)

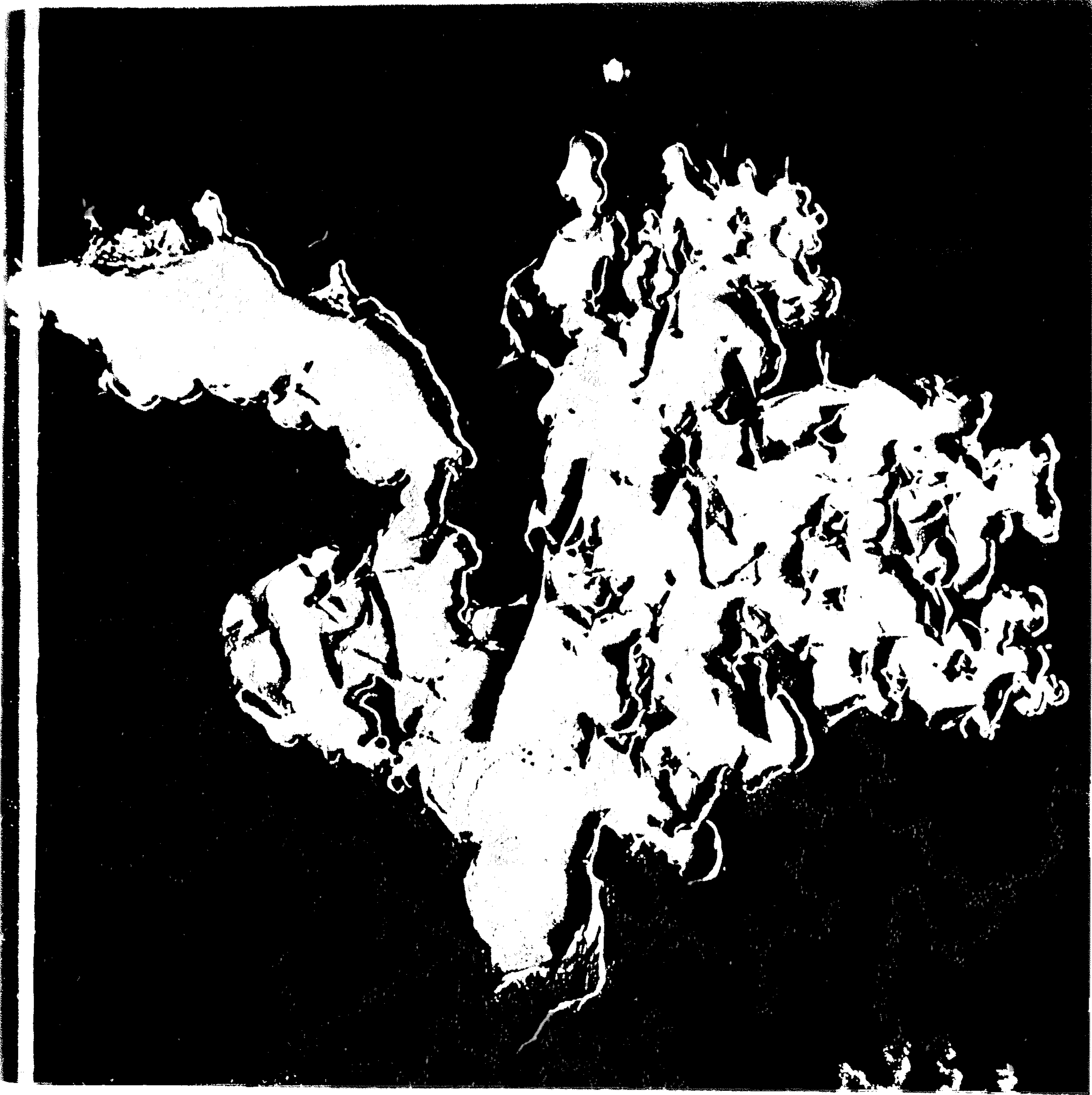


Fig. 63 Ag. electrode (X 160)

$$V_b < \eta_m$$

┌
63 μ

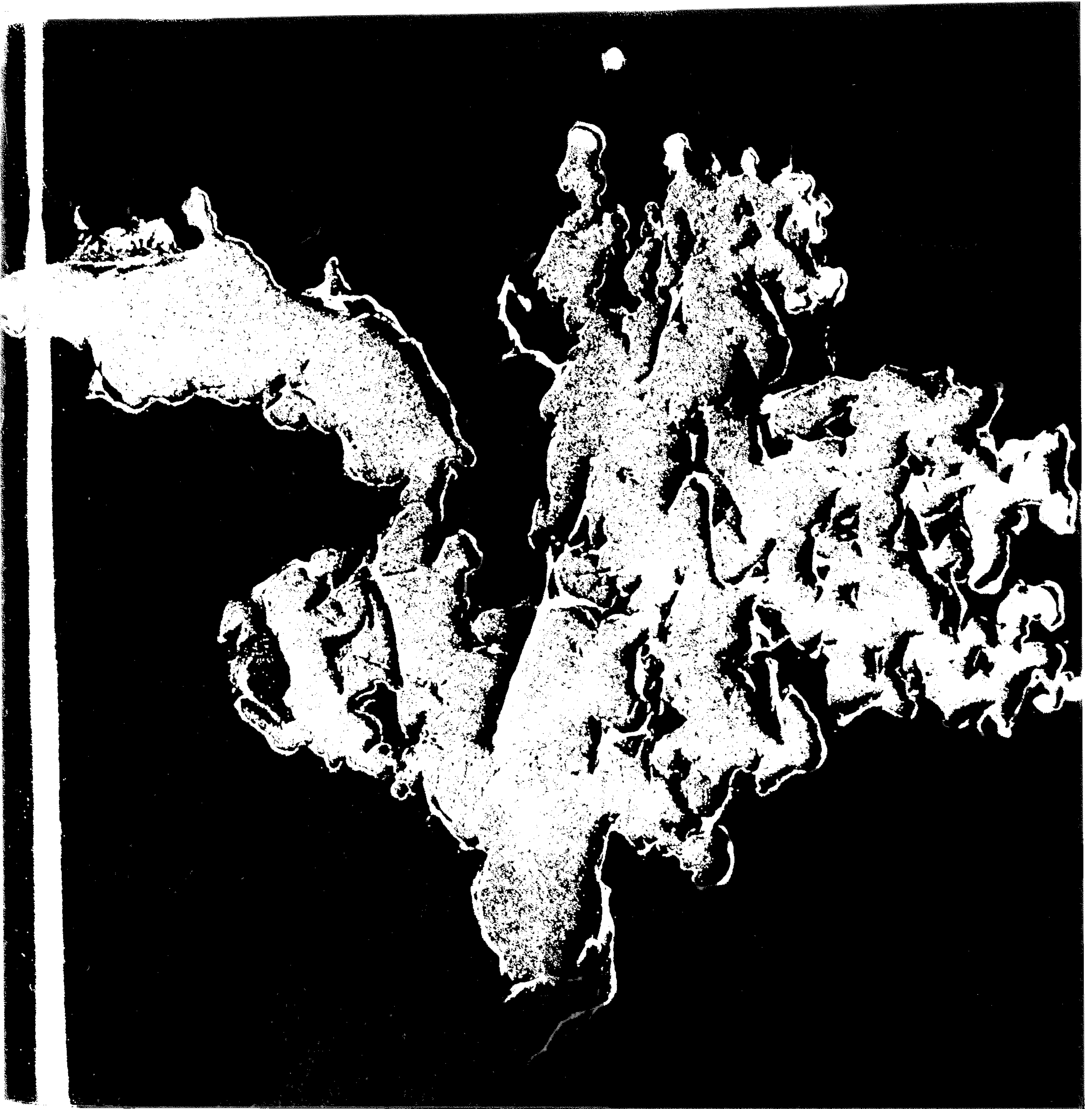


Fig. 64 Ag. electrode (X 160)

$$V_b > V_m$$

12.5 μ

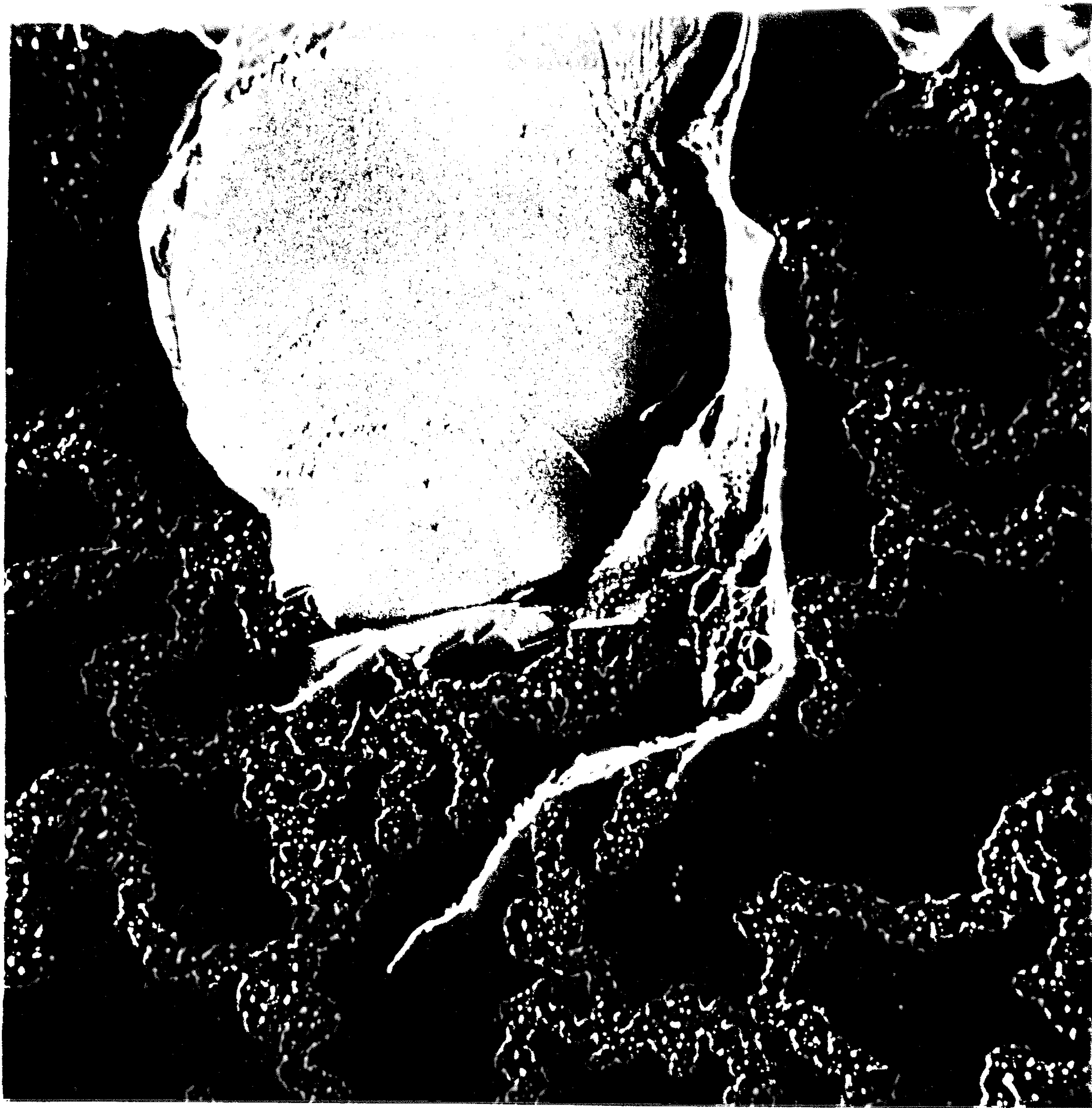


Fig. 65 Ag. electrode (X 300)

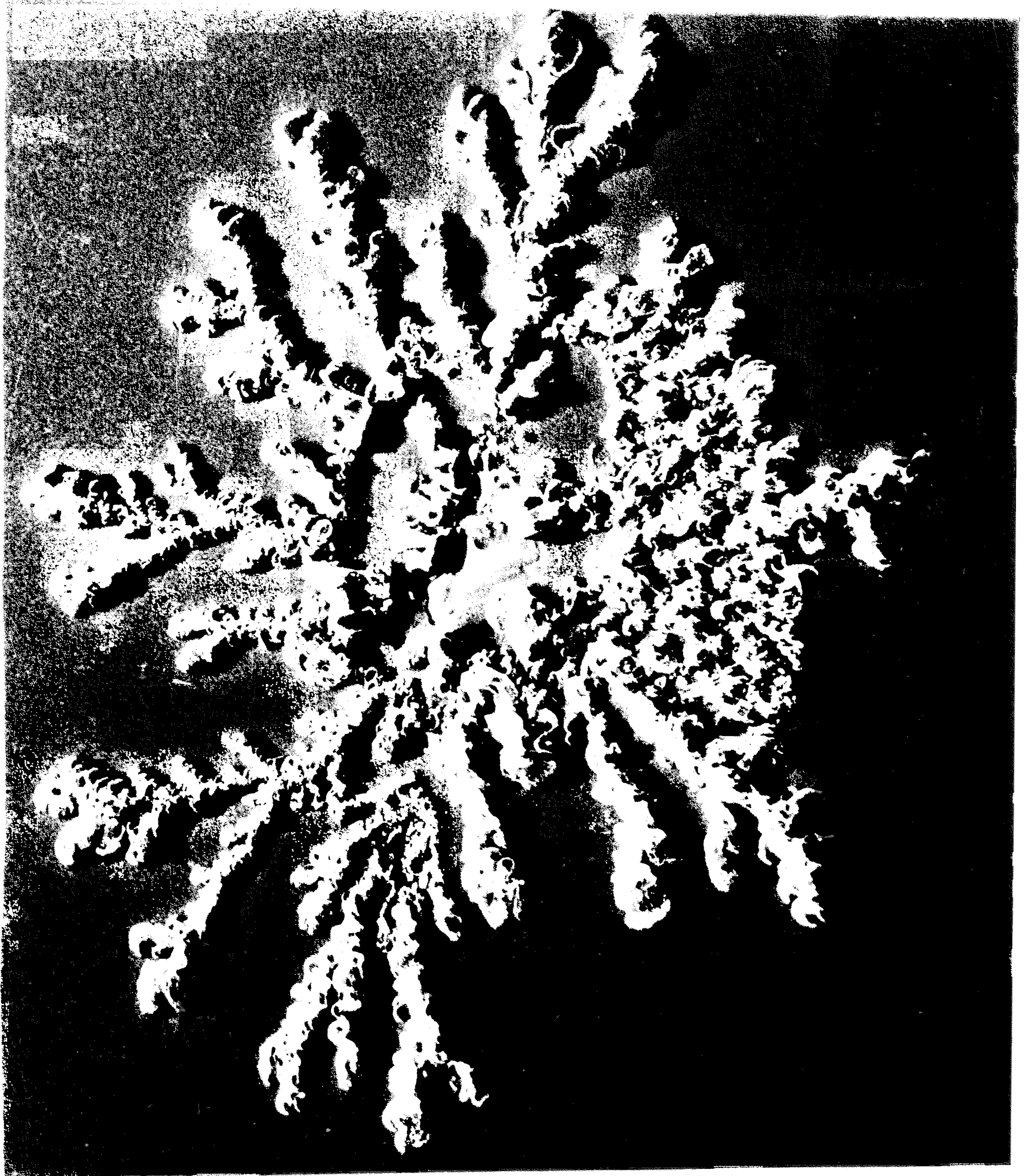


Fig. 66

Cu electrode (X 280)

┌
62.5μ

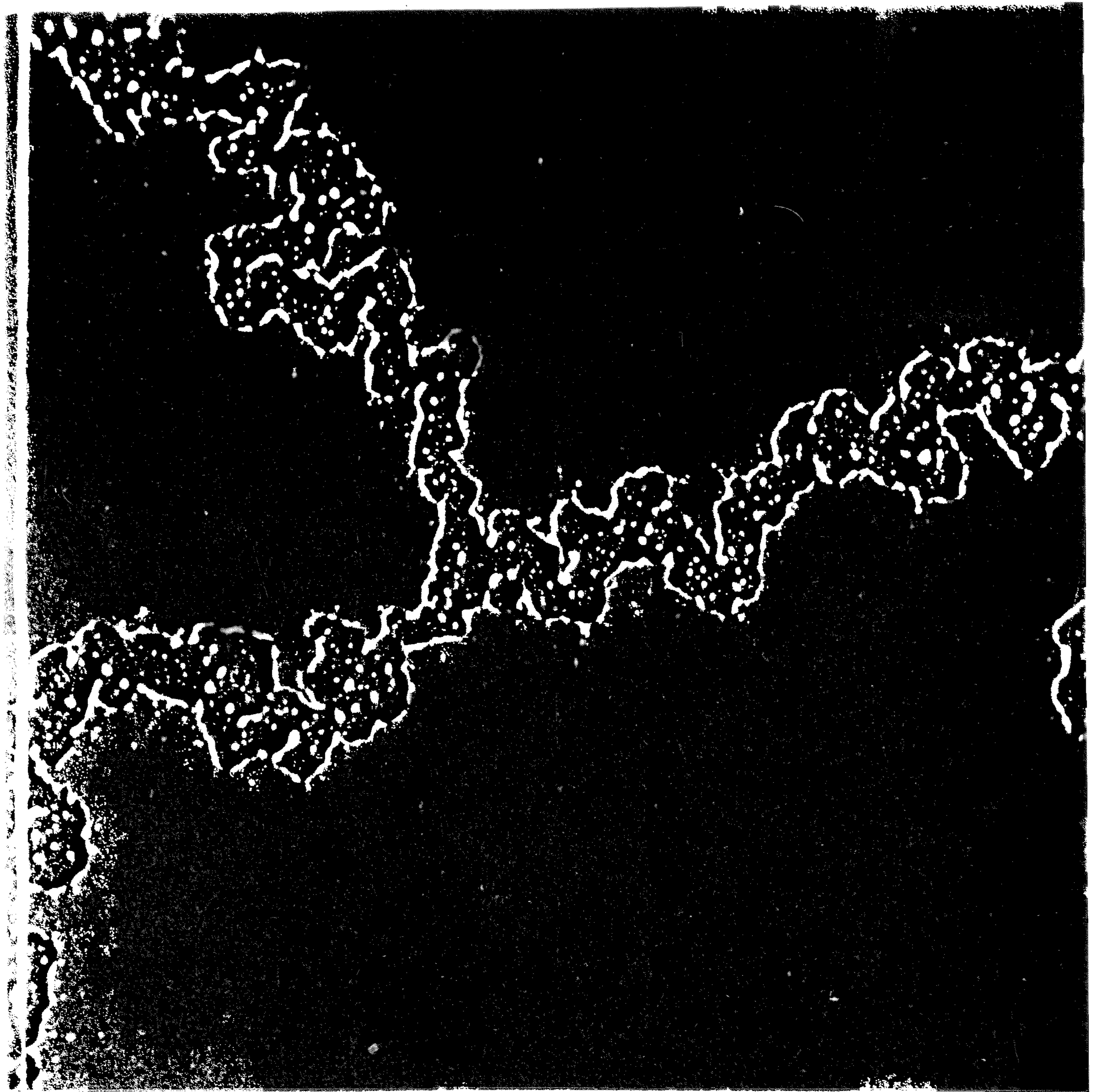


Fig. 67

Ag. electraea (X 1300)

This world must long survive our poor departure,
Persisting without name or note of us.

Could my heart know, in life, life's hidden secrets,
Death could inform me of God's hidden secrets.

from The Rubaiyyat of.

Omar Khayaam.